

NASA Contractor Report 3762

ARR yes
HHL
HHL
Log garden

Lightning Protection Guidelines and Test Data for Adhesively Bonded Aircraft Structures

J. E. Pryzby and J. A. Plumer

CONTRACT NAS1-15884
JANUARY 1984

DECLASSIFICATION STATEMENT II
Approved for public release
Distribution Unlimited

FOR EARLY DOMESTIC DISSEMINATION
Because of its significant early commercial potential, this information, which has been developed under a U.S. Government program, is being disseminated within the United States in advance of general publication. This information may be duplicated and used by the recipient with the express limitation that it not be published. Release of this information to other domestic parties by the recipient shall be made subject to these limitations.
Foreign release may be made only with prior NASA approval and appropriate export licenses. This legend shall be marked on any reproduction of this information in whole or in part.
Date for general release January 31, 1986

DEPARTMENT OF DEFENSE
ELASTICS TECHNICAL EVALUATION CENTER
ABRADCOM, DOVER, N. J. 07801

19960321 074

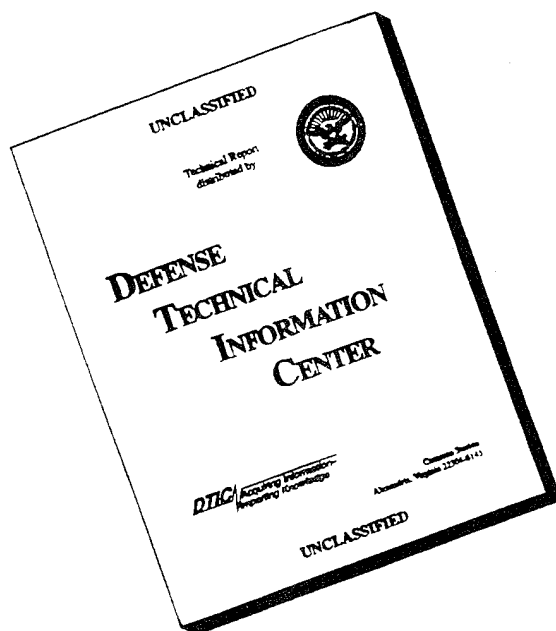
NASA

THIS QUALITY INSURED 1

PLASTEC

2/5/84
12/1/84

DISCLAIMER NOTICE



THIS DOCUMENT IS BEST QUALITY AVAILABLE. THE COPY FURNISHED TO DTIC CONTAINED A SIGNIFICANT NUMBER OF PAGES WHICH DO NOT REPRODUCE LEGIBLY.

NASA Contractor Report 3762

Lightning Protection Guidelines and Test Data for Adhesively Bonded Aircraft Structures

J. E. Pryzby and J. A. Plumer

Lightning Technologies, Inc.

Pittsfield, Massachusetts

Prepared for
Langley Research Center
under Contract NAS1-15884



National Aeronautics
and Space Administration

**Scientific and Technical
Information Office**

1984

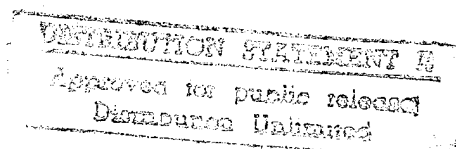


TABLE OF CONTENTS

	Page
1.0 SUMMARY	1
1.1 Introduction	3
1.2 Lightning Protection Design Guidelines	5
1.2.1 General	5
1.2.2 Basic Steps in Lightning Protection Design	5
2.0 EXPERIMENTAL PROGRAM	18
2.1 Purpose	18
2.2 Test Methods	19
2.2.1 Impulse voltage tests	19
2.2.2 Impulse current tests	20
2.2.3 Test chamber	21
2.2.4 Detection of electrical sparks	25
2.3 Adhesively bonded aluminum	26
2.3.1 Bonded aluminum lap joint specimens	27
2.3.2 Bonded aluminum fuel line brackets	37
2.3.4 Comparison of test results for various adhesives	43
2.3.5 Adhesively bonded aluminum honeycomb panel specimens	46
2.4 Hardware Interfaces with Metals	50
2.4.1 Access doors riveted, fastened, or bonded and fastened	50
2.5 Adhesively Bonded Graphite/Epoxy (gr/E)	62
2.5.1 Bonded gr/E lap joint specimens	63
2.5.2 Bonded gr/E stiffeners	69
2.6 Metal to gr/E Interfaces	69
2.6.1 Rivets in gr/E laminates	71
2.6.2 Access door dome nuts in gr/E laminates	76
2.6.3 Specimen description	78
3.0 FULL SCALE STRUCTURES TEST PROGRAM	83
3.1 Purpose	83
3.2 Basic Test Methods	83
3.2.1 Test setup	83

TABLE OF CONTENTS - CONT'D.

	Page
3.2.2 Current distribution tests	84
3.2.3 Bond line voltage measurements	84
3.2.4 Ignition source tests	84
3.2.5 Induced voltage measurements in wing electrical wiring	84
3.2.6 Magnetic field measurements	84
3.3 Bonded aluminum structure	84
3.3.1 Specimen description	84
3.3.2 Test setup	85
3.3.3 Test procedures	91
3.3.4 Test results	103
3.4 gr/E Wing	131
3.4.1 Specimen description	131
3.4.2 Test setup	132
3.4.3 Test procedures	137
3.4.4 Test results	141
3.5 Discussion of Results	161
3.5.1 Comparison of the full scale structural environment with the subelement test results	161
3.5.2 Comparison of the bonded aluminum wing with the gr/E composite structure	165
References	170

1.0 SUMMARY

The information presented in sections 2.0 and 3.0 of this report were developed from electrical tests of groups of representative specimens of graphite/epoxy (gr/E) and adhesively bonded aluminum. The purpose of the subelement program reported in section 2.0 was to characterize the electrical performance of typical structural bonds and joints and to determine the voltage and/or current thresholds at which electrical sparking and loss of physical strength occur. Then, complete, fully assembled structures employing adhesive bonding techniques and other manufacturing concepts similar to those evaluated during the subelement test program were tested to see if spark or physical damage threshold conditions could be reached in typical structures. These data are reported in Section 3.0. The data from both of these experimental programs are intended for use by aircraft designers in avoiding hazardous lightning effects in other designs. Guidelines for use of this data and design of lightning protection design are presented in Section 1.2.

Tests were performed on bonded aluminum and gr/E coupon-type (sub-element) specimens to determine the dielectric voltage breakdown and spark threshold levels of insulating adhesively bonded specimens and the current spark threshold levels of electrically conductive, adhesively bonded specimens. The aluminum specimens included lap joint, fuel line bracket, stiffener and honeycomb sections, and fuel tank access doors. gr/E specimens included lap joint, stiffener, fuel line feed-through elbow, and access door dome nut specimens in gr/E laminates.

Results of the bonded aluminum subelement specimens showed that many of the bonded specimens were electrically conductive but conductivity was not related to bond line thickness. The electrically conductive specimens exhibited a wide scatter of current spark threshold levels and many of the visible sparks were due to burrs at the specimen edges and ends. Shear strength degradation became significant at 2500 A/in² except for specimens bonded with aluminum powder-filled adhesive which did not suffer appreciable loss of strength at this current density. The addition of rivets to the bonded specimens increased the spark threshold level by 400-900 percent above the level for non-riveted specimens.

For aluminum specimens with nonconductive bonds, a wide range of voltage breakdown levels existed and most were due to edge sparkovers. The highest sparkover voltages were exhibited by specimens bonded with supported modified epoxies; the lowest readings were obtained on specimens bonded with aluminum powder-filled adhesives. Controlled bond line specimens showed increasing bond line voltage thresholds for increasing bond line thickness.

Contrary to expectation, no significant differences were found in spark threshold levels for the several aluminum access door and fastener configurations tested.

Results on the gr/E subelement specimens showed that some of the lap joint specimens exhibited electrical conductivity prior to test. Due to the small number of samples tested, no conclusion could be made between adhesive used and bond line breakdown voltage. On specimens with controlled bond lines, the breakdown voltage increased with increasing bond line thickness. Generally, the current spark threshold level was low for specimens which sparked at voltage breakdown and high for specimens which had exhibited pretest conductivity. However, all of the stiffener specimens exhibited pretest conductivity and had a low spark threshold level.

Tests on the rivet, dome nut, and fuel line feed-through elbows installed in gr/E laminates showed that the current spark threshold level of these specimens was low. Tests of fuel tank sealants as a means of containing such sparking showed that one sealant resulted in somewhat higher spark threshold levels than the other.

Tests on full scale bonded aluminum and gr/E wings included measurements of current flow in individual components, bond line voltages, induced voltages in wiring, and magnetic field levels.

Test results on the bonded aluminum wing showed that less than 0.2% of the test current flowed through the fuel lines and that 86% of the current was transferred from the skin to the main spar. Low bond line voltages indicated that electrical continuity existed through the bonding adhesive. Photographs of the fuel tank interior during simulated strikes to the wing indicated that no ignition sources existed within the fuel tank.

Induced voltage measurements in electrical wiring within the bonded aluminum wing showed that circuits routed entirely within the wing structure were relatively immune to severe induced voltages, but wiring to apparatus located in the plastic wing tip was susceptible to induced voltages high enough to damage other electrical/electronic equipment powered from the same source. The magnetic fields within the wing fuel tank were approximately 5% of the level external to the fuel tank.

Current flow measurements in the gr/E wing showed that during the first few microseconds (μ s) of current flow, the majority of the current was carried by the gr/E skin and spars. After about 20 μ s had elapsed, a significant portion of the total current was carried by metal conductors, including a leading edge conduit and the control cables, with smaller portions remaining in the gr/E structure.

Bond line and structure voltage levels increased with increasing test current levels and increased distance between the measurement location and the wing reference plane. However, the gr/E skin resistivity was somewhat non-linear and decreased with increasing current level. Voltage levels induced in wiring routed through a metal conduit to equipment located within the gr/E wing tip were generally low enough to be tolerated by electrical/electronic equipment associated with this wiring. One circuit experienced levels that may require additional protection against the effects of a severe strike.

The magnetic field amplitudes measured within the gr/E wing interior were approximately 20% of the levels measured around the exterior surfaces of the structure.

Measurements in the bonded aluminum wing showed that test current levels of 7 kA to 11 kA resulted in bond line voltage readings of 0.15 volts or less. Extrapolation of these measurements for a 200 kA severe lightning stroke results in a voltage level of less than 5 volts. This level is below the 50 volt spark threshold recorded during tests on the lap joint subelement specimens. Fuel line currents were 160A or less during current distribution measurements; this was higher than current spark threshold levels measured on subelement fuel line bracket specimens ($\leq 100A$). Lack of visible fuel tank sparking during ignition source tests, however, indicated that the amplitude of the current flowing through any one individual fuel line bracket must have been lower than the subelement spark threshold level.

Measurements in the gr/E wing showed that a test current of 190 kA resulted in a bond line voltage reading of 200 volts. This is below the voltage spark threshold level of 1200 volts recorded on the lap joint specimens during the subelement tests. Fuel line currents, measured during application of 190 kA test currents, reached a peak amplitude of 2 kA which was lower than the 5 kA spark threshold level of the fuel line feed-through subelement specimens.

1.1 Introduction

The highly competitive marketplace and increasing cost of energy is motivating manufacturers of general aviation aircraft to achieve greater efficiency and economy through application of advanced technologies in the design of new aircraft.

Among these are an increased use of composite materials to obtain higher strength-to-weight performance and the use of metal-to-metal bonding with adhesives in place of conventional fasteners and rivets to obtain smoother outside surfaces and reduce drag and to reduce costly hole drilling and fastening operations. Other advantages include corrosion reduction and extension of fatigue life.

Standing in the way of widespread use of some of these new technologies, are potential problems posed by variability of properties, impact resistance, environment effects, lightning protection, and electromagnetic compatibility. The primary emphasis of this program was protection from lightning effects.

The program began with a survey of the participating manufacturers to obtain information on advance-technology materials and fabrication methods under consideration for future designs. From the survey, typical structural designs were selected, and these were fabricated as small "subelement" specimens which were subjected to voltages and currents representative of the lightning stroke. Measurements of bond line voltages, electrical sparking, and mechanical strength degradation were made to comprise a data base of electrical properties for new technology materials and basic structural configurations.

The second phase of the program involved tests upon full scale wing structures which contained integral fuel tanks and which were representative examples of new technology structures and fuel systems. The purpose of these tests was to provide a comparison between full scale structural measurements and those obtained from the "subelement" specimens.

The new technologies dealt with included adhesive metal-to-metal bonding; bonded honeycomb; kevlar, fiberglass and gr/E structures; bonding and fastening techniques; fuel system internal components, and electrical systems located within the new-technology structures.

The prime contractor was Lightning Technologies, Inc., Pittsfield, Massachusetts. Test specimens were provided by Beech Aircraft Corporation, Wichita, Kansas; Lear Fan Corporation (US), Reno, Nevada; and Cessna Aircraft Company, Wichita, Kansas. The above-named participants, in addition to the Materials Division and the Low-Speed Aerodynamics Division of NASA Langley Research Center, provided engineering guidance and analyses through a project steering group which met periodically to review test results and plan further tests. The program period of performance was 1 August 1979 through 1 July 1983.

This report is organized into three sections:

Section 1.0 contains the Summary, Introduction, and Design Guidelines, which include a discussion of the basic steps involved in lightning protection design, and some techniques for use in anticipating possible lightning effects problem areas and protection design approaches;

Section 2.0 describes the "subelement" specimens and test results:

Section 3.0 describes the full scale structure specimens, presents the test results, and compares the results with those

obtained from the "subelement" tests. Test data from sections 2.0 and 3.0 are intended for use by designers in anticipating lightning effects hazards in new designs.

Identification of commercial products in this report is to adequately describe the materials and does not constitute official endorsement, expressed or implied, of such products or manufacturers by the National Aeronautics and Space Administration.

1.2 Lightning Protection Design Guidelines

1.2.1 General

In this section of the report, the basic procedural steps in lightning protection design are reviewed and examples are given of how to use the test data in sections 2.0 and 3.0 to assess potential hazards or develop protection.

1.2.2 Basic Steps in Lightning Protection Design

In most cases, lightning protection designs are achieved most efficiently if the process is begun early in the design phase of a new aircraft and accomplished according to the following basic steps:

1. Determine the lightning strike zone(s) in which the structure is located.
2. Establish the lightning environment.
3. Identify structural components, systems or subsystems that may be vulnerable to hazardous effects.
4. Establish the degree of protection required.
5. Proceed with protection design.
6. Verify adequacy of design by analysis or test.

The design and verification process outlined above is least costly and results in the most efficient design if begun very early in the preliminary design phase of a new aircraft or major structure. Also, the design effort should be an interdisciplinary one, because lightning effects are both electrical and physical in nature, and often interact with the structures as well as with electrical and avionics, propulsion, fuel and other systems contained within the aircraft. The following paragraphs describe each of the above steps in greater detail.

1.2.2.1 Determine the lightning strike zone(s) in which the structure is located

Lightning strikes attach initially to the extremities of an aircraft, such as propeller tip, nose, or empennage tips. It is extremely rare for lightning to initially strike a flat surface

such as the top or bottom surface of a wing or the center of a fuselage; however, since most aircraft are moving forward when a strike occurs and since most lightning flashes have a lifetime of approximately a second, the lightning arc channel may reattach itself to aircraft surfaces aft of initial attachment points. For example, a strike to the nose may reattach at spots along the fuselage, and strikes initially reaching a propeller tip will often reattach to the nacelle or a flap that lies behind it. There are other surfaces of an aircraft which are not expected to receive any strikes. These usually include the leading edges and flat surfaces of wings and empennage structures that do not lie behind initial attachment points such as the nose or a propeller. These surfaces do not usually need to be designed to tolerate direct strike effects. Nonetheless, they may lie between other portions of the airframe which are subject to direct or swept strokes. The lightning attachment process is described more fully in Ref. 1.

In recognition of this fact, lightning strike zones have been defined for use by aircraft designers and regulatory authorities in establishing the lightning environment for each major section of an aircraft. These zones have been defined (Ref. 2) as follows:

- Zone 1A: Initial attachment point with low possibility of lightning arc channel hang-on.
- Zone 1B: Initial attachment point with high possibility of lightning arc channel hang-on.
- Zone 2A: A swept stroke zone with low possibility of lightning arc channel hang-on.
- Zone 2B: A swept stroke zone with high possibility of lightning arc channel hang-on.
- Zone 3: All of the vehicle areas other than those covered by zone 1 and 2 regions. In zone 3, there is a low possibility of any direct attachment of the lightning arc channel. Zone 3 areas may carry substantial amounts of electrical current, but only by conduction between some pair of direct or swept stroke attachment points.

The location of each zone on a particular aircraft depends on the geometry of the aircraft as well as other factors including its intended flight envelope and airspeed. The zone locations for a particular aircraft are usually established by comparison with inflight experience of existing aircraft of similar shape or by tests in which a scale model is subjected to simulated lightning strikes applied from a variety of directions. Further guidance on location of strike zones is available in Refs. 3 and 4.

Although some of the surfaces of an aircraft are not within a direct strike zone (zone 1A or 2A), nearly all internal structures are located within zone 3 because they lie between extremities. Thus, even though an aircraft skin may not need protection, the complete structure which is comprised of the skins plus all internal structural members, must be designed to safely conduct zone 1A currents (usually SAE current components A and C) from one end to the other, or perhaps from one surface to another. For riveted metal structures this requirement was easily met with little or no specific changes in design to accommodate the lightning current. However, adhesive bonds and composite structures may be susceptible to electrical sparking or loss of strength when subjected to the same current levels unless specific measures are employed in the design to counter these effects. Thus, it is important that the lightning strike zones be located before assessment of potential lightning hazards or protection design methods are begun. All parties involved in the aircraft design and certification process should be aware of and understand the location(s) of these zones.

1.2.2.2 Establish the lightning environment

In this section the actual amplitudes and other important characteristics of lightning currents are established for the surfaces and structures within each zone. If the criteria in references 5 or 6 are followed, this step follows directly from step one since the environments for each zone are defined. The design process then becomes the determination of the percentage of the total environment current that may be expected to pass through a specific structural component or across a joint of interest. For example, if an integral fuel tank within a wing is comprised of the upper and lower wing skins and three longitudinal spars as shown in Figure 1.1, and if the skins are to be adhesively bonded to the spars, the designer will have to estimate the amount of current expected to flow across the adhesive bond from the skin to each spar.

The calculation of electric current flow through structures as complex as an airframe is extremely difficult to accomplish without extensive computational facilities. In addition, considerable uncertainties surround the authenticity of even the most sophisticated current flow models presently available, and this aspect of lightning phenomenology remains the subject of research. Therefore, the designer must resort to simple estimation methods and considerable reliance upon test data (when available) to determine the electrical environment. This task is made possible by reliance on several "rules of thumb" as follows:

1. For metal structures, lightning currents flow initially on the outermost conductors, which usually include outer skins and leading edges, and diffuse more slowly into internal structural members such as spars and stringers. The current flow in an aluminum spar within an aluminum wing might appear as shown in Figure 1.2.

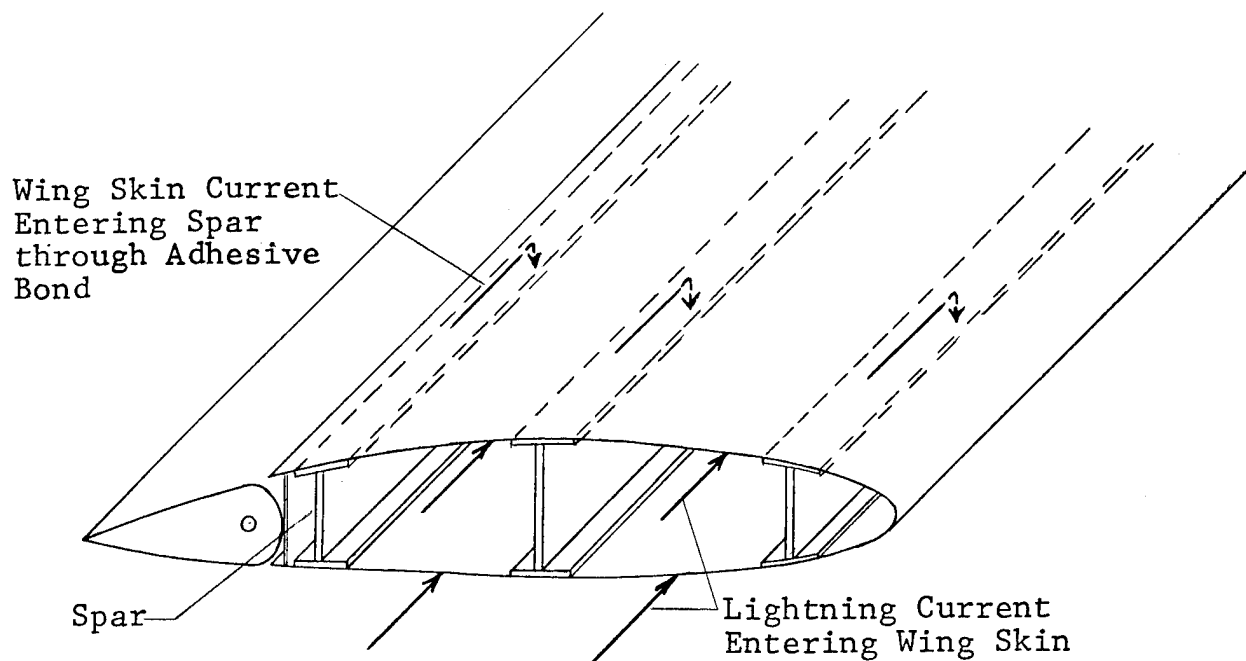


Figure 1.1 - Current Flow from Wing Skin to Spars through Adhesive Bonds.

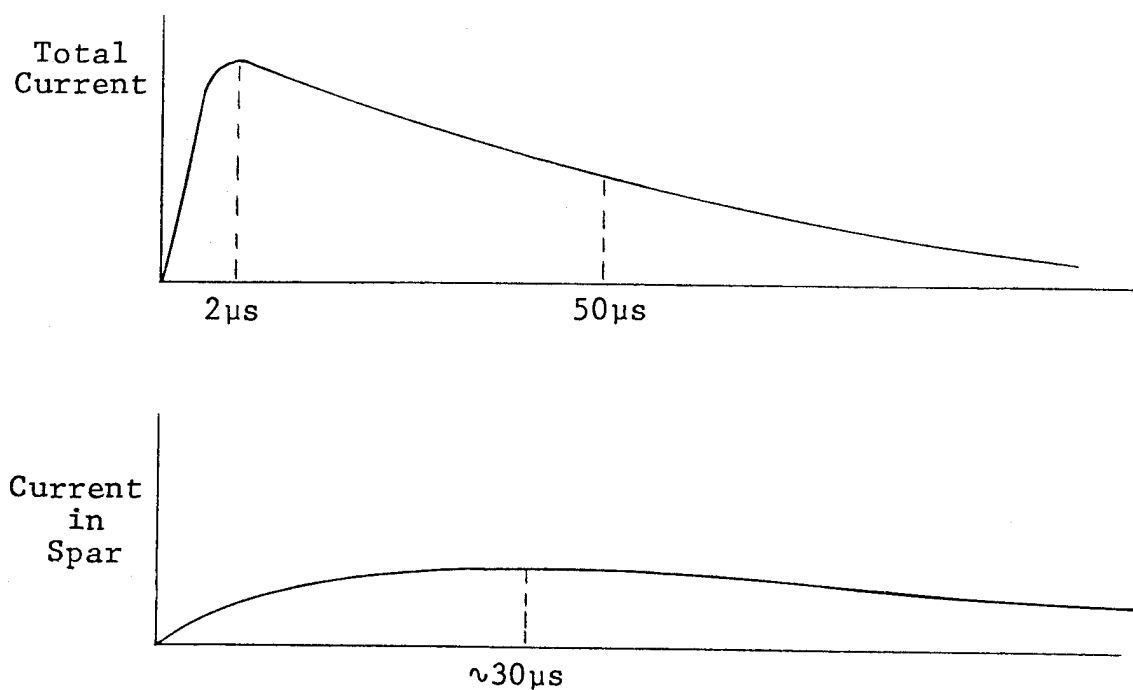


Figure 1.2 - Current Flow within an Aluminum Wing.
 • Top Waveform - Total Current in Wing
 • Bottom Waveform - Current in Spar

2. Electric currents diffuse much more rapidly throughout gr/E structures so the lightning current may be expected to flow into internal structural members (such as spars) at the same rate as in external skins.

3. During the first few microseconds of current flow, current divides inductively. At later times, after a few tens of microseconds have elapsed, currents divide in accordance with the relative conductivity of structural members. For example, in a gr/E structure containing some metallic items such as electrical conduits or control cables, current flows through all paths in accordance with their relative inductances (i.e. longer paths have higher inductances and thus carry lower currents than shorter paths) but at later times, the current will seek paths of lowest resistance and thus begin to concentrate in the metal conductors. This characteristic is illustrated in the measurements of current in the metal components within the gr/E wing, reported in paragraph 3.4.4.1. For estimating purposes, current division through a composite structure may be considered inductive during the first ten microseconds and resistive thereafter.

4. Current division through any structure is also influenced by the strike attachment point (i.e., the location(s) where currents enter and leave the structure). Since lightning currents usually enter or leave a structure at single points, the currents will become much more concentrated in the vicinity of these points than elsewhere in the structure. Thus, nearby joints, bonds, and materials usually must be designed to tolerate higher current densities than similar interfaces further away from current entry or exit points. Current concentration factors between four and ten should be applied in the vicinity of possible current entry or exit points.

5. Smaller structures will always have to tolerate higher current densities than larger airframes, since the total lightning current is the same regardless of aircraft size. The goal of spark or physical damage prevention within a general aviation aircraft structure is, therefore, usually more difficult than for structures of larger transport category aircraft.

With the above guidelines in mind, it is possible to make a rough assessment of the currents that must be tolerated in a typical structure. An example of how this may be done is as follows:

A. Determine the possible direction(s) of lightning current flow, based on the location of the structure within an aircraft.

B. Determine the cross-sectional areas of each of the conductive elements of the structure. This will include the upper and lower skins, main spars, and any longerons or stringers, plus any nonstructural components such as metal conduits or control cables.

C. Determine the division of lightning current among the elements. If the length of all of the above paths are approximately the same, the lightning current will initially divide among the elements in proportion to their relative cross-sectional areas.

D. Determine the electrical resistivities of each of the conducting paths, and calculate the resistances of each path or conductor by the following expression:

$$R = \frac{\rho L}{A}$$

where:

R = the total resistance of the conductor - ohms

ρ = the resistivity of the conductor material - ohm-in. (ohm-cm)

L = length of the conductor - in. (cm)

A = conductor cross-sectional area - in.² (cm²)

Electrical resistivities of typical airframe structural materials are presented in Table 1-1 (Ref. 7).

Table 1-1 - Electrical Resistivities of Typical Airframe Structural Materials

<u>Material</u>	<u>Resistivity</u>	
	<u>Ω-in. $\times 10^{-6}$</u>	<u>Ω-cm $\times 10^{-6}$</u>
Aluminum	1.1	(2.8)
Copper	0.67	(1.7)
Titanium	17.	(42.)
Stainless Steel (304)	28.	(72.)
Magnesium	1.8	(4.5)
gr/E	2000.	(5000.)

The total resistance of any structural path, of course, is comprised of joint and bond resistances as well as the resistances of the bulk structural materials themselves. In some cases, joint or bond resistance can be higher than the resistance of the structural member itself. Bulk structural resistances are readily calculated, but joint or bond resistances are very difficult to estimate and must usually be determined by test. These latter resistances are also dependent on the amplitude of current flowing

through them. Tests on candidate joint and bond configurations should be performed to obtain these resistances. If such data is available it should be included in the resistance calculation. If not available, these resistances will have to be neglected during the initial estimates.

Examples of the magnitude of structural resistance (including joint and bond resistance) which may be expected in bonded aluminum and gr/E wings are recorded in paragraphs 3.3.4.4.2 and 3.5.2.1. For the bonded aluminum wing this value was 0.3 mΩ; for the gr/E wing the value was 25 mΩ.

E. Estimate the lightning current in each structural element at later times (after a few tens of microseconds), when current flow is inversely proportional to the resistance of each structural member or other conductor. The following expression should be used for this purpose:

$$i_1 = \frac{i_T R_T}{R_1}$$

where:

i_1 = Current in a structural element or other conductor of interest (amperes)

i_T = Total lightning current in entire structure (amperes, usually 200 kA)

R_T = Electrical resistance of entire structure along direction of current flow (ohms)

R_1 = Electrical resistance of structural element or other conductor of interest (amperes)

In most cases, it will be found that current distribution based on element resistances is different than distribution determined by comparative inductances. This would seem to necessitate current flow from one conducting element to another and this is actually what happens. The result may be a concentration of currents at interfaces between gr/E and metal conductors. Such current concentrations may produce sparking or loss of strength at gr/E-to-metal interfaces, presenting difficult protection problems. These problems can sometimes be avoided by breaking or eliminating the current path through the metal conductor. Within a fuel tank, for example, metal fuel or vent lines can be replaced with tubes made of nonmetallic materials, or provided with nonmetallic inserts to prevent current flow.

F. Design structural materials, joints, bonds and other critical interfaces to tolerate the highest current estimated for each structural element. This may be the current determined by either inductive or resistive distribution.

G. Determine if concentration factors are needed. At locations remote from lightning entry or exit points, the structural element currents for design purposes may be assumed to be as estimated by the foregoing procedures. However, in the vicinity of the lightning entry or exit points, the estimated current densities should be increased by a "concentration factor". For structures directly beneath attachment points, such as a skin-to-spar bond, the estimated current density should be increased by a multiple of ten. In other cases, the multiple may be as low as four. In cases where a higher degree of doubt exists, the highest multiple should be applied.

H. Determine if spark or physical damage thresholds will be exceeded. Refer to the spark or physical damage threshold data presented in section 2.0 of this report to determine if these thresholds are likely to be approached or exceeded at similar interfaces within the structure being designed. For example, if adhesively bonded gr/E spar-to-skin joints are planned, the data of paragraph 2.5.1.2.3. may be applicable. These data indicate that sparking occurs at current densities of 248 A/in.² or greater. An example of how these data may be used in aircraft design is shown in paragraph 3.5.1.2. In this example, the average current density through the spar caps of the tested gr/E wing was calculated to be 75 A/in.². When current distributions, as shown in Figure 3.36, were factored into the calculations, it was found that the average current density through the spar caps was approximately 55 A/in.² or 25% of the level which may cause sparking as indicated by the subelement test results. If the calculations had indicated that the current densities would exceed 248 A/in.², then additional protection methods would need to be considered.

If the data of section 2.0 are not applicable to particular structural designs, similar tests of appropriate subelement specimens representative of the structure should be performed in the same manner as described in section 2.0.

1.2.2.3 Identify structural components, systems or subsystems that may be vulnerable to hazardous effects

The next step in the lightning protection design process is to identify structural components and other associated systems, subsystems or components that might be vulnerable to damage, electrical sparking, or other adverse effects from the lightning environment determined in the second step, paragraph 1.2.2.2.

A study of section 2.0 and 3.0 will illustrate particular areas of concern. Some of these areas are:

Airframe and Structures

- Puncture of skins
- Delamination of composite skins and other structural members
- Adhesive debonding
- Crimping due to magnetic force effects

Fuel Systems

- Electrical sparking at rivets, removable fasteners, nut plates, and other types of fasteners. This hazard will be found most often in gr/E structures where current concentrations near metal fasteners are high; however, sparking has also been found to occur at rivets and fasteners within all-metal fuel tank structures. The reason is that most metal components are treated with primers or other corrosion-resistance surfaces prior to assembly, thus forcing lightning currents to flow via rivets or fasteners.
- Electrical sparking at fuel tank plumbing components such as flexible couplings, bulkhead fittings, support clamps and at other joints not specifically designed to tolerate lightning-like currents. Here again, this hazard will be most prevalent in plumbing contained within a composite structure; however, it also may occur within all metal structures.
- Electrical sparking at adhesively bonded joints. This hazard will appear most often in locations where no rivets or fasteners are used in either composite or all metal structures. The ability of a rivet to increase the spark threshold level of an adhesively bonded joint was shown by the test results on aluminum lap joint specimens reported in paragraph 2.3.1.2.3. The results showed that the addition of a rivet to the lap joint increased the spark threshold level from 1 kA to 5 kA.
- Incendiary Sparks. The minimum electrical energy required to produce an incendiary spark has been found to be 0.2 millijoules (Ref. 8). Although the amount of current expected to flow in an individual structural element can be estimated by the methods described in paragraph 1.2.2, the amount of energy that might be released in a spark between two structural elements would be extremely difficult to estimate. The minimum spark energy is, however, equivalent to the energy released by a current of several amperes flowing through a spark of several microseconds duration. Since most structural elements will experience currents of several hundred or several thousand

amperes, the possibility of at least one or two of those amperes flowing in any spark that might occur must be considered a certainty.

- Hot Spots. In addition to sparking, hot spots of sufficient temperature and duration to ignite flammable vapors may be formed. These hot spots would be formed by direct lightning strikes to integral tank skins. It has generally been found that the melting temperature of aluminum (1200°F) will be reached before the short-time ignition temperature (2400°F) of fuel air vapor is reached. This, however, may not be true for composites. No work on this hazard was conducted during this program.
- Sparking at electrical apparatus such as fuel quantity probes or float switches due to lightning-induced voltages in associated electrical wiring.

Electrical and Avionics

- Surge voltages due to structural IR voltages that arise during lightning current flow, appearing in electrical circuits referenced to the airframe at two or more locations. This hazard is most prevalent in composite structures whose resistances are comparatively high. gr/E wing resistance, calculated from data obtained during the full scale structures tests, was found to be approximately 25 mΩ. Thus, a full threat 200 kA lightning strike could result in a voltage potential as high as 5 kV near the wing tip. Electrical circuits routed along these structures will "see" these IR voltages, which are capable of driving substantial currents through electronic equipment located at the ends of the circuits.
- Surge voltages induced in electrical circuits by changing magnetic fields associated with lightning currents. This hazard occurs most often in circuits that pass adjacent to apertures in the airframe, such as windshields or along wing trailing edges. Electric wiring that is completely contained within metallic structures is least susceptible to this hazard especially if the structure is assembled with rivets. Circuits within gr/E structures are more susceptible to magnetically induced effects, but still less so than those exposed to large apertures. A comparison of the shielding effectiveness of aluminum and gr/E was demonstrated during magnetic field intensity tests on the bonded aluminum and gr/E wings. The ratio of the magnetic field intensity measured within the bonded aluminum wing to that of the gr/E wing was calculated in paragraph 3.5.2.2 and found to be approximately 4:1. Additional data that shows the relative effectiveness of metallic and non-metallic shielding is presented in paragraph 3.3.4.4.3 and Table 3-5. These data show the voltages induced in electrical

wiring, located within the bonded aluminum wing, as a result of a simulated lightning strike to the wing tip. Voltages induced in wiring located entirely within the aluminum skin ranged from 15V to 60V for test currents of 7 kA. Voltages induced in navigational light wiring, which was partially routed through the plastic wing tip, ranged from 2.9 kV to 4.1 kA for test currents of 7 kA. These higher voltage levels resulted from a lack of electromagnetic shielding provided by the plastic wing tip, thus allowing greater magnetic flux interaction with these wires than for those located entirely within the shielded environment of the aluminum skin.

- Transient voltages "induced" in aircraft electrical wiring. These voltages are a combination of magnetically induced and structural IR voltages. In gr/E structures, the IR voltages usually predominate; in metal airframes, the magnetically induced voltages are usually highest.
- Electrical wiring installed within nonconducting composite structures such as those made of fiberglass or kevlar reinforced composites, may itself become the sole lightning conductor, resulting in puncture of the structure, explosion and severe electrical damage to associated electrical or electronic equipment. The effects of a lightning strike to a navigation light mounted in a fiberglass wing tip can be very destructive, for example, unless protective measures are applied

Whether the above hazards, or other potential hazards actually exist depends on the details of the specific design. The data of sections 2.0 and 3.0 are intended as useful references against which to compare new designs; however, development testing of more representative specimens specimens is often advisable. Factors such as adhesive type, bond line thickness, surface preparation, edge treatments, and type and locations of fasteners have significant impact on spark and physical damage thresholds. Thus, especially when new materials, bonding of fastening techniques are being considered for critical structural or fuel tank applications, development testing should be conducted. The types of tests require are similar to those described in section 2.0.

1.2.2.4 Establish the degrees of protection required

Once the potentially hazardous effects have been defined for particular structures or systems, the extent of the desired protection can be determined. If the consequences of the lightning effect would result in a flight safety hazard (i.e. ignition of fuel vapors), protection design will be required. However, other situations often exist, in which the lightning effect would not be

a hazard to flight safety but could result in an expensive repair or partial impairment of aircraft performance. In these cases, a decision might be made to forego protection, especially if such protection would incur a weight or cost penalty. Therefore, proper completion of this step usually requires that alternative methods be assessed, and costs, weight, and performance penalties be determined. On more complex systems, trade-off studies are also performed.

1.2.2.5 Proceed with protection design

Once the need for protection has been established, work may progress on designing specific protection measures. Here again, development testing is often appropriate to evaluate the effectiveness of various alternatives. Several alternatives may be appropriate for each hazard. The total number of possibilities is very large and limited only by the imagination of the designer. Brief descriptions of some common approaches are:

- Improvements in electrical bonding at joints and other interfaces by conductive additives in adhesives or sealants, use of rivets, conductive inserts within adhesive bonds or external bond straps.
- Elimination of electrical sparking by breaking or altering current flow paths through structures, improvement of electrical bonding, or design of highly conductive, spark-free interfaces.
- Containment of sparking, by encapsulating or covering spark sources with fuel tank sealant or other material capable of withstanding spark pressures.
- Provision of metallic ground planes or electromagnetic shielding for wiring harnesses.
- Provision of surge suppression devices at the terminals of electrical/electronic equipment.

Additional information on lightning protection devices is contained in Ref. 9.

1.2.2.6 Verify adequacy of design by analysis or test

The final step in the lightning protection design process is verification of design adequacy. This can be accomplished by simulated lightning tests of production-like structures, systems, or components; or by analytical procedures which may be combined with development tests. Qualification or certification testing is most often used because it provides the most direct assessment of performance. Typically, voltage or current waveforms of the stroke components appropriate to the zone(s) in which the structure or component is located are applied, and the condition of the

structure is carefully assessed afterwards. The test object may range from a flight critical component such as an access door installation or a wing tip assembly to a complete structure such as a wing containing an integral fuel tank. Due to the complex nature of many structures, it is not possible to verify a spark-free design without subjecting the entire structure to full scale lightning currents. Similarly, the response of internal electrical wiring to magnetic fields and structural IR voltages is dependent on characteristics of the complete structure (or possibly the complete airframe); therefore the complete structure must be represented in the tests. Tests similar to those described in section 3.0 are often applied.

There are other cases in which testing is not practical, or perhaps not necessary. These include situations where the design is sufficiently similar to previous designs formerly qualified by test, or structures that are so large as to make testing of them very difficult or impossible. In such cases, verification is achieved by combining the results of development tests on critical component specimens with analysis of current flow patterns or other effects in order to achieve a high confidence in design adequacy. An example of this latter procedure might be a wing structure in which current densities have been estimated by analysis, followed by individual or component tests of representative adhesively bonded joints and other potential spark sources. To account for possible errors in the current flow analysis, test current levels are usually set higher by a factor of approximately 100%.

Whichever approach is used, it should be carefully planned in advance to address, as a minimum, all flight-critical lightning protection designs. It is often appropriate to review the intended verification plan with airworthiness regulatory authorities prior to commencement. The verification plan should include definition of the pass/fail criteria applicable to each test. For fuel tanks, passage will be evidenced by lack of sparks or other ignition sources. For other structures or systems, passage of the verification test will be established by some tolerable degree of damage.

Frequently, data from development tests conducted during earlier phases of the lightning protection design program can be used for verification purposes, if the development test specimen(s) is sufficiently representative of the final design(s), and if the development tests have been sufficiently documented. This is an excellent way to reduce the cost of design verification.

2.0 EXPERIMENTAL PROGRAM

2.1 Purpose

The purpose of the experimental program was to determine the effects of lightning-like currents on typical bonded aluminum and gr/E aircraft structures, and acquire sufficient electrical effects data from which to develop guidelines for protection of these structures against physical damage or electrical sparking that could ignite flammable vapors.

The first phase of the experimental program included electrical tests of small subelement specimens representative of adhesively bonded metal and gr/E interfaces that occur throughout adhesively bonded aluminum or gr/E structures. Emphasis was on interfaces found in integral fuel tank construction, where small electrical sparks may be a hazard. Where possible, the subelement specimens selected were identical to mechanical strength test specimens already in use so that adhesive bond strength degradation due to electric current flow could be compared with adhesive strength data bases already in existence. Other subelement specimens included typical hardware interfaces with aluminum and gr/E skins, because these interfaces are often in the paths of lightning currents flowing in fuel tank plumbing, control cables or other electrically conductive parts. The types of subelement specimens that were tested are listed in Table 2-1.

Table 2-1 - Subelement Specimens

Adhesively Bonded Aluminum:

- Bonded aluminum lap joint specimens:
 - with varied adhesives
 - with varied bond line thicknesses
- Bonded aluminum lap joint specimens:
 - with one rivet
- Bonded aluminum fuel line brackets
- Bonded aluminum stiffeners
- Bonded aluminum honeycomb panels

Hardware Interfaces with Metals:

- Access doors riveted, fastened, or bonded and fastened

Table 2-1 - Subelement Specimens (cont'd)

Adhesively bonded gr/E:

Bonded gr/E lap joint specimens:
 with varied adhesives
 with varied bond line thicknesses

Bonded gr/E lap joint specimens:
 with one rivet

Bonded gr/E stiffeners

Metal-to-gr/E interfaces:

Rivets in gr/E laminates:
 covered with fuel tank sealant
 uncovered

Access door dome nuts in gr/E laminates

Fuel line feed-through elbows in gr/E laminates

Basically, the subelement test program included impulse voltage tests to determine the voltage required to break down nonconductive adhesive bond lines or cause visible sparks to appear, and impulse current tests to establish physical damage and spark thresholds due to current flow across adhesive bonds or metal-to-gr/E interfaces. The test methods utilized are described in the following paragraph. Subsequent paragraphs describe each type of specimen and the test results in detail.

2.2 Test Methods

2.2.1 Impulse voltage tests

Voltage breakdown tests were made on all of the subelement specimens that were adhesively bonded with electrically nonconductive epoxies. The tests were conducted by applying a rapidly rising voltage between both sides of the bonded specimen and recording the voltage level reached when sparkover or breakdown occurred. The test circuit and a typical voltage oscillogram are shown on Figure 2.1

The test voltage was measured by a 100:1 resistance voltage divider and recorded by a cathode ray oscilloscope (CRO). The generator charging voltage was set to provide a constant rate of rise to peak of several thousand volts, well above the region where breakdowns were expected. For most of the tests, the rate of voltage rise was set at 600 volts per microsecond, which is typical of the rate of voltage rise that may be produced throughout a gr/E structure by rapidly rising lightning stroke currents.

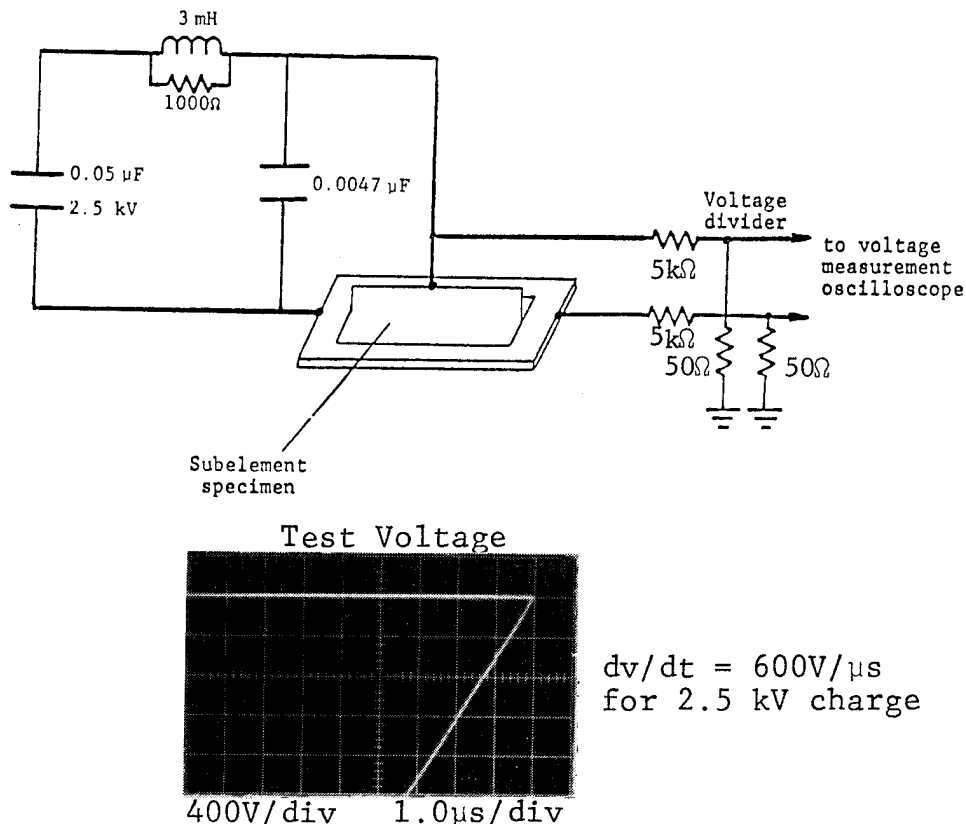


Figure 2.1 - Test Circuit for Applying a Controlled Voltage Rate-of-Rise to Specimen for Determining Adhesive Breakdown Levels.

2.2.2 Impulse current tests

Impulse current tests were made on all of the subelement specimens that were adhesively bonded with either conductive or nonconductive epoxies, the access door specimens, and the metal-to-gr/E interfaces. The purpose of the tests was to determine visible spark and physical damage thresholds. Most of the bonded specimens were tested at currents of 20 kA or less, whereas riveted specimens and the complete fuel tank access door and skin panel specimens were tested at currents of up to 200 kA. The test circuit utilized to produce the impulse currents is shown in Figure 2.2 together with a typical current oscillogram. The circuit parameters shown produced the 3kA, 2 x 50 μs current pictured in the oscillograms. Different parameters were utilized to produce currents higher than this level.

The 2 x 50 μs (2 μs to crest, 50 μs to 50% of crest on decay) waveform is most representative of a natural lightning stroke current, but could not be produced at peak currents higher than about 15 kA because of the circuit resistance required. Therefore, for testing beyond this level, a unidirectional waveform

of shorter duration ($8 \times 20 \mu\text{s}$) was utilized. To produce currents above 50 kA, more resistance had to be removed from the test circuit, necessitating a damped sine waveform of approximately 25 kilohertz (kHz) frequency. Oscillograms of the three test waveforms utilized are shown in Figure 2.3.

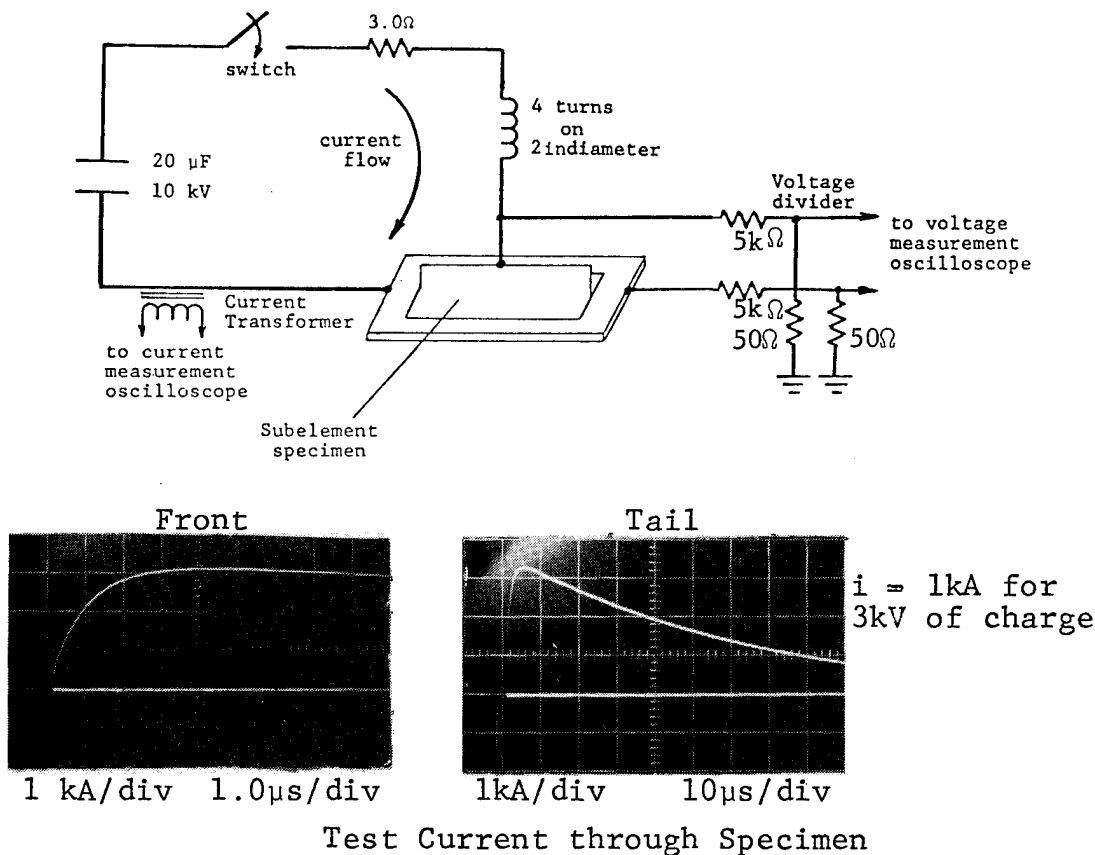


Figure 2.2 - Test Circuit Parameters for Generating the $2 \times 50 \mu\text{s}$ Simulated Lightning Current Pulse.

During some of the impulse current tests, the voltage across the bond line was measured, utilizing the same voltage divider and CRO that was used for the impulse voltage tests.

2.2.3 Test chamber

Most of the subelement specimens were tested with a 2 ft. x 2 ft. x 6 ft. wooden, light-tight test chamber constructed for this program. The chamber is pictured in Figure 2.4.

The chamber was fitted with a removable end panel to enable arc entry tests of fuel tank access door specimens, and threaded steel rods through opposite side walls to provide support and electrical connections to smaller specimens suspended inside.

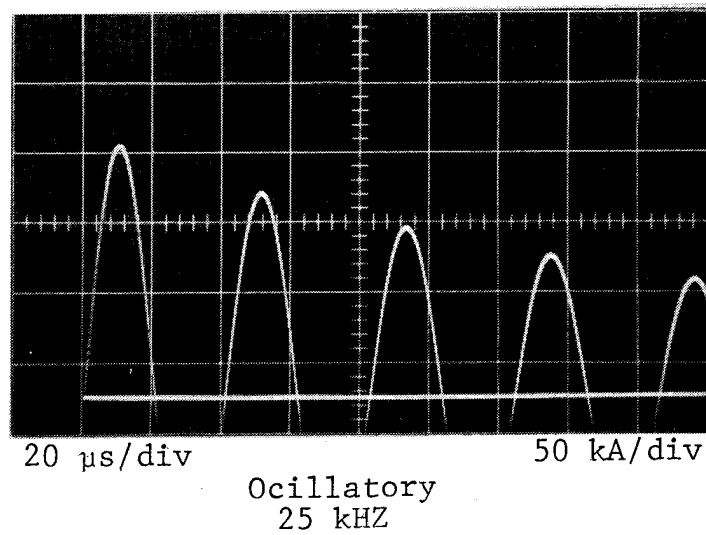
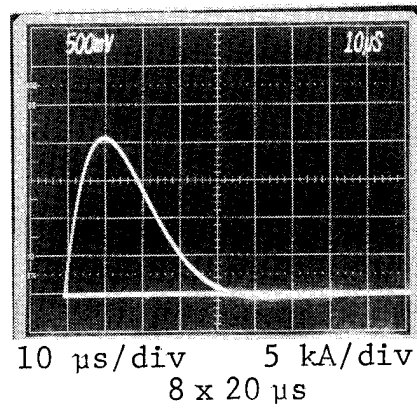
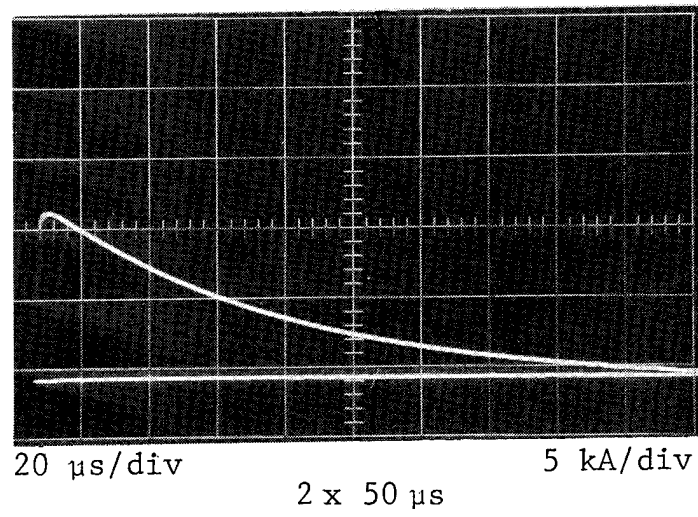


Figure 2.3 - Test Current Waveforms.

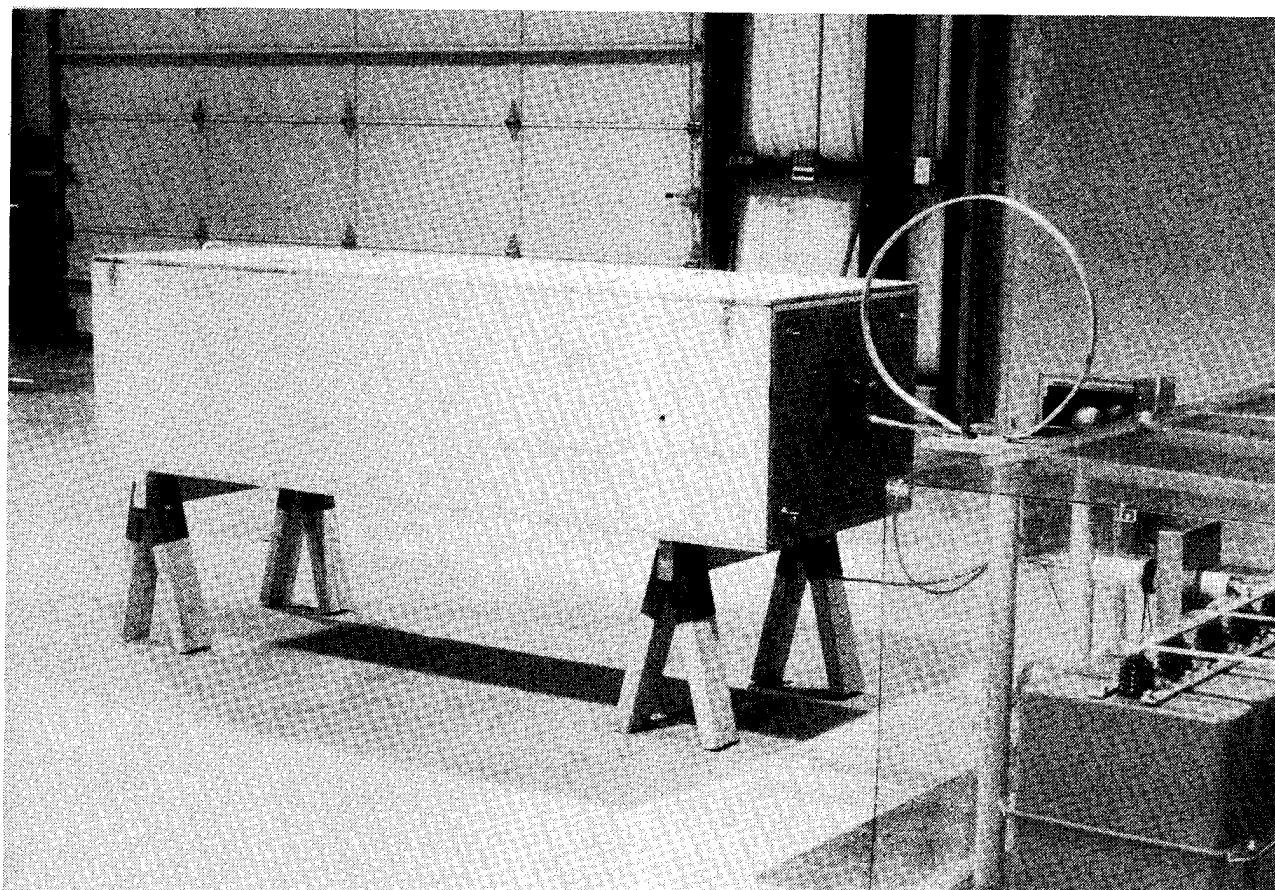


Figure 2.4 - Light-Tight Chamber in which Subelement Specimens were Tested.

These test voltages or currents were conducted into and out of these specimens via the steel rods. The light-tight chamber was also fitted with a fiber-optic light source to serve as a reference light during photographs of electrical sparking and hinged access doors to provide access to cameras and test specimens.

2.2.4 Detection of electrical sparks

Photography was selected for detection of electrical arcs or sparks on the test specimens. ASA 2000 speed polaroid-type film exposed through an F 4.7 lens opening has been shown to be capable of detecting a spark of 0.2 millijoule which has been established as the lowest spark energy capable of igniting a flammable vapor (Ref. 10). At the beginning of the subelement test program, cameras with polaroid-type 3000 speed film were utilized. Later in the subelement test program, a 35 mm camera with 400 speed film was added, to achieve improved definition of the spark locations and background. When exposed at a lens opening of F 3.5 and developed to 1600 speed with special developing procedures, the film sensitivity is equivalent to polaroid-type 3000 speed film exposed at F 4.7.

To assure that incendiary sparks could be successfully photographed, a series of tests were performed to determine the minimum energy necessary to ignite a flammable fuel-air mixture, with a spark produced between electrodes typical of the component interfaces found within an aircraft structure, and to verify that a spark of this magnitude could be identified on exposed film. Tests were performed with a set of flat electrodes cut from 0.5 in. wide, 0.020 in. thick aluminum bar stock as shown in Figure 2.5.

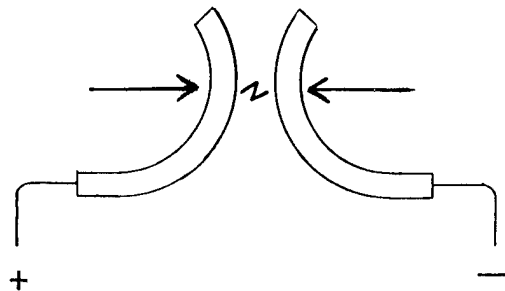


Figure 2.5 - Spark Electrode Configuration.

In this respect, the tests differed from those reported in Ref. 10 in which point-tipped electrodes were utilized.

To create a spark, the electrodes were moved toward each other until the gap breakdown voltage was exceeded.

Since a spark produced by a capacitor charged to 0.2×10^{-3} joules of energy has been previously established as the minimum energy necessary to ignite a flammable vapor, a test circuit capable of storing and discharging this much energy was arranged. The circuit is shown in Figure 2.6.

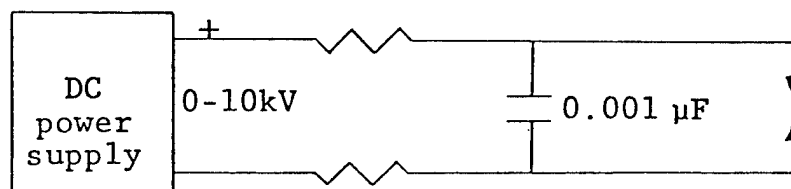


Figure 2.6 - Test Circuit to Produce Small Electrical Sparks.

A charging level of 632.5 volts results in a stored energy of 0.2×10^{-3} joules (0.2 millijoule).

For the ignition tests, a stoichiometric mixture of 100 octane aviation gasolene and air at room temperature was placed in a sealed explosion chamber. 0.2 millijoule electrical sparks were produced by a $0.001 \mu\text{F}$ capacitor charged to 632.5 volts. Sparks of higher intensity were produced by charging the capacitor to higher voltage.

Tests were begun with the capacitor charged to produce 0.2 millijoules. It was not possible to ignite the fuel with 0.2 millijoule sparks, so the tests were repeated at successively higher spark intensities until ignition occurred. Three tests were conducted at each energy level prior to moving to the next higher level. The capacitor charging voltages stored energies, and test results are presented in Table 2.2.

Table 2-2 - Spark Ignition Test Results

Test No.	Charging Voltage	Stored Energy (millijoules)	Test Results
1	632	0.2	No ignition on three sparks
2	1250	0.8	No ignition on three sparks
3	2000	2.0	No ignition on three sparks
4	3000	4.5	No ignition on three sparks
5	5000	12.5	No ignition on three sparks
6	7500	28.1	Ignition on third spark

The failure of the 0.2 millijoule spark to ignite the fuel-air mixture is probably due to the shape of the electrodes, which were flat and thus presented a comparatively large heat sink to the spark and the forming kernel of flame, thus quenching it. Laboratory tests in which 0.2 millijoule was capable of igniting a flammable vapor have always been performed with thin, needle electrodes of low thermal mass. The flat-electrodes selected for investigation were more representative of the thermal capacity that might exist among structural parts.

Spark tests were continued to establish that light from a small spark could be identified on photographic film. The light from a 2.0×10^{-3} joule spark at a distance of 4 ft from the camera is shown on Figure 2.7. The camera was placed 4 ft away from the specimen in the light-tight box during all of the subelement tests in Phase I.

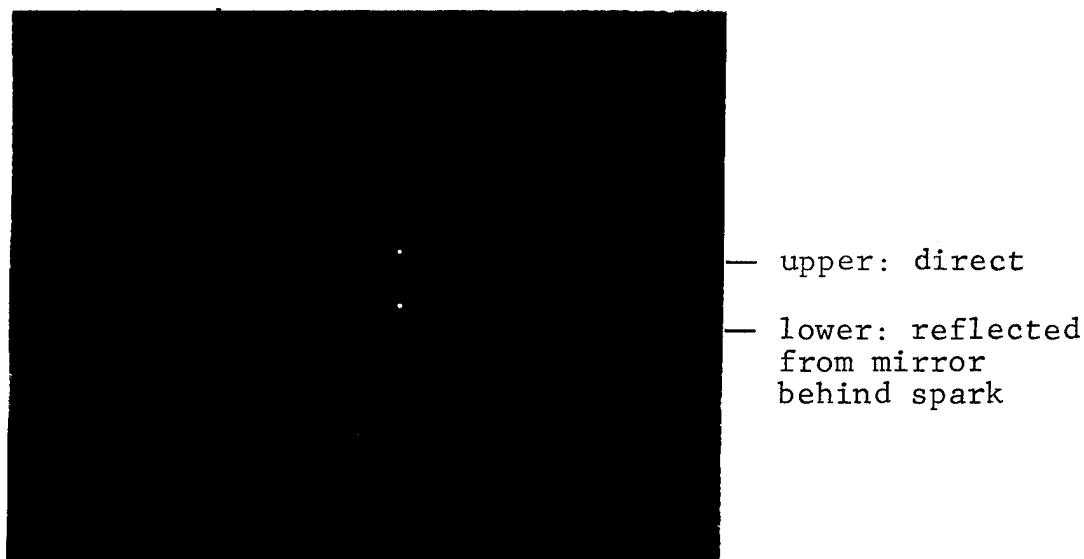


Figure 2.7 - Light from 2.0×10^{-3} Joule Spark. Camera is 4 ft from light source. Polaroid-type 3000 film photographed via F8.8 lens.

All of the subelement tests in which sparking thresholds were to be determined were conducted within the light-tight chamber pictured in Figure 2.4. Detailed descriptions of each type of test specimen and the results obtained are presented in the following paragraphs.

2.3 Adhesively bonded aluminum

Adhesively bonded aluminum specimens included aluminum lap joint specimens as are commonly used to evaluate adhesive shear

strength; "T" section stiffeners and aluminum fuel line brackets adhesively bonded to aluminum skins; sections of typical adhesively bonded aluminum honeycomb panels; and specimens of riveted, fastened, or bonded and fastened, aluminum skin panels and access doors. The latter specimens included typical rivet and fastener installations coated with fuel tank sealant. All of these specimens are representative of configurations being utilized in new aircraft design.

Groups of the adhesively bonded specimens were tested with each of eight different commercially available structural adhesives so that possible relationship(s) between adhesive properties and electric current transfer characteristics could be determined. Two of the adhesives were partially electrically conductive due to incorporation of aluminum powder. The rest were electrically nonconductive and no attempt was made to improve their electrical conductivity. Both supported and unsupported type adhesives were used. Supported adhesives utilize a carrier material, such as a nylon or polyester woven scrim, for bond line control or enhancement of bond line strength in thick bond lines. Unsupported adhesives lack a carrier material and may be used when low moisture absorption or good filleting action are required.

2.3.1 Bonded aluminum lap joint specimens

2.3.1.1 Specimen description

The bonded aluminum lap joint specimens were fabricated of 0.060 in. aluminum with an overlap of 1 in. as shown in Figure 2.8. The aluminum adherends were primed and bonded together with a single layer of adhesive in accordance with the manufacturers' recommendations. Most of the adhesives met the requirement of US Military Standard MIL-A-25463 (Ref. 11) and US Federal Specification MMM-A-132 (Ref. 12).

Groups of seven specimens plus an untested control specimen were cut from single lap joint panels. For each adhesive, four such panels were prepared so the number of specimens available for electrical tests was 28. The aluminum adherends were vapor or alkaline degreased, acid etched, rinsed and dried prior to priming and bonding. The characteristics of each adhesive and primer are described in Table 2-3.

All but two of the adhesives were electrically nonconductive; two of the adhesives exhibited partial electrical conductivity due to aluminum powder incorporated in the epoxy. The purpose of the aluminum powder was to maintain adhesive properties at elevated temperatures rather than to provide electrical conductivity.

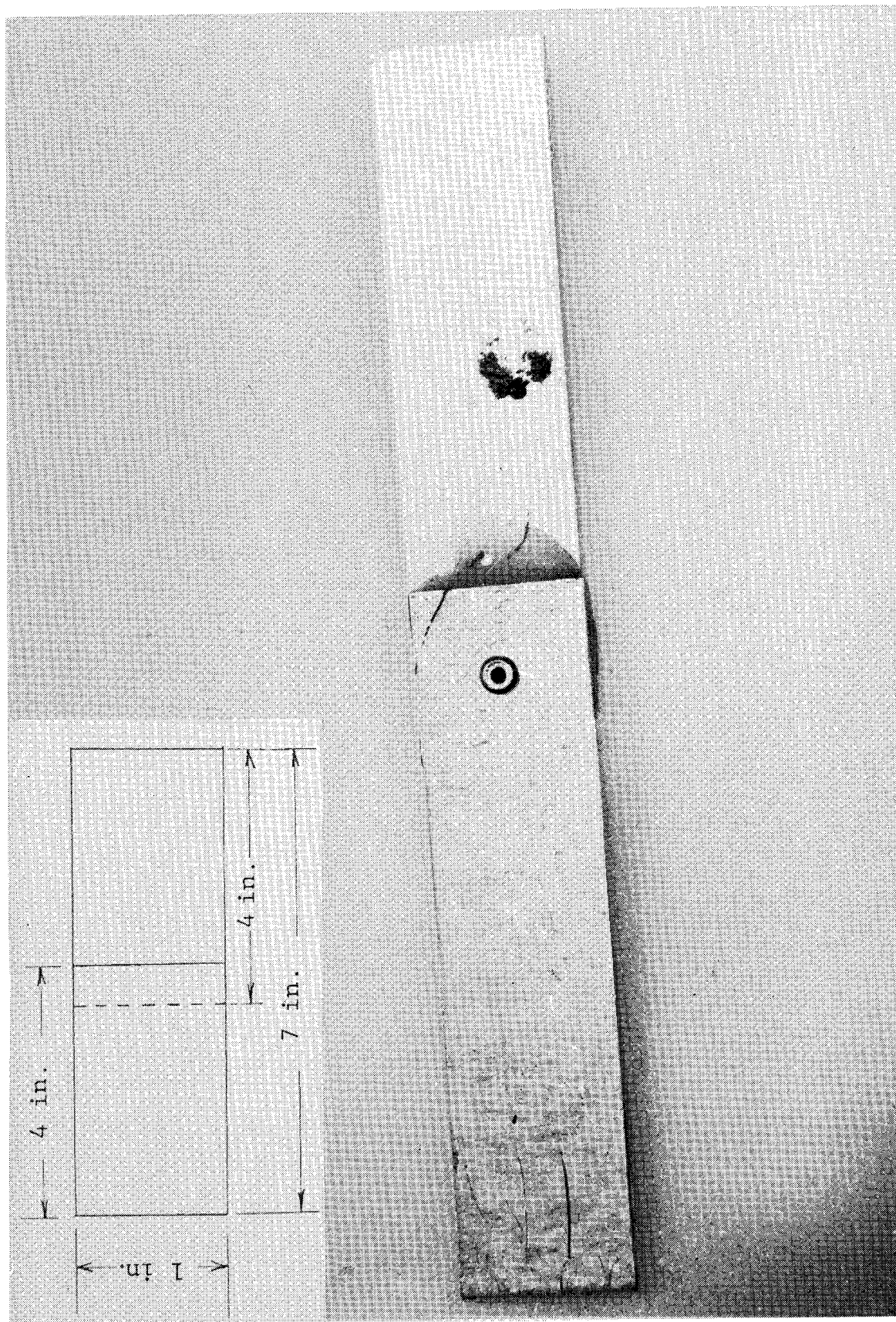


Figure 2.8 - Bonded Aluminum Lap Joint Specimen.

Table 2-3 - Characteristics of Adhesives in Bonded Aluminum Specimens

Adhesive Manufacturer	Adhesive Manufacturer's Part No.	Type of Adhesive	One Hour Nominal Cure Temp. (°F)	Film Weight (lbs/ft ²)	Manufacturer's Rated Tensile Shear Strength at 75°F (lbs/in ²)	Primer Used	Electrical Conductivity
3M Co.	AF-126-2	Supported modified epoxy film	250	0.060	5200	EC-3909	none
Dexter Corp. (Hysol Div.)	EA 9602.3	Supported modified epoxy film	250	0.060	5700	EA-9202	none
Narmco Materials Inc.	MB 1113	Supported modified epoxy film	250	0.060	6270	MB-6726	none
Reliable Manufacturing Co.	R 7114	Supported modified epoxy film	250	0.060	6140	EA-9202	none
American Cyanamid Co.	HT 424	Supported, aluminum filled, modified epoxy phenolic resin	350	0.135	3550	HT-424	partial
American Cyanamid Co.	FM 1000	Unsupported, modified polyimide epoxy film	350	0.040	6150	BR-1009-49	none
American Cyanamid Co.	FM 61	Supported composite film	350	0.075	3030	BR-227A	none
American Cyanamid Co.	FM 400	Supported aluminum filled, modified epoxy film	350	0.100	4120	BR-400	partial

Bond line thicknesses ranged from a minimum of 0.001-0.002 in. to 0.008-0.010 in. for the unsupported adhesives. Supported adhesives had bond line thicknesses ranging between 0.002-0.006 in.

2.3.1.2 Test results

Prior to test, each lap joint specimen was given an electrical continuity check with a battery-operated ohmmeter to see if physical contact existed between aluminum adherends. The numbers of specimens in each group of 28 which exhibited conductivity prior to test are presented in Table 2-4.

Table 2-4 - Electrical Continuity of Aluminum Lap Joint Specimens Prior to Test

<u>Adhesive Designation</u>	<u>Nominal Bond Line Thickness (in.)</u>	<u>No. of Conductive Specimens/Group</u>	<u>Type</u>
AF-126-2	0.002	11/28	supported
FM 1000	0.001-0.002	1/28	unsupported
EA 9602.3	0.002-0.004	2/28	supported
R 7114	0.002-0.004	1/28	supported
MB 1113	0.003-0.005	18/28	supported
FM 61	0.005-0.007	2/28	supported
HT 424	0.006-0.008	10/28	supported
FM 400	0.008-0.010	5/28	supported

There was no apparent relationship between bond line thickness and occurrence of pre-test conductive paths, since even a thin layer of adhesive may electrically isolate the adherends. Even the aluminum-loaded adhesives appeared non-conductive in some specimens at the low voltage (several volts) applied by the battery-operated meter. The conductivity exhibited by some of the specimens was undoubtedly due to burrs left on the edges of the adherends by cutting operations.

The specimens that were nonconductive prior to the start of tests were given voltage breakdown tests as described in Para. 2.2.1 to determine the voltage necessary to cause sparkover across or through the adhesives. Those that exhibited continuity would, of course, require no voltage to initiate conductivity. Hence, these specimens were tested initially with impulse currents as described in Para. 2.2.2 to determine the amounts of such currents that may produce visible sparks.

2.3.1.2.1 Bond line breakdown voltages. - Breakdown voltages of bonds made with non-conducting adhesives ranged between 50 and 8 000 volts. In general, the thicker bond lines produced the highest breakdown voltage, but the relationship was not well defined due to the presence of burrs or other imperfections at the edges. For this reason, most of the breakdowns were visible as sparks at the edges of the specimens. Only 10% of the specimens indicated breakdown within the bond line, and in these cases sparks were not visible.

Following these tests, a second set of specimens was prepared with controlled bond line thicknesses. The burrs were also removed from these specimens to eliminate this source of sparking. This group of specimens was identical to the previous group except that only AF-126-2 adhesive was used. None of the specimens exhibited electrical conductivity prior to the tests. The results showed that breakdown voltage increases with bond line thickness, as shown in Table 2-5.

Table 2-5 - Breakdown Voltage vs. Bond Line Thickness
(AF-126-2 adhesive only)

<u>Bond Line Thickness</u> in.	<u>Breakdown Range</u>
0.0035	1200 - 2400 volts
0.007	2400 - 2800 volts
0.010	3600 - 4700 volts
0.015	4000 - 4800 volts
0.020	4000 - 4800 volts

For thin bond lines, the breakdown voltage is about 500 volts per mil (0.001 in.) thickness. For thicker bonds, the voltage required to cause sparkover diminishes to about 200 volts per mil. All breakdowns occurred at the edges of the specimens, indicating that the voltage withstand capability of the adhesive is greater than that of air.

2.3.1.2.2 Spark threshold due to current flow.- Following the breakdown tests, all lap joint specimens were subjected to impulse currents as described in Para. 2.2.2 to establish the minimum currents which would cause visible sparking. Since many of the lap joint test specimens were nonconductive to start with and breakdown occurred at the edges, visible sparks occurred upon initial application of generator voltage and no appreciable current flow was necessary to produce sparks. These specimens were therefore eliminated from the current flow tests. Thus, specimens given current flow tests included those with partially conductive adhesive (FM 400 and HT 424) and those with nonconductive adhesives in which breakdown has occurred within the bond.

Spark threshold ranged from less than 100A to greater than 10 000 A as shown in Table 2-6 (the highest level applied). The wide range of spark thresholds was undoubtedly due more to the random locations of breakdowns within the bond line than to characteristics of the adhesive.

Table 2-6 - Spark Threshold Currents for Bonded Aluminum Lap Joint Specimens (All specimens exhibited electrical conductivity prior to test. Bonded surfaces were 1 in²).

<u>Adhesive Designation</u>	<u>Range of Currents to Produce Visible Spark (kA)</u>	<u>Adhesive Conductivity</u>
AF-126-2	<0.10-0.50	none
EA 9602.3	0.20	none
FM 61	<0.10	none
FM 400	0.20-5.0	partial
FM 1000	<0.10->10	none
HT 424	>0-1.0	partial
MB 1113	<0.10-10	none
R 7114	<0.10	none

It should be noted that inclusion of the aluminum particles in the FM 400 and HT 424 adhesives did not increase the spark thresholds. Whereas the particles make the adhesive partially conductive, current flow among the particles undoubtedly causes minute sparks,

and if these should occur at or near the edges of such a bond, the sparks are likely to be visible and may therefore constitute a source of ignition of fuel vapors.

The data presented in Table 2-6 were derived from tests to specimens including a 1 in.² bond. Due to the wide variations in spark thresholds, the data should not be extrapolated to predict the current that can be allowed to pass through a larger adhesively bonded surface. Instead, the data indicate that breakdown and visible sparks may occur under widely varying conditions, and means other than the adhesive must be provided to allow spark-free transfer of current among adhesively bonded metal parts.

2.3.1.2.3 Spark thresholds of sealed and riveted aluminum lap joints. - One means of improving electrical continuity across an adhesively bonded or sealed aluminum lap joint is to install rivets through the bonded joint. To determine the spark threshold with a rivet installed, additional lap joint specimens were prepared, with a single rivet installed through the center of the bonded surfaces, as pictured in Figure 2.9. Groups of five specimens each were bonded with either of two commercially available fuel tank sealants, in a manner typical of sealed and riveted fuel tank construction. The rivets were installed "wet" with sealant but their heads were not sealed over after installation.

Similar groups of five non-riveted specimens with the same tank sealants as used for the riveted specimens were prepared and tested to establish a baseline for comparison with the riveted specimens. Photographs of the riveted and non-riveted specimens are shown on Figure 2.9.

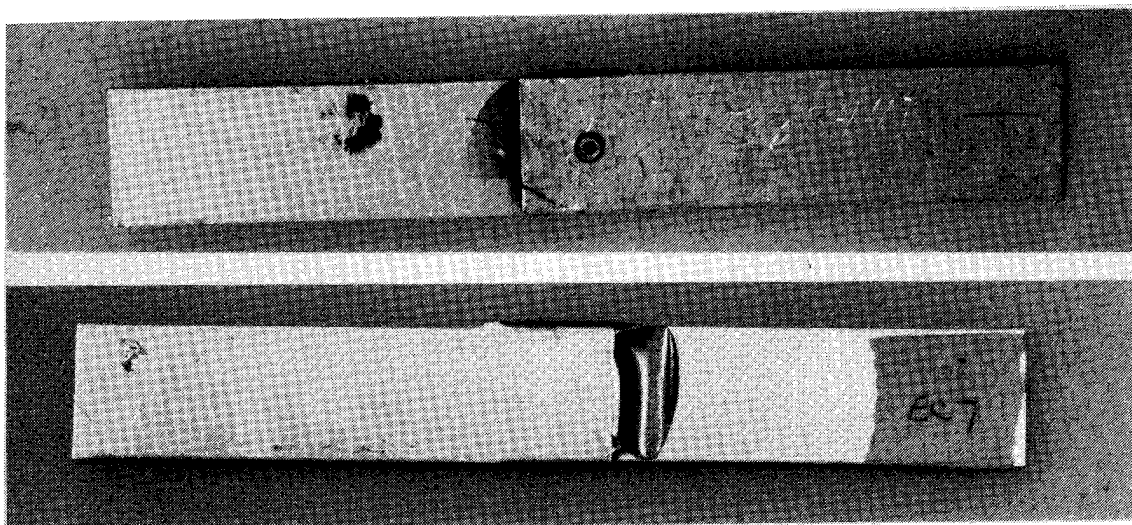


Figure 2.9 - Sealed Aluminum Lap Joint Specimens with and without Rivet.

The specimens were bonded with nonconductive sealants, so that all current would be forced (initially, at least) to flow through the rivet. At moderate current levels all current is conducted through the rivet and no sparking is visible. At higher currents, of 5-10 kA per rivet, the voltage rise through the rivet path is sufficient to establish other paths, which result in visible sparks. A typical test is shown on Figure 2.10.

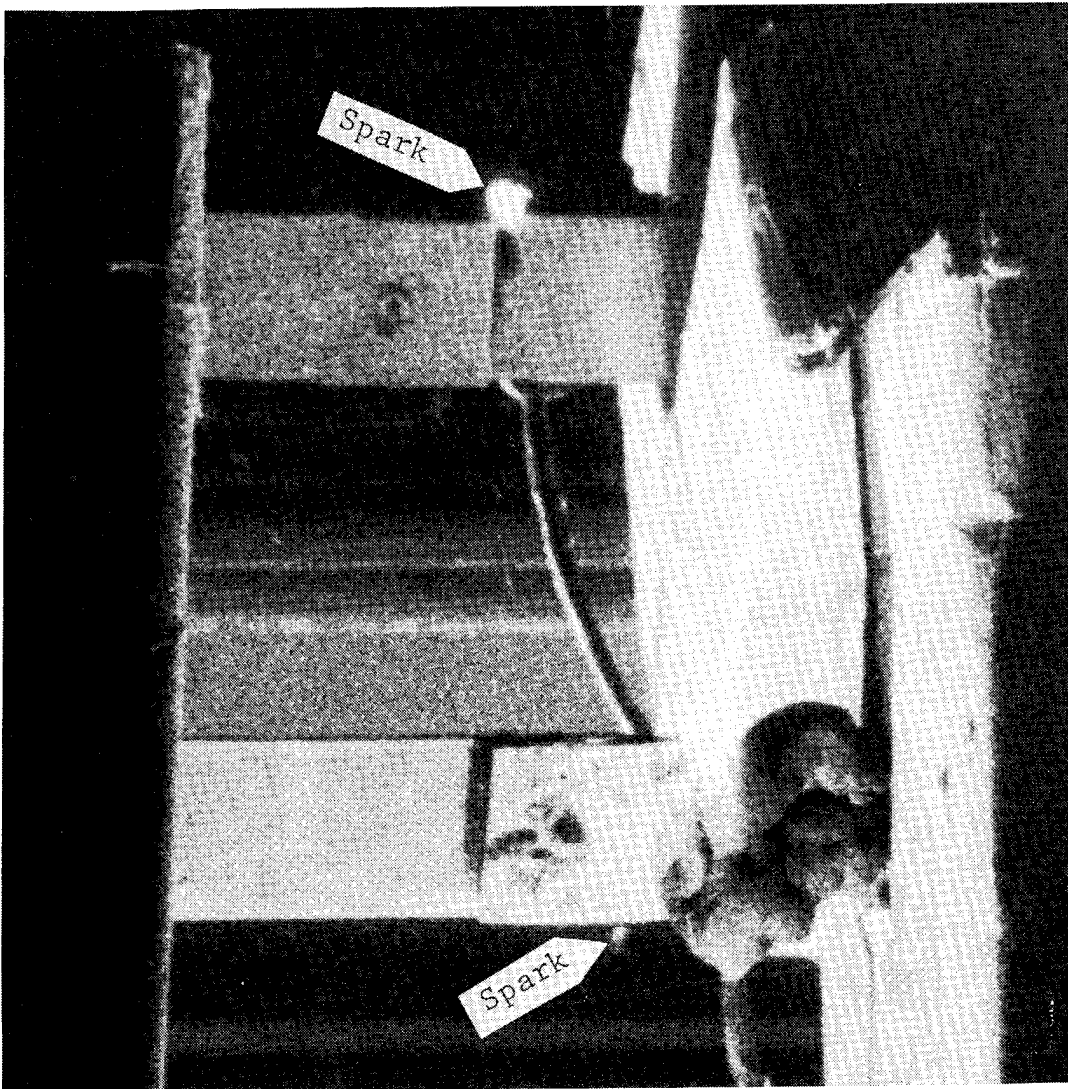


Figure 2.10 - Typical Test of Riveted Aluminum Lap Joint Specimen. Spark at 20 kA occurs at corner of bond. Reverse side of specimen is visible in mirror.

With the rivet installed, the impulse current spark threshold was raised to 5 kA when the bond was filled with one type of tank sealant and 10 kA for the other type. Sparks occurred at the edges or corners of the adherends in all cases. Comparisons of test results with and without the rivet installed are presented on Figure 2.11.

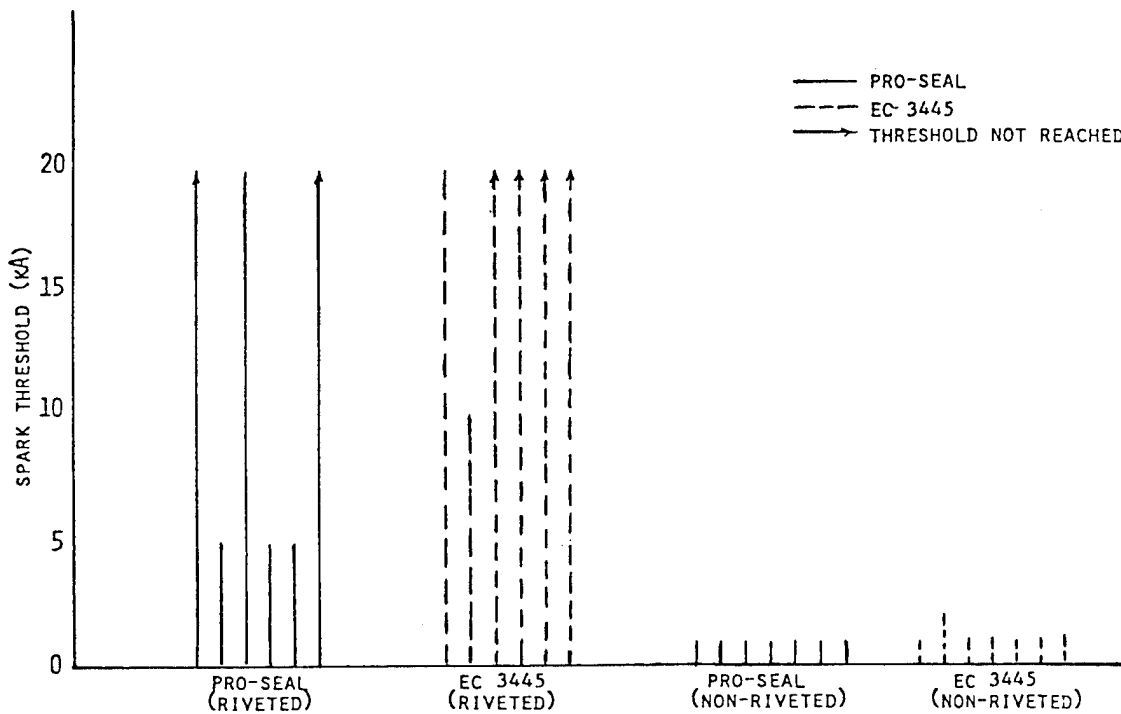


Figure 2.11 - Spark Threshold of Riveted and Non-Riveted Sealed Aluminum Lap Joints.

2.3.1.2.4 Current density vs. shear strength. - Following the spark threshold level tests, three aluminum lap joint specimens with each of the adhesives described in Table 2-3 were tested with impulse currents of 1 kA, 5 kA, 10 kA, and 50 kA peak amplitudes. The shear strength of each specimen was determined following these tests and is listed in Table 2-7. All of the specimen bonds were destroyed at the 50 kA impulse current amplitude.

Table 2-7 - Adhesive Shear Strength of Bonded Aluminum Lap Joint Specimens following Conduction of Current

Adhesive Shear Strength (lbs/in ²)				
Adhesive Designation	Before Test	After 1kA	After 5kA	After 10kA
FM 400	2820	2860	2507	897
FM 61	2898	2813	2813	2153
FM 1000	--	5507	6047	5690
HT 424	--	3580	3869	3600
MB 1113	5600	6180	5973	5760
R 7114	4300	4420	2436	2407
AF-126-2	5270	5413	3580	5333
EA 9602.3	4940	4873	4500	4243

The data in Table 2-7 are plotted graphically on Figure 2.12.

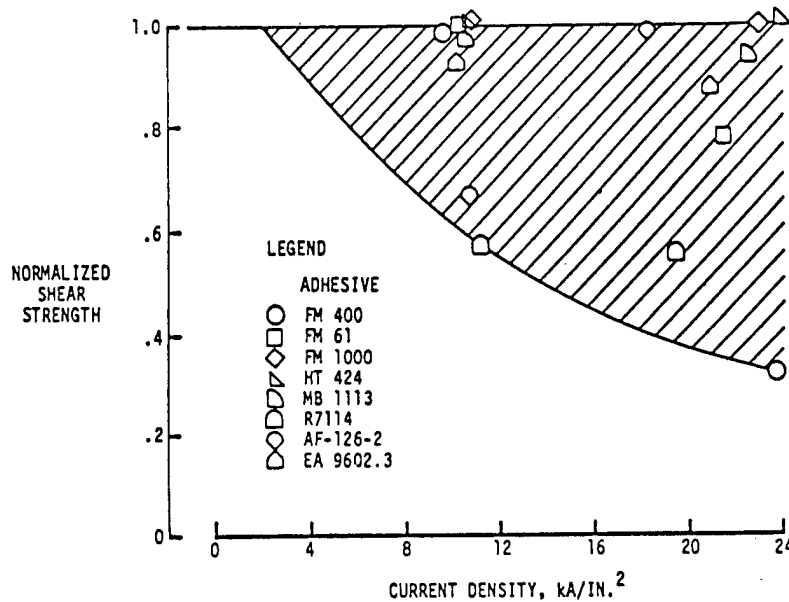


Figure 2.12 - Effect of Current Density on Adhesive Shear Strength of Bonded Aluminum Lap Joint Specimens.

2.3.2 Bonded aluminum fuel line brackets

2.3.2.1 Specimen description

The bonded aluminum fuel line brackets are typical of brackets utilized to support small fuel or vent lines within fuel tanks, as well as conduits or hydraulic lines in other locations. The brackets were fabricated from 0.032 in. aluminum 0.5 in. wide. Groups of 12 brackets were bonded to single sheets of primed aluminum with each of the adhesives described on Table 2-3. Thus, twelve specimens with each type of adhesive were available. A typical set of brackets is pictured on Figure 2.13.

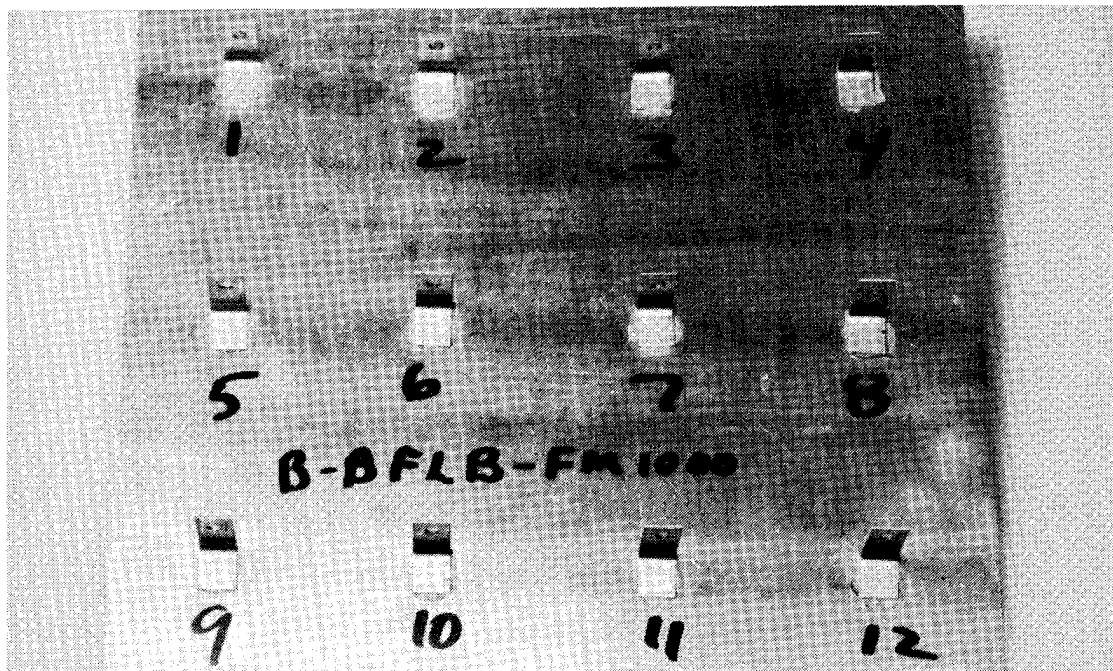


Figure 2.13 - Adhesively Bonded Aluminum Fuel Line Bracket Specimens.

The aluminum brackets and panels were vapor degreased, acid etched, rinsed and dried prior to priming and bonding. The characteristics of each adhesive and primer are described in Table 2-3. These are the same adhesives as used for the lap joint specimens. The bond line thicknesses were not controlled or measured, but probably ranged between 0.005 and 0.020 in.

2.3.2.2 Test Results

Prior to test, each bracket was given a continuity check with a battery-operated ohmmeter to see if electrical contact existed

between the brackets and the aluminum panel. Except for the partially conductive adhesives, the presence of conductivity means that physical contact existed between the bracket and the panel. The numbers of brackets in each group that exhibited conductivity prior to test are presented in Table 2-8.

Table 2-8 - Electrical Continuity of Bonded Aluminum Lap Joint Specimens Prior to Tests

<u>Adhesive Description</u>			No. of Conductive Specimens Group
<u>Designation</u>	<u>Type</u>	<u>Conductivity</u>	
AF-126-2	supported	none	8/12
FM 1000	unsupported	none	10/12
EA 9602.3	supported	none	3/12
R 7114	supported	none	2/12
MB 1113	supported	none	5/12
FM 61	supported	none	1/12
HT 424	supported	partial	11/12
FM 400	supported	partial	11/12

The partially conductive and unsupported adhesive exhibited the highest incidence of conductivity. Electrical resistances of "conductive" specimens ranged from a fraction of one ohm to several thousand ohms.

2.3.2.2.1 Spark thresholds due to voltage stress.- Specimens originally nonconductive exhibited bond line sparkover at the voltages shown on Table 2-9 when tested as described in Para. 2.2.1. Most of the sparkovers were visible.

Since the range of sparkover voltages was so wide, no relationship could be derived between type of adhesive and sparkover voltages. Some of the specimens with partially conductive adhesives also exhibited high sparkover voltages. Others showed some degree of electrical conductivity to start with, as indicated in Table 2-8.

Table 2-9 - Breakdown Voltage of Fuel Line
Bracket Specimens

<u>Adhesive Description</u>			<u>Range of Breakdown Voltages (kV)</u>
<u>Designation</u>	<u>Type</u>	<u>Conductivity</u>	
AF-126-2	supported	none	1.8-3.5
EA 9602.3	supported	none	<0.1-5.5
FM 61	supported	none	1.0
FM 400	supported	partial	0.5-10.0
FM 1000	unsupported	none	0.2-10.0
HT 424	supported	partial	0.1-10.0
MB 1113	supported	none	0.2-5.0
R 7114	supported	none	0.5-2.0

2.3.2.2.1 Spark thresholds due to current flow.- Following the sparkover tests, all bonded fuel line brackets which had indicated some conductivity prior to test were subjected to impulse currents as described in Para. 2.2.2 to establish the minimum currents which would cause sparking. The ranges of currents which produced visible sparking for each type of adhesive are shown on Table 2-10.

Spark thresholds ranged from less than 0.10 kA to greater than 10 kA (the highest level applied) as shown in Table 2.10. The wide range of spark thresholds was undoubtedly due more to the random locations of breakdowns within the bond line than to characteristics of the adhesive.

Table 2-10 - Spark Threshold Currents for Bonded Aluminum Fuel Line Brackets
(All specimens exhibited electrical conductivity prior to test. Bonded surfaces were 0.25 in.²)

<u>Adhesive Description</u>			<u>Range of Currents to Produce Visible Sparks (kA)</u>
<u>Designation</u>	<u>Type</u>	<u>Conductivity</u>	
AF-126-2	supported	none	0.2-2.0
EA 6902.3	supported	none	<0.1-10.0
FM 61	supported	none	1.0
FM 400	supported	partial	0.5-10.0
FM 1000	unsupported	none	0.2-10.0
HT 424	supported	partial	0.1-10.0
MB 1113	supported	none	0.2-5.0
R 7114	supported	none	0.5-2.0

2.3.3 Bonded aluminum stiffeners

2.3.3.1 Specimen description

The bonded aluminum stiffeners are typical of "T" section stringers or stiffeners used in wing and integral fuel tank construction. Three stiffeners were fabricated from 0.120 in. aluminum and adhesively bonded to sheets of primed aluminum with each of the adhesives described on Table 2-3. "T" sections were 1.5 in. wide and 10 in. long, so the bonded surface area was 15 in.². Thus, the stiffeners represented the largest bonded areas tested. Typical specimens are shown in Figure 2.14.

2.3.3.2 Test results

Prior to test, each lap joint specimen was given an electrical continuity check with a battery-operated ohmmeter to see if physical contact existed between aluminum adherends. The numbers of specimens in each group of 28 which exhibited conductivity prior to test are presented in Table 2-11.

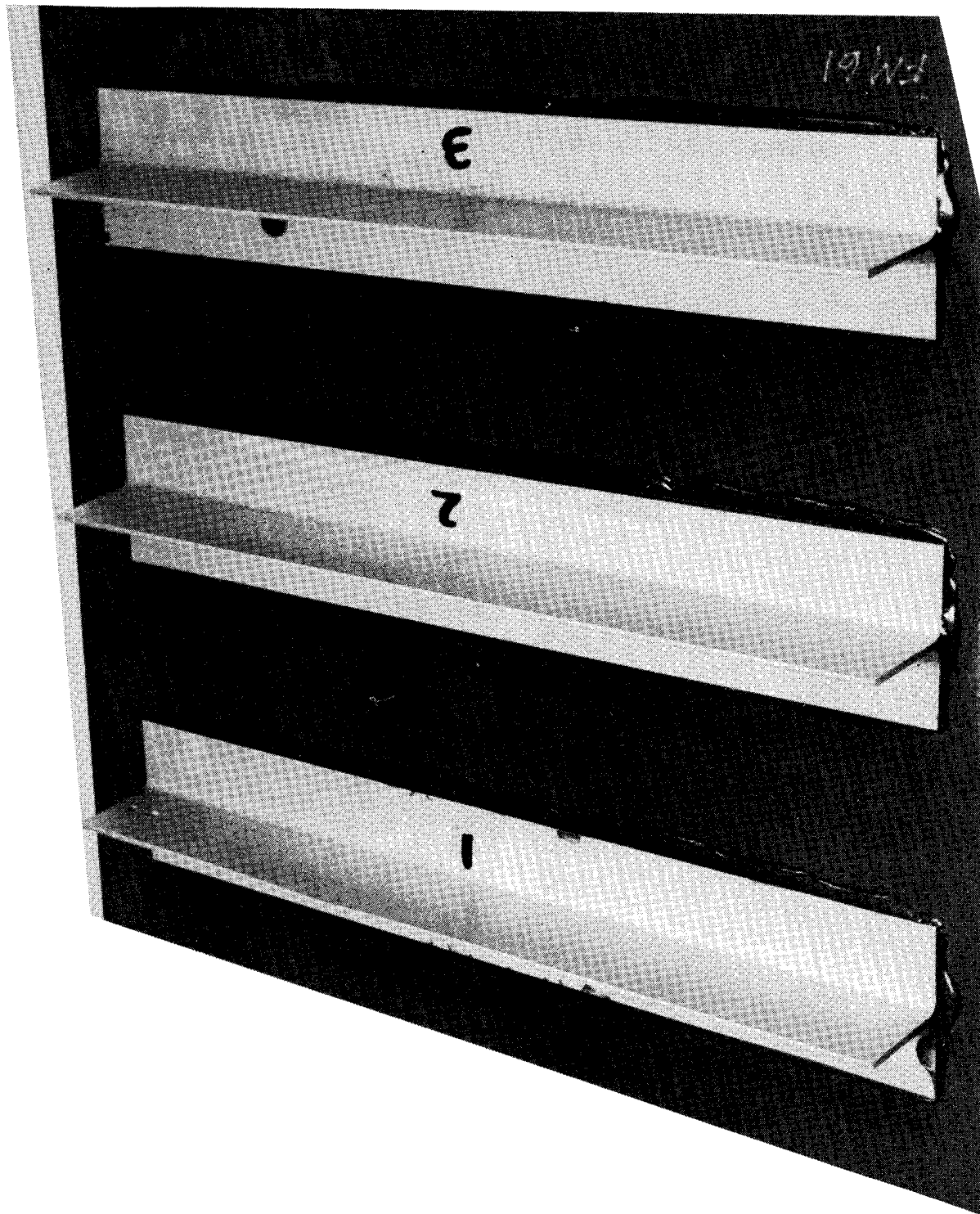


Figure 2.14 - Bonded Aluminum Stiffener Specimens.

Table 2-11 - Electrical Continuity Tests of Bonded Aluminum Stiffener Specimens Prior to Test

<u>Adhesive Description</u>			<u>Nominal Bondline Thickness (in.)</u>	<u>No. of Conductive Specimens Group</u>
<u>Designation</u>	<u>Type</u>	<u>Conductivity</u>		
AF-126-2	supported	none	0.002	3/3
FM 1000	unsupported	none	0.001-0.002	3/3
EA 9602.3	supported	none	0.002-0.004	2/3
R 7114	supported	none	0.002-0.004	3/3
MB 1113	supported	none	0.003-0.005	3/3
FM 61	supported	none	0.005-0.007	0/3
HT 924	supported	partial	0.006-0.008	3/3
FM 400	supported	partial	0.008-0.10	0/3

The specimens that were nonconductive prior to the start of tests were given voltage breakdown tests as described in Para. 2.2.1 to determine the voltage necessary to cause sparkover across or through the adhesives. Those that exhibited continuity would, of course, require no voltage to initiate conductivity. Hence, those specimens were tested initially with impulse currents as described in Para. 2.2.2 to establish the visible spark thresholds due to current flow.

2.3.3.2.1 Spark thresholds due to voltage stress.- Sparkover voltages of the seven specimens that exhibited no conductivity prior to test ranged between 100 volts and 7100 volts. Visible sparks occurred at the edges or corners of the specimens, and the low sparkover voltage and pre-test conductivity was due to metal burrs or other cutting tool marks along the edges or ends of the specimens.

2.3.3.2.2 Spark thresholds due to current flow.- All bonded aluminum stiffener specimens that exhibited some degree of electrical conductivity were subjected to impulse currents as described in para. 2.2.2 to establish the minimum currents which would cause visible sparking. The ranges of currents that caused visible sparking are shown in Table 2-12.

Table 2-12 - Spark Threshold Currents for Bonded Aluminum Stiffener Specimens
(All specimens exhibited electrical conductivity prior to test. Bonded surfaces were 15 in.²)

<u>Adhesive Description</u>			<u>Nominal Bondline Thickness (in.)</u>	<u>Range of Sparkover Currents (kA)</u>
<u>Designation</u>	<u>Type</u>	<u>Conductivity</u>		
AF-126-2	supported	none	0.002	0.1-0.5
FM 1000	unsupported	none	0.001-0.002	5.0-10.0
EA 9602.3	supported	none	0.002-0.004	2.0-10.0
R 7114	supported	none	0.002-0.004	1.0-5.0
MB 1113	supported	none	0.003-0.005	0.2-10.6
FM 61	supported	none	0.005-0.007	0.0-2.0
HT 424	supported	partial	0.006-0.008	1.0-5.0
FM 400	supported	partial	0.008-0.010	0.2-5.0

2.3.4 Comparison of test results for various adhesives

Bond line sparkover voltages for aluminum lap joints, fuel line brackets and stiffener specimens bonded with each of the eight adhesives are presented on Figure 2.15.

The sparkover voltages were highest (up to 8.6 kV) for the supported modified epoxies, probably due to the presence of the nylon carrier which maintains a positive separation between

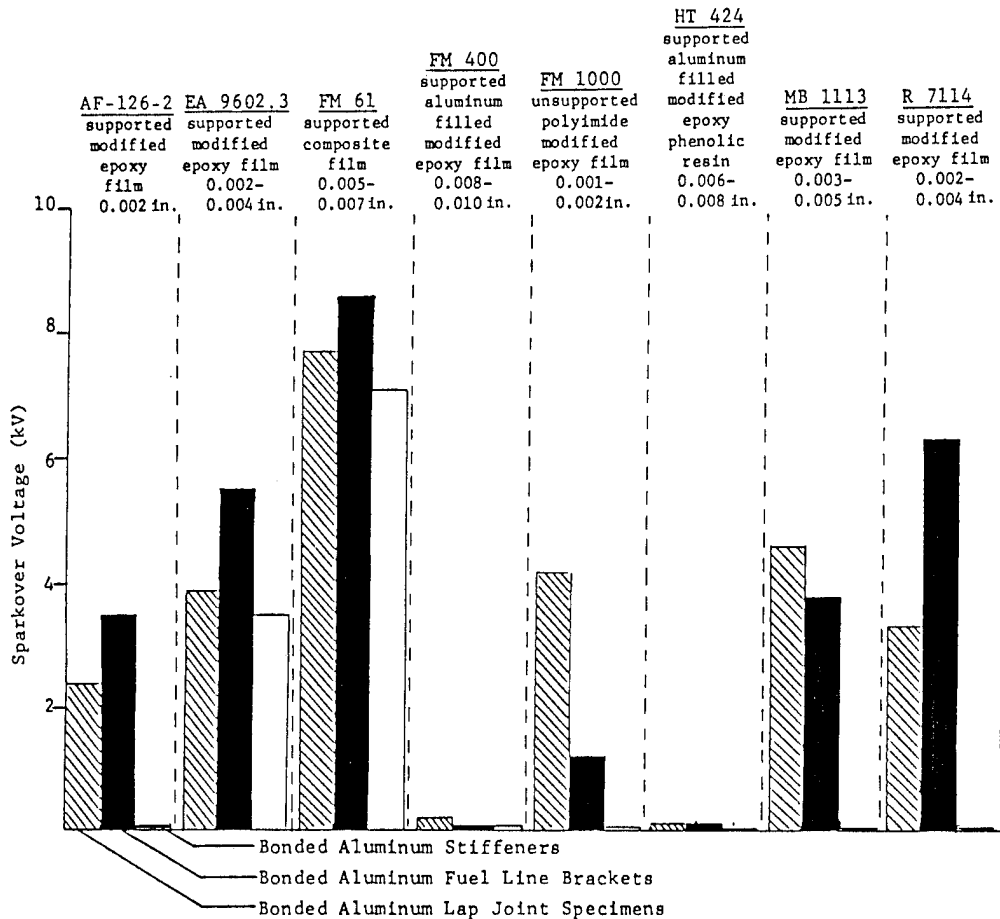


Figure 2.15 - Ranges of Sparkover Voltages for Bonded Aluminum Specimens.

bonded surfaces. Within this group, the adhesives with the thickest bond lines allowed the highest voltage. The low sparkover voltages that sometimes occurred were due to burrs which penetrated the adhesive at the edges of the specimens, or to sparkovers across the adhesive at the edges of the specimens.

The highest sparkover voltage (1200 V) for the unsupported adhesive was somewhat less than that recorded for the supported adhesives, due to the absence of the carrier.

The sparkover voltages of the two aluminum filled adhesives did not exceed 100 volts due to the aluminum particles. In contrast to the other adhesives, which usually sparked over at the specimen edges, the aluminum filled adhesives allowed conduction to take place within the bond, and visible sparks were not usually visible until higher currents of sufficient magnitude were applied to blow arc products out of the bond.

Loss of adhesive shear strength due to current flow is due to arcing and pressure buildup within the bond. Thus, shear strength was affected only when the sparkover took place within the bond. Sparkovers that occurred at an edge of one of the adherends or between the sides of the adherends did not result in pressure buildup within the bond line, nor affect the bond in any other way. Thus, loss of bond strength depends greatly on whether sparkovers may occur within the bond. The adhesives that permitted this to occur most often were the aluminum powder filled modified epoxies or unsupported modified epoxies. Those for which sparkovers occurred most often at the edges were the supported modified epoxies with no aluminum powder.

Normalized shear strengths following exposure to lightning-like currents are presented as a function of current density for each of the adhesives on Figure 2.16.

The amount of current necessary to degrade or debond a lap joint depends on the number of sparkover paths that exist through the adhesive. If a large number of paths exist, as is possible when aluminum powder is present throughout the adhesive, arcing of a large number of partially conducting paths may occur so the current and pressure buildup associated with each path would be small. Beneath some level it would be insufficient to degrade the bond. On the other hand, if the adhesive bond is a comparatively good electrical insulator, only a few sparkovers may occur within the bond, but these will conduct much higher amounts of current and the associated pressure buildups can be sufficient to cause loss of bond strength. For this reason, data that relate loss of shear strength to current density (amperes per unit of bonded surface) give a very general indication only. Since the number and location(s) of internal sparkovers are random occurrences, data produced from small coupon-type test specimens give only a general indication of the capability of much larger bonded surfaces. From Figure 2.16, it may be concluded that:

1. The shear strength of all adhesives degrade a minimum of 20% when sparkovers occur inside the bond, regardless of current level.
2. For nonconductive adhesives, strength degradation becomes significant at 2500 A/in.², at which level very little shear strength may remain.
3. Aluminum-filled adhesives do not suffer appreciable loss of shear strength at 2500A.

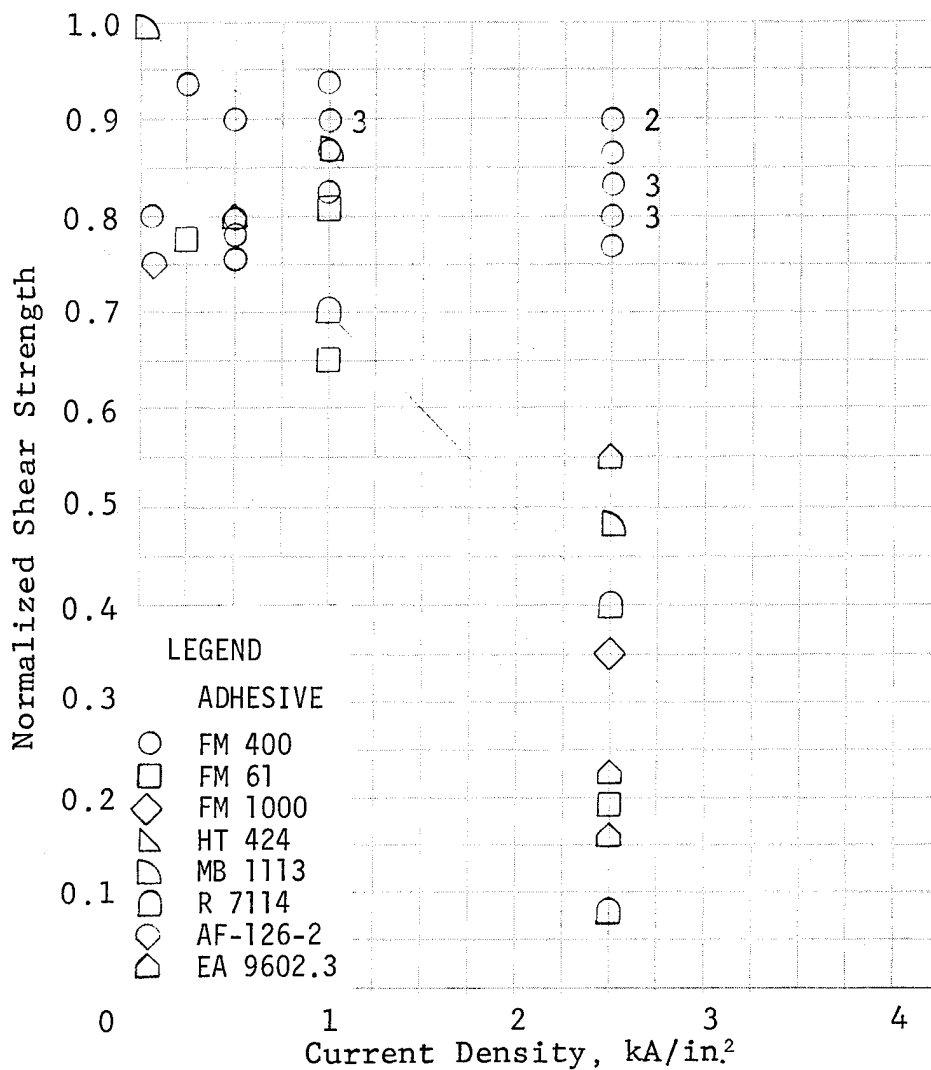


Figure 2.16 - Normalized Shear Strength of Bonded Aluminum Lap Joint Specimens Following Current Flow (data shown is for internal sparking only).

Note: Numbers next to symbols indicate replicated data.

2.3.5 Adhesively bonded aluminum honeycomb panel specimens

2.3.5.1 Specimen description

The bonded aluminum honeycomb panel specimens are representative of structural members used for rib or spar applications. They are comprised of aluminum face sheets adhesively bonded to an aluminum trussgrid core. Each specimen was 1 in. wide and 15 in. long. Eight specimens were provided with each of the eight adhesives described on Table 2-3. A typical specimen is shown in Figure 2.17.

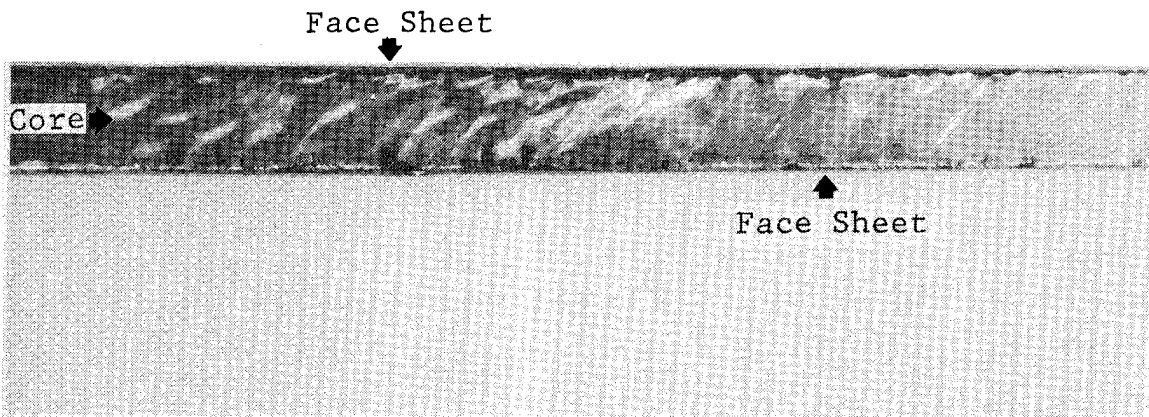


Figure 2.17 - Edge View of Adhesively Bonded Aluminum Honeycomb Panel Specimen.

2.3.5.2 Test results

Since the adhesive bond between the aluminum core and face sheets is not normally exposed to fuel vapors, and since much of the bonded interfaces are out of view, no attempt was made to determine sparking thresholds. Instead, tests were conducted to determine the current levels at which adhesive bond strength becomes degraded, or other physical damage effects occur.

For this purpose, test currents were conducted from one face sheet to the other, so that currents would have to flow across adhesive bonds on both sides of the core. The test setup is pictured on Figure 2.18.

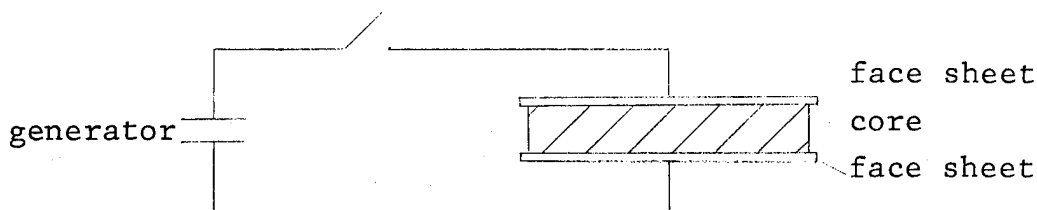


Figure 2.18 - Circuit for Aluminum Honeycomb Panel Specimen Tests.

Test currents of between 20 kA and 100 kA were applied to the specimens. Following the current applications, each specimen was given a peel test in which the force necessary to peel a face sheet from the core was measured. This also permitted inspection of the bonded surfaces for evidence of arcing or other damage.

In general, currents of 50 kA or less (equivalent to 3.33 kA/in.^2) produced up to 30% loss of peel strength and some evidence of sparking at the bonds was evident after the face sheets had been peeled away. Currents of from 50 to 100 kA ($3.33\text{-}6.67 \text{ kA/in.}^2$) caused considerable loss of bond strength and the pressure buildup due to internal arcing caused some of the core to be blown out of the edges of the specimens. A typical example is shown on Figure 2.19.

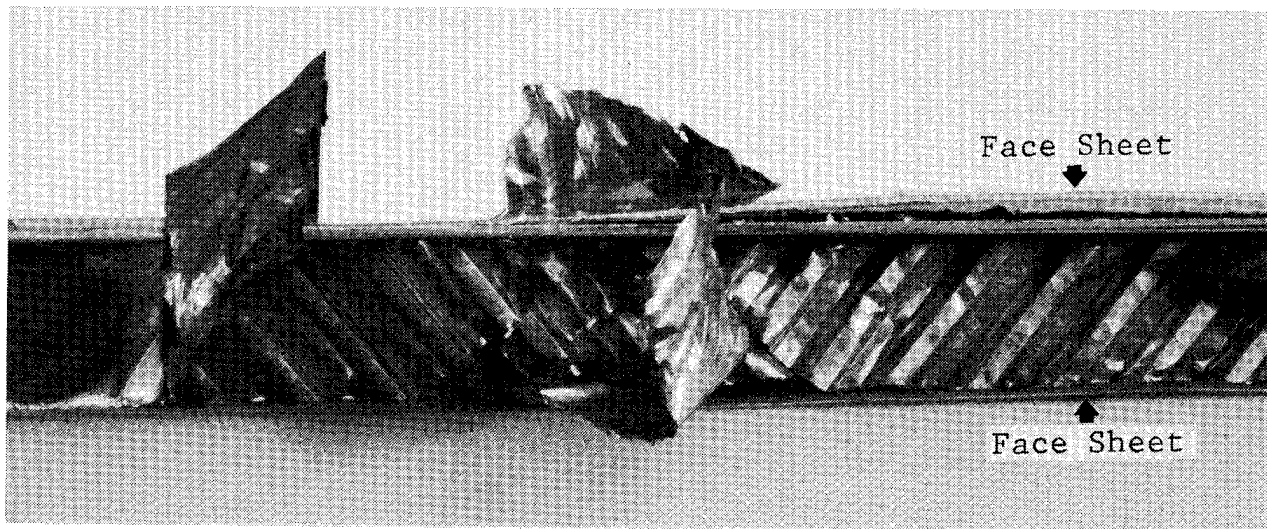


Figure 2.19 - Bonded Aluminum Honeycomb Panel
Specimen following 100 kA Test.
Current was applied between Face
Sheets.

The test results for each adhesive are plotted on Figure 2.20, which shows normalized peel strength versus current density. This is the same format in which the lap joint shear strength data are presented in Figure 2.16. Due to the scatter of peel test results, it is not possible to discern a difference that is attributable to type of adhesive, except that the three specimens which sustained the greatest loss of peel strength contained aluminum powder and were partially conductive. This may simply be an extension of data scatter and not related to adhesive properties. No other explanation is apparent.

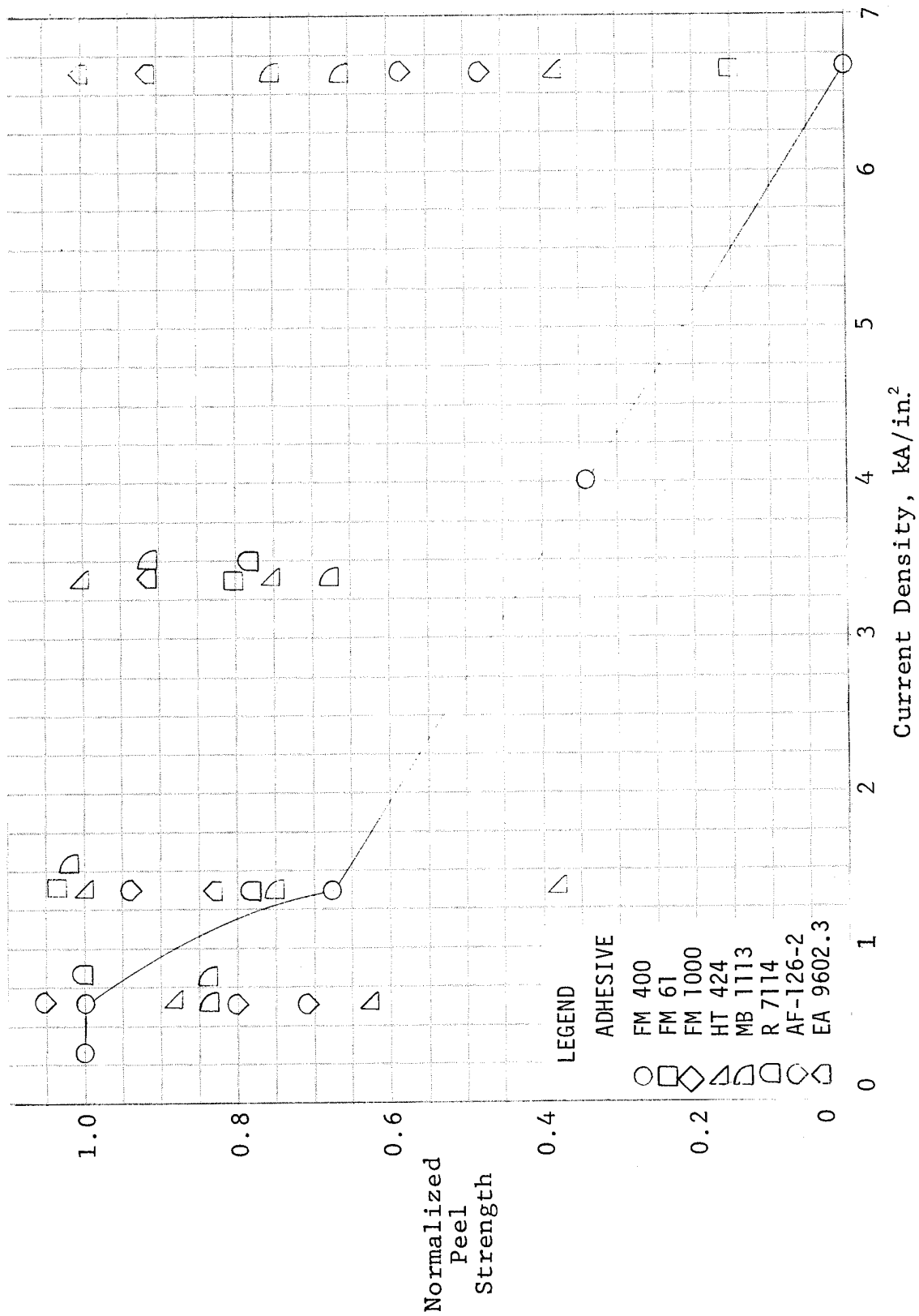


Figure 2.20 - Normalized Peel Strength of Bonded Aluminum Honeycomb Panel Specimens following Current Flow.

2.4 Hardware Interfaces with Metals

The specimens in this category included access doors which were riveted, fastened, or bonded and fastened. They represented typical access door configurations utilized in aluminum aircraft structure.

Each type of specimen was subjected to impulse currents as described in Para. 2.2.2 to establish the minimum current which would cause visible sparking. The test specimens were constructed to evaluate the effect of various access door bonding and fastening configurations on spark threshold level.

2.4.1 Access doors riveted, fastened, or bonded and fastened

2.4.1.1 Specimen description

The entire access door assemblies were fabricated in 17.5 in. by 22.5 in. aluminum panels which were 0.040 in. thick. The access door was also of aluminum construction and 0.040 in. thickness. A 0.050 in. thick aluminum splice plate was fastened to the aluminum "skin" and access door using rivets, fasteners, and adhesive in various configurations which included the following:

- Configuration 1 & 2 - Single rows of LZ4 rivets
- Configuration 3 - Stagger rows of LZ4 rivets
- Configuration 4 - Single rows of LZ5 rivets
- Configuration 5 - Single row of LZ4 rivets
attaching the "skin" to
splice plate. #10 screws
attaching the access door-to-
splice plate
- Configuration 6 - Adhesive bonding between "skin"
and splice plate. #10 screws
attaching the access door-to-
splice plate

All rivets were "wet" installed. Fuel tank sealant was applied to all fasteners on the wet side and to the skin-to-splice and access door-to-splice interfaces. In addition, panel configurations 5 and 6 included T-section stringers representative of typical aircraft construction. The test specimens are further described in Figures 2.21 through 2.24.

Photographs of typical panel configurations with and without the T-section stringers are shown in Figure 2.25.

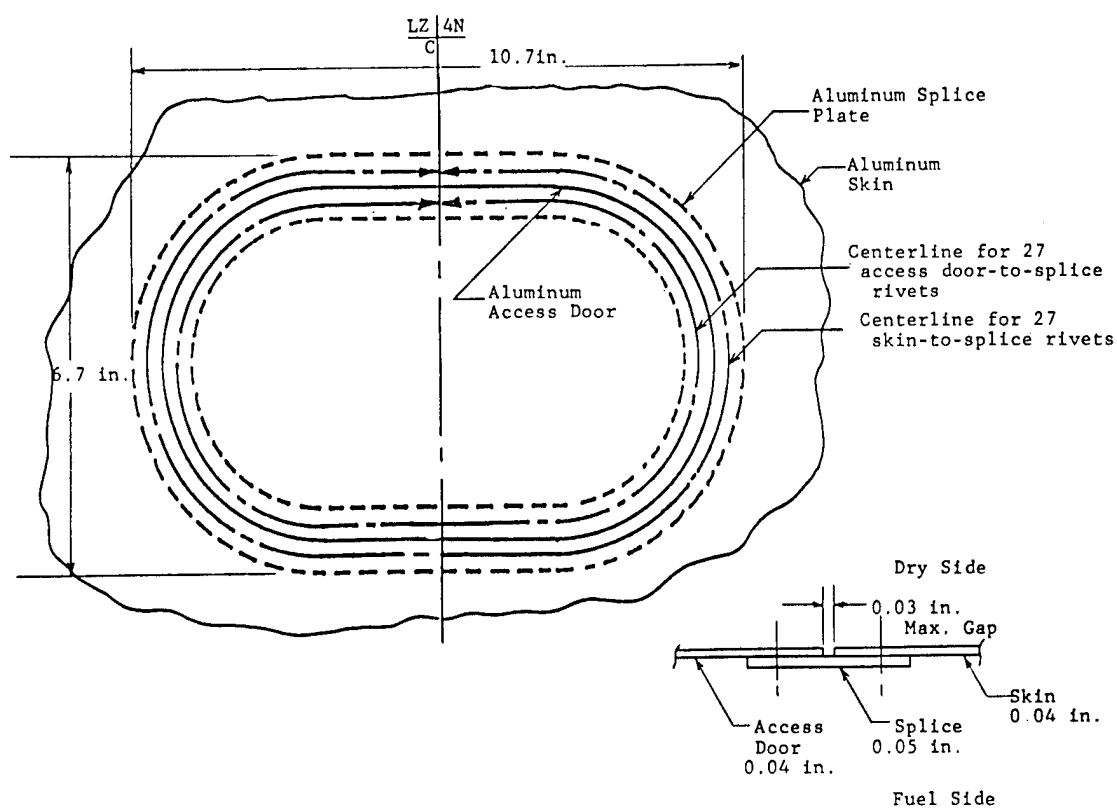


Figure 2.21 - Access Door Configurations 1 and 2.

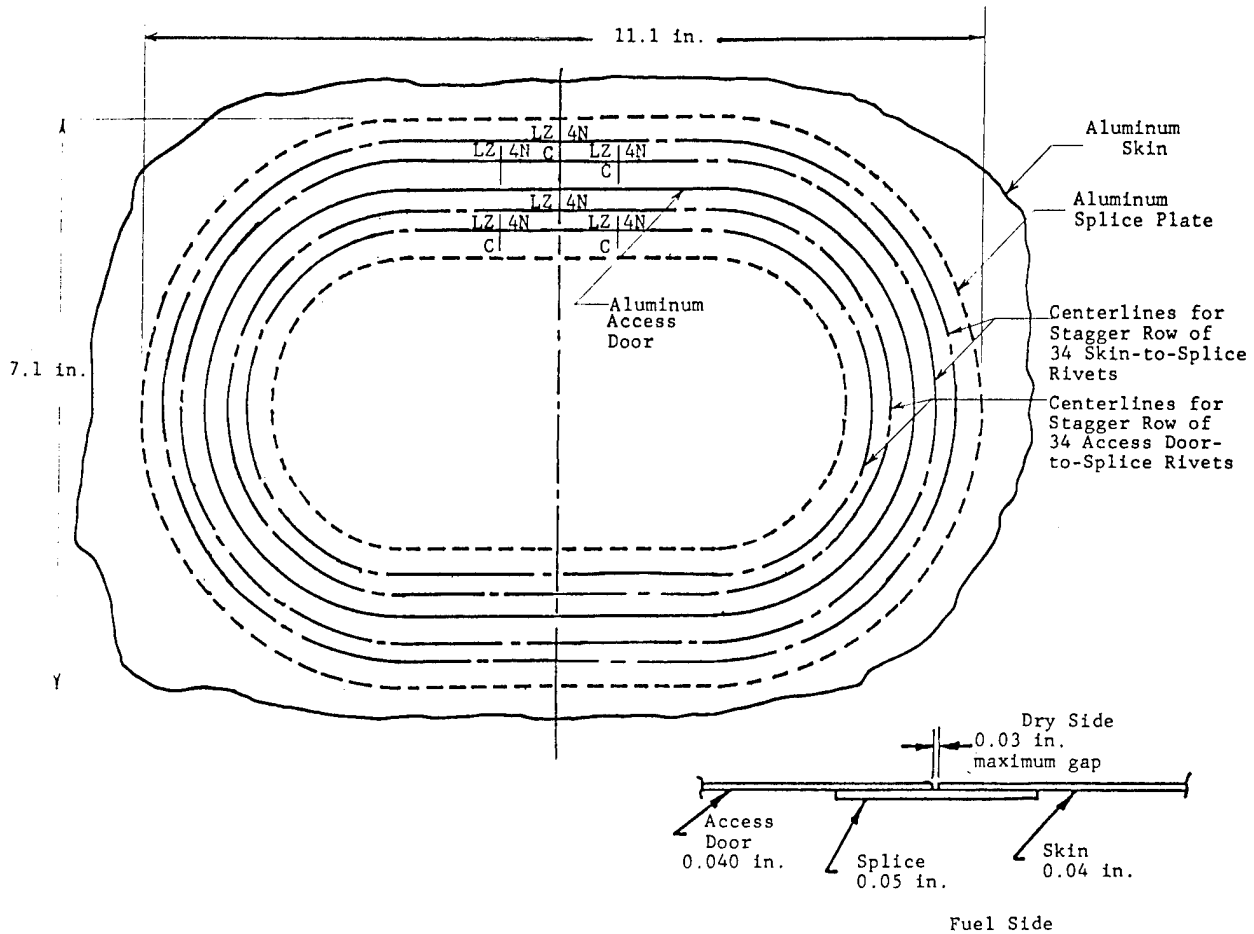


Figure 2.22 - Access Door Configuration 3.

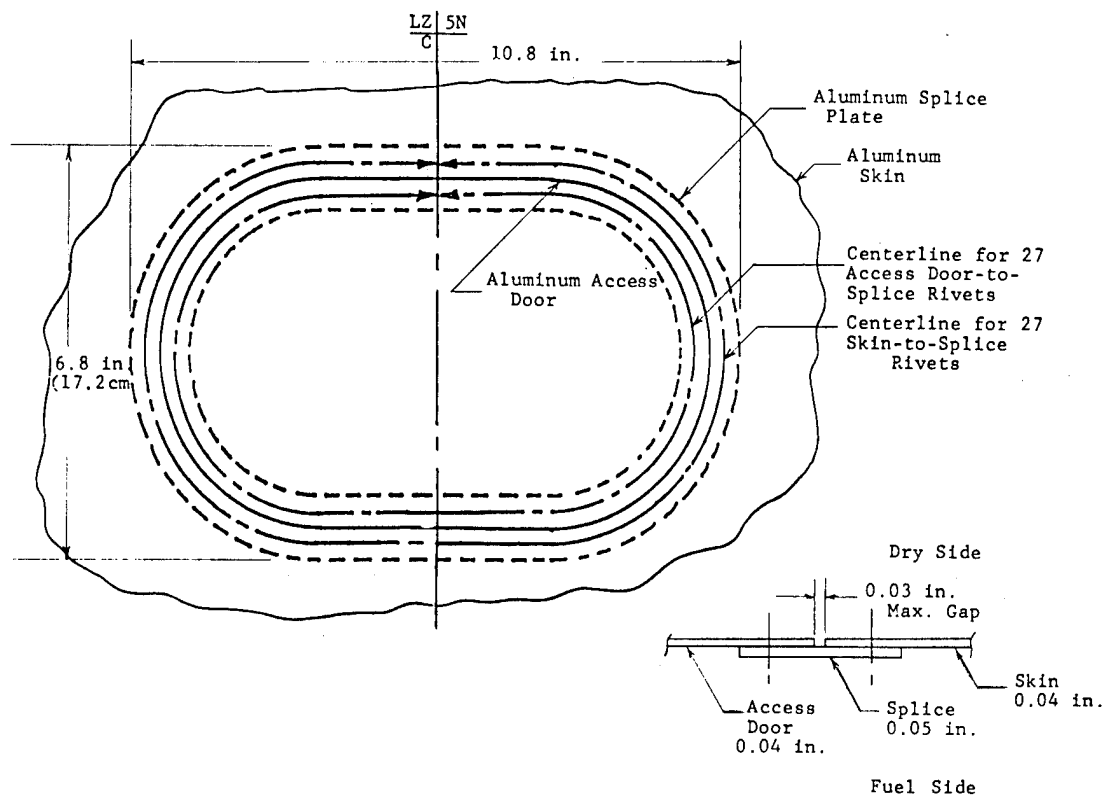


Figure 2.23 Access Door Configuration 4.

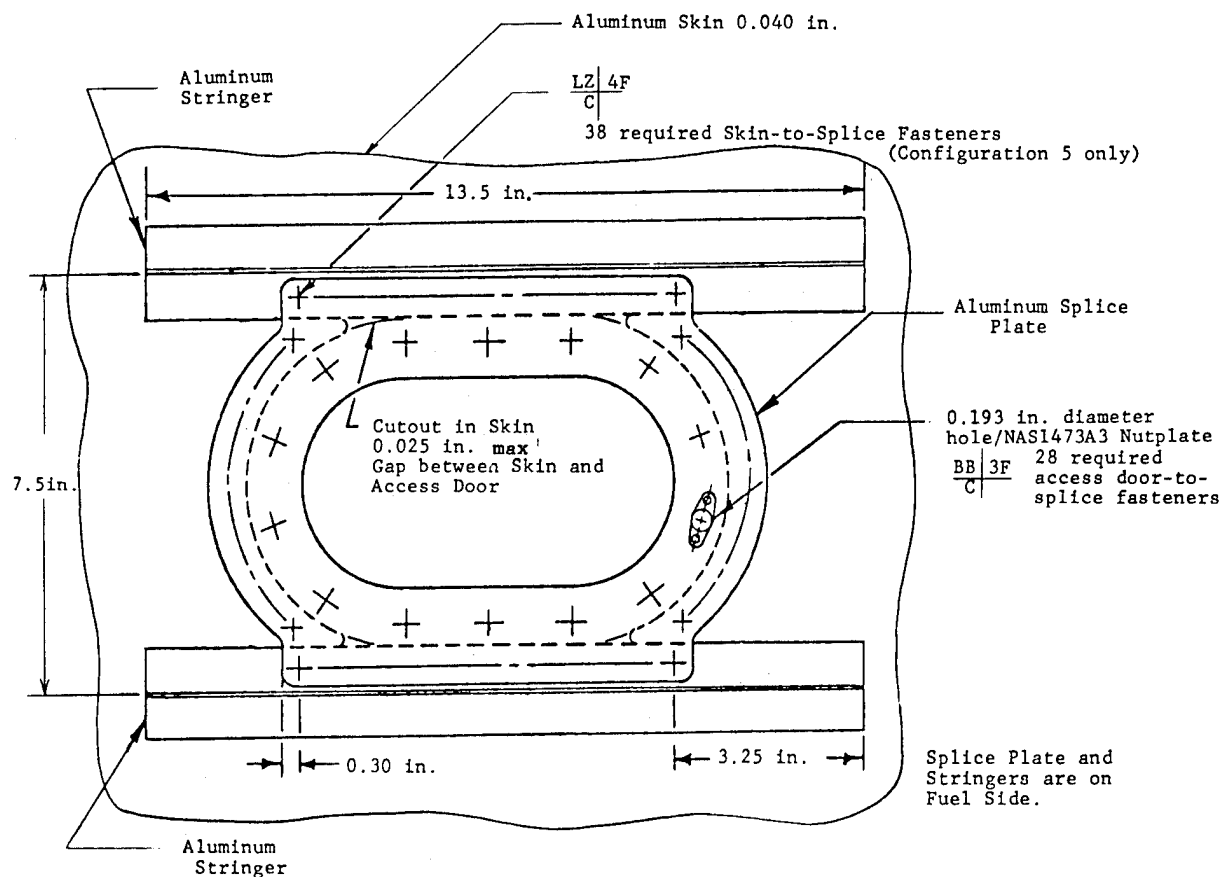


Figure 2.24 - Access Door Configurations 5 and 6.
Note: Configuration 6 is the same
as above except splice plate is
bonded to aluminum skin.

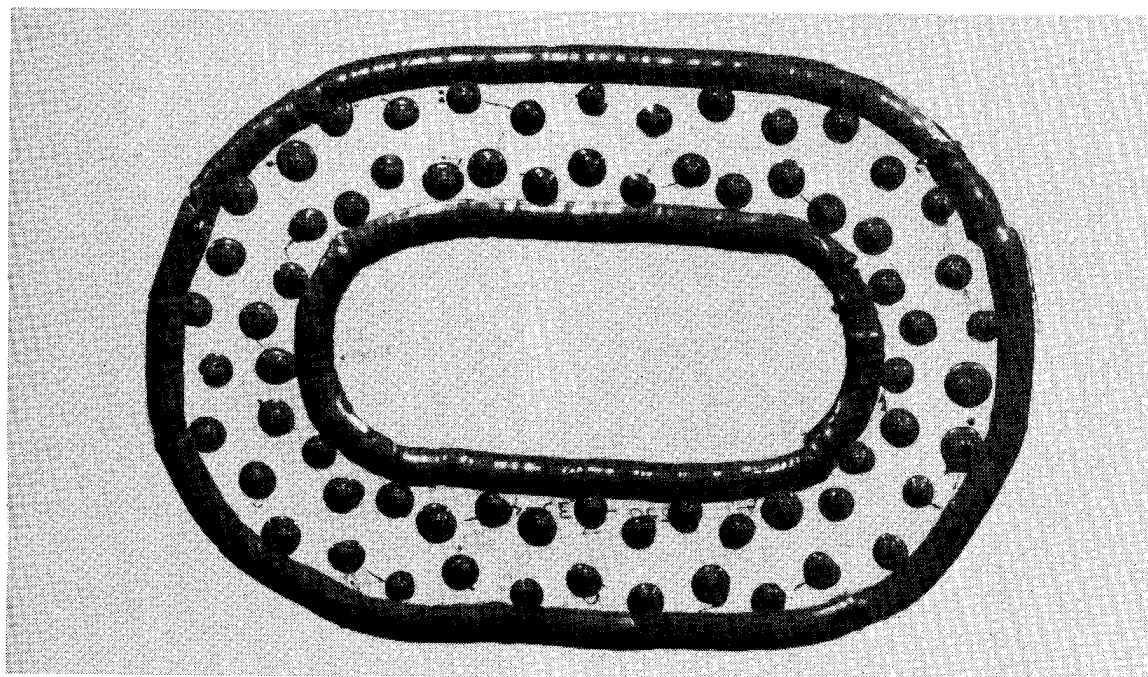
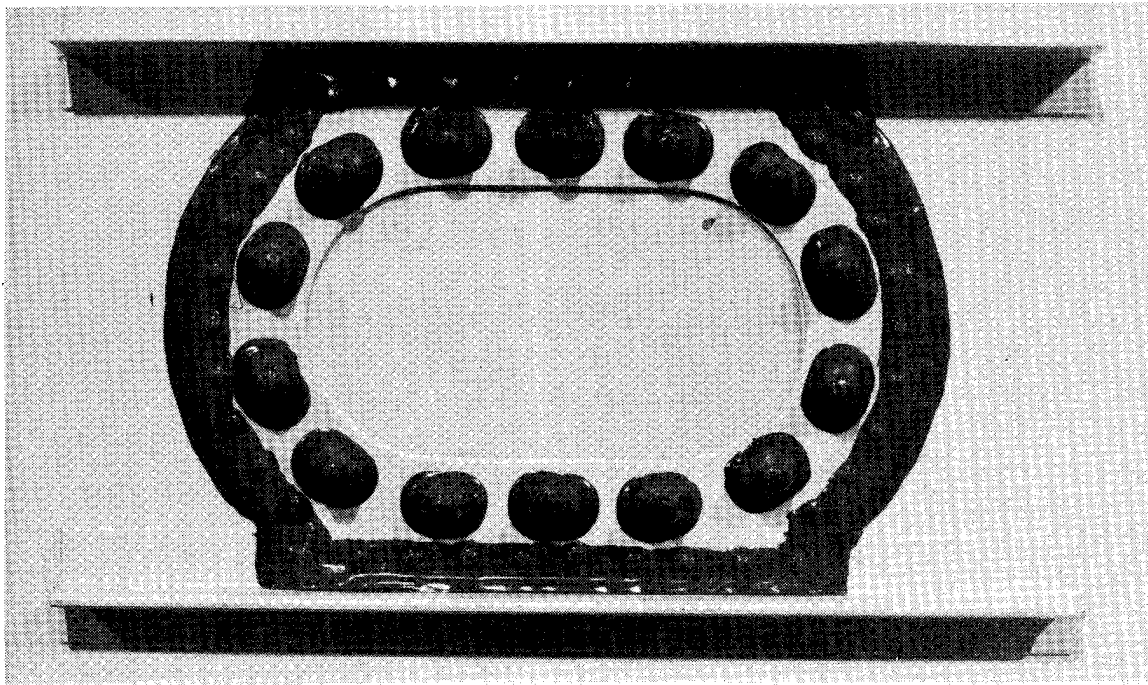


Figure 2.25 - Photographs Showing Typical Access Door Panels.
Top photo - with T-section stringers
Bottom photo - without stringers

2.4.1.2 Test results

Direct lightning strikes to the skin-to-splice and the access door-to-splice fasteners and to the center of the access door were simulated during the tests. Each fastener or access door was struck only once. During the fastener tests, the applied current level was increased in the sequence of 10, 20, 50, 100, 150 and 200 kA until a fastener sparked. The sequence was repeated several times as allowed by the number of fasteners available.

Each access door was struck only once at the highest current level available (150-200 kA), thus a spark or no spark result occurred indicating the ability of the access door configuration to suppress a fuel ignition spark. The test results are shown in Figures 2.26 to 2.28.

The test results for a direct strike to the center of the access door are shown in Figure 2.26. A no spark result is shown by an upward pointing arrow indicating that the spark threshold was higher than the tested level. The lowest spark threshold level was 150 kA. Due to the limited number of tests and specimens, no definite relationship between spark level and fastener configuration could be concluded.

A typical example of visible sparks resulting from a strike to the access door is shown in Figure 2.29. As this photo shows, the pressure built up by the transfer of current from the access door to the splice plate caused the arc products to blow past the door "O" ring causing visible sparking within the fuel tank area.

Figure 2.27 shows the spark threshold level for strike to the skin-to-splice fastener. The minimum spark threshold level was 180 kA for the series of tests. The graph indicates that there was no configuration that was significantly better or worse than the others - all appeared to provide about the same level of protection as the others. Figure 2.30 shows the results of a 200 kA strike to a skin-to-splice rivet. Pressure buildup beneath the fuel tank sealant due to current transfer from the rivet to the skin tore through the sealant at the rivet/splice plate interface causing a potential fuel ignition spark in the fuel tank interior.

Figure 2.28 shows the results of strike to the access door-to-splice plate fasteners. The minimum spark threshold level was 50 kA. In general, fastener configuration did not seem to affect spark threshold level except for configuration No. 5. In this configuration, the simulated strikes were to #10 screws and the current return paths to the skin were through LZ4 rivets. Due to their larger size, the #10 screws may have provided a lower current density path from the access door to the splice plate than either the LZ4 or LZ5 rivets of the other configurations. The

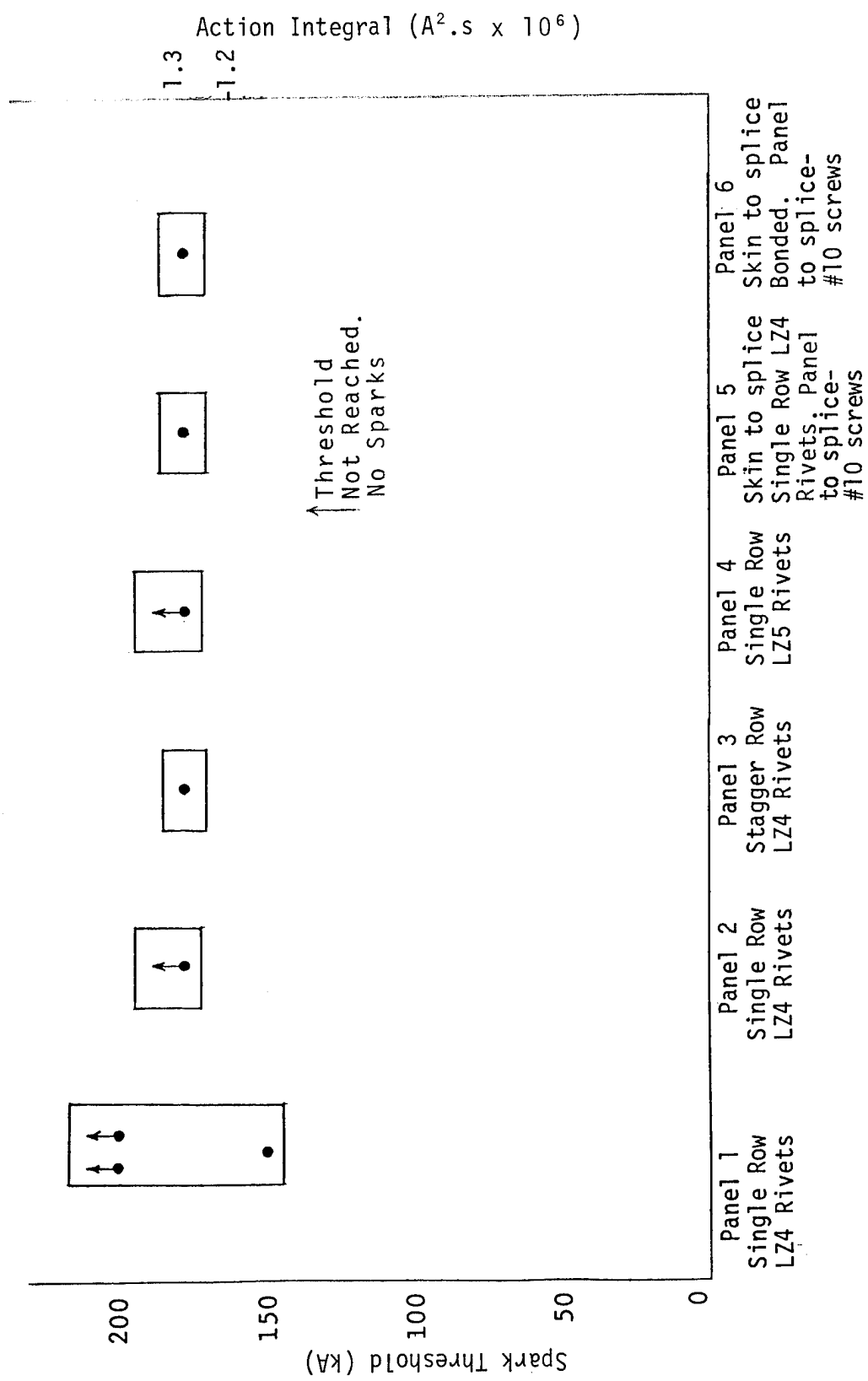


Figure 2.26 - Spark Threshold Levels - Direct Strike to Center of Access Door.

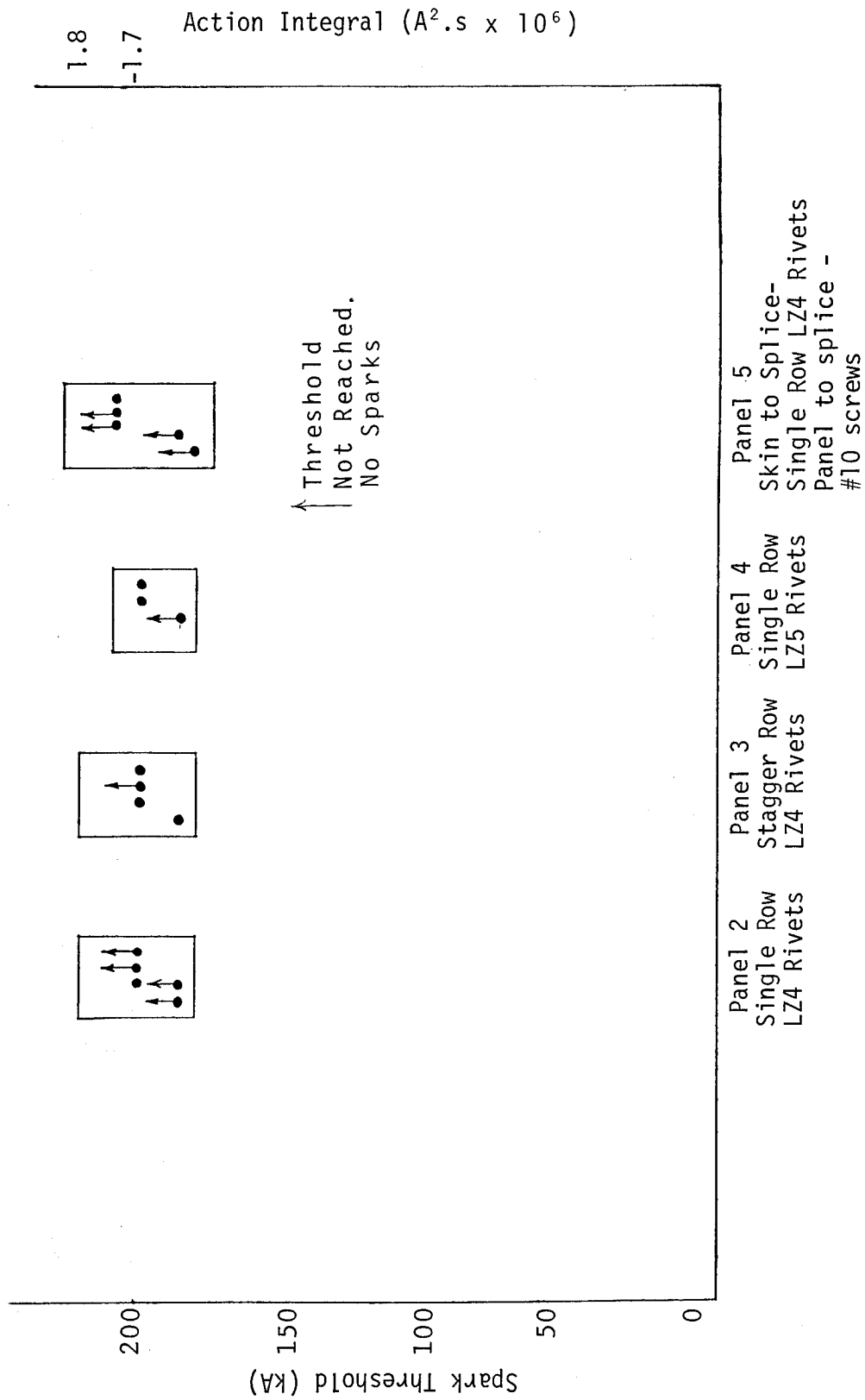


Figure 2.27 - Spark Threshold Levels - Direct Strike to Skin-to-Splice Fastener.

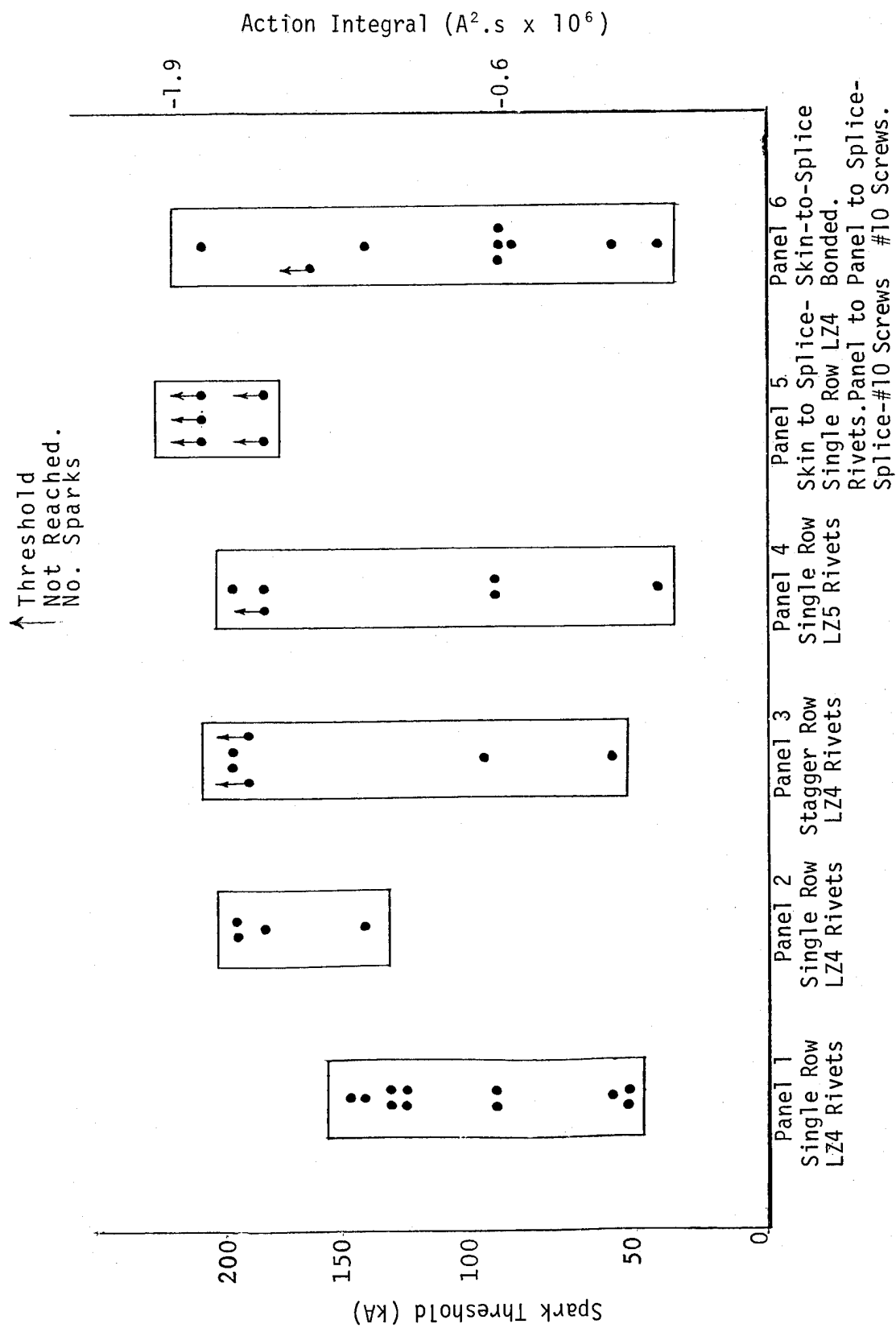


Figure 2.28 - Spark Threshold Levels - Direct Strike to Access Door-to-Splice Fastener.

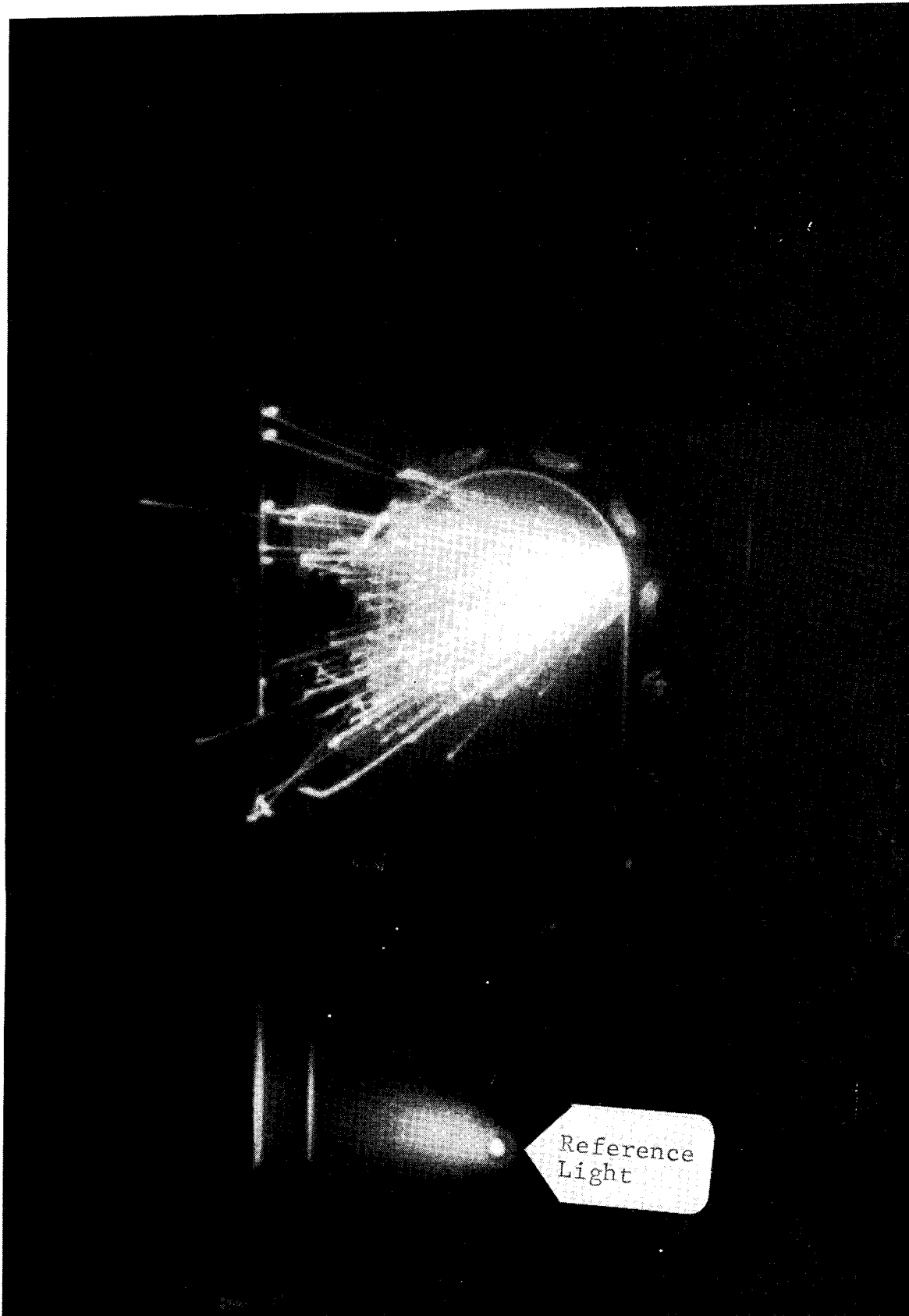


Figure 2.29 - Transfer of Current from Access Door to Splice Plate.

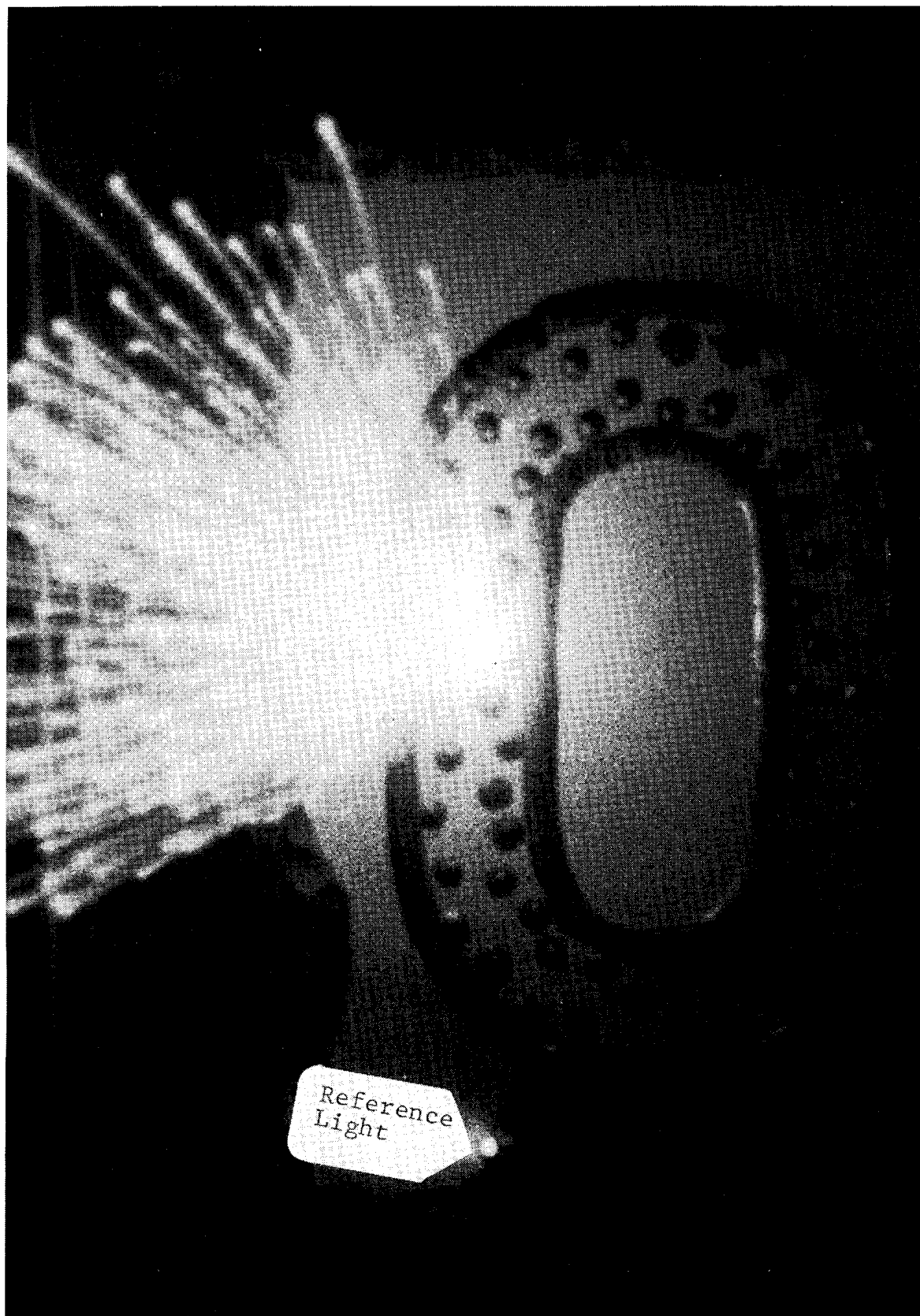


Figure 2.30 - Results of 200 kA Strike to Skin-to-Splice Rivet.

lower current concentration would have prevented excessive pressure from building up to a level sufficiently high to tear through the fuel tank sealant. Configuration six also utilized #10 screws to fasten the access door to the splice plate; however, the current return path to the aluminum skin provided by that specimen configuration was through a bonding adhesive which was electrically nonconductive. Thus, the adhesive would have tended to aid in pressure buildup due to its nonconductive properties.

Figure 2.31 shows internal sparking as a result of a 200 kA strike to an access door-to-splice rivet.

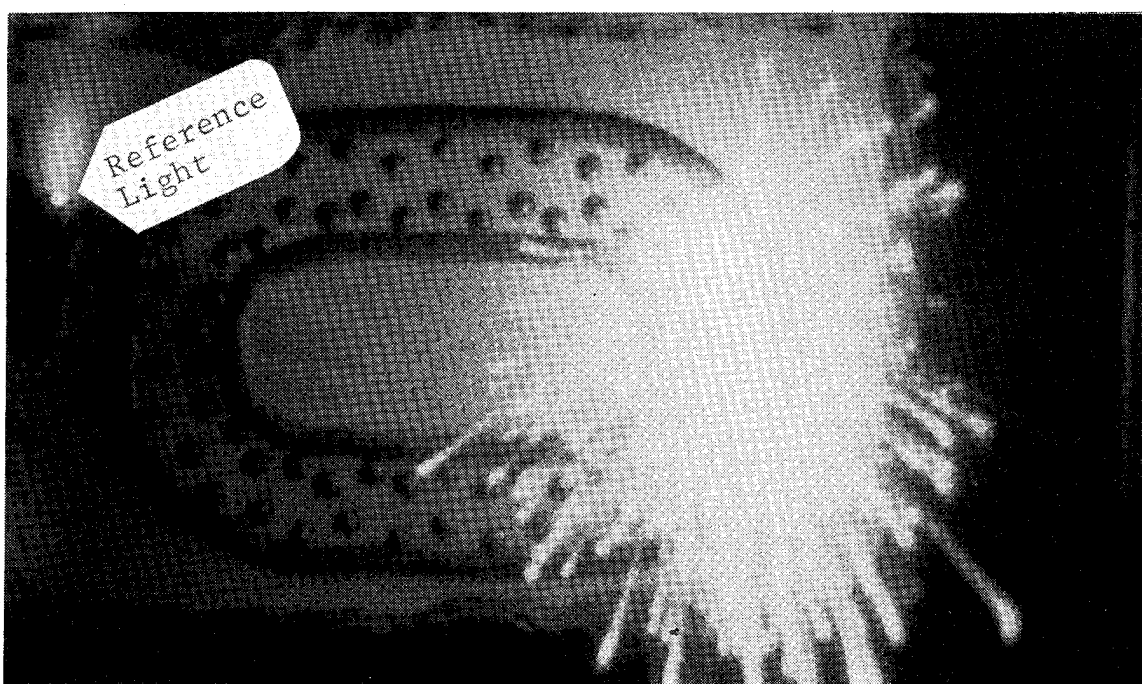


Figure 2.31 - Internal Fuel Tank Sparking as a Result of a 200 kA Strike to an Access Door-to-splice Rivet.

Current transfer from the rivet to the splice plate resulted in pressure buildup beneath the sealant, eventually exceeding the strength of the fuel tank sealant and tearing a hole in it at the rivet/splice plate interface.

2.5 Adhesively Bonded gr/E

Adhesively bonded gr/E specimens included single lap joints used to evaluate adhesive shear strength and bonded "T" section

stiffeners. The lap joint specimens were evaluated using varied adhesives to determine if a possible relationship between adhesive properties and electrical transfer characteristics could be determined. All the adhesives tested were electrically nonconductive. Additional tests on controlled bond line lap joint specimens were evaluated for a relationship between bond line thickness and dielectric voltage breakdown. All of the specimens were representative of configurations being utilized in new aircraft design.

2.5.1 Bonded gr/E lap joint specimens

2.5.1.1 Specimen description

The bonded gr/E lap joint specimens were fabricated of 4 ply 0.056 in. gr/E, and were 2 in. in width, 12 in. in length and had an overlap of 0.5 in. as shown in Figure 2.32. The gr/E adherends were bonded together with a single layer of adhesive in accordance with the manufacturers' recommendations. The characteristics of each adhesive are described in Table 2-13.

The controlled bond line specimens had bond line thicknesses ranging from 0.003 in. to 0.028 in.

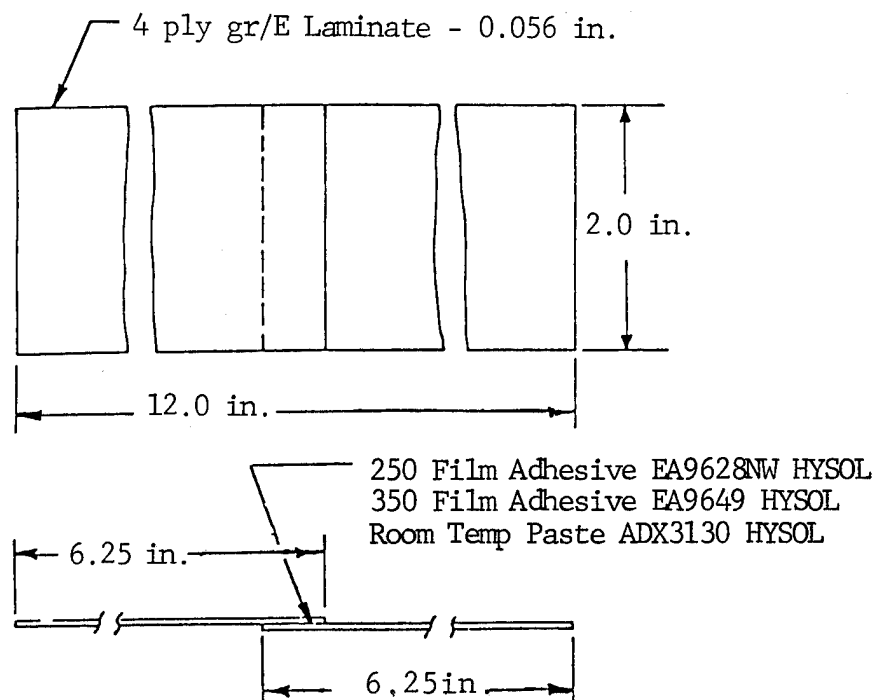


Figure 2.32 - gr/E Lap Joint Specimen.

Table 2-13 - Characteristics of Adhesives in Bonded gr/E Specimens.

Adhesive Manufacturer	Adhesive Manufacturer's Part No.	Type of Adhesive	One Hour Nominal Cure Temp(°F)	Film Weight (lbs/ft ²)	Manufacturer's Rated Tensile Shear Strength at 70°F (lbs/in ²)	Electrical Conductivity
Dexter Corp. (Hysol Div.)	EA9628NW	non-woven mat supported modified epoxy	250	0.045	4720	None
Dexter Corp. (Hysol Div.)	EA9649	supported adhesive	350	0.085	3800	None
Dexter Corp. (Hysol Div.)	ADX3130	unsupported room temp. resin adhesive	(a)	(b)	4500	None

Notes:

(a) minimum cure - 2.5 hrs. at 165°F

(b) not supplied by manufacturer

2.5.1.2 Test results

Prior to test, each lap joint specimen was given an electrical continuity check with a battery-operated ohmmeter to see if physical contact existed between the gr/E adherends. The number of specimens in each adhesive group which exhibited conductivity prior to test is presented in Table 2-14.

Table 2-14 - Electrical Continuity of gr/E Lap Joint Specimens Prior to Test.

<u>Adhesive Type</u>	<u>Nominal Bond Line Thickness</u>	<u>Number of Conductive Specimens/Group</u>
EA9628NW	0.005-0.007 in.	0/12
EA9679	0.005-0.007 in.	3/3
ADX3130	0.005-0.007 in.	0/3

The three EA9649 adhesive samples were conductive prior to test, apparently due to incidental penetration of yarns through the adhesive. Due to the small number of samples involved, no relationship could be determined between electrical conductivity and type of adhesive or bond line thickness.

The specimens that were nonconductive prior to the start of tests were given voltage breakdown tests, as described in Para. 2.2.1, to determine the voltage necessary to cause spark-over across or through the adhesives. Those that exhibited continuity would require no voltage to initiate continuity, hence, those specimens were tested initially with impulse currents that may produce visible sparks.

2.5.1.2.1 Bond line breakdown voltages.- Table 2-15 shows the breakdown voltage levels for the two nonconductive adhesives tested. The lap joints bonded with EA9649 were not subjected to voltage breakdown tests since they exhibited continuity prior to test. Breakdown voltages for specimens bonded with EA9628NW ranged from 1200V to 8000V for 11 of the 12 specimens tested, one specimen broke down at less than 100 volts. The breakdown voltage range for the ADX3130 adhesive was 1600V to 2000V.

Visible sparking at breakdown, which was due to edge flash-overs, occurred in twenty-five percent of the specimens bonded with EA9628NW and all of the specimens bonded with ADX3130. Thus, the majority of the specimens bonded with EA9628NW (seventy five percent) and none of the ADX3130 specimens broke down within the bond line.

Table 2-15 - Breakdown Voltage vs. Bond Line Adhesive of
Nonconductive gr/E Lap Joint Specimens.

<u>Sample</u>	<u>Adhesive</u>	<u>Breakdown Voltage</u>
1	EA9628NW	4600
2	EA9628NW	3700
3	EA9628NW	6000 (a)
4	EA9628NW	6000 (a)
5	EA9628NW	4000
6	EA9628NW	<100
7	EA9628NW	3600
8	EA9628NW	3200
9	EA9628NW	1200
10	EA9628NW	6800
11	EA9628NW	8000 (a)
12	EA9628NW	3400
1	ADX3130	1600 (a)
2	ADX3130	2000 (a)
3	ADX3130	2000 (a)

(a) visible spark

An additional set of specimens was tested to determine the relationship between bond line thickness and voltage breakdown level. The test results are summarized in Table 2-16. This group of specimens was identical to the previous group except that only EA9628NW adhesive was used. Prior to the tests, continuity measurements were made between the adherends to determine if electrical contact existed between them. None of the specimens exhibited continuity.

The results showed that the overall breakdown voltage level increased with increasing bond line thickness. The voltage "gradient", however, decreased from 350 volts per mil for "thin" bond lines to about 150 volts per mil for "thick" bond lines. All breakdowns occurred at the edges of the specimens indicating that the voltage withstand capability of the adhesive was greater than that of air.

Table 2-16 - Breakdown Voltage vs. Bond Line Thickness for gr/E Lap Joint Specimens.
(EA9628NW Adhesive only)

<u>Bondline Thickness</u> (in.)	<u>Breakdown Range</u> (volts)
0.003	1100
0.008	1700-1800
0.010-0.013	2100
0.015	2200-2400
0.027-0.028	4200-4400

2.5.1.2.2 Spark threshold due to current flow.- Following the voltage breakdown tests, all lap joint specimens were subjected to impulse currents as described in Para. 2.2.2 to establish the minimum currents which would cause visible sparking. Since some of the specimens showed visible sparking during the breakdown voltage tests, they conducted no appreciable current before sparking occurred. The test results are summarized in Table 2-17 and indicate that the specimens which were bonded with EA9649 and which exhibited pretest conductivity were able to conduct up to 5000 amperes before producing visible sparks. This was more than five times the current conducted by the EZ9628NW specimens before they exhibited visible sparking.

Table 2-17 - Spark Threshold Currents for gr/E Lap Joint Specimens.
Bonded surfaces were 1 in.²

<u>Adhesive</u>	<u>Range of Currents to Produce Visible Sparks</u> (amperes)
EA9628NW	<100-900
EA9649	5000
ADX3130	<100

2.5.1.2.3 Current density vs. shear strength.- Following the current flow spark tests, the gr/E lap joint specimens were tested for shear strength. A comparison of the post test shear strength with untested control samples is given in Table 2-18.

Loss of shear strength is due to arcing and pressure buildup within the bond due to current flow. Thus, shear strength was affected only when the sparkover took place within the bond. Sparkovers that occurred at an edge or between the

Table 2-18 - Shear Strength of Bonded gr/E Lap Joint Specimens
Following Current Spark Threshold Tests.

<u>Specimen No.</u>	<u>Adhesive Type</u>	<u>Current Density (A/in.²)</u>	<u>Test Failure Load (lbs./in.²)</u>	<u>Failure Mode</u>
Control #1	EA9628NW	--	3190	interlaminar
Control #2	EA9628NW	--	3158	interlaminar
Control #3	EA9628NW	--	3693	interlaminar
1	EA9628NW	796	2043	interlaminar
2	EA9628NW	874	2022	interlaminar
3 (a)	EA9628NW	<100	3075	interlaminar
4 (a)	EA9628NW	<100	3919	interlaminar
5	EA9628NW	345	1318	interlaminar
6	EA9628NW	259	1711	interlaminar
7	EA9628NW	305	2715	interlaminar
8	EA9628NW	259	2362	interlaminar
9	EA9628NW	248	1908	interlaminar
10	EA9628NW	275	2741	interlaminar
11 (a)	EA9628NW	<100	2545	interlaminar
12	EA9628NW	819	1761	interlaminar
Control #1	EA9649	--	1716	interlaminar
Control #2	EA9649	--	2119	interlaminar
Control #3	EA9649	--	1784	interlaminar
1	EA9649	~5000	--	bond destroyed
2	EA9649	~5000		bond destroyed
3	EA9649	5176	590	interlaminar
Control #1	ADX3130	--	1641	adhesive
Control #2	ADX3130	--	2385	adhesive
Control #3	ADX3130	--	1660	adhesive
1 (a)	ADX3130	<100	1541	adhesive
2 (a)	ADX3130	<100	2011	adhesive
3 (a)	ADX3130	<100	2220	adhesive

(a) visible sparking during voltage breakdown tests

sides of the adherends did not result in pressure buildup within the bond line or affect the bond in any other way.

Those specimens which exhibited visible sparking during voltage breakdown subsequently produced very low current spark threshold levels. Since those specimens sparked over externally (rather than internally within the bond), it was expected that no loss of shear strength would result. Table 2-19 summarizes the shear strength of the test specimens compared to the test sparking mechanism. Those specimens which exhibited external sparking showed little, if any, loss of shear strength when compared to the control specimen values. Those specimens which sparked within the bond showed loss of shear strength when compared to the control specimens.

2.5.2 Bonded gr/E stiffeners

2.5.2.1 Specimen description

The bonded gr/E stiffeners were typical of "T" section stringers or stiffeners used in wing and integral fuel tank construction. The "T" sections were of 4 ply 0.056 in. gr/E construction and were 1.5 in. wide and 6 in. long, so the bonded surface area was 9 in.². They were bonded to 5.5 in. by 10 in., 4 ply gr/E "skins" with EA9628NW adhesive. The specimen is shown in Figure 2.33.

2.5.2.2 Test results

Prior to test, each gr/E stiffener specimen was given an electrical continuity check with a battery-operated ohmmeter to see if physical contact existed between the gr/E adherends. All 9 specimens showed electrical continuity. Since no voltage would be required to initiate conductivity, the specimens were tested only with impulse currents as described in Para. 2.2.2 to establish the visible spark thresholds due to current flow.

2.5.2.2.1 Spark thresholds due to current flow.- All nine gr/E stiffener specimens produced visible sparks at applied current levels of less than 100 amperes. Apparently, incidental penetration of yarns through the adhesive at the specimen edges resulted in visible sparks.

2.6 Metal to gr/E Interfaces

The metal to gr/E interfaces included rivets, access door dome nuts and fuel line feed-through elbows in gr/E laminates. These subelement specimens represented typical interfaces utilized in the production of gr/E integral fuel tanks and which could be a source of fuel ignition sparks due to lightning currents flowing through them.

Table 2-19 - Summary of Shear Strength Levels Compared to Current Threshold Sparking Mechanism for Bonded gr/E Lap Joint Specimens

Adhesive Designation	Control Specimens	Shear Strength (lbs./in. ²)	
		Specimens Sparking within Bond	Specimens Sparking Externally
EA9628NW	3158-3693	1711-2741	2545-3919
EA9649	1716-2119	590	---
ADX3130	1641-2385	---	1541-2220

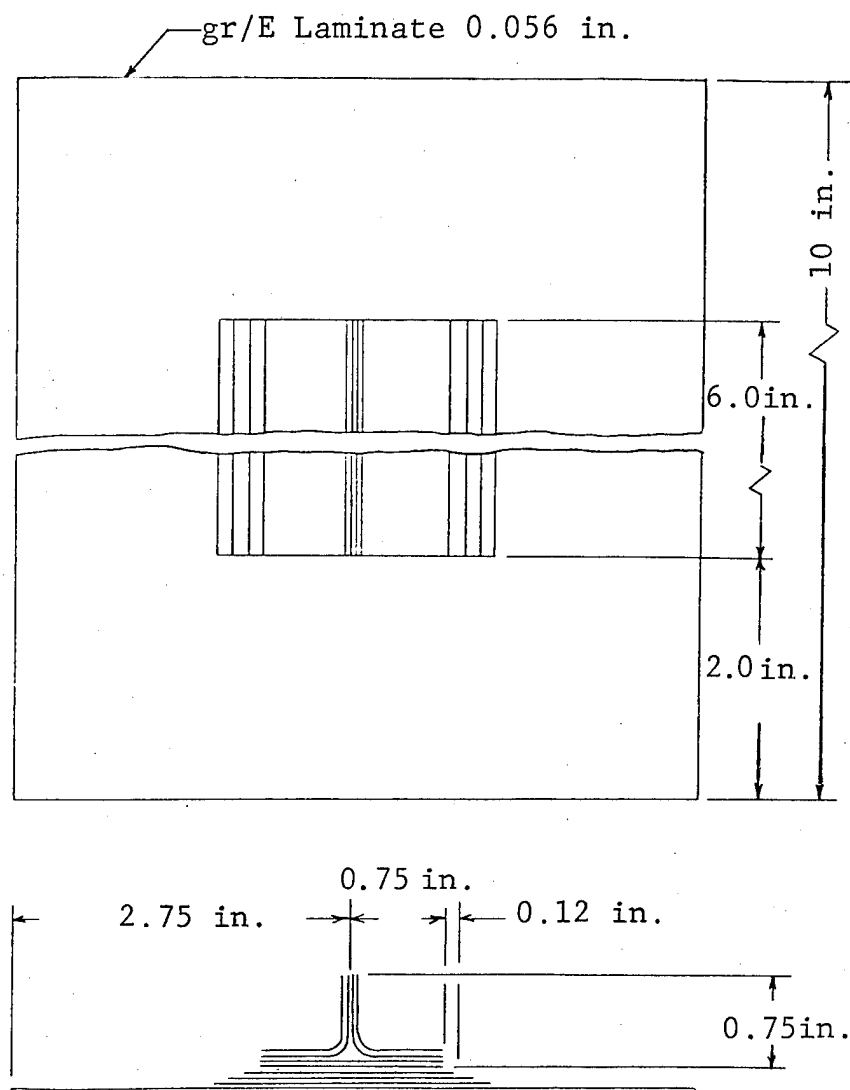


Figure 2.33 - Bonded gr/E Stiffener.

Each type of specimen was subjected to impulse currents as described in Para. 2.2.2 to establish the minimum currents which would cause visible sparking. Test specimens were fabricated to evaluate the effect of fuel tank sealant, to compare different sealants, and to compare results with and without the use of an adhesive carrier cloth.

2.6.1 Rivets in gr/E laminates

2.6.1.1 Specimen description

The rivet in gr/E laminate specimens represented metal-to-graphite interfaces utilized in gr/E integral fuel tank construction. Lightning currents conducted across this interface could cause sparking which would be a fuel ignition hazard.

The specimens consisted of a 0.04 in. thick, 2.5 in. by 0.75 in. aluminum tab which was riveted to a gr/E skin with a 0.125 in. diameter titanium rivet. The gr/E skin was 3 in. by 6 in. and was constructed of four plies of gr/E laminate 0.056 in. thick. In addition, some of the specimens also contained a 0.005 in. one ply layer of fiberglass between the aluminum tab and gr/E skin to simulate an adhesive carrier cloth. The test specimen is shown in Figure 2.34.

2.6.1.2 Test results

Currents were conducted through the rivet to gr/E interface by connecting the generator "high" side to the aluminum tab and returning the current to generator "ground" through a connection to the gr/E "skin". Initial specimen tests were to determine the effect of the carrier cloth and fuel tank sealant on the spark threshold level. The applied test current levels were increased in a 1, 2, 5 sequence on each specimen until a spark was detected. The test results are shown in Figures 2.35 and 2.36.

The test results indicate that, in general, the spark levels were higher for specimens without the carrier cloth than those containing the carrier cloth. Apparently, the carrier cloth forced all of the current to pass through the rivet; thus, the carrier cloth increased the current density at the rivet-gr/E interface resulting in visible sparks at lower applied current levels. Comparison of specimens with the adhesive cloth carrier to those without the cloth carrier indicates that the application of fuel tank sealant had the effect of increasing the spark threshold level. For the specimens with the adhesive carrier cloth and sealant, the spark threshold level was 4.3 kA; for specimens without the adhesive cloth but with sealant, the spark threshold level was 7.5 kA. Without sealant, the threshold

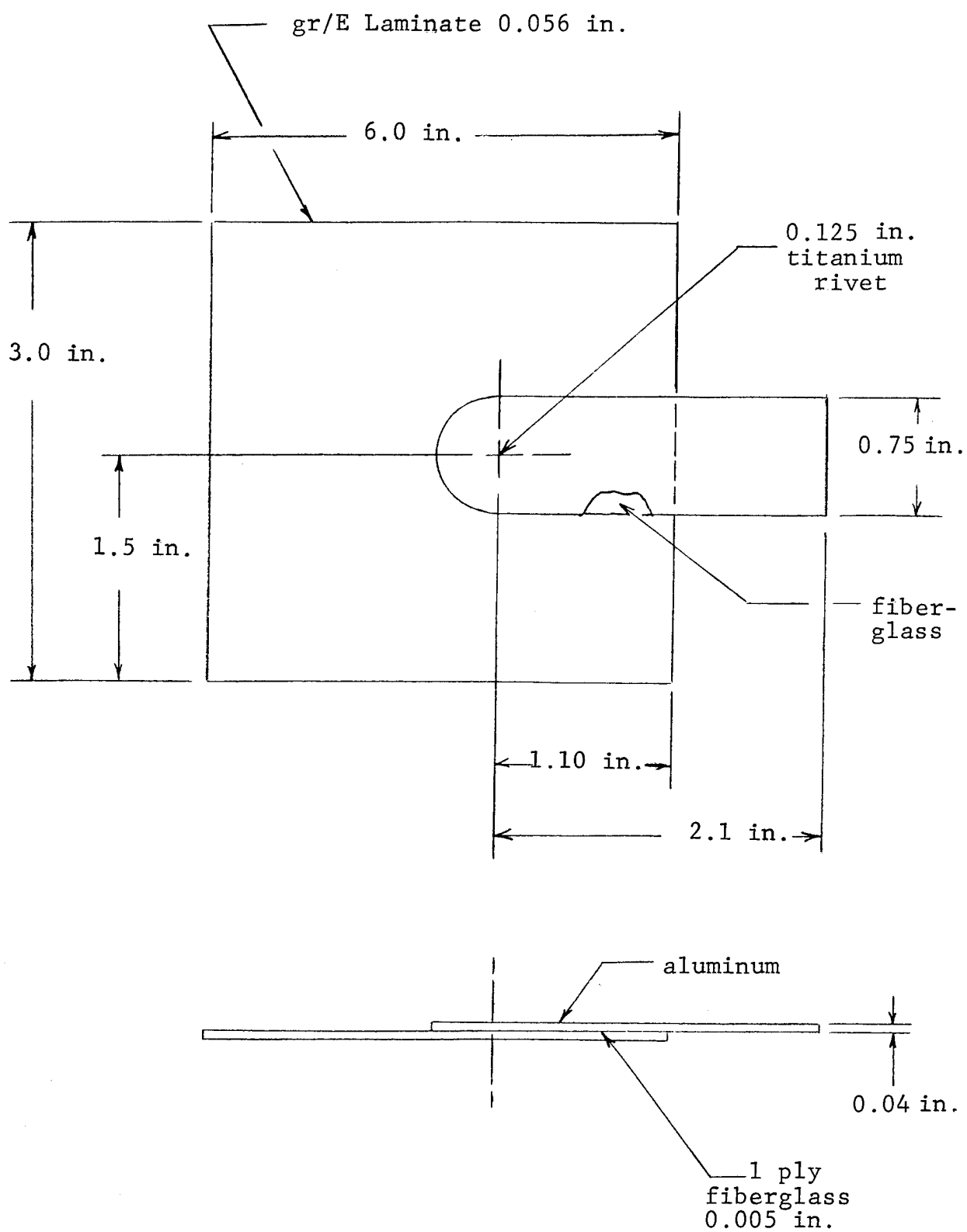


Figure 2.34 - Rivet in gr/E Laminate Test Specimen.

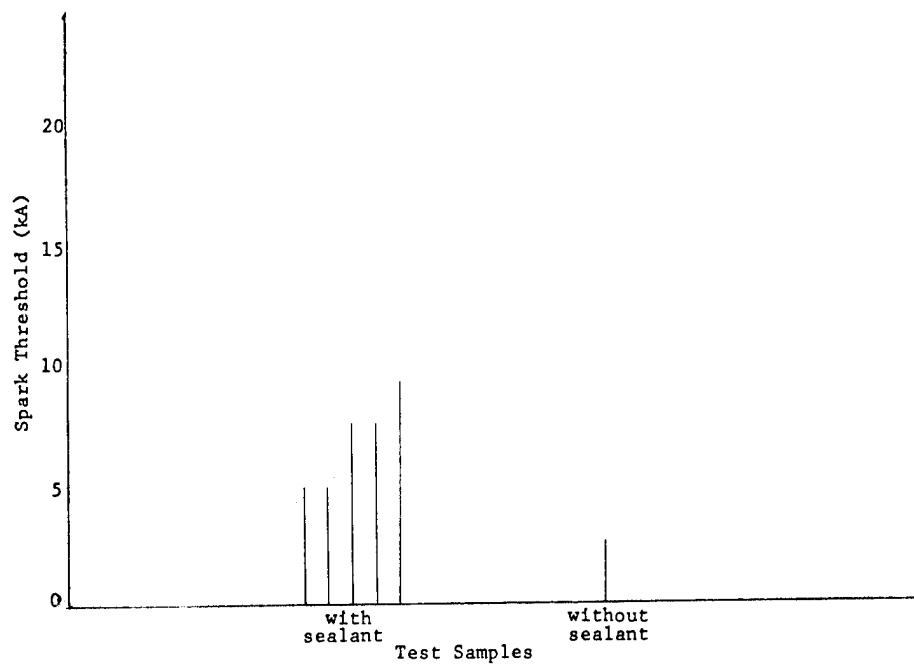


Figure 2.35 - Spark Threshold Levels for Rivet in gr/E Laminate with Adhesive Carrier Cloth.

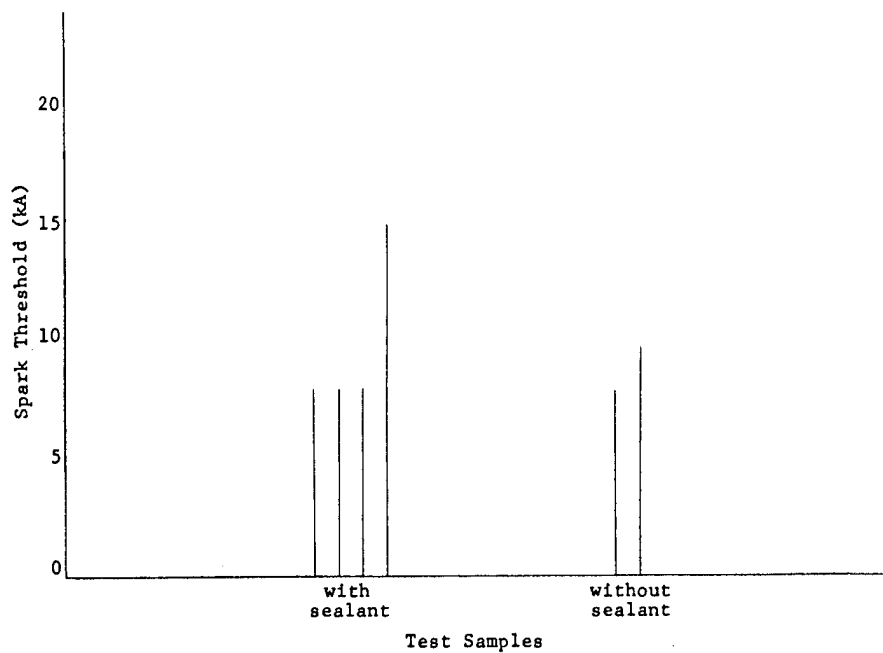


Figure 2.36 - Spark Threshold Levels for Rivet in gr/E Laminate without Adhesive Carrier Cloth.

level for the carrier cloth specimens was 2.1 kA; those without the carrier cloth were able to tolerate 7.5 kA before sparking.

A second series of tests utilized two types of fuel tank sealant to determine if sealant characteristics had an effect on the spark threshold level. Specimens with and without an adhesive carrier cloth were tested. Table 2-20 lists the characteristics of the sealants tested.

Table 2-20 - Characteristics of Fuel Tank Sealants
Utilized in gr/E Test Specimens

<u>Sealant Manufacturer</u>	<u>Manufacturer Part No.</u>	<u>Type of Sealant</u>	<u>Tensile Strength (lbs/in.²)</u>
Essex Chemical Corp.	PRO-Seal 890	Two part polysulfide integral fuel tank and fuselage sealant	300(a)
Products Research and Chemical Corp.	SEMKIT 654	Two part, polysulfide integral fuel tank and fuselage sealant	269(b)

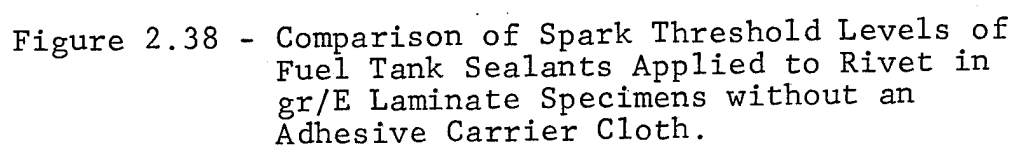
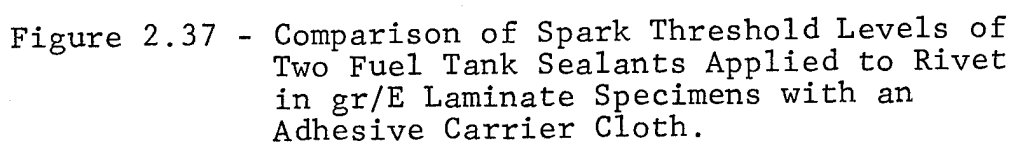
Notes:

- (a) 14 day cure
- (b) 28 day cure

Applied current levels to each specimen were initiated at 5 kA and increased in 5 kA steps until a visible spark was detected. The test results are shown in Figures 2.37 and 2.38.

The specimens containing the simulated adhesive carrier cloth, in general, sparked at lower current levels than those without a carrier cloth. This result was the same as that obtained during tests on the first set of rivet in gr/E laminate specimens.

The test results also indicated that the Semkit 654 specimens had, on the average, higher spark threshold levels than did the specimens coated with Pro-Seal 890 sealant. In some cases the Semkit sealant prevented visible sparking up to and including 17 kA which was the limit of the generator. The difference in spark threshold level was less well defined between specimens coated with a thin coat of Pro-Seal and those coated with a normal coat of Pro-Seal. Most likely, this was the result of difficulty in applying a thin coat of Pro-Seal.



The spark threshold level of the Pro-Seal specimens, with and without the carrier cloth was 5 kA; the spark threshold level of the Semkit specimens, with and without the carrier cloth was 10 kA. In general, the Semkit sealed specimens conducted greater amplitude current levels before sparking than did the Pro-Seal specimens. Figure 2.39 shows a typical spark produced during these tests. The transfer of current from the gr/E skin to the rivet resulted in pressure buildup beneath the sealant and subsequent release through a tear in the sealant at the gr/E skin surface.

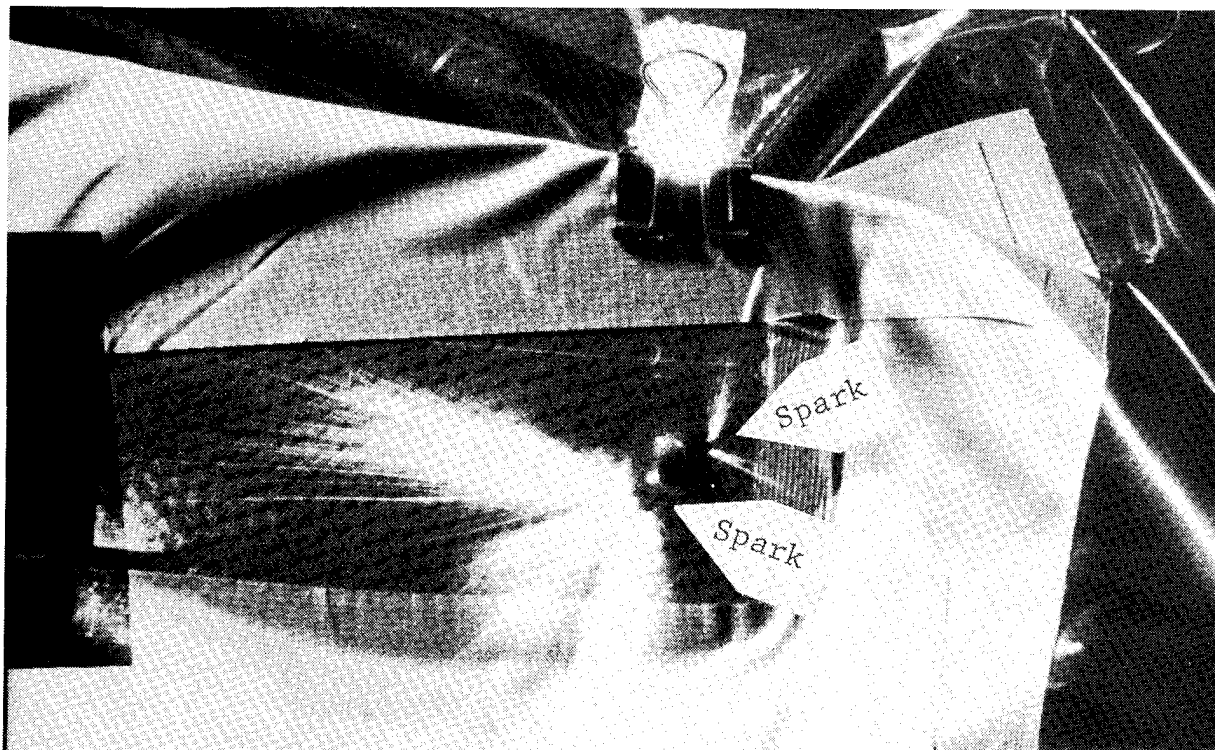


Figure 2.39 - Spark at Rivet to gr/E Interface Due to 17 kA Simulated Lightning Strike.

2.6.2 Access door dome nuts in gr/E laminates

2.6.2.1 Specimen description

The access door dome nut specimen consisted of a 1.5 in. by 2.88 in. 7 ply, 0.10 in. gr/E skin section to which a nutplate was fastened by two rivets. A second 7 ply gr/E skin section of identical dimensions was fastened to the first section by a countersunk machine screw which threaded into the nutplate. A synthetic rubber gasket between the gr/E skin sections was used to insure that all of the impulse current flowed through the dome nut. The specimen is shown in Figure 2.40.

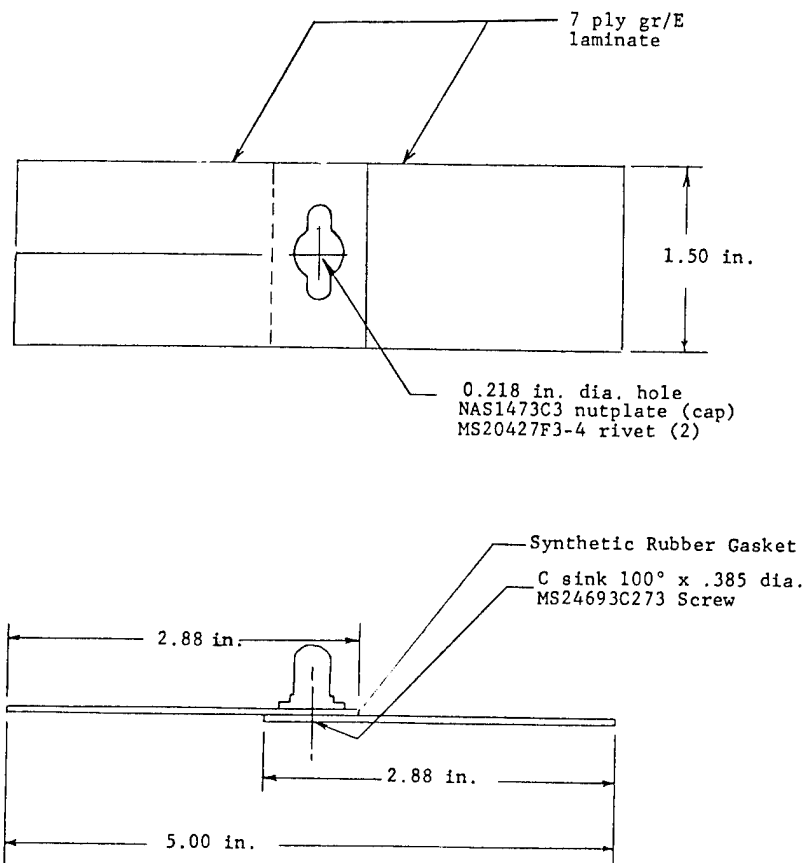


Figure 2.40 - Access Door Dome Nut in gr/E Laminate.

2.6.2.2 Test results

Generator current levels of 5, 11 and 17 kA were applied to one gr/E skin section, conducted through the dome nut assembly, and returned to generator "ground" from the second gr/E section. Tests on a specimen were concluded when a visible spark occurred. Test specimens were prepared with either Pro-Seal or Semkit fuel tank sealant applied to the fuel side of the dome nut assembly. The test results are shown in Figure 2.41.

The tests indicated that, in general, the Semkit sealed specimens sparked at higher current levels than did the Pro-Seal specimens. The minimum spark threshold level of the Semkit sealant was, however, at 5 kA which was lower than the 10 kA level of the normally applied Pro-Seal specimens and the same as the specimens with the thinly applied coat of Pro-Seal. Thus, the minimum spark threshold level for either the Pro-Seal or the Semkit sealant was 5 kA.

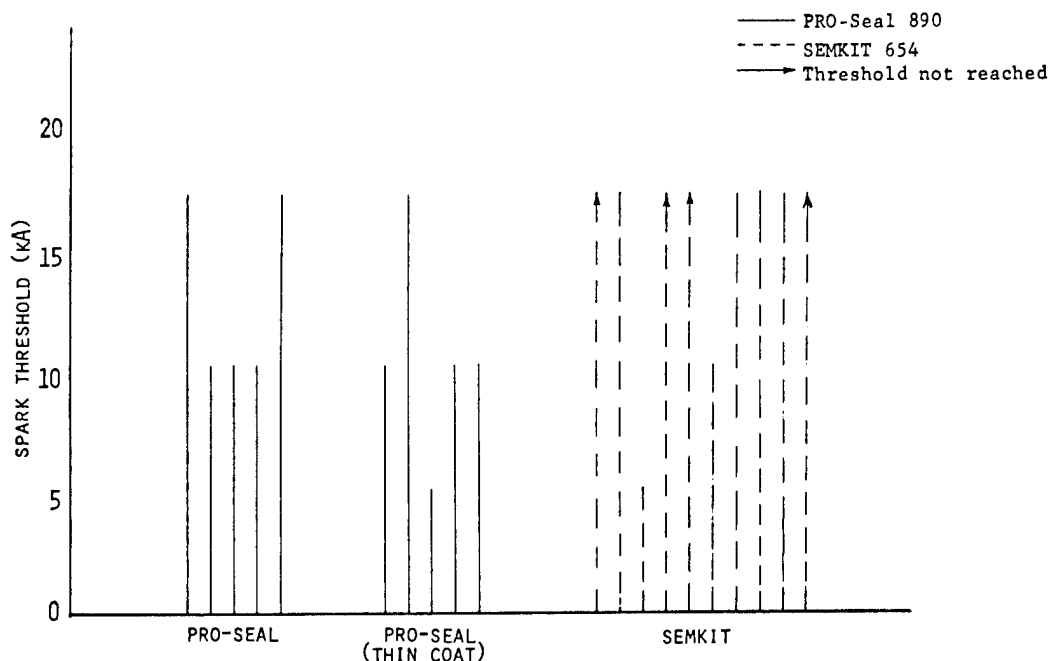


Figure 2.41 - Spark Threshold Levels of Access Door Dome Nuts in gr/E Laminates.

Figure 2.42 shows a photograph of a 17 kA spark through Pro-Seal sealant. The spark was the result of current transfer from the first gr/E skin section, through the dome nut assembly and into the second gr/E skin section. The internal pressure buildup, which resulted from current flow through the specimen, tore through the sealant at the gr/E skin surface as shown by the photograph. This spark was typical of those observed during these tests.

2.6.3 Fuel line feed-through elbows in gr/E laminates

2.6.3.1 Specimen description

The fuel line feed-through elbow specimens were metal-to-graphite interfaces which represented interfaces between fuel lines and internal fuel tank structural configurations such as ribs.

Five feed-through elbows were mounted on a 3.0 in. x 18 in. 4 ply, gr/E laminate. Each surface of the laminate made contact with the feed-through elbow by a 0.036 in. thick, 2.06 in. diameter washer. A drawing and a photo of the test specimen are shown in Figure 2.43.

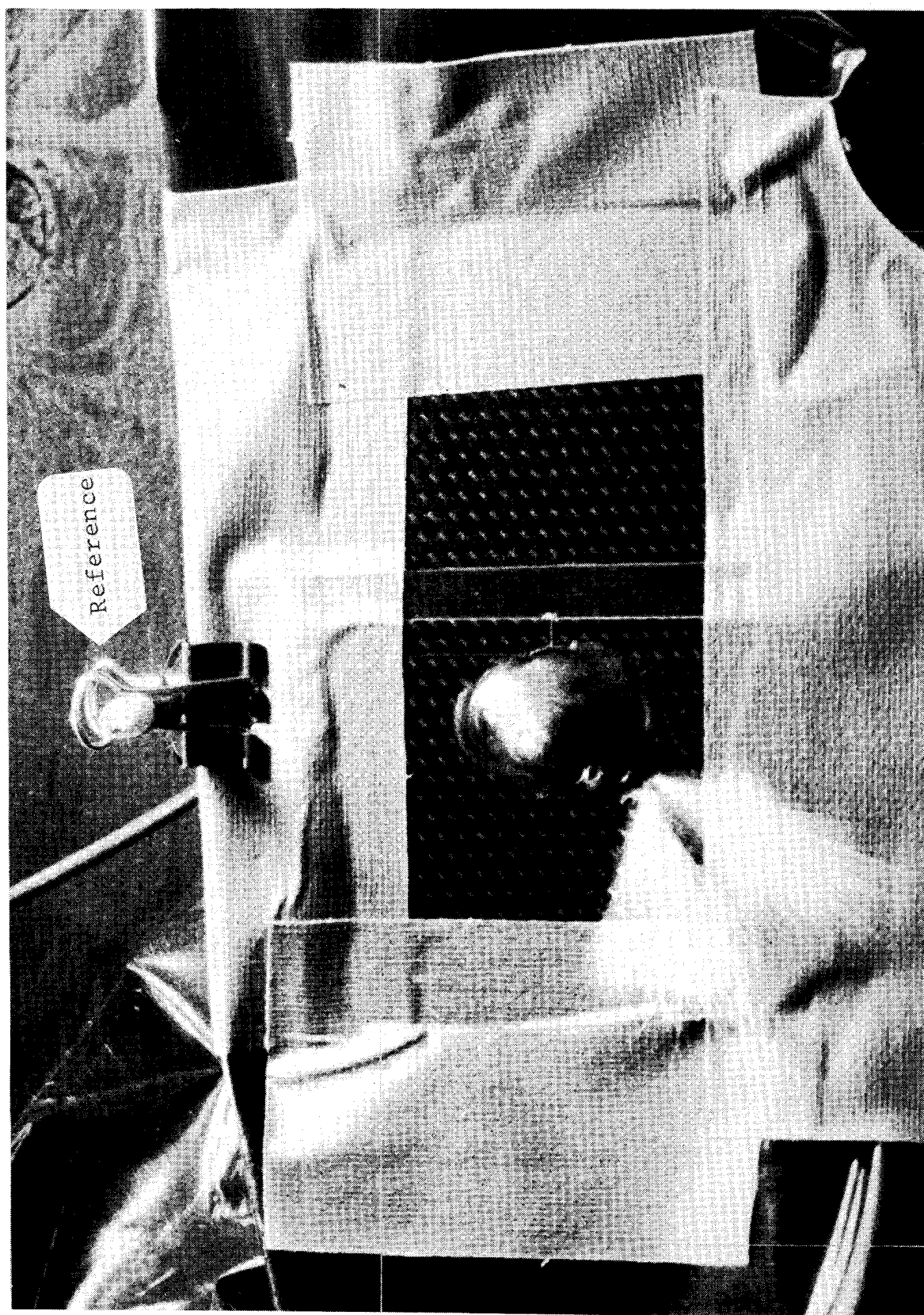


Figure 2.42 - Spark at Access Door Dome Nut due to 17 kA Current Strike.
"Wet" Side View Shown.

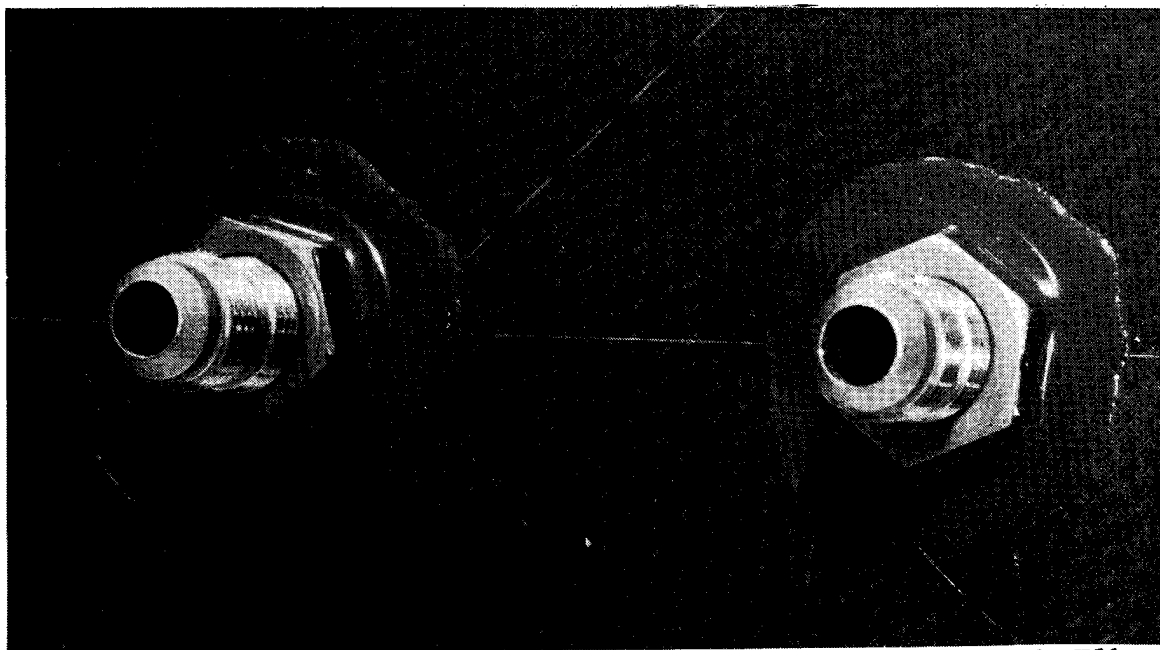
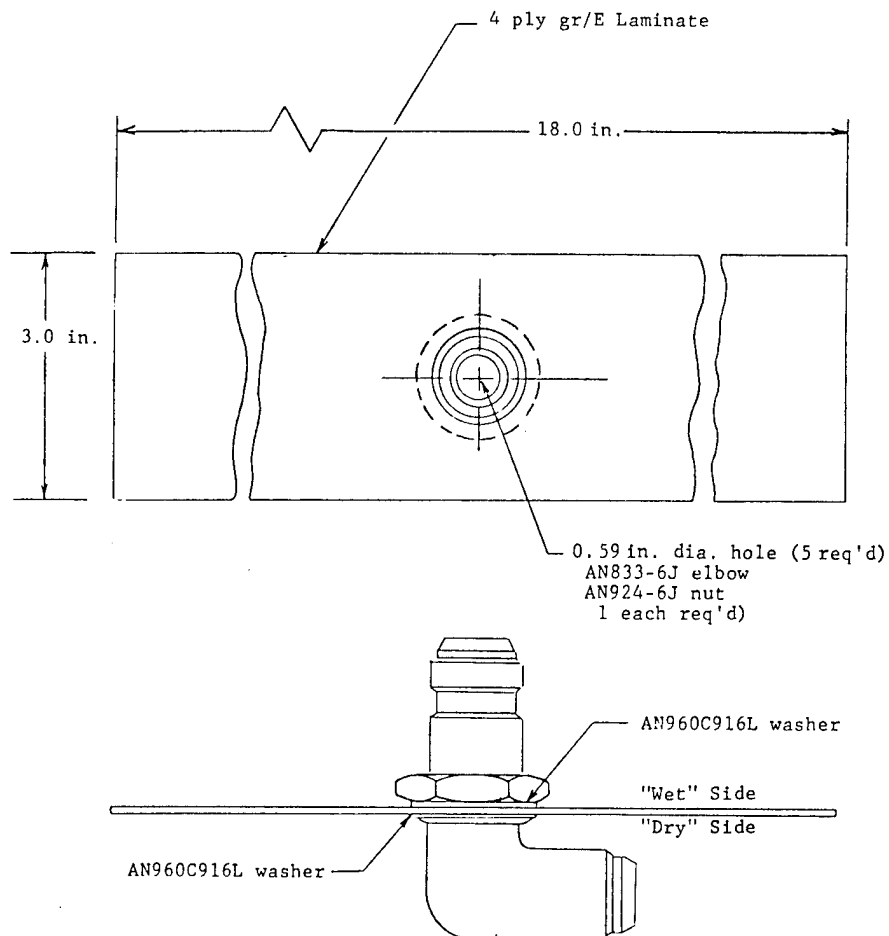


Figure 2.43 - "Wet" Side View of Fuel Line Feed-Through Elbow in gr/E Laminate.

2.6.3.2 - Test Results

The generator "high" side was connected to the "dry" side of the feed-through elbow and generator return was connected to the gr/E "skin". Thus, current flow was into the metallic feed-through elbow, across the washer-gr/E interface, into the gr/E skin and then returned to generator "ground". This circuit, then, represented possible current flow through internal fuel lines as a result of a lightning strike to the wing tip.

Each feed-through elbow was tested with a series of increasing current levels (6, 10, 14, 17 kA) using a $4 \times 50 \mu\text{s}$ wave and 20, 25, 30 and 40 kA using an $8 \times 20 \mu\text{s}$ current wave. Testing on an elbow ceased when a visible spark was detected. Both Pro-Seal and Semkit fuel tank sealant was applied over the washer - gr/E interface on both the "wet" and "dry" skin surfaces. A mirror was positioned to provide a view of the specimen "dry" side during test.

The test results are shown in Figure 2.44.

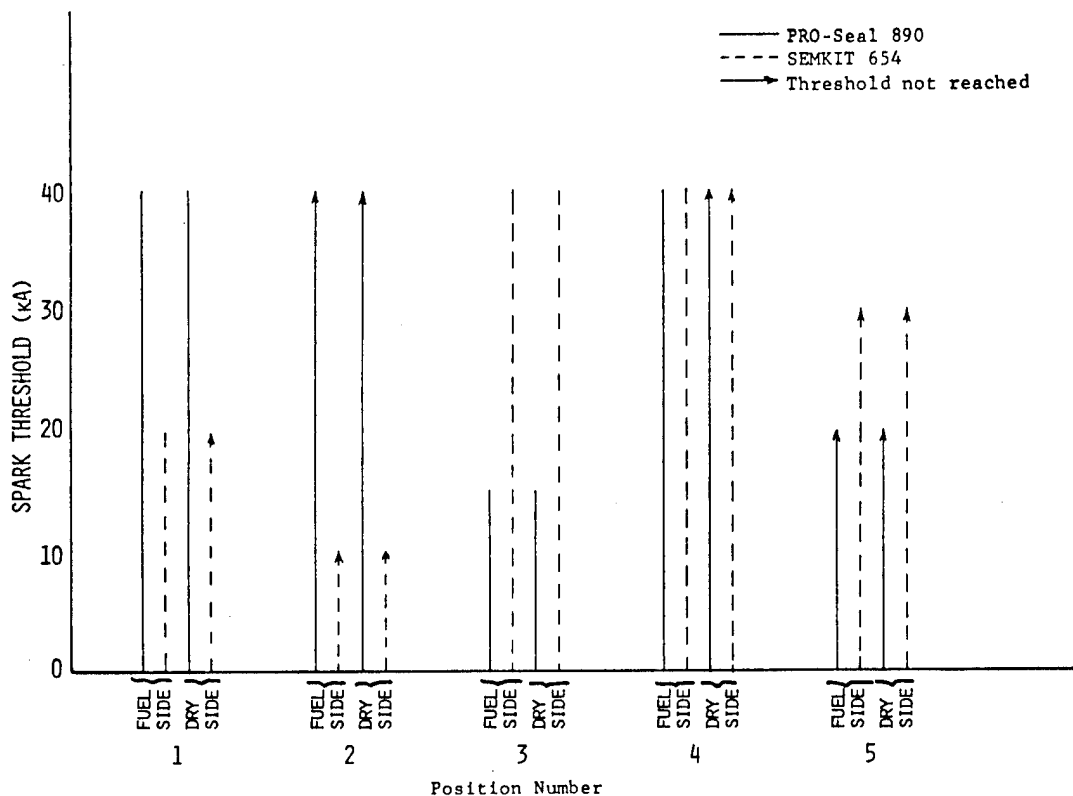


Figure 2.44 - Spark Threshold Levels of Feed-through Elbows in gr/E Laminates.

Examination of the test results indicates that, in general, both Pro-Seal and Semkit sealants provided equal protection against visible sparks. This is in contrast to the results on the rivet and dome nut gr/E interfaces in which the Semkit sealant appeared to provide higher spark threshold levels. The metal to gr/E contact surface provided by the feed-through elbow washers was greater than the contact surfaces provided by the rivet or dome nut specimens; hence, the current density at the interfaces was lower. The lower current density level may have tended to "equalize" the results between the two sealants due to lower internal pressure buildups and could also explain the higher current threshold levels obtained with these specimens. Both sealants were able to prevent visible sparks at levels of 40 kA or higher in some specimens. The minimum threshold level was 10 kA for the Semkit specimens and 14 kA for the Pro-Seal specimens. No difference in spark threshold levels was noted between the "fuel" side and the "dry" side.

Figure 2.45 shows a spark at a feed-through elbow resulting from a current of 15 kA applied to the feed-through elbow. The spark was the result of pressure buildup beneath the sealant due to current flow across the metal washer to gr/E interface. The pressure caused the sealant to tear at the metal-graphite interface allowing release of the arc products and producing a visible spark.

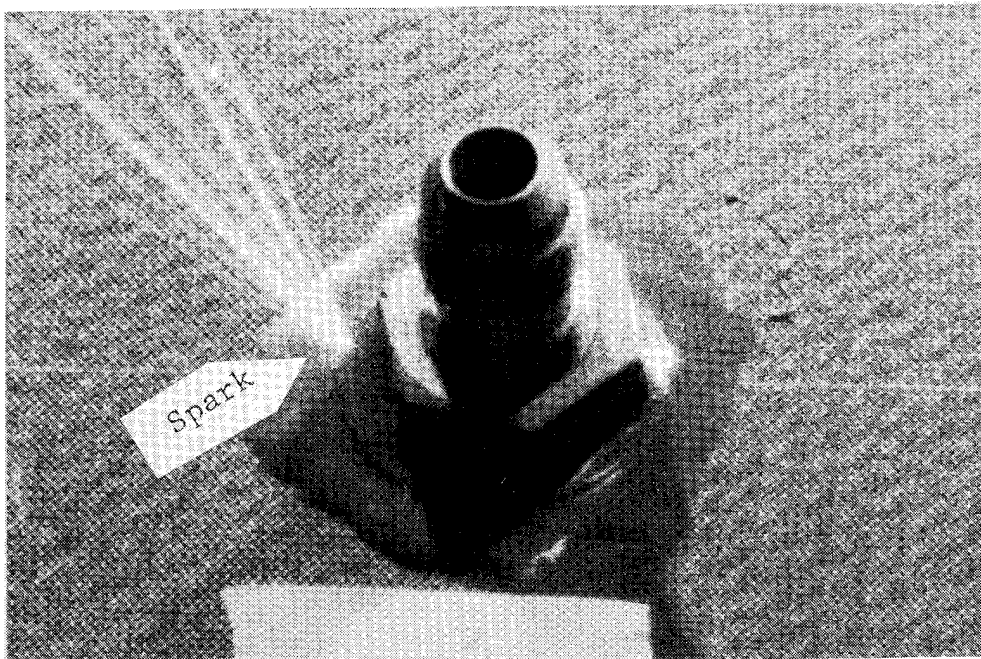


Figure 2.45 - Spark at Washer to gr/E Interface Resulting from a 15 kA Current Strike to the Fuel Feed-through Elbow. Wet side view shown.

3.0 FULL SCALE STRUCTURES TEST PROGRAM

3.1 Purpose

Measurements of the electrical behavior of adhesively bonded aluminum and gr/E coupon-type subelement specimens were conducted during phase one of the program. Whether the voltage and current levels measured during these tests actually existed in full scale structures was the subject of investigation during phase two. Specifically, measurements and tests conducted included the following:

1. Current distribution
2. Bond line voltages
3. Ignition source locations
4. Induced voltages in wing electrical wiring
5. Magnetic field levels

The structures tested were full scale wings containing integral fuel tanks and were typical of general aviation aircraft construction.

The first of the two structures tested was a right hand aluminum wing which contained an adhesively bonded integral fuel tank and outboard leading edge assembly. The remainder of the structure was constructed with conventional rivets and fasteners.

With the exception of the leading edge, tip, and some control surfaces, the second structure was constructed entirely of gr/E composites. The wing was fabricated as one unit (left and right) but only the right wing was tested.

3.2 Basic Test Methods

A brief description of the test setup and procedures is presented in paragraphs 3.2.1 through 3.2.6. A more detailed description of the test specimens and test procedures is presented together with the test results in paragraphs 3.3 and 3.4.

3.2.1 Test setup

The full scale structure was positioned adjacent to the high current generator. Connections between the generator and wing simulated a strike to the wing tip with currents flowing through the wing structure to an exit point at the wing root. Measurement signals were conducted from the wing structure through shielded cables and electrical conduit to a nearby RF shielded room where they were recorded by oscilloscopes.

3.2.2 Current distribution tests

Currents in fuel lines, conduits, control cables and other structural members were measured using a wide-band current transformer which was placed around the conductor to be measured. The measurement signals were transferred through shielded cables and recorded by the oscilloscope.

3.2.3 Bond line voltage measurements

Voltages across bond lines were measured in the fuel tank interiors. One measurement lead was connected to the wing skin and the second was connected to a rib, spar, or stringer. The signals were transmitted by shielded cable to the differential inputs of an oscilloscope and the measurement waveform recorded on an oscillogram.

3.2.4 Ignition source tests

Possible fuel vapor ignition sources were investigated by the placement of cameras within the sealed fuel tank during a simulated strike to the structure. The appearance (or absence) of light ("sparks") on the film negative indicated the presence (or absence) of an ignition source.

3.2.5 Induced voltage measurements in wing electrical wiring

The voltages induced in the wing circuits by the simulated lightning currents were measured using the differential measurement technique. The circuit conductor under test was connected to one input of the oscilloscope differential preamplifier; circuit "ground" was connected to the second input. The measurement cable and instrumentation were shielded to minimize measurement errors due to external fields and electrical "noise".

3.2.6 Magnetic field measurements

Both internal and external magnetic fields were measured using a search coil positioned in each of three orthogonal directions. The signal induced in the coil was transmitted through shielded cable, integrated and recorded by an oscilloscope. The magnetic field intensity was calculated using the search coil calibration factor.

3.3 Bonded aluminum structure

3.3.1 Specimen description

The wing extended from inboard of the right engine nacelle out to and including the wing tip. Except for the wing tip which was made of acrylonitrile-butadiene-styrene (ABS) plastic, the

wing was of aluminum construction. The wing contained one integral fuel tank and outboard leading edge assembly of adhesive bonded construction spanning from nacelle to tip. This was the only part of the wing which was adhesively bonded; elsewhere conventional rivets and fasteners were utilized. Sketches of the wing are shown in Figures 3.1 and 3.2.

The wing test locations hereafter referred to in this report will be referenced in inches from fuselage center line by a wing station (WS) number. For example, the wing box closeout rib which is located 220 in. outboard of the fuselage center line, would be designated WS 220.

3.3.2 Test setup

Figure 3.3 is a photograph showing the laboratory set-up for tests on the bonded aluminum wing.

The wing was arranged to simulate a strike to the wing tip with the lightning currents flowing inboard to an exit point elsewhere on the plane.

The wing was suspended from the ceiling with the leading edge up and the inboard end located at the lightning current generator. Twelve in. width aluminum flashing, connected to the generator output, encircled the wing with provision for attachment to the taxi and navigation lights as shown in Figure 3.4. This arrangement allowed the current to be injected into the wing tip, flow through the wing skin, and return to generator "ground" through the front main, and rear spars at the wing root.

Currents flowing in the aluminum flashing conductors produced nearly equal and opposite magnetic fields between them; thus, the influence of the test circuit magnetic fields on the wing was minimized. In addition, the use of wide conductors minimized the test circuit inductance which was necessary for generation of peak currents of 100 kA or greater. The conductors were positioned as far as practical from the wing surface to enable access to the fuel filler cap and access doors for instrumentation purposes and to minimize the influence of their magnetic fields on the wing structure.

The simulated lightning currents were generated by a 17.25 μ F 70 kV high current capacitor bank in conjunction with waveshaping elements. The currents were measured by a 100:1 ferrite core, impulse current transformer (C.T.) and were recorded by a Tektronix 535A oscilloscope. The simulated lightning current waveform oscillograms are shown in Figure 3.5.

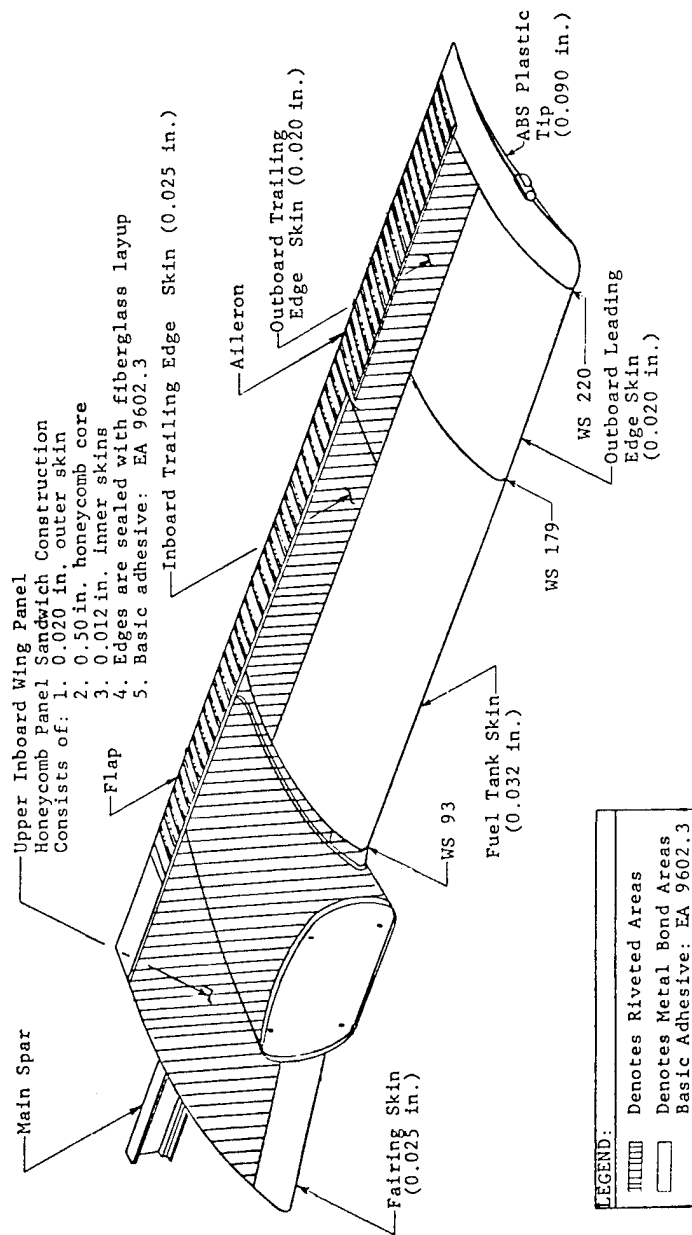


Figure 3.1 - Bonded Aluminum Wing - Exterior View

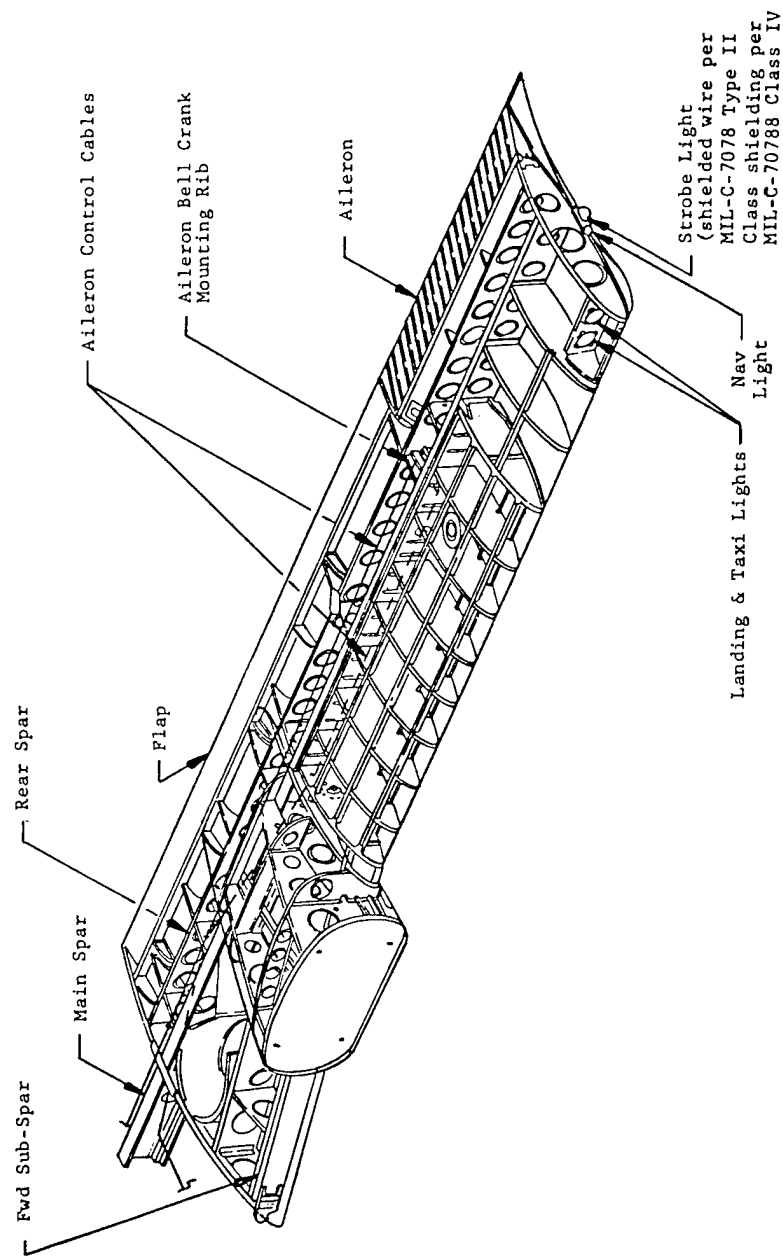


Figure 3.2 - Bonded Aluminum Wing - Interior View.

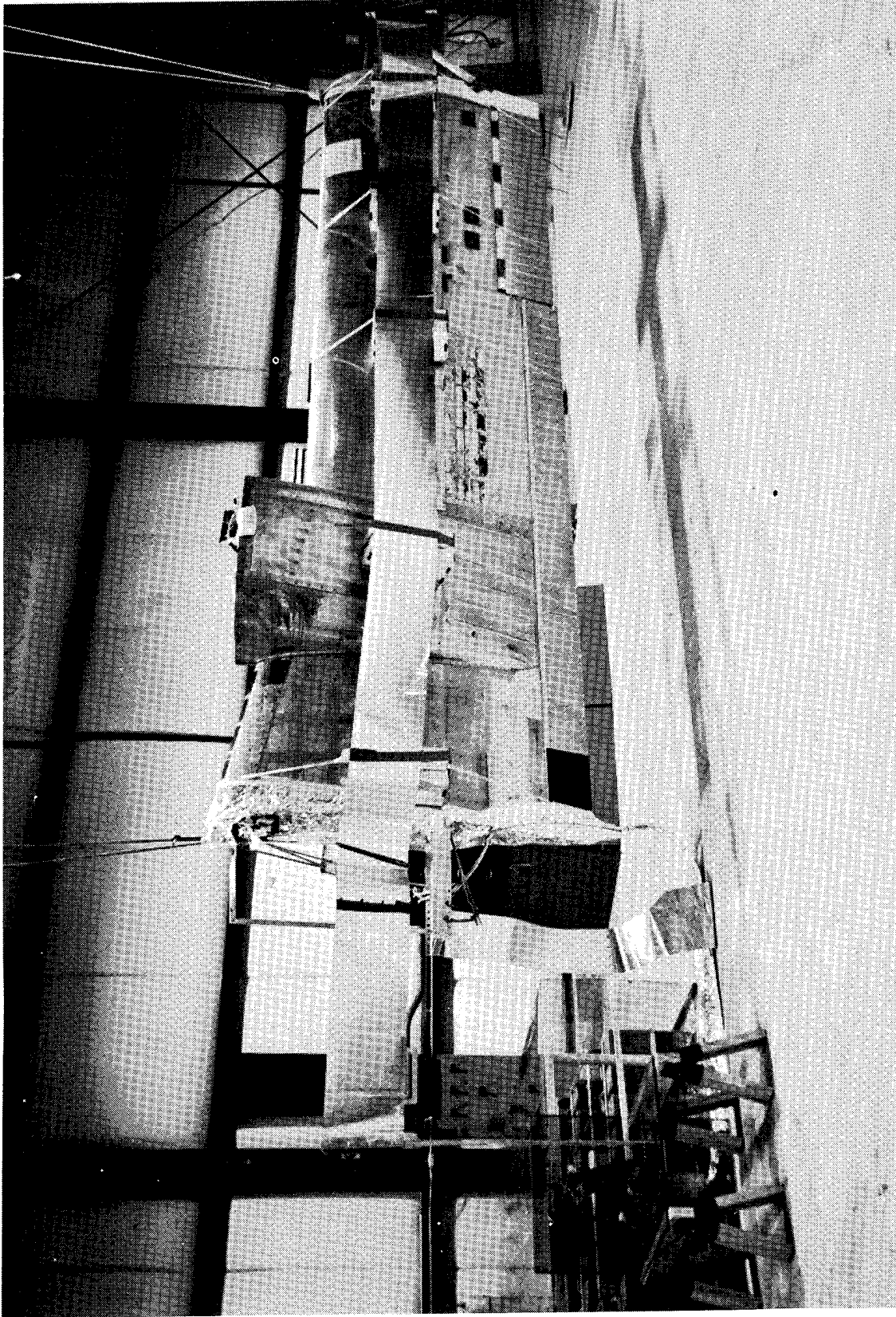


Figure 3.3 - Laboratory Setup of Bonded Aluminum Wing.

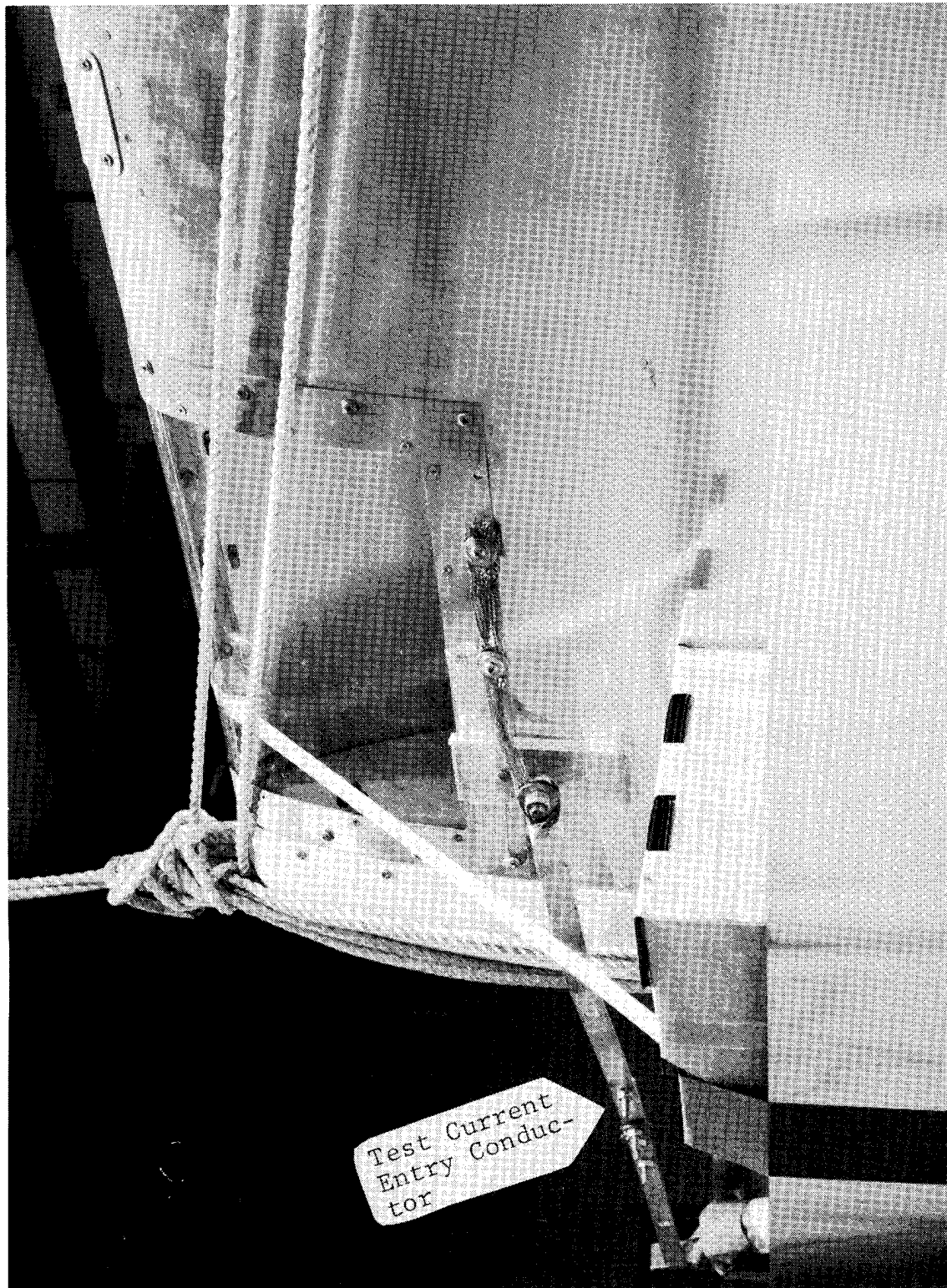
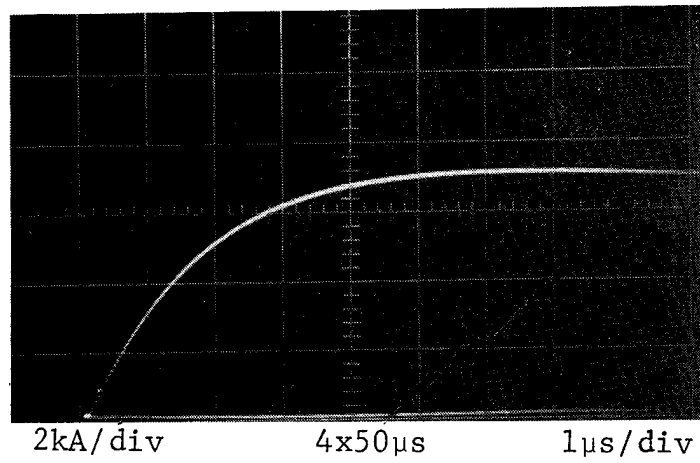
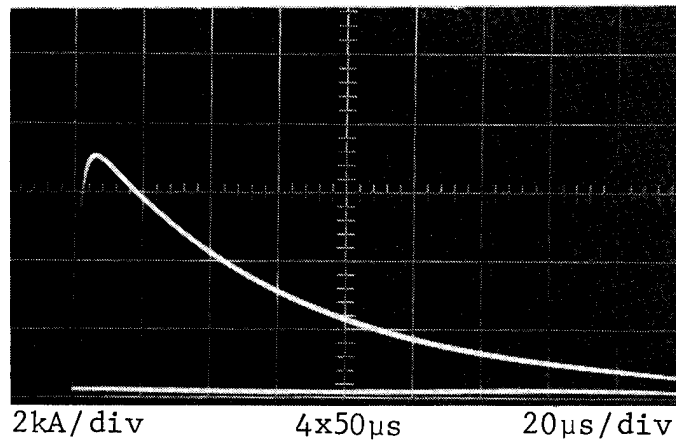


Figure 3.4 - Connection for Simulated Strike to Taxi Light Housing
on Bonded Aluminum Wing.

Test 2146



Test 2145



Test 2207

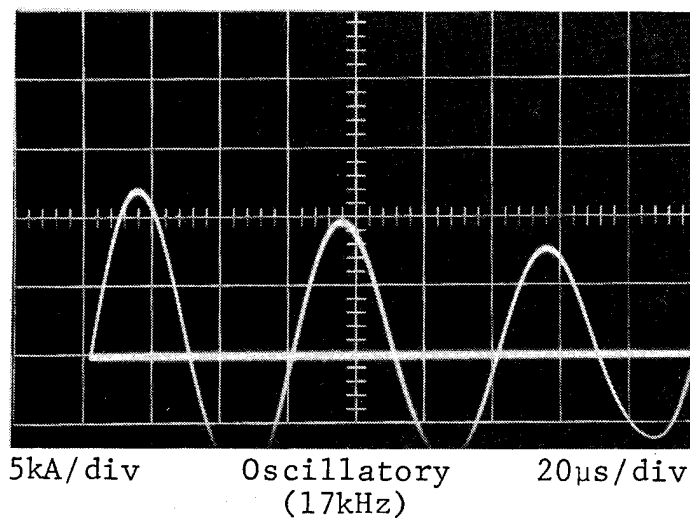


Figure 3.5 - Simulated Lightning Current Waveforms.

3.3.3 Test procedures

3.3.3.1 Current distribution

Measurement of currents in internal structural members and fuel lines was limited to those members which could be physically fitted with the current transformer. The current transformer was a Pearson Model 110A which had a current times time (IT) product of 0.5 A.s and a frequency response of 1 Hz to 35 MHz. RG-58/U coaxial cable connected to the current transformer, routed the measurement signal from the wing to a Tektronix 7704A oscilloscope located in the RF shielded room. The cable was routed as far as practicable within the wing structure to shield the signal from the influence of external fields. Aluminum foil and electrical conduit provided shielding between the wing and the RF shielded room.

The cable was terminated in 50 Ω at the Tektronix 7704A oscilloscope.

The simulated lightning current, which was injected into the taxi light housing, was a 16 kHz oscillatory wave with peak amplitudes ranging from 12 to 88 kA.

Measurements were made of currents in fuel lines (outside the fuel tank) and the forward and rear spars.

3.3.3.2 Bond line voltages

Lightning currents flowing through the aluminum wing skin can raise its voltage potential with respect to structural or fuel system components which may be electrically isolated from the skins. If the voltage potential difference between the skin and these components exceeds the withstand capability of the insulating medium (adhesive or air), breakdown will occur and the resulting spark could be a possible fuel ignition source.

Measurements were recorded across bond lines with the fuel tank interior between wing locations WS 153.75 and WS 164.65. Both spar-to-skin and rib-to-skin bond line voltages were measured.

A "ground" measurement reference plane was established at the fuel tank skin by attaching 14 in. wide aluminum flashing between the skin and a grounded electrical junction box. Two RG-58/U coaxial cables, shielded with aluminum foil, conducted the measurement signals from the tank interior, to the electrical box, and through electrical conduit to the measurement oscilloscope located in the RF shielded room. The influence of external magnetic fields was minimized by maintaining contact between the shielded measurement cables and the aluminum flashing ground plane as shown in Figure 3.6.

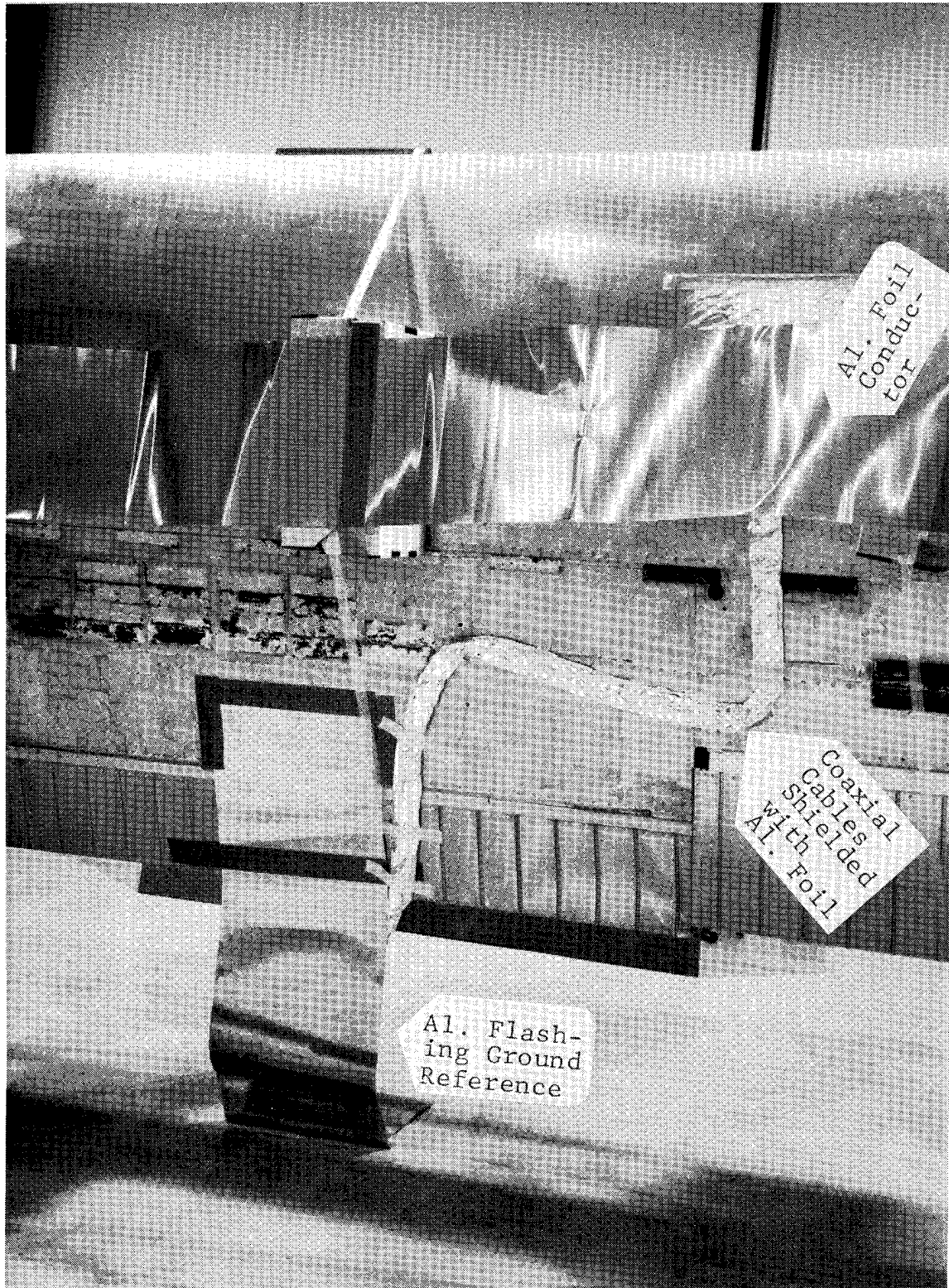


Figure 3.6 - Lab Setup for Measurement of Bond Line Voltages on Bonded Aluminum Wing.

One test lead was connected to the wing lower skin with a self-tapping screw; the second lead was connected to the rib or stringer under test.

The simulated lightning current unipolar and oscillatory waves were injected into the wing at the taxi light housing. The voltage potential which developed across the bond lines was measured by the shielded coaxial cables and recorded by a Tektronix 7704A oscilloscope with a type 7A13 preamplifier. The test circuit schematic is shown in Figure 3.7.

3.3.3.3 Ignition source tests

Lightning Currents flowing through an aircraft structure, such as a wing, can produce sparking across joints, especially those which are bonded with a nonconductive adhesive. In the aluminum wing, bonded joints were located within the fuel tank area; thus, a spark across one of these joints would present an ignition source hazard.

The method employed to detect possible sparks in the fuel tank was similar to that described in paragraph 2.2.4 for spark detection during the subelement tests. The size of the fuel filler cap opening prevented insertion of a Polaroid camera into the fuel tank; the spark detection was limited to the use of a more compact 35 mm camera equipped with an equivalent lens/film speed combination.

The simulated lightning strikes of 85 kA - 100 kA peak amplitude were conducted into the taxi light housing and returned to the generator through the front, main, and rear spars at the wing root end to represent the effects of stroke currents being conducted through the structure between the wing tip and wing root. It was recognized that direct strikes to the fuel tank skin were also possible since portions of this tank lie aft of the propeller. However, as noted in paragraph 1.2.2.3 the effects of direct strikes to integral fuel tank skins were not a part of this investigation. The 85 kA - 100 kA peak current, which represents a moderately severe stroke, represented the limits of the test facility generator.

The camera lens was positioned in each of the four orthogonal wing directions during the simulated strikes to the taxi light housing. These directions included views toward the upper and lower wing skin surfaces and toward the wing tip and root ends. The fuel tank was sealed for each tests and a test frame was recorded prior to each test to verify that the fuel tank was light-tight. The test circuit schematic is shown in Figure 3.8.

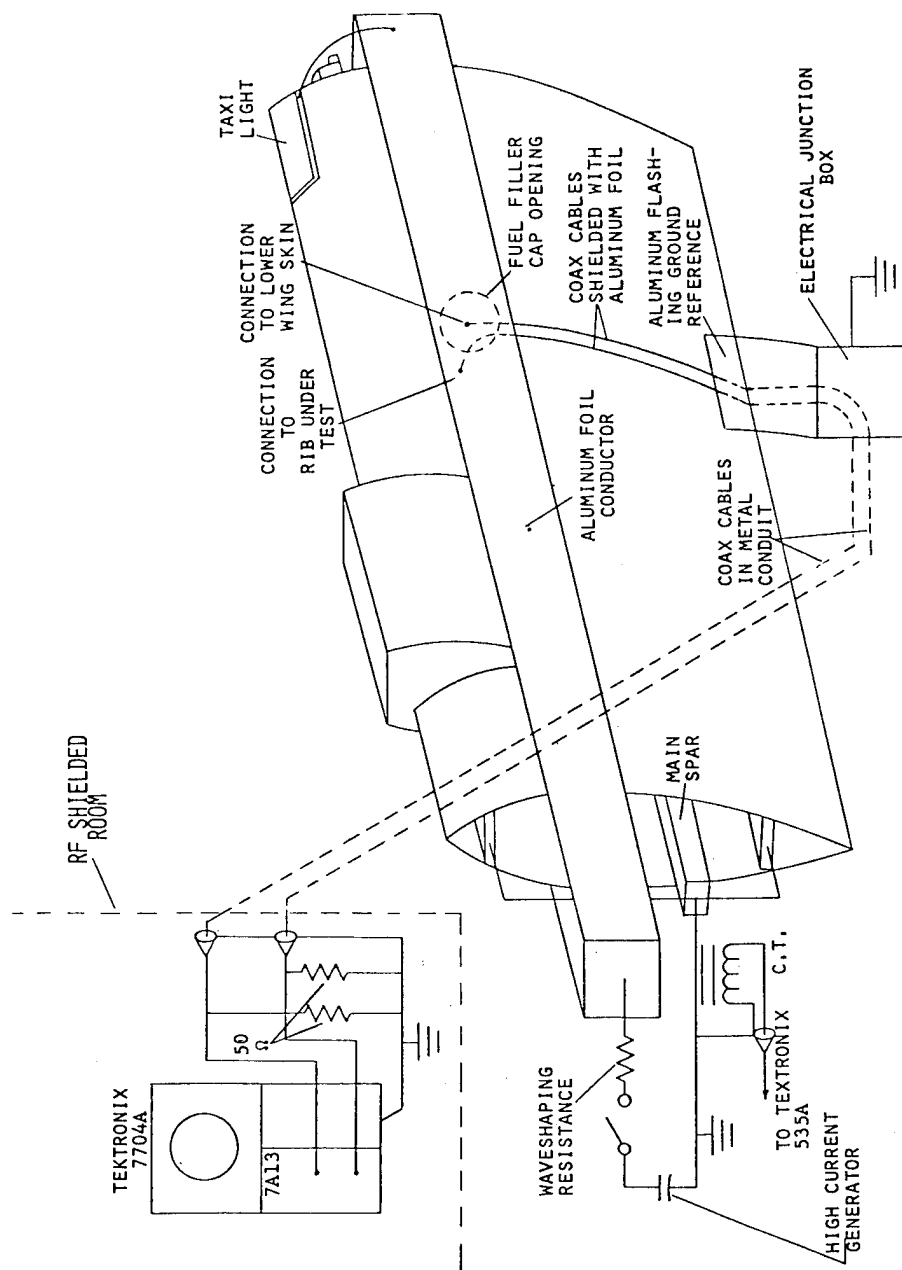


Figure 3.7 - Schematic for Measuring Bond Line Voltages in Fuel Tank of Bonded Aluminum Wing.

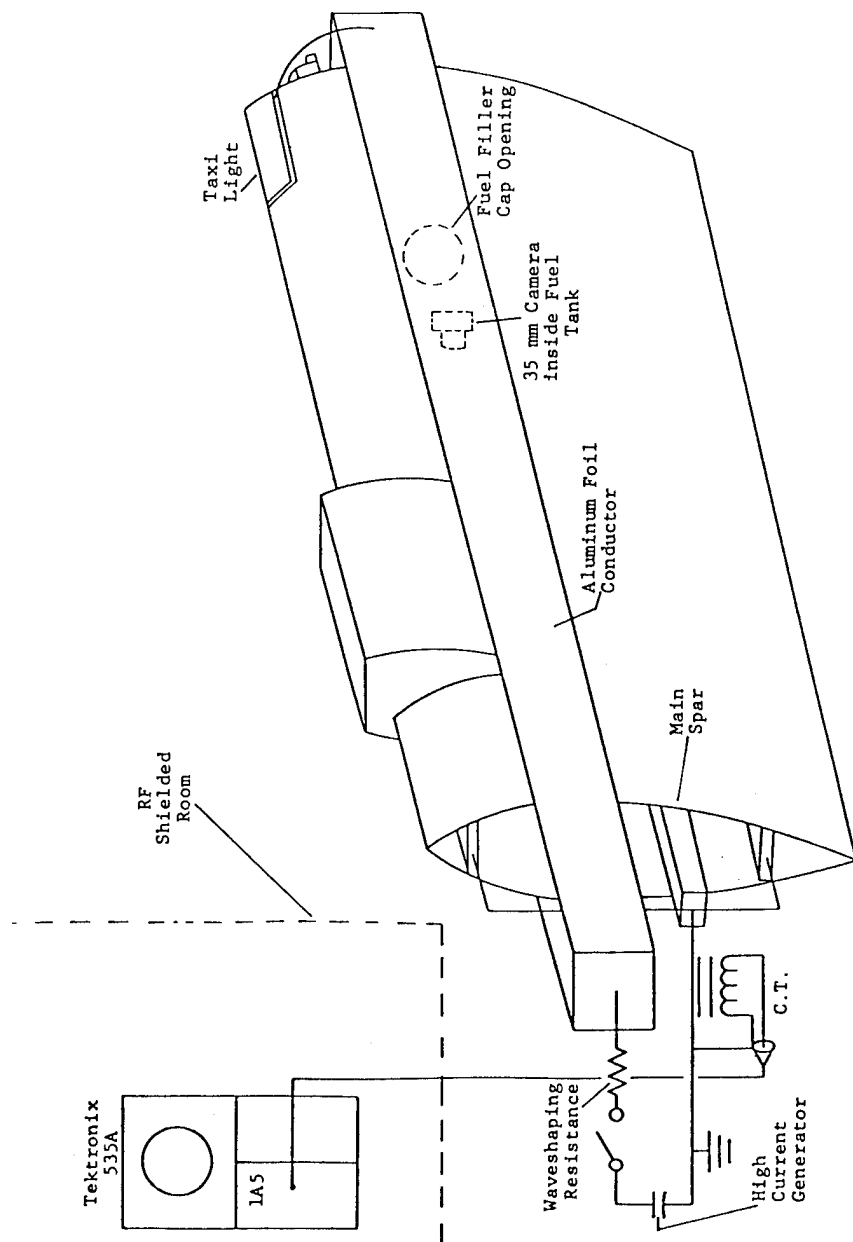


Figure 3.8 - Circuit for Ignition Source Tests in Bonded Aluminum Wing.

3.3.3.4 Induced voltages in wing electrical wiring

The electrical circuits contained within the bonded aluminum wing included the following:

- Right hand taxi light
- Right hand navigation light
- Strobe lamp and power supply
- Inboard & outboard fuel quantity transmitters
- Auxiliary fuel pump
- Alternator
- Overvoltage relay
- Fuel primer solenoid
- Heater fuel solenoid
- Right hand oil pressure transducer
- Right hand cylinder head temperature transmitter
- Right hand oil temperature sensor
- Voltage regulator
- Right hand stall switch
- Fuel pressure transducer

A wire from each of these circuits was accessible for test connections at the wing root. RG-58/U coaxial cable connected each circuit under test to channel "A" of a Tektronix 7704A type 7A13 differential preamplifier. A second coaxial cable (circuit return) connected a wing inboard rib to the preamplifier channel "B" input. By differentially subtracting the readings of the measurement and return lines, errors due to electrical "noise" were minimized. Additional noise reduction techniques included shielding of the coaxial cable measurement lines with aluminum foil and electrical conduit, and locating the measurement instruments within an RF shielded room.

A 10:1 resistive voltage divider, inserted into the measurement circuit, protected the oscilloscope preamplifier circuitry by limiting the voltage level appearing at its terminals. The divider consisted of two sets of five 100 Ω resistors which fed the coaxial cables terminated in 50 Ω at the oscilloscope preamplifier. Simulated lightning currents were injected into the taxi or navigation lights and were removed from the wing at its root end through connections between the forward, main, and rear spars and generator "ground"

A photograph of the instrument cable and test current connections is shown in Figure 3.9. The test circuit schematic is shown in Figure 3.10.

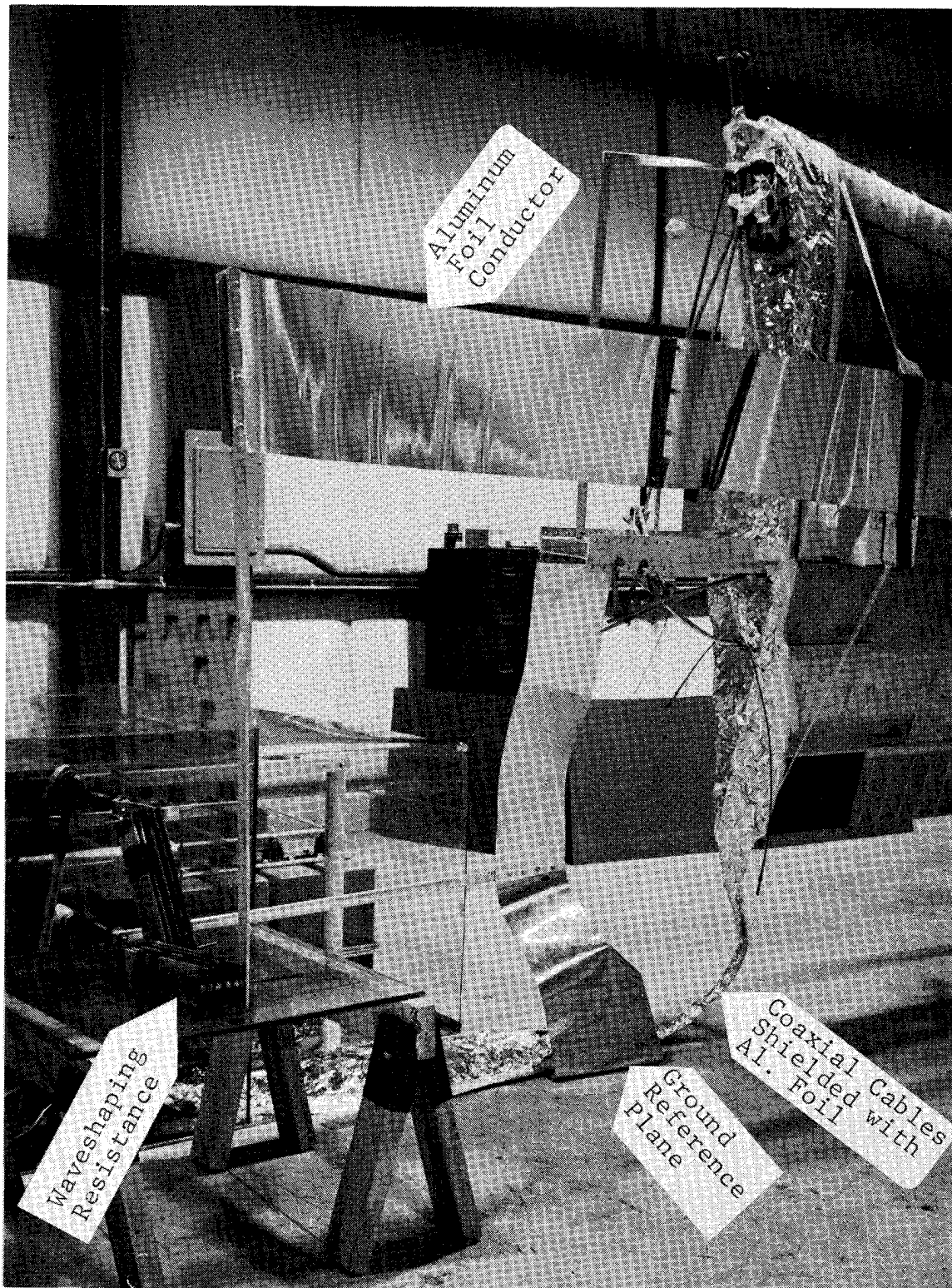


Figure 3.9 - Root End of Bonded Aluminum Wing Showing Shielded Instrument Cables and Test Current Connections for Measuring Induced Voltages in Wing Electrical Wiring.

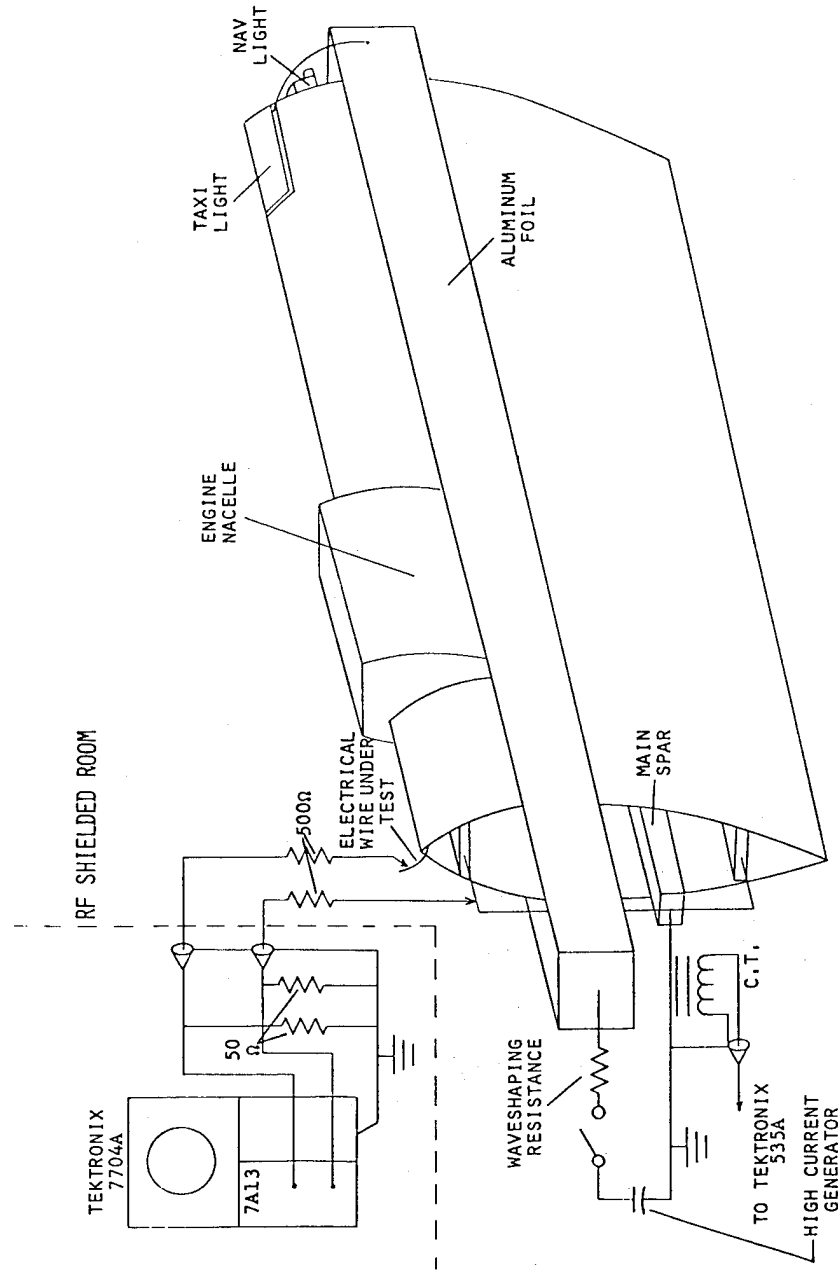


Figure 3.10 - Circuit for Measurements of Induced Voltages in Bonded Aluminum Wing Electrical Wiring.
Note: Connection to taxi light shown.

3.3.3.5 Magnetic field measurements

The magnetic field intensity within the wing fuel tank and along its exterior surface was measured with the aid of search coils. The changing magnetic flux ($d\phi/dt$) produced by these fields induced a voltage signal in the search coil. This signal was then integrated by a passive RC integrator and recorded by a Tektronix 7704A oscilloscope with Type 7A13 preamplifier. The magnetic field intensity (H) at the coil measurement location was then calculated from the measurement oscillogram and the calibration factor of the search coil.

Three different search coils and two passive integrators were utilized. The specifications are given in Table 3-1.

Table 3-1 - Specifications for Search Coils and Passive Integrators Utilized in Magnetic Field Measurements

	<u>Search Coil</u>		
	<u>Single Layer</u>	<u>Multi-Layer</u>	<u>Single Layer</u>
Number of Turns	20	20	100
Effective Diameter	2.4 inches	2.4 inches	2.4 inches
Inductance	$\sim 30\mu\text{H}$	$\sim 23\mu\text{H}$	$\sim 885\mu\text{H}$
Resistance	$\sim 0\Omega$	$\sim 0\Omega$	$\sim 30\Omega$

<u>Passive Integrator</u>		
<u>R</u>	<u>C</u>	<u>Time Constant</u>
10 k Ω	0.10 μF	1 ms
1 k Ω	0.01 μF	10 μs

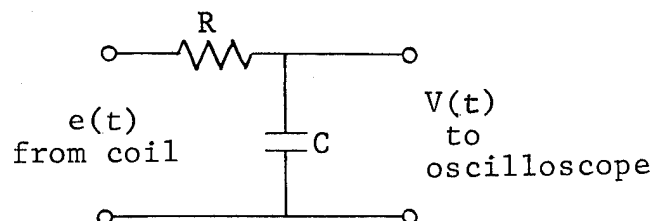


Figure 3.11 - Passive Integrator Schematic.

The magnetic field intensity can be related to the integrated coil signal as follows (refer to schematic diagram of passive integrator in Figure 3.11).

$$\frac{e(t)}{R} = C \frac{dV(t)}{dt} \quad (R \gg |X_C|) \quad (3.1)$$

$$V(t) = \frac{1}{RC} \int_0^t e(t) dt \quad (3.2)$$

$$e(t) = N \frac{d\phi}{dt} = NA \frac{dB}{dt} = \mu_0 NA \frac{dH}{dt} \quad (3.3)$$

$$V(t) = \frac{\mu_0 NA}{RC} \int_0^t \left(\frac{dH}{dt} \right) dt \quad (3.4)$$

$$H(t) = \frac{RC}{\mu_0 NA} V(t) \quad (3.5)$$

where:

$e(t)$ = search coil voltage (volts)

$V(t)$ = integrator output voltage (volts)

ϕ = magnetic flux through coil (webers)

B = magnetic flux density through coil (webers/meter²)

H = magnetic field intensity (amperes/meter)

μ_0 = permeability of free space ($4\pi \times 10^{-7}$ weber/ampere-meter)

N = no. of turns of search coil

A = area of search coil (meter²)

R = resistance of integrator coil (ohm, Ω)

C = capacitance of integrator (farads, F)

t = time (seconds)

Equation (3.5) gives the theoretical relationship between the magnetic field intensity at a given point and the integrated signal of a search coil responding to the changing magnetic field at that point.

The coil calibration factors was determined experimentally using the test setup shown in Figure 3.12.

The calibration test fixture was approximately 10 ft long with a center wire conductor which was connected to the simulated lightning current generator "high" side. The conductor was connected to 16 return wires at the far end of the test fixture (Figure 3.12 shows only four return wires to retain clarity). The return wires were strung back to the near end of the fixture in a radial configuration with each return wire equidistant from the center conductor. The return wires were fastened together and connected to the ground side of the generator. The search coil being calibrated was located at a known distance, r , from the center conductor of the test fixture with its axis perpendicular to the conductor.

A current impulse which was measured by a current transformer and recorded by a Tektronix 535A oscilloscope, was applied to the center conductor, and the voltage induced in the search coil was measured by the integrator and recorded on a Tektronix 7704A oscilloscope. The magnetic field intensity (H) at the search coil location was calculated from the relationship

$$H = \frac{I}{2\pi d} \quad (3.6)$$

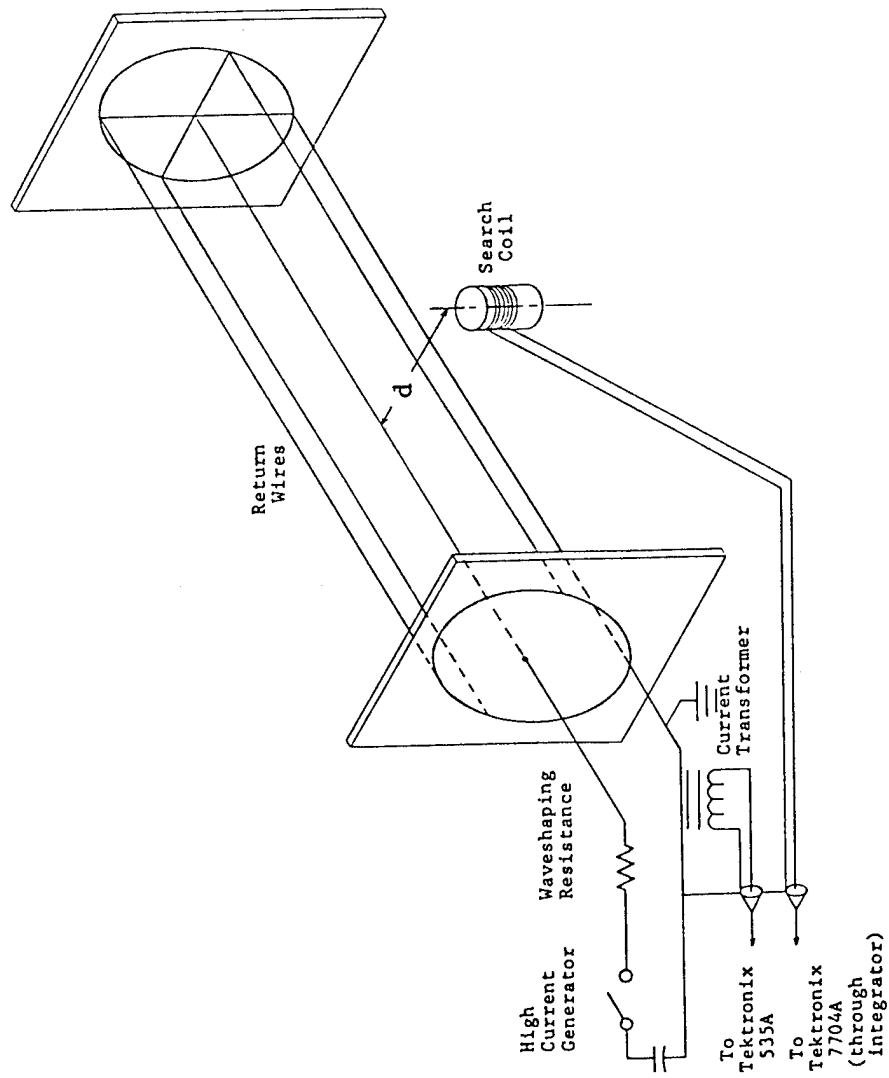


Figure 3.12 - Test Setup for Search Coil Calibration.

where the field intensity (H) is in A/m, the current, I, is in amperes and the distance is in meters. The coil calibration factor, then, is H/V or the magnetic field intensity per volt of the integrated coil signal and has the units of amps per meter per volt.

The test circuit used for the measurement of magnetic field intensity within the wing structure is shown in Figure 3.13.

The RG-58/U coaxial cable measurement lines, which conducted the search coil signals to the measurement and recording instruments, were routed as far as practical within the wing structure to utilize its shielding capabilities. Externally, the cables were shielded by aluminum foil and metal conduit until their entrance into the RF shielded room. The coil signals were measured by a Tektronix 7704A oscilloscope with a Type 7A13 preamplifier.

Measurements of the magnetic field intensities were made in the three orthogonal axes as shown in Figure 3.13.

The magnetic fields were generated by simulated lightning currents as they flowed through the wing structure from the taxi light housing at the wing tip to their exit point from the forward, main and rear spars at the root end of the wing. Unipolar and oscillatory current waves were utilized for these tests.

3.3.4 Test results

3.3.4.1 Current distribution

A summary of test results is shown in Table 3-2 and typical current oscillograms are shown in Figure 3.14. The locations of the test measurements are given in Figure 3.15.

The noise level measured during test 2409 was 2 amperes. Currents in the fuel lines ranged from a maximum of 16 amperes to a minimum of less than 1 ampere for a test current of 12 kA. Increasing the test current to 88 kA resulted in a fuel line current level of 160 amperes and a noise level of 30 amperes. At either level, the currents measured in the fuel lines were less than 0.2% of the test current.

The distribution of currents in the spar was recorded during tests 2423-2426. During a 19 kA test current strike, a current of 2.5 kA was measured in the forward spar and 190A was measured in rear spar. The data indicate that the main spar carried 86% of the stroke current, the forward spar 13% and the rear spar 1%.

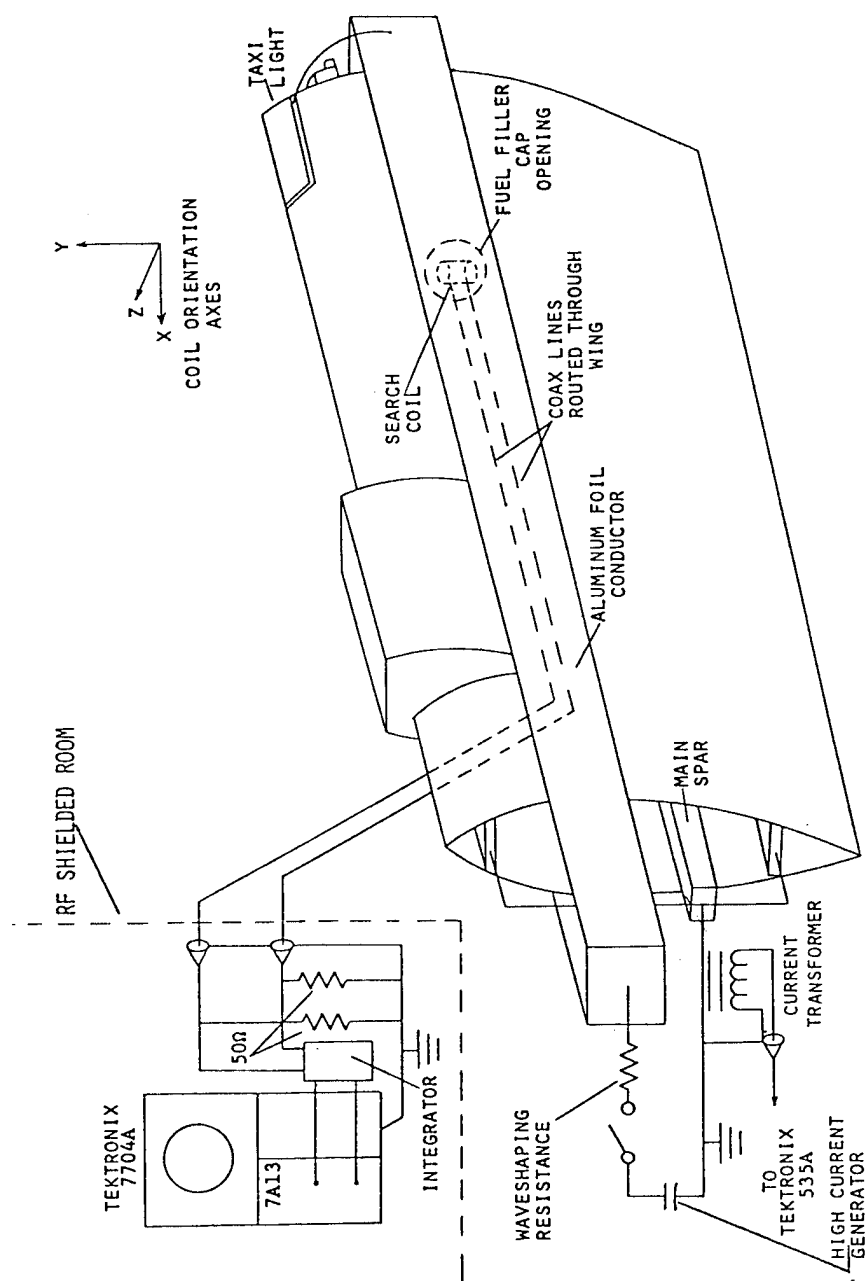


Figure 3.13 - Test Circuit for Measuring Magnetic Field Intensities in Bonded Aluminum Wing.

Table 3-2 - Current Distribution in Fuel Lines and Spars of the Bonded Aluminum Wing

<u>Test No.</u>	<u>Measurement Location</u>	<u>Test Current kA</u>	<u>Measured Current A</u>	<u>Remarks</u>
2409	Fuel line	12	2	Noise measurement
2410	Fuel line	12	2	
2411	Fuel line	12	16	
2412	Fuel line	12	14	
2413	Fuel line	12	<1	
2414	Fuel line	12	<1	
2421	Fuel line	88	160	
2422	Fuel line	88	30	Noise measurement
2423	Forward Spar	19	2500	
2424	Forward Spar	19	800	Noise measurement
2425	Rear Spar	19	60	Noise measurement
2426	Rear Spar	19	190	

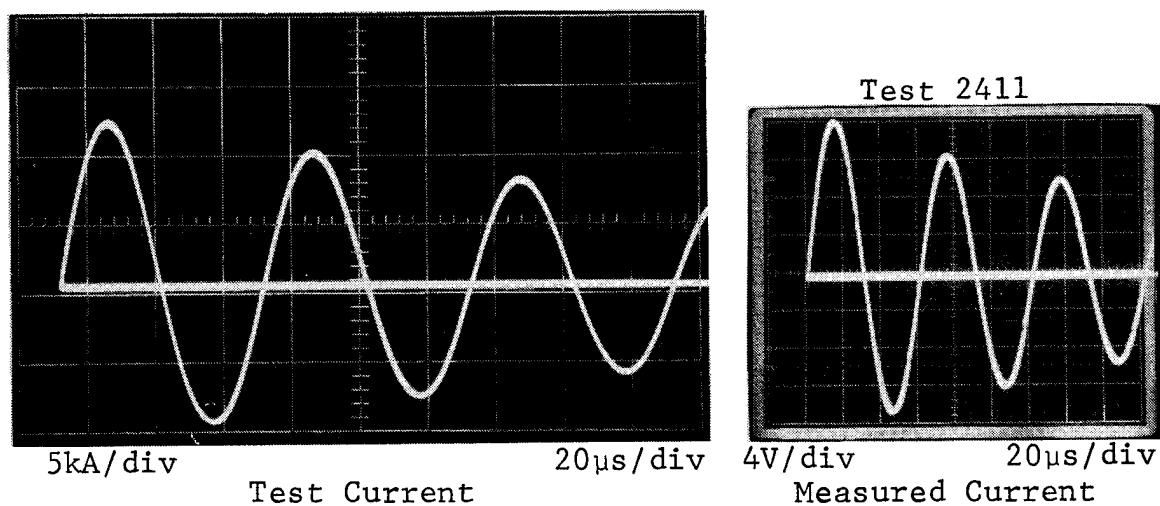


Figure 3.14 - Typical Current Oscillograms Obtained during Current Distribution Measurements in Bonded Aluminum Wing.

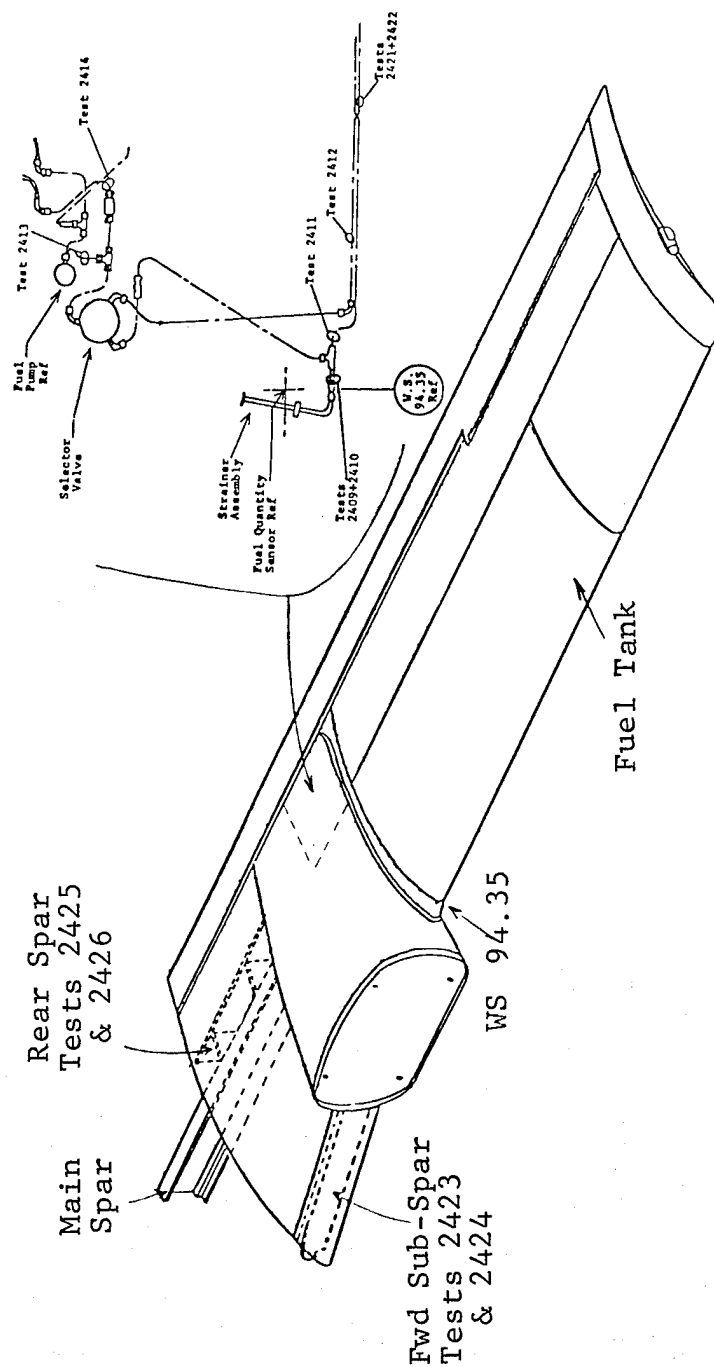


Figure 3.15 - Locations of Current Distribution Measurements.

3.3.4.2 Bond line voltages

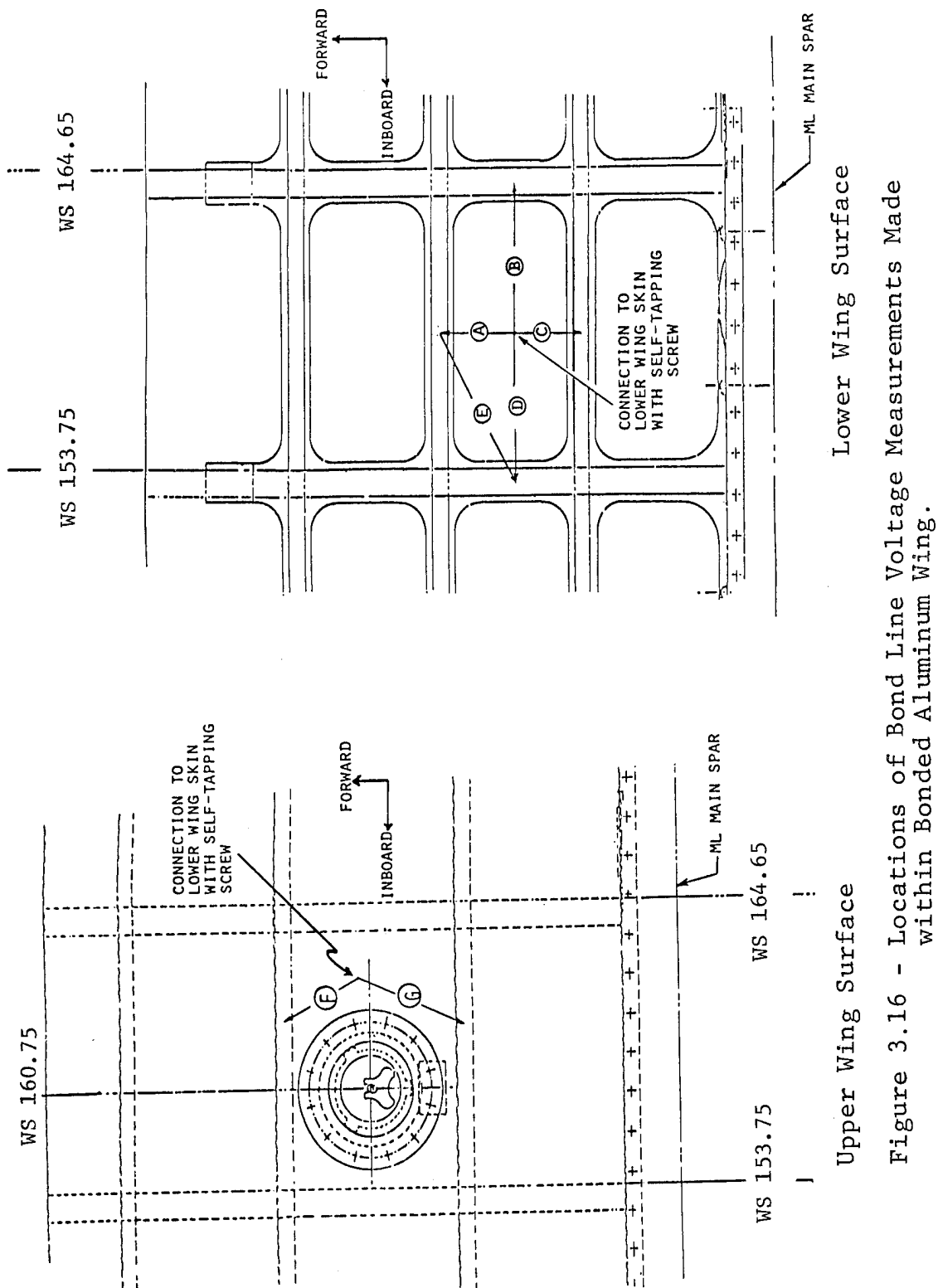
Measurements of bond line voltages were made in the fuel tank interior between WS 153.75 and WS 164.65 as shown in Figure 3.16. The test results are summarized in Table 3-3.

Table 3-3 - Bond Line Voltages Inside Bonded Aluminum Wing Fuel Tank. Simulated Strike to Taxi Light Housing.

<u>Test No.</u>	<u>Input Current</u>	<u>Measurement Location(a)</u>	<u>Measured Voltage (V)</u>	<u>Remarks</u>
2236	11kA, 17kHz	--	0.04	Noise check - Test leads shorted to each other inside tank
2237	11kA, 17kHz	A	0.10	
2238	11kA, 17kHz	C	0.14	
2239	11kA, 17kHz	D	0.10	
2240	11kA, 17kHz	E	0.10	
2241	11kA, 17kHz	B	0.11	
2242	11kA, 17kHz	G	0.05	
2243	11kA, 17kHz	F	0.06	
2244	7kA, 4x50 μ s	F	0.05	
2245	7kA, 4x50 μ s	G	0.03	
2246	7kA, 4x50 μ s	B	0.10	
2247	7kA, 4x50 μ s	E	0.04	
2248	7kA, 4x50 μ s	D	0.07	
2249	7kA, 4x50 μ s	C	0.10	
2250	7kA, 4x50 μ s	A	0.08	
2251	7kA, 4x50 μ s	-	0.02	Noise check - Test leads shorted to each other inside tank

(a) See Figure 3.16

Readings obtained with each of the input current waves were 0.14 volts or less. The noise level, which was 0.04 volts or less, was greater than 10% of the measured values. The low test readings seemed to indicate that the bond line voltage readings were primarily due to noise pickup. Apparently the adhesive joints were not isolated but had metal-to-metal contact at one or more locations.



3.3.4.3 Ignition source tests

Table 3-4 is a summary of results. The test photographs showed that no light sources existed during the simulated lightning strikes to the taxi light housing indicating the lack of a fuel vapor ignition source. Figures 3.17 through 3.20 are photographs of the fuel tank interior during these tests.

Table 3-4 - Summary of Ignition Source Test Results on Bonded Aluminum Wing

<u>Test No.</u>	<u>Test Current (kA)</u>	<u>Camera Lens Direction</u>	<u>Results</u>	<u>Photograph Figure No.</u>
2417	100	Inboard	No light	3.17
2418	85	Lower wing surface	No light	3.18
2419	90	Upper wing surface	No light	3.19
2420	90	Outboard	No light	3.20

3.3.4.4 Induced voltage in wing wiring

Table 3-5 is a complete record of the induced voltage measurement test results. In addition to the measured values, the test results have been extrapolated for an average stroke of 20 kA and a severe stroke of 200 kA.

Table 3-6 summarizes the induced voltage measurement test results which have been grouped by the circuit return path configuration. These paths include an independent return within the wing, airframe return within the wing, and airframe return from the plastic wing tip. Representative circuits for each of these configurations are presented in Figures 3.21 to 3.24. The figures include wire numbers, connectors, and pertinent interfacing electronics. The accompanying oscillograms, which show the induced voltage waveforms, are referenced by arrows to the measurement point. Each oscillogram includes the amplitude, sweep scale settings and test number.

3.3.4.4.1 Independent return within wing: Figure 3.21 shows voltage induced in the right hand stall switch to battery line W4C22 by the 4 x 50 μ s unipolar and the 17 kHz oscillatory simulated lightning current waves. Since the wing structure is not utilized for circuit return, the induced voltage is proportional only to the rate of change of the simulated lightning current (i.e. there is no structural IR component). This concept is illustrated in Table 3-7. The initial rates-of-rise of the unipolar and



Figure 3.17 - Interior of Fuel Tank during Ignition Source Tests.
(camera view - inboard) No Light Sources.



Figure 3.18 - Interior of Fuel Tank during Ignition Source Tests.
(camera view-lower wing surface) No Light Sources.

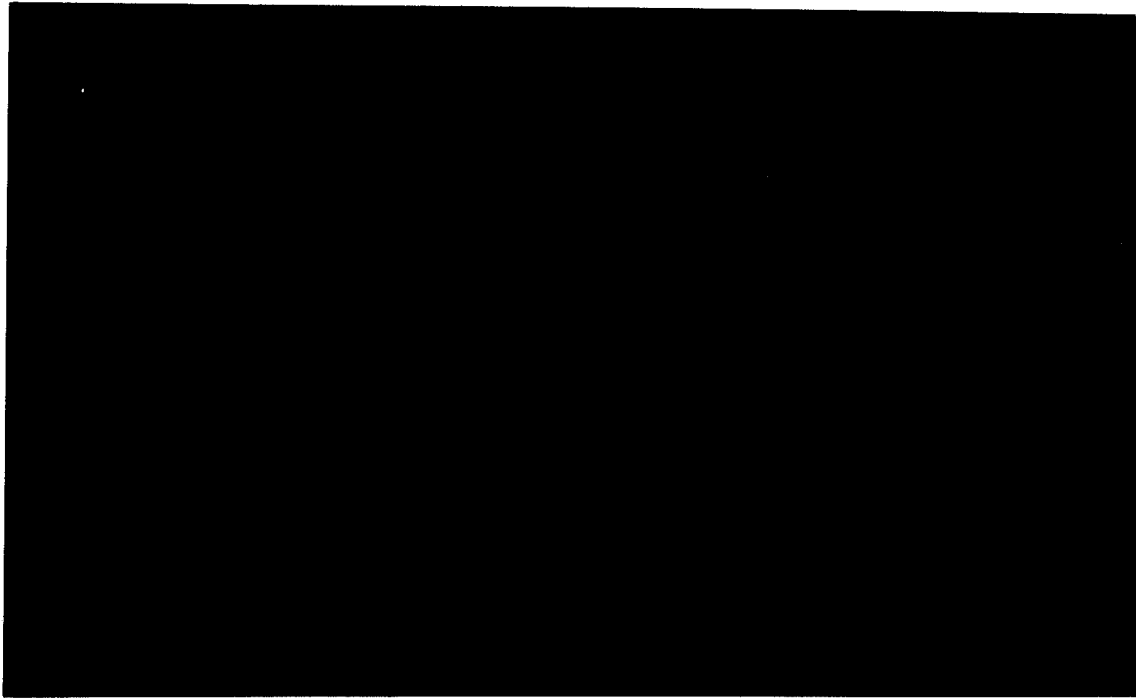


Figure 3.19 - Interior of Fuel Tank During Ignition Source Tests. (camera view-upper wing surface)
No Light Sources.



Figure 3.20 - Interior of Fuel Tank During Ignition Source Tests. (camera view-outboard) No Light Sources.

Table 3-5 - Induced Voltages in Electrical Wiring
7kA, 4x50 μ s Simulated Strike

Test No.	System & Wire No.	Lightning Strike Location	Lightning Induced Voltages			Notes
			Measured at 7kA (V)	Extrapolated to Average Stroke of 20kA (V)	Extrapolated to Severe Stroke of 200kA (V)	
2149 2150	Taxi Light L8A18	Taxi Light	50	145	1430	
2151 2153	Nav Light L9F22	Nav Light	2900	(a)	(a)	
2156 2157	Nav Light L9F22	Nav Light	4100	(a)	(a)	0.25 in. (0.06cm) Electrode to Nav Light Air Gap
2158 2159	Strobe Power Supply 72A18	Taxi Light	60	170	1700	
2160 2161	Fuel Quantity Transmitter E6A22	Taxi Light	50	145	1400	
2163 2164	Aux Fuel Pump Q7A22	Taxi Light	35	100	1000	
2173 2174	Low Voltage Comparator P29A22	Taxi Light	25	70	700	

(a) Voltage limited to 10kV or less due to dielectric breakdown

Table 3-5 - (continued)

Test No.	System & Wire No.	Lightning Strike Location	Lightning Induced Voltages			Notes
			Measured at 7kA (V)	Extrapolated to Average Stroke of 20kA (V)	Extrapolated to Severe Stroke of 200kA (V)	
2175 2176	Alternator Output P23A6	Taxi Light	20	55	570	
2180 2181	Alternator Output P23A6	Taxi Light	35	100	1000	Alternator Line P22C6 Grounded at Nacelle
2177 2178	Parallel Ckt LH Volt. Reg. P27A18	Taxi Light	25	70	700	
2182 2183	Overvoltage Indicator Light P31A22	Taxi Light	25	70	700	
2184 2185	Overvoltage Relay Power P25A18	Taxi Light	25	70	700	
2186 2187	Fuel Primer Solenoid Q9A22	Taxi Light	15	45	430	
2188 2189	Heater Fuel Solenoid H19A14	Taxi Light	30	85	860	

Table 3-5 - (continued)

Test No.	System & Wire No.	Lightning Strike Location	Lightning Induced Voltages			Notes
			Measured at 7kA (V)	Extrapolated to Average Stroke of 20kA (V)	Extrapolated to Severe Stroke of 200kA (V)	
2190 2191	RH Oil Pressure Transducer E16A22	Taxi Light	25	70	700	
2192 2193	RH Oil Temp. Bulb E12A22	Taxi Light	40	115	1140	
2194 2195	RH Cyl. Head Temp. Transmitter E14A22	Taxi Light	40	115	1140	
2196 2197	RH Fuel Pressure Transducer E18A22	Taxi Light	35	100	1000	
2198 2199	Stall Switch to Battery W4C22	Taxi Light	40	115	1140	Stall Switch in Open Position
2200 2201	Stall Switch to Horn W5A22	Taxi Light	20	55	570	Stall Switch in Closed Position
2202 2203	Stall Switch W5A22	Taxi Light	20	55	570	Stall Switch in Closed Position

Table 3-5 - (concluded)

Test No.	System & Wire No.	Lightning Strike Location	Lightning Induced Voltages			Notes
			Measured at 7 kA (V)	Extrapolated to Average Stroke of 20kA (V)	Extrapolated to Severe Stroke of 200kA (V)	
2204	Stall Switch W4C22	Taxi Light	15	45	430	Stall Switch in Closed Position
2152	Noise Check	NAV Light	90	250	2600	Both Leads Shorted to Inboard Rib
2205	Noise Check	Taxi Light	2	5	260	" " "
2206	Stall Switch to Horn W5A22	Taxi Light	at 12 kA 8	15	130	Stall Switch in Open Position
2207	Stall Switch to Battery W4C22	Taxi Light	at 12 kA 10	15	170	Stall Switch in Open Position
2209 2210	RH NAV Light L9F22	Taxi Light	at 12 kA 19	30	330	
2208	Noise Check	Taxi Light	at 12 kA 3	5	50	Both Test Leads Shorted to Inboard Rib

Table 3-6 - Summary of Induced Voltage Measurements
in Bonded Aluminum Wing

<u>Range of Peak Voltages (V)</u>	<u>Waveform and Strike Location</u>	<u>Structural IR (Ω)</u>	<u>Traveling Wave Frequencies (MHz)</u>	<u>Figure No's.</u>
<u>Independent Return within Wing</u>				
20-40	7kA, 4x50 μ s Taxi Light	--	--	3.21, 3.22
<u>Airframe Return within Wing</u>				
15-50	7kA, 4x50 μ s Taxi Light	0.3(10 ⁻³)	8	3.23
<u>Airframe Return from Plastic Wing Tip</u>				
20	12kA, 17kHz Taxi Light	--	--	
2900	7kA, 4x50 μ s NAV Light	14(10 ⁻³)	8	3.24
11,000	85kA, 17kHz NAV Light	--	--	

Table 3-7 - Induced Voltage Measurements Rate-of-Rise Comparison
in Bonded Aluminum Wing.

<u>Circuit</u>	<u>Waveform</u>	<u>Rate-of-Rise (A/s)</u>	<u>Induced Voltage (V)</u>
Stall Switch to Battery	7kA, 4x50 μ s	$\sim 6.0 \times 10^9$	40
	12kA, 17 kHz	$\sim 1.4 \times 10^9$	10
Stall Switch to Horn	7kA, 4x50 μ s	$\sim 6.0 \times 10^9$	40
	12kA, 17 kHz	$\sim 1.4 \times 10^9$	8

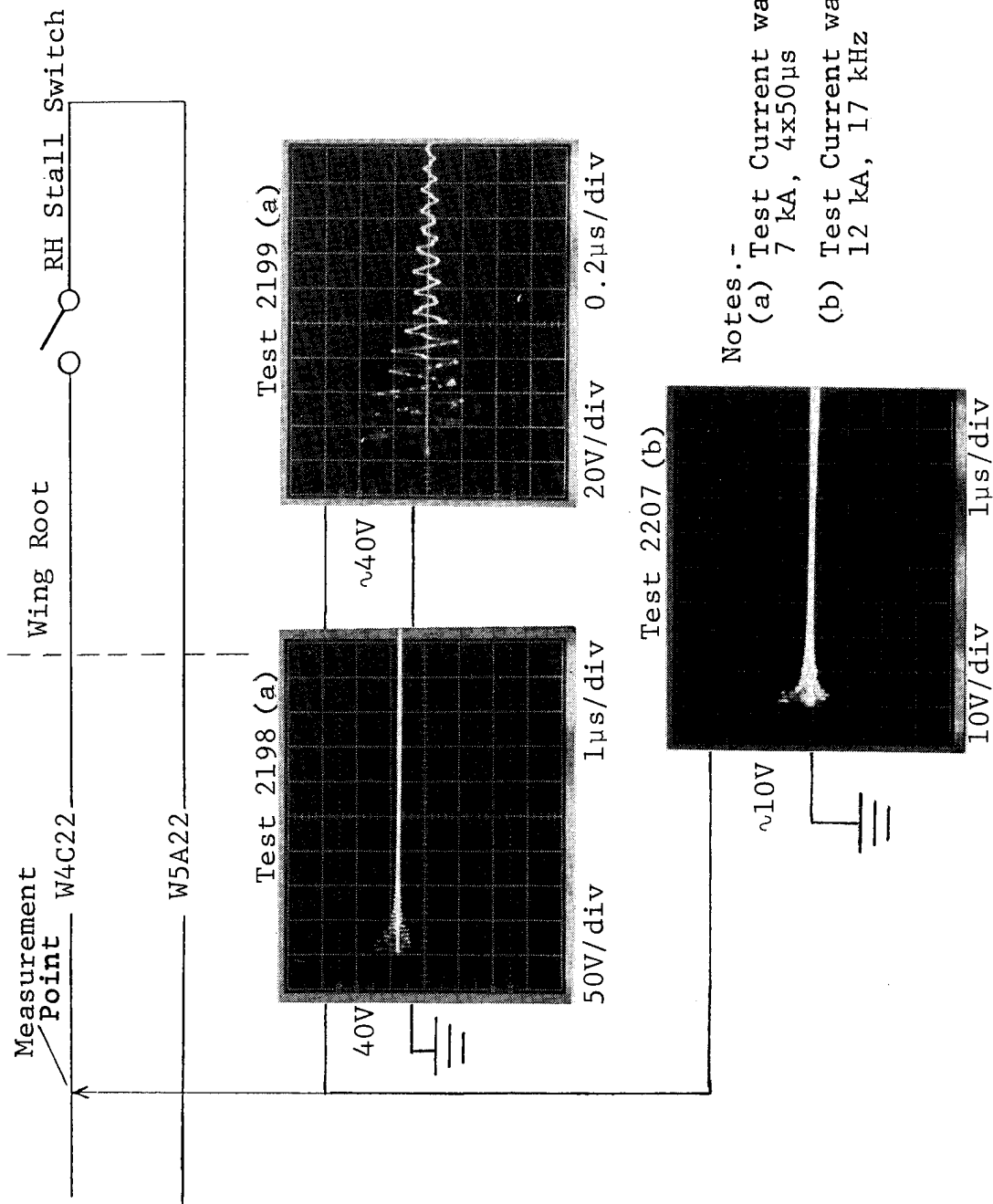


Figure 3.21 - Voltage Induced in RH Stall Switch to Battery by Simulated Lightning Strike to Taxi Light Housing of Bonded Aluminum Wing.

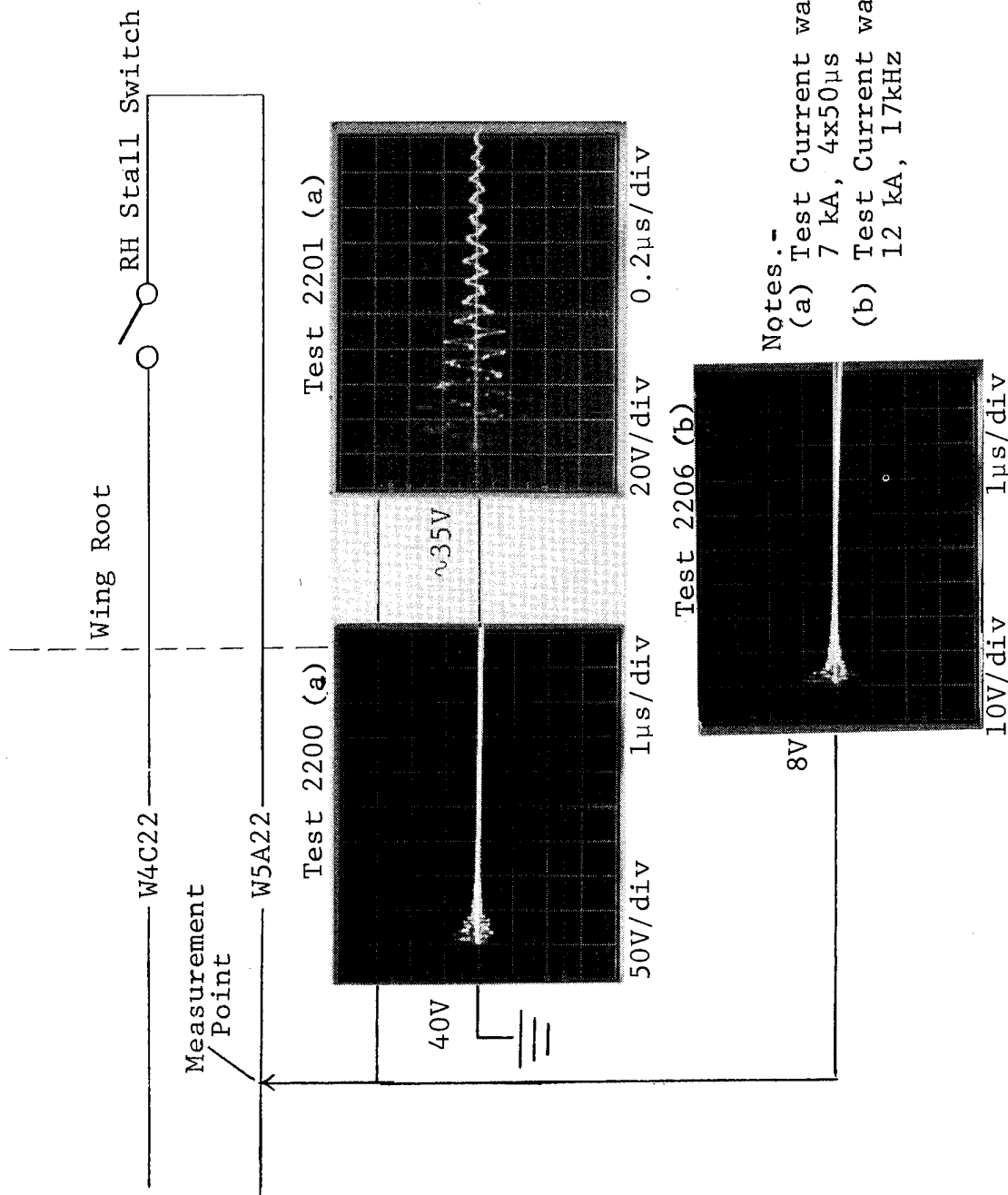


Figure 3.22 - Voltage Induced in RH Stall Switch to Horn by Simulated Lightning Strike to Taxi Light Housing of Bonded Aluminum Wing.

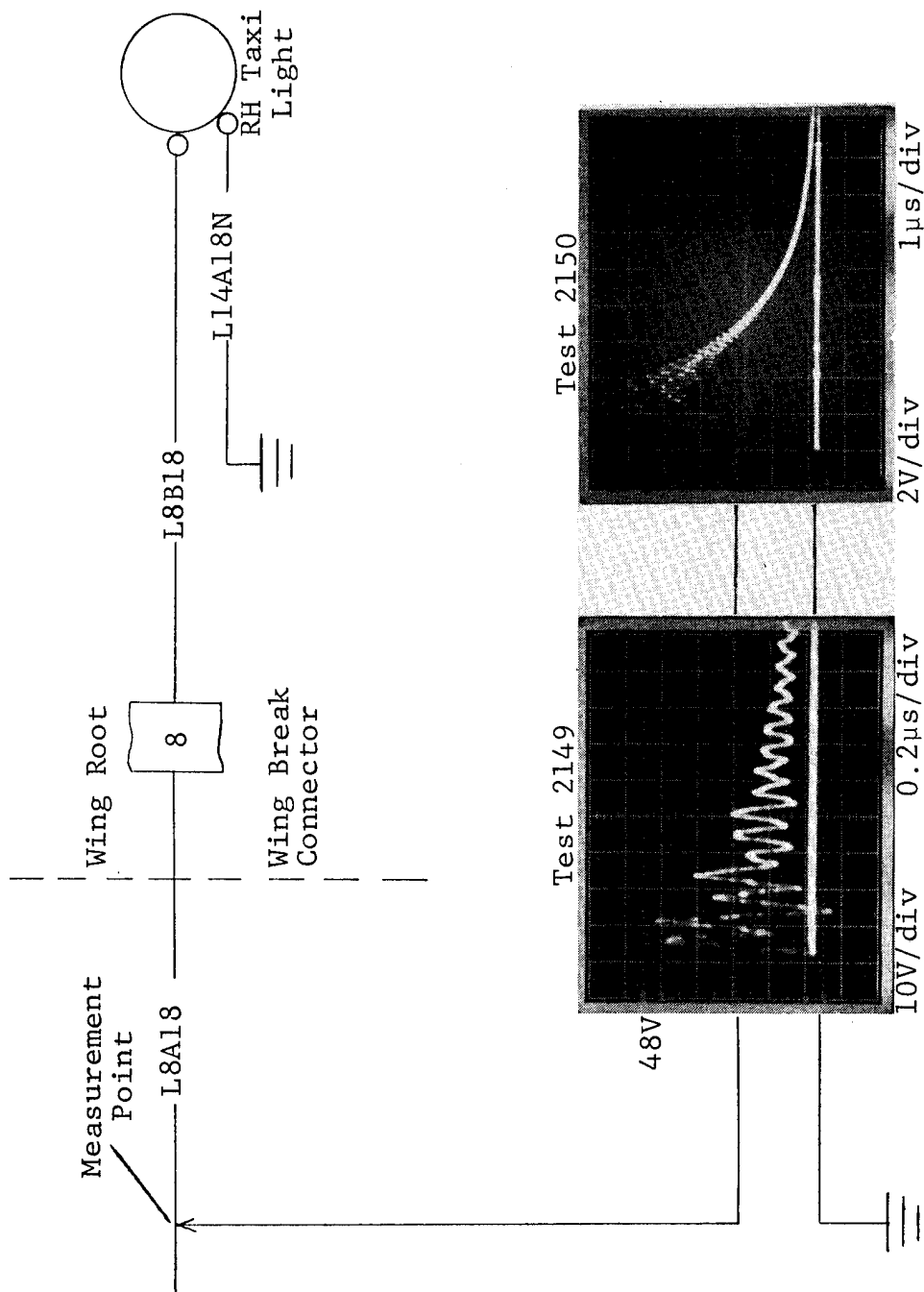


Figure 3.23 - Induced Voltage in RH Taxi Light Wiring by 7kA, 4x50 μs Simulated Lightning Strike to Taxi Light Housing of Bonded Aluminum Wing.

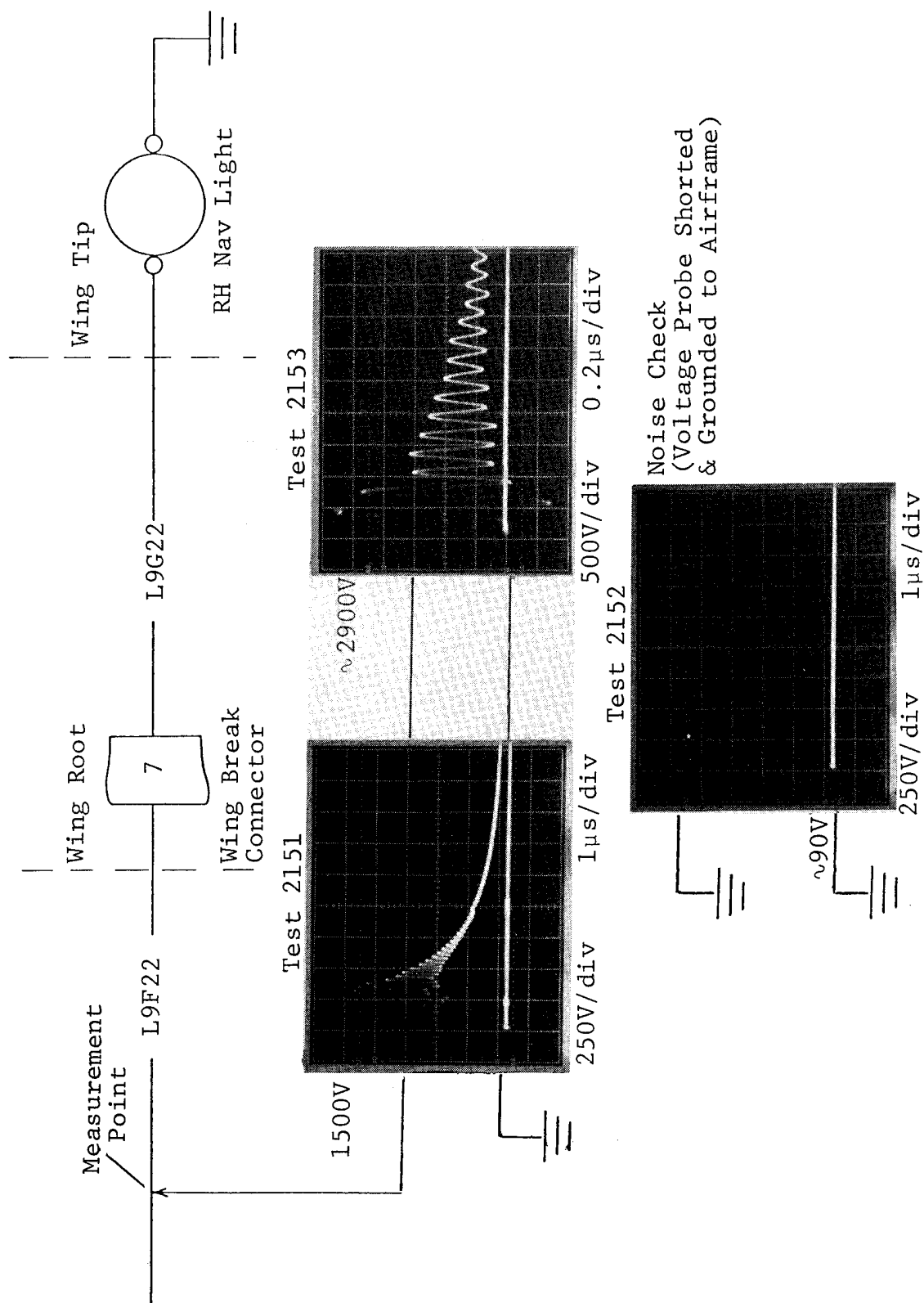


Figure 3.24 - Voltage Induced in RH Navigation Light Circuit, by 7 kA, 4x50μs Simulated Lightning Strike to RH Nav Light Housing of Bonded Aluminum Wing.

oscillatory currents were approximated by dividing the peak test voltage by the circuit inductance. The calculations indicated that the initial rate-of-rise of the unipolar wave was approximately four times that of the oscillatory wave. The peak values of the voltages induced by these currents also approximated a 4:1 ratio.

The 8 MHz oscillations which appear on the induced voltage oscillograms were due to traveling waves being reflected at each end of the wing.

A second example illustrating the relationship of peak induced voltage to current rate-of-rise is shown in Figure 3.22. Induced voltages were measured on the right hand stall switch to horn circuit (line W5A22) during unipolar and oscillatory current strikes to the wing taxi light housing. The measurement oscillograms indicated induced voltage levels of 35 to 40 volts for the unipolar current wave and approximately 8 volts for the oscillatory wave. As before, the ratio of the two induced voltage levels was in the same proportion as the initial rates-of-rise of the test current waves as shown in Table 3-7.

3.3.4.4.2 Airframe return within wing.- The electrical circuits in this group utilize the wing airframe for measurement return. Figure 3.23 illustrates a representative circuit. The measurement oscillogram indicated that the voltage on line L8A18 was the sum of two voltage components. One component was proportional to the test current rate-of-rise as previously illustrated in Table 3-7. The second component was the result of structural voltage rise (IR) due to the test current flowing in the wing skin. The equation for the measured voltage can be written as follows:

$$V = IR + L \frac{di}{dt} \quad (3.7)$$

where IR represents the component due to the structural voltage rise and $L \frac{di}{dt}$ represents the component proportional to the rate-of-rise of the test current. The wing resistance (between the taxi light and wing root) can be calculated from equation 3.7 by measuring the voltage and current amplitudes at a time, t , at which the rate-of-change of the test current is zero ($di/dt = 0$). Equation 3.7 then becomes

$$V = IR$$

$$R = \left. \frac{V}{I} \right|_{di/dt=0} \quad (3.8)$$

For the unipolar current wave, $di/dt = 0$ at $t = 5 \mu s$ (see Figure 3.5). At $5 \mu s$, the test current amplitude was 7 kA and the voltage amplitude was 2 volts (Figure 3.23, test 2150).

The wing resistance, from equation 3.8, is then

$$R = \frac{V}{I} \Big|_{di/dt=0}$$

$$R = \frac{2V}{7kA}$$

$$R = 0.3 (10^{-3}) \Omega$$

3.3.4.4.3 Airframe return from plastic wing tip.- Figure 3.24 illustrates the right hand navigation light circuit and measurement oscillograms. Because the navigation light was located at the end of the plastic wing tip, a separate wire was necessary to connect the navigation light return to airframe ground.

Figure 3.24, test 2151, shows that the induced voltage was the result of a component proportional to the test current-rate-of-rise and a component due to the wing voltage rise (IR).

The wing resistance can be calculated as before using equation 3.8:

$$R = \frac{V}{I} \Big|_{di/dt=0}$$

As before, $di/dt = 0$ at time $t = 5 \mu s$. At $t = 5 \mu s$ the test current amplitude was 7 kA and the voltage amplitude was 175 volts, (see Figure 3.24, test 2151). Substituting these values into equation 3.8 yields the wing resistance as follows:

$$R = \frac{V}{I} \Big|_{di/dt=0}$$

$$R = \frac{175V}{7kA}$$

$$R = 25(10^{-3}) \Omega$$

This calculation results in a higher wing resistance than that previously calculated for the taxi light circuit. The additional circuit return wires and connections required in the navigation light circuit may account for this difference.

It should also be noted that the peak induced voltage magnitude of the navigational light circuit was greater than that of the electrical circuits located entirely within the metallic wing. This is because the plastic wing tip did not provide electromagnetic shielding for the navigation light circuit wires, thus allowing greater magnetic flux interaction with these

wires than for those located entirely within the shielded environment of the metallic wing structure.

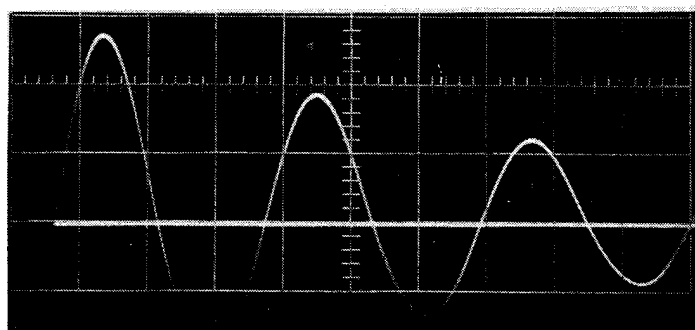
Test 2152 of Figure 3.24 shows that the electrical "noise" in the measurement lines was less than 10% of the voltage measurement signal.

3.3.4.5 Magnetic field measurements

Table 3-8 summarizes the results of the search coil calibration tests. Voltage and current oscillograms recorded during calibration of the single layer 20-turn coil are shown in Figure 3.25

Table 3-8 Summary of Results Obtained during Search Coil Calibration Tests

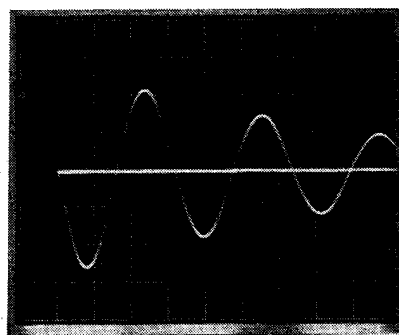
Coil Description	Integrator	Magnetic Field Intensity(H)		Integrated Voltage V	Calibration Factor	
		A/ft	(A/m $\times 10^3$)		A/ft/V	A/m/V
Multi-layer 20 Turn	10 μ s	935	(3.07)	11.50	0.81	(0.28)
	1 ms	935	(3.07)	0.32	2.90	(9.60)
Single layer 20 Turn	10 μ s	970	(3.18)	15.50	0.063	(0.21)
	1 ms	935	(3.07)	0.26	3.60	(12.00)
Single layer 100 Turn	10 μ s	935	(3.07)	45.00	0.021	(0.068)
	1 ms	902	(2.96)	0.63	1.40	(4.60)



2kA/div

20 μ s/div

Test Current



0.1V/div

20 μ s/div

Integrated Coil Signal

Figure 3.25 - Oscillograms Recorded during Calibration of a Single Layer 20-turn Search Coil with 1 ms Integrator.

The peak amplitude of the test current, as shown in Figure 3.25, was 5.4 kA, and the distance, d , of the coil from the current-carrying conductor was 0.92 ft. Substitution of these values into equation 3.9 yields the magnetic field intensity, H , at the position of the coil.

$$H = \frac{I}{2\pi d}$$

$$H = \frac{5.4\text{kA}}{2\pi(0.92\text{ft})}$$

$$H = 935 \text{ A/ft } (3.07(10^3) \text{ A/m})$$

The field intensity value of 935 A/ft ($3.07(10^3)$ A/m) obtained above, divided by the integrated coil signal of 0.26 volts (obtained from Figure 3.25), results in a calibration factor for this coil-integrator combination of $3.6 (10^3) \text{ A/ft/V}$ ($11.8(10^3) \text{ A/m/V}$).

Initial measurements of the field intensity within the fuel tank are summarized in Table 3-9. A typical measurement oscillogram is shown in Figure 3.26.

The search coil was oriented in each of the three orthogonal axes for the tests as defined in Figure 3.13. Measurements were initiated with the coil positioned midway between the upper and lower skin surfaces in the vicinity of the fuel filler cap. The fuel filler cap was in place during the tests to simulate the actual structural configuration that exists during a lightning strike. Table 3-9 indicates that the magnetic intensity amplitude readings ranged from 4.6 to 7.9 A/ft (15 to 26 A/m). Electrical noise in the measurement cables was equivalent to 4.6 A/ft (15 A/m).

For comparison purposes, additional tests were made with the coil positioned midway between the fuel filler cap and the wing leading edge, at the wing leading edge, and at the wing trailing edge. Table 3-9 shows that the field intensity measurement amplitudes were higher at the leading and trailing edges than at the fuel filler cap location, but not significantly so. A noise measurement made with the search coil located at the wing trailing edge, yielded an equivalent field intensity level of 6.4 A/ft (21 A/m).

These measurements indicated that the amplitude of the magnetic field intensity within the wing tank was not significantly higher than the amplitude of the electrical "noise" within the measurement cables.

Table 3-9 - Summary of Magnetic Field Intensity Measurements within a Bonded Aluminum Wing Fuel Tank, 20-turn Search Coil, 1 ms Passive Integrator. 2.4 kA 4x50 μ s Conducted Current Strike to Taxi Light Housing.

Coil Axis Orientation	(a)	Search Coil Location	Magnetic Intensity(H) A/ft (A/m)		Notes
X		midway between skin surfaces at fuel cap location	7.3	(24)	
Y		"	7.9	(26)	
Z		"	4.6	(15)	
-		"	4.6	(15)	Noise measurement
X		midway between skin surfaces and midway between fuel cap and leading edge	9.5	(31)	
Y		"	7.9	(26)	
Z		"	7.9	(26)	
X		midway between skin surfaces at trailing edge	7.9	(26)	
Y		"	9.5	(31)	
Z		"	7.3	(24)	
-		"	6.4	(21)	Noise measurement
Z		midway between skin surfaces at leading edge	9.2	(30)	

(a) See Figure 3.13.

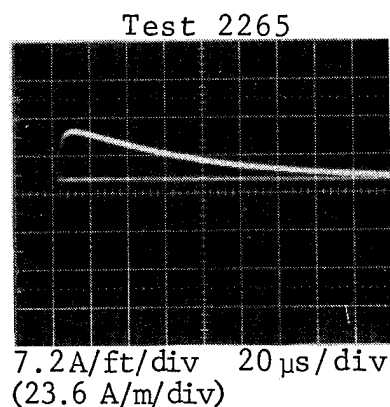


Figure 3.26 - Typical Magnetic Field Intensity Oscillogram Obtained during Measurements within Fuel Tank of Bonded Aluminum Wing.

A search coil wound with 100 turns of wire was utilized during additional tests of the magnetic fields within the wing fuel tank. Since the output signal of the search coil is proportional to the number of turns of wire in its construction, as shown by equation 3.3, theory would predict that the signal amplitude from this coil would be approximately 5 times that of the 20-turn coil used during the previous tests.

$$\frac{e(t)_{100T \text{ coil}}}{e(t)_{20T \text{ coil}}} = \frac{N_{100T} d\phi/dt}{N_{20T} d\phi/dt} \quad (3.10)$$

$$\frac{e(t)_{100T \text{ coil}}}{e(t)_{20T \text{ coil}}} = \frac{N_{100T}}{N_{20T}} = \frac{100}{20} = 5 \quad (3.11)$$

Two sets of tests were conducted with this coil. The first set of tests, with the search coil located in the vicinity of the fuel filler cap, was performed with a 2.4 kA, 4 x 50 μ s, conducted entry current to the taxi light housing. The second set of tests was performed with a 16 kHz, 11 kA oscillatory current wave. For comparison purposes, each set of tests consisted of measurements taken with the fuel cap in place and with it removed. Figure 3.27 shows oscillograms of the test current waveforms and typical integrated coil response oscillograms. Tables 3-10 and 3-11 summarize the measurement results of these tests.

Table 3-10 - Summary of Magnetic Field Intensity Tests within an Aluminum Wing Fuel Tank near the Fuel Filler Cap. 100 Turn Search Coil, 1 ms Passive Integrator. 2.4 kA, 4 x 50 μ s Conducted Current Strike to Taxi Light Housing.

Coil Axis Orientation (a)	Magnetic Intensity (H)		Notes
	A/ft	(A/m)	
X	5.5	(18)	Fuel cap ON
"	7.0	(23)	Fuel cap OFF
Y	8.5	(28)	Fuel cap ON
"	5.5	(18)	Fuel cap OFF
Z	20.0	(64)	Fuel cap ON
"	20.0	(64)	Fuel cap OFF
--	1.5	(5)	Fuel cap ON - Noise check

(a) See Figure 3.13

TEST CURRENT

INTEGRATED COIL RESPONSE (H)

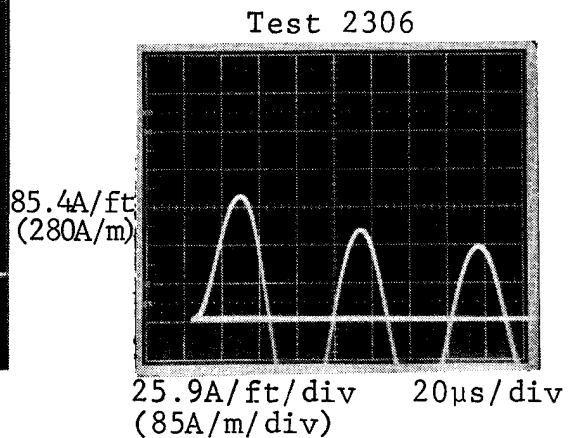
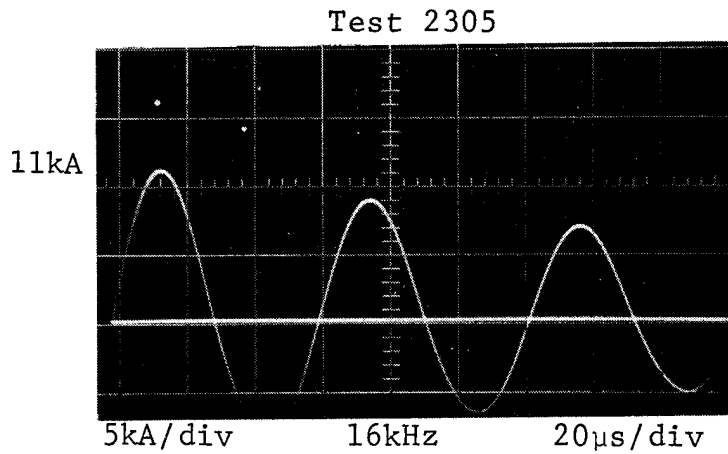
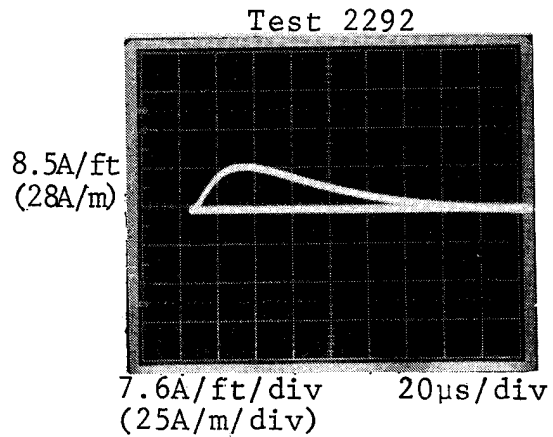
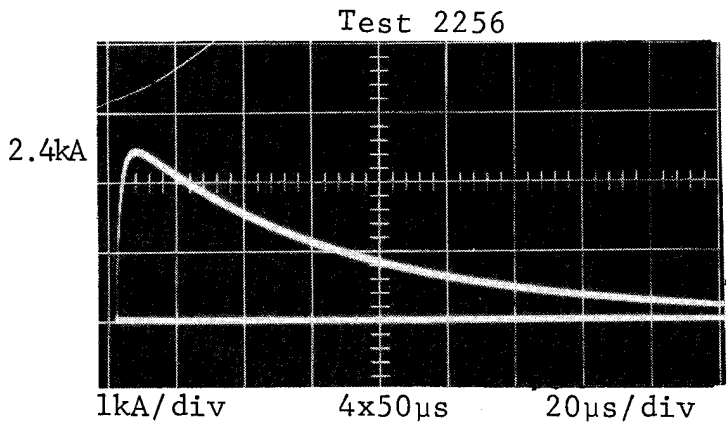


Figure 3.27 - Typical Test Current and Integrated Coil Response Oscillograms. 100 turn search coil; 1 ms passive integrator. Conducted entry strike to taxi light housing of bonded aluminum wing. Measurement inside fuel tank with filler cap on. See Table 3-12.

Table 3-11 - Summary of Magnetic Field Intensity Tests within a Bonded Aluminum Wing Fuel Tank near the Fuel Filler Cap. 100 Turn Search Coil, 1 ms Passive Integrator. 11kA, 16 kHz Conducted Current Strike to Taxi Light Housing

<u>Orientation (a)</u>	<u>Magnetic Intensity (H)</u>		<u>Notes</u>
	<u>A/ft</u>	<u>(A/m)</u>	
X	14.0	(46)	Fuel cap ON
"	14.0	(46)	Fuel cap OFF
Y	43.0	(140)	Fuel cap ON
"	43.0	(140)	Fuel cap OFF
Z	85.0	(280)	Fuel cap ON
"	98.0	(320)	Fuel cap OFF
--	1.5	(5)	Fuel cap ON - Noise check
--	2.8	(9)	Fuel cap OFF- Noise check

(a) See Figure 3.13

The test results shown in Tables 3-10 and 3-11 showed that the presence or absence of the fuel filler cap made little difference in the test results. This indicated that the internal fields were the result of diffusion flux rather than aperture flux penetration. Tables 3-10 and 3-11 also indicate that stronger magnetic fields existed in the Z axis orientation than in either the X or Y axis orientations. The Z axis field, as defined by Figure 3.13, can be represented by field vectors normal to the upper and lower wing skin surfaces. This field is the result of wing skin penetration by the external magnetic field lines of flux. The Y-axis field intensity measurements were approximately one half the magnitude of the Z axis amplitude levels recorded during the 11 kA oscillatory tests (Table 3-11) and were in the noise level range for the 2.4 kA unipolar current tests (Table 3-10). The X axis orientation field amplitude levels were less than 10 times the amplitude level of the electrical noise in the measurement cable for both sets of tests.

A comparison of the fuel tank internal field measurements is shown in Table 3-12.

Magnetic field intensity measurements along the external surface of the wing were recorded utilizing a 20 turn multi-layer search coil and a 1 ms passive integrator. The wing circumference at WS 160.75 was divided into eight equidistant sections. Figure 3.28 is a schematic representation of the wing outline showing the

Table 3-12 - Comparison of Magnetic Field Intensity Measurements in A/ft (A/M) within a Bonded Aluminum Wing Fuel Tank near the Fuel Filler Cap for Conducted Current Strikes to the Taxi Light Housing.

2.4 kA, 4x50 μ s Test Current

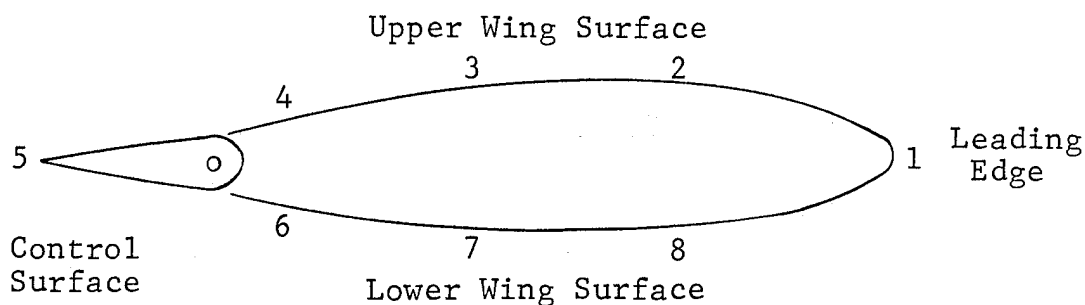
<u>Coil Axis Orientation (a)</u>	<u>X</u>	<u>Y</u>	<u>Z</u>	<u>Electrical Noise Reading</u>
20 Turn Coil Filler Cap ON	7.3 (24)	7.9 (26)	4.6 (15)	4.6 (15)
100 Turn Coil Filler Cap ON	5.5 (18)	8.5 (28)	20.0 (64)	1.5 (5)
100 Turn Coil Filler Cap OFF	7.0 (23)	5.5 (18)	20.0 (64)	-- --

11 kA, 16 kHz Test Current

100 Turn Coil Filler Cap ON	14 (46)	43 (100)	85 (280)	1.5 (5)
100 Turn Coil Filler Cap OFF	14 (46)	43 (140)	93 (320)	2.8 (9)

(a) See Figure 3.13

field measurement locations and the magnetic intensity amplitudes. The measurement amplitudes were greater than eight times the noise level.



Measurement Location	Magnetic Field Intensity(H) <u>A/ft x 10³</u>	(A/m x 10 ³)
1	0.61	(2.0)
2	2.10	(6.9)
3	0.89	(2.9)
4	0.28	(0.9)
5	0.28	(0.9)
6	0.18	(0.6)
7	1.00	(3.4)
8	1.70	(5.5)

Figure 3.28 - External Magnetic Field Intensity Measurements and Locations for a Bonded Aluminum Wing. Distance between measurement locations was approximately 1.2 ft. Test current was 12 kA.

The average magnetic field intensity around a current-carrying conductor is given by the equation

$$H_{AV} = \frac{I}{P} \quad (3.12)$$

where I is the conducted current and P is the circumference. For a conductor with an irregular shape, such as an aircraft wing, the field intensity will be greater than average where the radius of curvature is smaller than average (such as the leading and trailing edges) and less than average where the radius of curvature is greater than average (as midway between the leading and trailing edge).

For the tested wing, the circumference was 9.5 ft at WS 160.75 and the test current level was 12 kA. From equation (3.12), then, the average magnetic field intensity along the external wing surface was

$$H_{AV} = \frac{I}{P} = \frac{12\text{kA}}{9.2\text{ft}}$$

$$H_{AV} = 1.3(10^3)\text{A/ft} \quad (4.3(10^3) \text{ A/m}) \quad (3.13)$$

Magnetic field intensity measurements were made at locations 1 through 8 as shown in Figure 3.28. They indicated that the tested wing did not follow the theoretical intensity distribution. The maximum field intensity amplitudes occurred at locations 3 and 7. A sharp drop in amplitude is recorded at locations 4 and 6 with an equally low reading at the wing trailing edge. Location 1 at the wing leading edge also recorded an intensity level lower than average but was greater than twice the reading recorded at the trailing edge.

Comparison of the field distribution readings shown in Figure 3.28 with the photograph of the wing laboratory setup reveals an explanation for the divergence of the wing field pattern from that predicted by theory. The aluminum flashing, which conducted the test currents from the generator to the taxi light housing, was positioned along the wing skin approximately 1/3 to 1/2 of the distance between the leading and trailing edges. This corresponds to the region of highest field intensity levels. Apparently, the close proximity of the test current-carrying conductor to the skin surface strongly influenced the magnetic field distribution in their immediate vicinity.

3.4 gr/E Wing

3.4.1 Specimen description

The gr/E wing was fabricated as a single structure. The wing box extended from the fuselage centerline to the close-out rib 226 in. outboard. With the exception of the leading edge and some control surfaces, the wing was constructed of gr/E. The skin thicknesses ranged from 0.05 in. at the wing tip to 0.125 in. inboard. The wing had three full length spars with an integral fuel tank between the front and the rear spars and extending throughout much of the wing. The leading edge, which was to be fabricated of nonconducting composite beneath a de-ice boot, was not fastened to the wing structure during the test program. The wing tip was fabricated of gr/E containing interwoven wires for lightning protection. The wing was complete with ailerons, flaps, internal sealants, wiring and components.

Electrical circuits contained within the tested wing included navigation light, position light, strobe light, trim tab actuator motor, and capacitance-type fuel quantity probes. The quantity probe wiring was located within the fuel tanks; the wiring for all other circuits was routed through an aluminum conduit located within the leading edge of the wing.

The gr/E skins were adhesively bonded to the spars and ribs. Some mechanical fasteners were utilized to provide additional strength and to fasten hardware such as control surfaces, hinges, etc. to the wing.

Rib, access door, connector, and test locations hereafter referred to in this report will be referenced in inches from the fuselage center line by a wing station (WS) number. For example, the wing box closeout rib which is located 226 in. outboard of the fuselage center line, would be designated WS 226.

A drawing of the wing is shown in Figure 3.29.

3.4.2 Test setup

A photograph of the test setup is shown in Figure 3.30. The wing was positioned on a specially constructed wooden framework with the tip of the right wing positioned at the simulated lightning current generator. The wing was positioned with its lower skin surface facing up to allow access to the fuel tank access doors. The framework structure provided for the positioning of eight equally-spaced radial lightning current return lines. These lines originated at a metallic ground plane, which simulated the conductive cabin floor located in the aircraft fuselage, and were terminated at generator "ground". By spacing the return lines in an equidistant, radial pattern around the wing, the magnetic fields created by these wires would have little or minimal effect on wing measurements; this is because the magnetic fields surrounding each wire would cancel in the areas between them. This is shown schematically in Figure 3.31.

The simulated ground plane is shown in the photo of Figure 3.32.

The output of the generator "high" side was connected to the static discharger which was located on the trailing edge of the wing tip. The lab setup simulated a strike to the wing tip with current flow through the wing skin to an exit point elsewhere on the aircraft.

The simulated lightning currents were generated by a 20 μ F, 100 kV high current capacitor bank in conjunction with waveshaping elements. The currents were measured by a 100:1 current transformer and recorded by an oscilloscope located within an RF shielded room.

All Graphite Construction
Consists of:

1. Skin thickness ranging from 4 plies to 72 plies
2. 250°F cure adhesive/material
3. Wing span 39 ft. 4 in. (11.9 m)
4. Wing area 162.9 ft² (15.1 m²)
5. "Wet Wing" design fuel tank

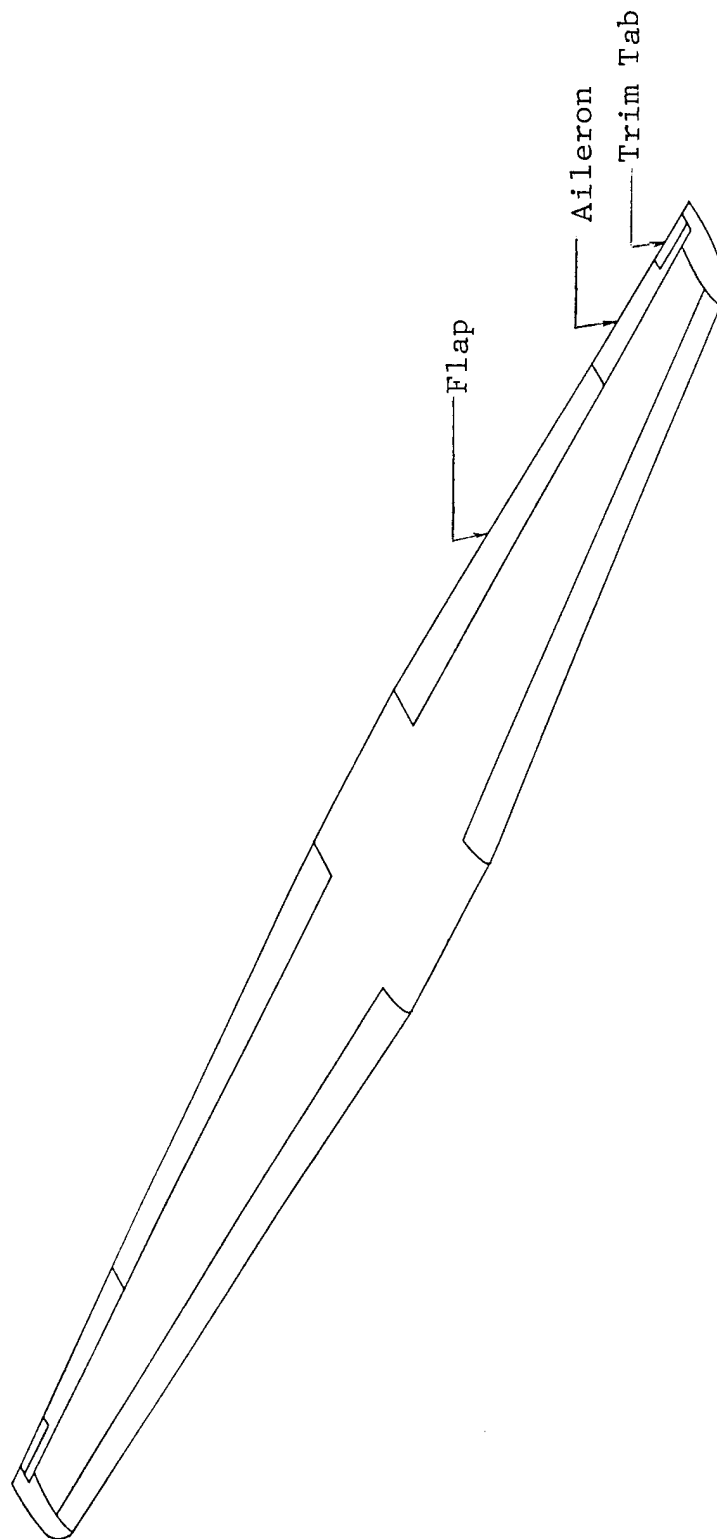


Figure 3.29 - Gr/E Wing - Exterior View.

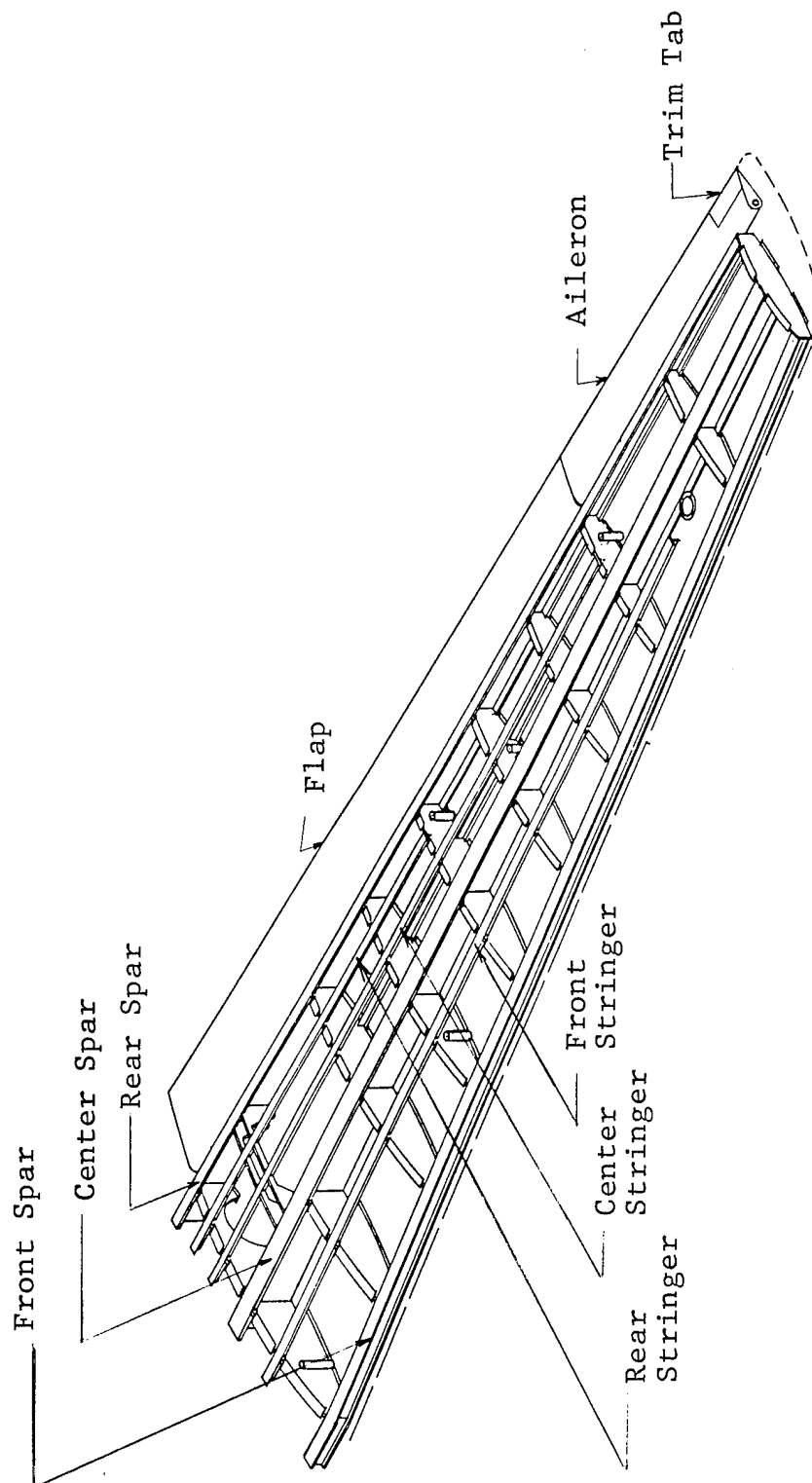


Figure 3.29 Gr/E Wing - Interior View.

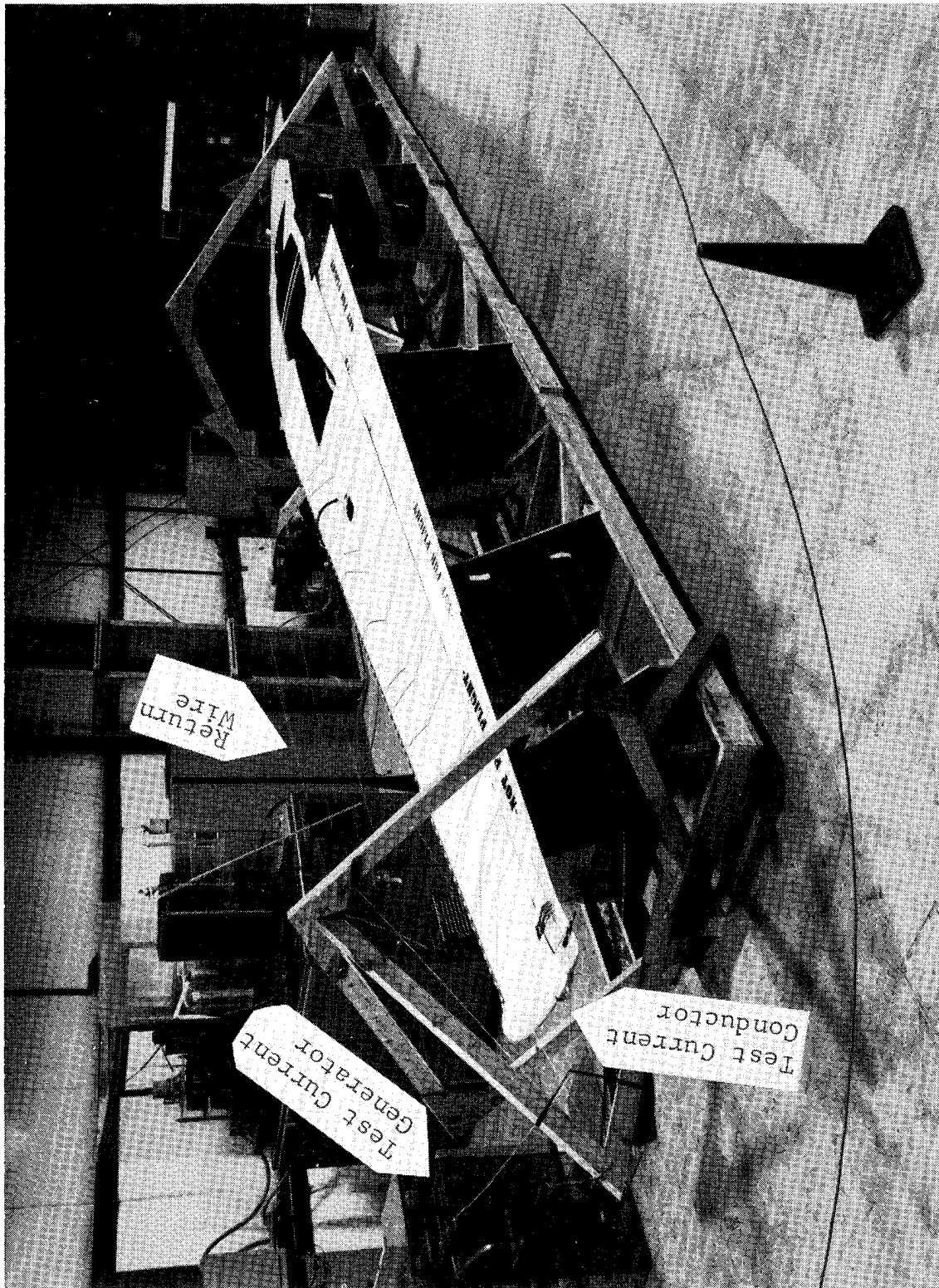


Figure 3.30 - gr/E Wing Test Setup.

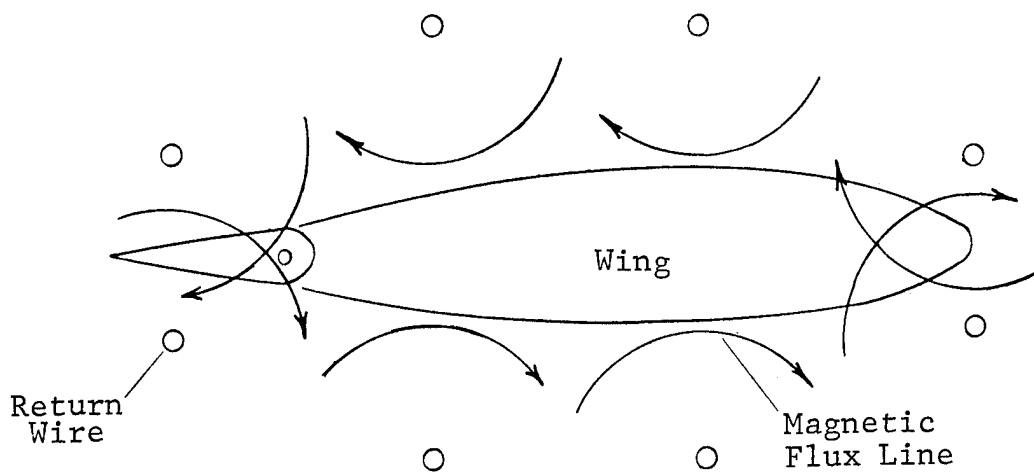


Figure 3.31 - Cancellation of Return Wire Magnetic Fields in Vicinity of gr/E Wing.

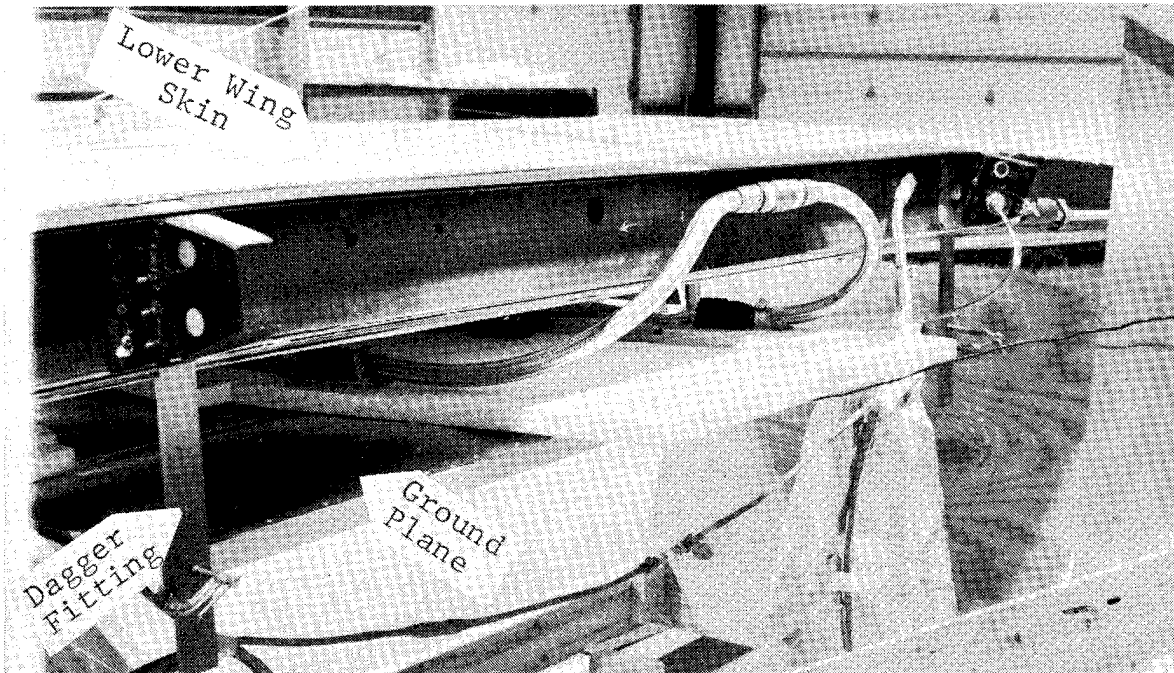


Figure 3.32 - Photo Showing Connections to Simulated Ground Plane in gr/E Wing.

3.4.3 Test procedures

3.4.3.1 Current distribution

Measurements were made of current through the following structural elements:

- Conduit in wing leading edge (aluminum)
- Conduit braid (copper)
- Wing attach fittings (titanium)
- Drag angles (gr/E)
- Hydraulic lines (aluminum)
- Fuel lines (steel reinforced)

Each of the above elements was connected to the ground plane; for the drag angles, four equally spaced copper braids connected each drag angle to the ground plane. The wing attach fittings (dagger fittings) were connected to the ground plane through 0.087 in. gr/E skins to simulate actual conditions in the aircraft, as shown on Figure 3.33.

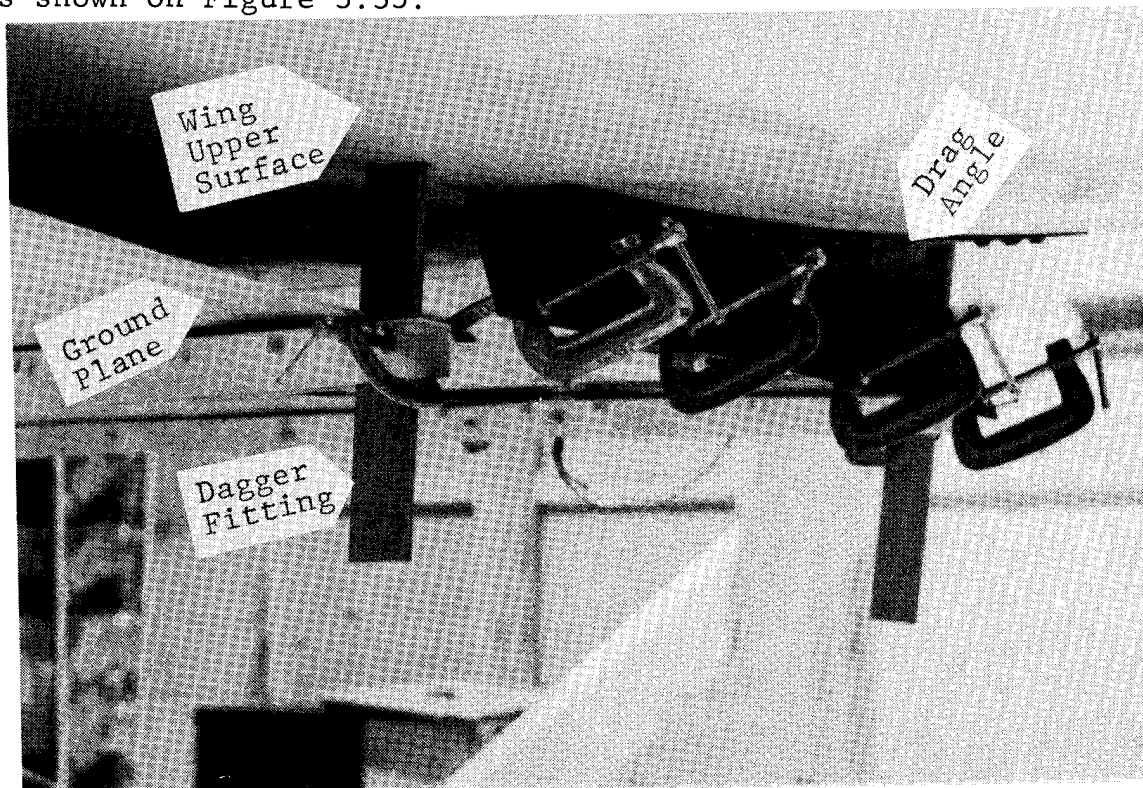


Figure 3.33 - Connections of Drag Angle and Wing Attach Fittings (dagger fittings) to Ground Plane in gr/E Wing.

The current measurements were made by a Pearson Model 110A current transformer which had an IT product of 0.5 A.s and a frequency response of 1 Hz to 35 MHz. RG 58 coaxial conductor cable routed the measurement signal from the current transformer to the RF shielded room where the measurement was recorded by a Tektronix 535A oscilloscope with a type 1A1 preamplifier.

Test currents of 900 A and 4450 A peak amplitude and $4 \times 50 \mu\text{s}$ waveform were conducted into the static discharger located at the trailing edge of the right wing tip and flowed through the wing to the ground plane where they were conducted by the radial return wires to the lightning current generator "ground". The test current peak amplitudes were kept low to avoid "conditioning" the wing structure.

3.4.3.2 Bond line and fuel probe voltages

Lightning currents flowing through the resistive gr/E wing skin can raise its voltage potential with respect to structural or fuel system components which may be electrically isolated from the skins. If the voltage potential difference between the skin and these components exceeds the withstand capability of the insulating medium (adhesive or air), breakdown will occur and the resulting spark could be a possible ignition source.

Measurements were recorded across bond lines located within the wing structure between locations WS 28 and WS 212. The bond lines included upper skin to front, center, and rear spars and stringers.

The number of measurements which could be made at each wing location was determined by the physical accessibility of the locations and the ability to insure a low resistance electrical contact between the skin and measurement leads. Since the epoxy resin electrically insulated the wing skin surface, modified test procedures were employed to insure low contact resistance between the skin and measurement leads. Experimentation with several test methods resulted in the following procedure. The insulating epoxy resin surface was removed by sanding the surface area with medium grade sandpaper. Copper braid, approximately 0.75 in. in length, was taped to the sanded surface with aluminum foil tape, with a sufficient length of braid extending beyond the aluminum tape to allow connection of the voltage measurement probe. A wooden dowel was wedged between the aluminum foil/copper braid and the opposite skin surface to provide the pressure needed to insure good electrical contact between the braid and the skin surface. This procedure was repeated at the adjacent spar or stringer measurement point. The contact resistance of each copper braid location was measured with an ohmmeter and the whole procedure repeated if the contact resistance was too high.

The measurement signals were conducted by twinaxial cable to the recording oscilloscope (Tektronix 535) located within the RF shielded room.

Measurements of fuel probe to skin voltages were made using a test procedure similar to that employed during bond line voltage measurements. One measurement lead was connected to a fuel probe terminal and the second lead was connected to the adjacent wing skin surface using the technique described above. The fuel probe circuits were electrically tied to the ground plane through a dummy fuel quantity meter circuit.

Initial measurements were made using test currents of 900A - 1800A conducted into the static discharger on the wing tip. During the latter part of the test series, test current levels of 190 kA were injected into the aluminum rib at wing location WS 226, the wing tip attachment point. A photograph of the test setup is shown in Figure 3.34.

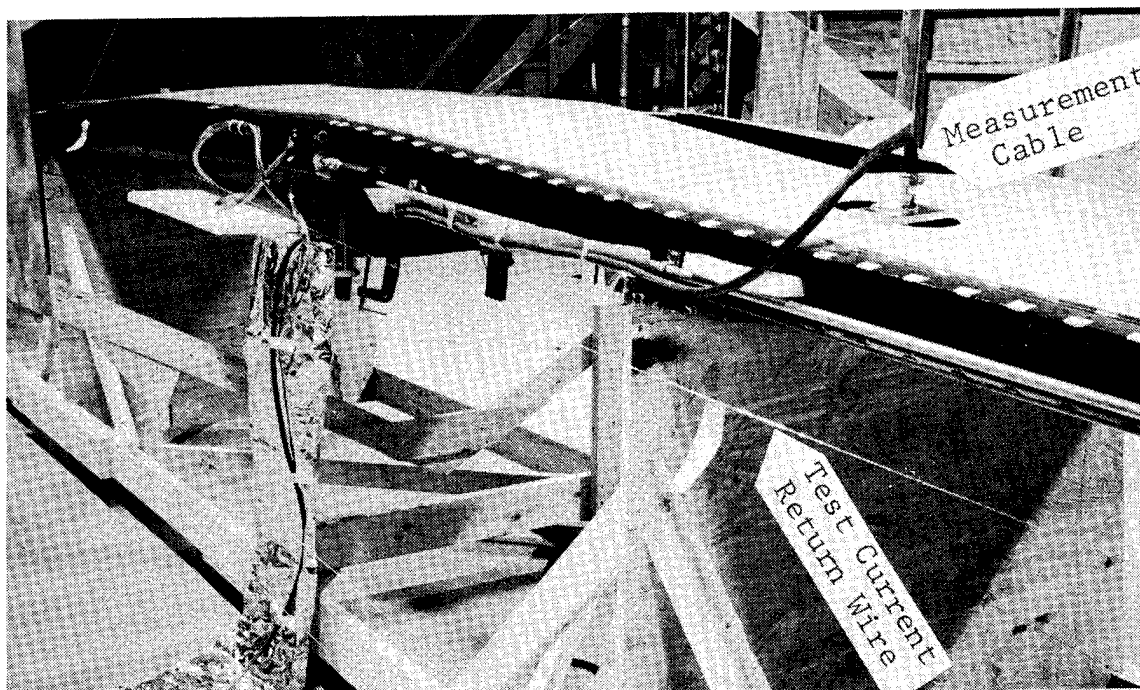


Figure 3.34 - Lab Setup for Bond Line and Fuel Probe Voltage Measurements in gr/E Wing.

3.4.3.3 Induced voltages in wing electrical wiring

Measurements of voltages induced in the leading edge conduit harness wires were recorded during 36 kA oscillatory test currents conducted into the navigation light housing. In addition, one

170 kA oscillatory test current strike was applied across a 1 in. air gap to the navigation light and the voltage in the navigation light circuit conductor measured with respect to the conduit braid. A schematic of the measurement circuit is shown in Figure 3.35 for the 170 kA test current strike to the navigation light. The conduit braid was connected to the simulated ground plane (not shown). The circuit wire under test was pulled through the conduit braid at the connector located at the inboard end of the conduit and measured with respect to the conduit braid by a 100:1 voltage measurement divider. The divider consisted of two measurement leads each of which had 5000 Ω of resistance at the measurement end and 50 Ω to ground at the recording (oscilloscope) end. The signals measured by the divider were conducted through twinaxial cable to a Tektronix 535 oscilloscope located in an RF shielded room where they were recorded differentially by the oscilloscope equipped with a type 1A5 preamplifier.

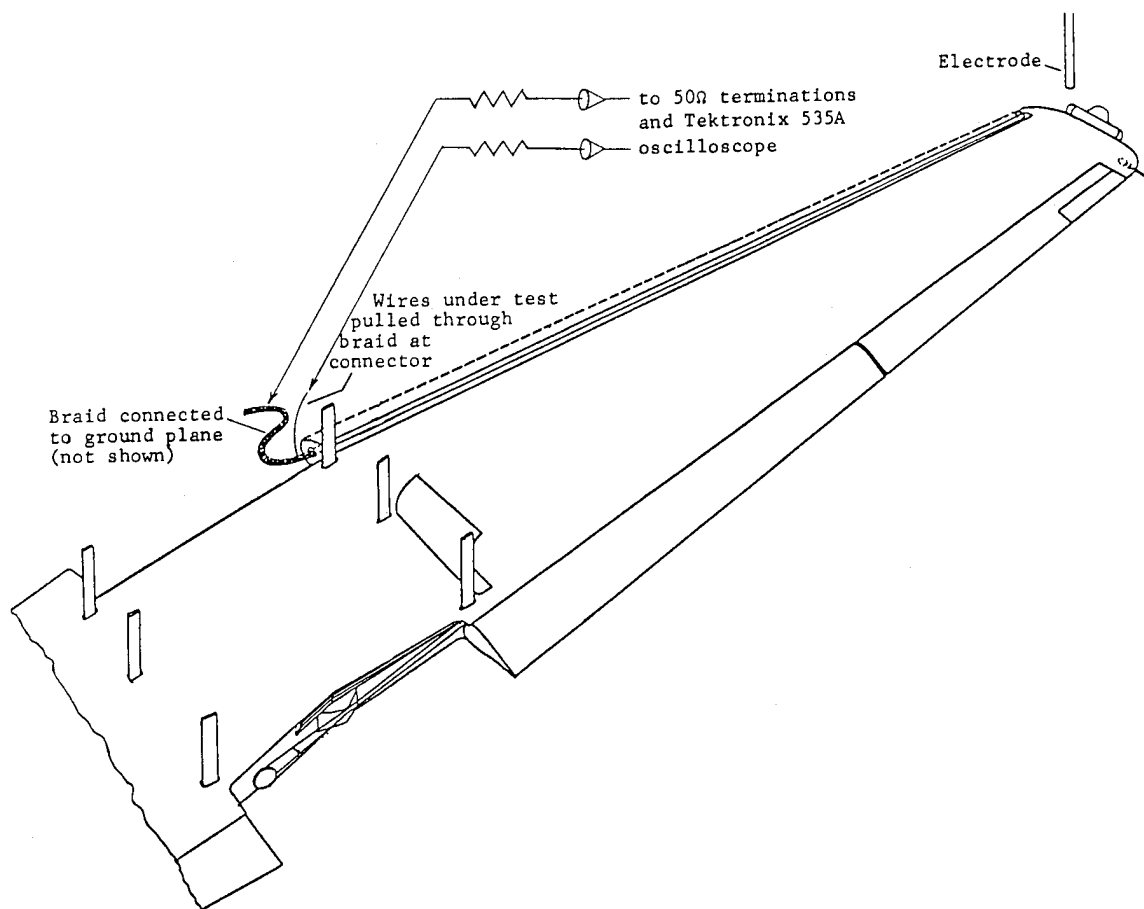


Figure 3.35 - Circuit of Induced Voltage Measurement Circuit. Arc Entry Strike to Navigation Light Shown on gr/E Wing. (Ground plane not shown.)

3.4.3.4 Magnetic field measurements

Magnetic field intensity readings were recorded for six wing interior locations and two wing exterior locations utilizing the 20 turn multilayer search coil and 1 ms passive integrator employed during field measurement tests on the bonded aluminum structure described in paragraphs 3.3.3.5 and 3.3.4.5.

The measurement coil was attached to shielded twinaxial cable which conducted the signals to the 1 ms passive integrator and Tektronix 535A oscilloscope located within an RF shielded room. The internal field measurements were at the location of six wing access doors. Aluminum flashing was used to shield the access door opening during the test measurements with the exception of the door at WS 40, since this door was constructed of kevlar and would not normally have provided any shielding. The coil was oriented in each of the three orthogonal axes as defined in Figure 3.13, i.e., the X-axis direction is inboard to outboard, the Y-axis direction is leading edge to trailing edge, and the Z-axis direction is upper to lower skin surfaces.

Measurements of external magnetic fields were made at wing location WS 182 and WS 80 with the axis of the coil positioned in the axis of highest field intensity. Measurements at WS 182 were made at 10 equidistant location points around the wing perimeter. Measurements at WS 80 were made at five locations along the wing lower skin which were also located at equidistant points along the wing surface.

Test currents were conducted into the wing through the static discharger located on the wing tip trailing edge and were removed from the wing at the simulated ground plane and returned to generator "ground" through the radial return line configuration.

3.4.4 Test Results

3.4.4.1 Current distribution

The test results are shown on the schematic drawings of Figures 3.36 through 3.38. Typical oscillograms of total current and currents measured in a metallic conductor are shown in Figure 3.39.

Figure 3.36 shows the initial current distribution at time $t = 4\mu s$ the time at which the applied current is at its maximum value. At this time, 74% of the current was conducted by the graphite skin and the remaining 26% by the metal conduit, control cables, and hydraulic lines. The gr/E skin current was returned to the ground plane through the two drag angles and the six dagger fittings. It is interesting to note that the skin current returning to the ground plane through the dagger fittings did not divide equally among them. Almost twice as much current returned through

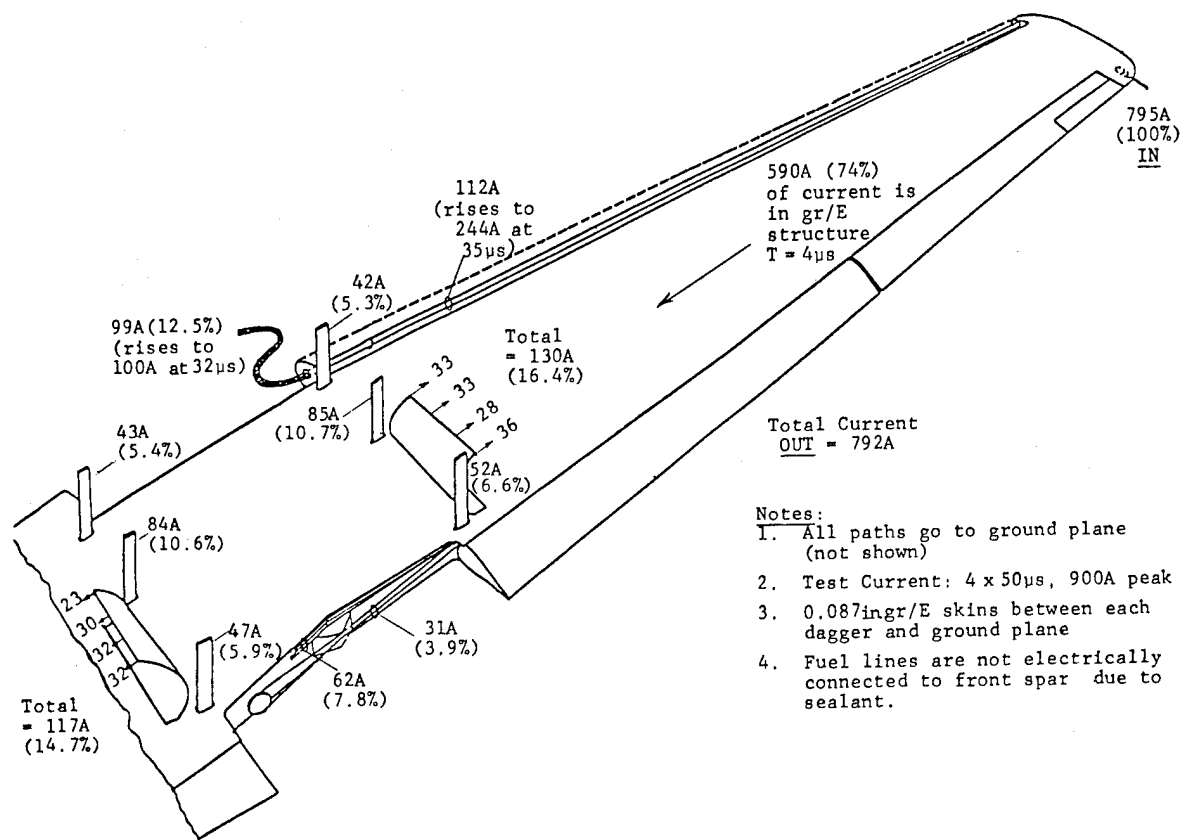


Figure 3.36 - Current Distribution in gr/E Wing at $T = 4 \mu s$ for a 900 A Current during a Simulated Strike to Static Discharger.

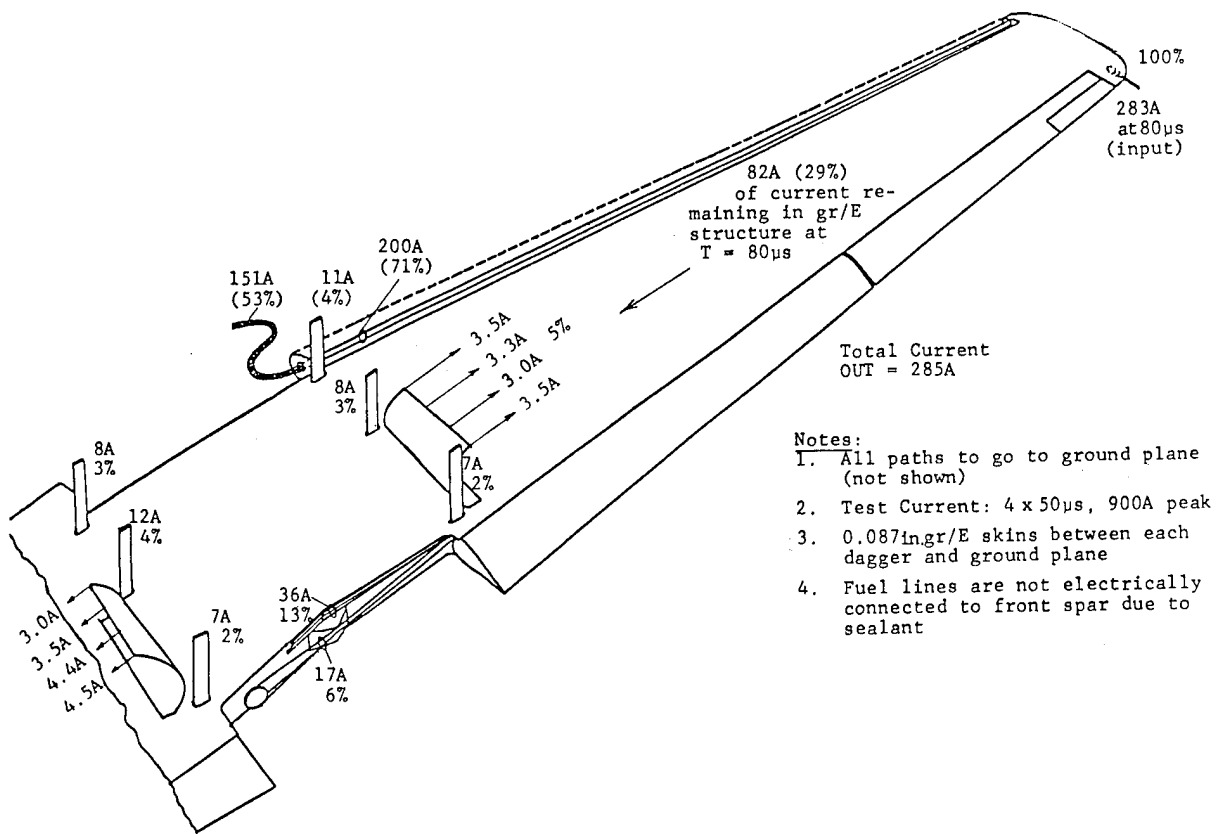


Figure 3.37 - Current Distribution in gr/E wing at $T = 80 \mu s$ for 900 A Current during a Simulated Strike to Static Discharger.

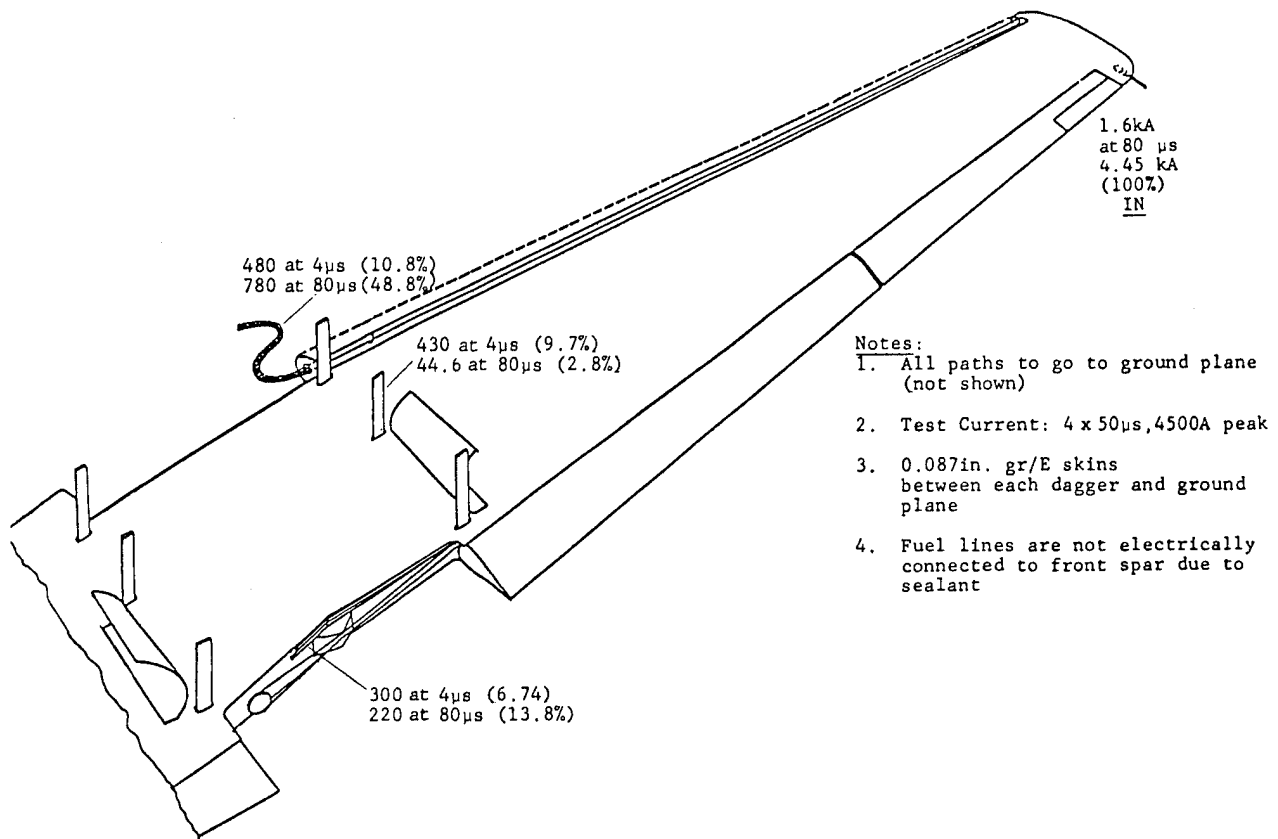


Figure 3.38 - Current Distribution in gr/E wing at $T = 4 \mu s$ and $T = 80 \mu s$ for a 4500 A Current during a Simulated Strike to Static Discharger.

the center fittings as through either the forward or aft fittings. It is reasonable to assume that the conduit braid at the leading edge and the hydraulic lines and control cables at the trailing edge bled off some of the current that might normally have been carried by the forward and aft dagger fittings.

Figure 3.37 shows that during the latter part of the strike, at $t = 80 \mu\text{s}$, the percentage of current conducted by the skin decreased from 75% to 29% as the metal conduit, control cables, and hydraulic lines began to conduct a greater percentage of the input current. Most of the current previously conducted by the graphite skin was transferred to the metal conduit; a much smaller percentage was transferred to the control cable and hydraulic lines since trailing edge currents were also conducted by the wire mesh along the rear spar.

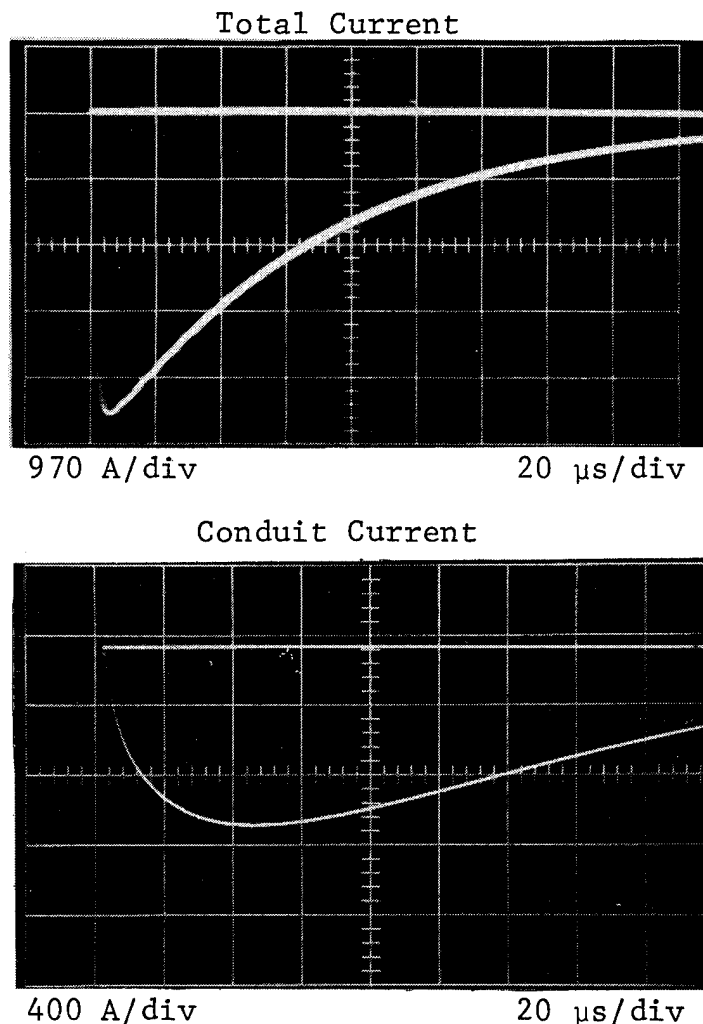


Figure 3.39 - Typical Oscillograms of Total Test Current and Current in Conduit of gr/E wing.

Additional current measurements were made in the leading edge conduit braid, the right center dagger fitting, and the hydraulic lines during a limited number of 4500A $4 \times 50 \mu\text{s}$ conducted test

current strikes. The purpose of these additional tests was to determine if the current distribution varied as a function of peak current amplitude. The results are shown in Figure 3.38. A comparison of current distributions at 4 μ s and 80 μ s for the two levels of test current showed that the current distribution percentages for the 4500 ampere test currents were within 5% of the readings obtained for the 900 A test current.

Measurements of current amplitudes in the fuel lines were recorded during 190 kA conducted entry test currents to the aluminum closeout rib at WS 226. The current amplitudes measured in the large and small diameter fuel lines, which exited at the front spar, were 200 A and 1.96 kA, respectively.

3.4.4.2 Bond line and fuel probe voltages

A summary of bond line voltage levels is shown in Table 3-13. Test currents, conducted into the static discharger, included a 900 A - 18 kA, 4x50 μ s unipolar wave and a 45kA - 190kA, 16 kHz oscillatory wave (waveforms are shown in Figure 3.5). Positive voltage readings indicate that the stringer or spar under test was at a lower voltage potential than the adjacent wing skin; negative readings indicate that the stringer or spar under test was at a higher voltage potential than the adjacent wing skin. Typical bond line and fuel probe voltage measurement oscillograms are shown in Figure 3.40.

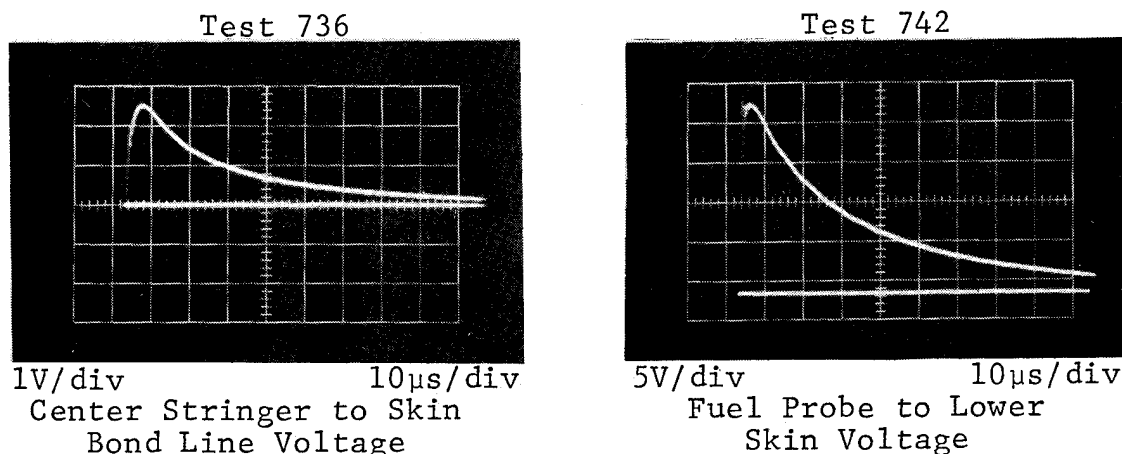


Figure 3.40 - Typical Bond Line and Fuel Probe Voltage Oscillograms at gr/E Wing Location WS 128 for a 900 A Test Current.

Bond line readings obtained during the 960 A conducted entry test currents ranged from 0.07 volts to 4.4 volts. Readings were also obtained at selected locations during application of 4.5 kA test currents. The bond line voltages recorded at this level were approximately five times those recorded at 900 A; thus the bond line voltages increased in the same proportion as the test current levels for this test current range.

Two 45 kA test current strikes were applied to the wing following the 900 A and 4500 A test current series. The rear stringer-to-skin bond line voltage was 63 volts.

Table 3-13 - Bond Line Voltages in gr/E Wing

	Total Current Level (kA)				
	<u>0.9</u>	<u>4.5</u>	<u>18.0</u>	<u>45.0</u>	<u>190.0</u>
<u>REAR SPAR TO UPPER SKIN</u>					
WS 88	0.25	1.50			
after 45 kA	0.40	--			
WS 128	0.80	4.00	--	--	--
WS 183	1.80	11.00	--	--	--
WS 206	1.90	--	--	--	--
<u>REAR STRINGER TO UPPER SKIN</u>					
WS 88	4.40				
after 45 kA	1.80	--	36	63.0	200.0
WS 128	2.50	--	--	--	--
<u>CENTER SPAR TO UPPER SKIN</u>					
WS 28	2.50	--	--	--	--
WS 69	0.07	--	--	--	--
WS 88	1.40	--	--	--	--
WS 128	-0.70	--	--	--	--
WS 212	1.60	--	--	--	--
<u>CENTER STRINGER TO UPPER SKIN</u>					
WS 88	-0.70	--	--	--	--
WS 128	2.5	--	--	--	--
<u>FRONT STRINGER TO UPPER SKIN</u>					
WS 28	2.90	--	--	--	--
WS 69	-1.20	--	--	--	--
<u>FRONT SPAR TO UPPER SKIN</u>					
WS 28	2.20	--	--	--	--
WS 69	1.50	--	--	--	--
WS 88	--	--	--	--	--
WS 128	--	--	--	--	--
WS 168	--	--	--	--	--
WS 183	--	--	--	--	--
WS 212	1.60	7.00			

A retest of WS 88 bond lines at 900A indicated that the rear stringer-to-skin voltage which was previously 4.4 volts, was 1.8 volts. This second measurement showed better correlation with bond line voltages of other locations indicating that the initial reading may have resulted from a high resistance measurement contact. The rear spar-to-skin bond line voltage was 0.4 volts, an increase of 0.15 volts from the first measurement at this location. Variation in the measurement probe contact resistance may account for the difference in reading.

At the conclusion of an intervening series of tests at 45 kA and 190 kA, voltages at WS 88 were remeasured at test currents of 900 A. A comparison of the remeasured voltages with the initial voltage readings at 900 A is shown in Table 3-14. Examination of the data shows that there was no significant difference in the fuel probe to lower skin voltage. The rear spar to upper skin bond line voltage increased by 20%, but the remaining spar and stringer-to-skin bond line voltages decreased by 20% - 57%.

Table 3-14 - Voltages in gr/E Wing at WS 88 for
900 A Test Currents

	<u>Initial</u> <u>Voltage</u> <u>(V)</u>	<u>Voltage After</u> <u>2 Tests at 45 kA</u> <u>(V)</u>	<u>Voltage After</u> <u>20 Tests at 198 kA</u> <u>(V)</u>
Fuel Probe to Lower Skin	19.00	20.00	20.00
<u>BOND LINE</u>			
Rear Spar to Upper Skin	0.25	0.40	0.30
Rear Stringer to Upper Skin	4.40	1.80	3.00
Center Stringer to Upper Skin	-0.70	--	-0.50
Center Spar to Upper Skin	1.40	--	0.60
Rib to Upper Skin	1.50	--	1.20

Front and rear spar bond line voltages are plotted in Figure 3.41. The graph indicates that the bond lines in the vicinity of the wing tip developed higher potentials than those further inboard. This is consistent with the fact that the

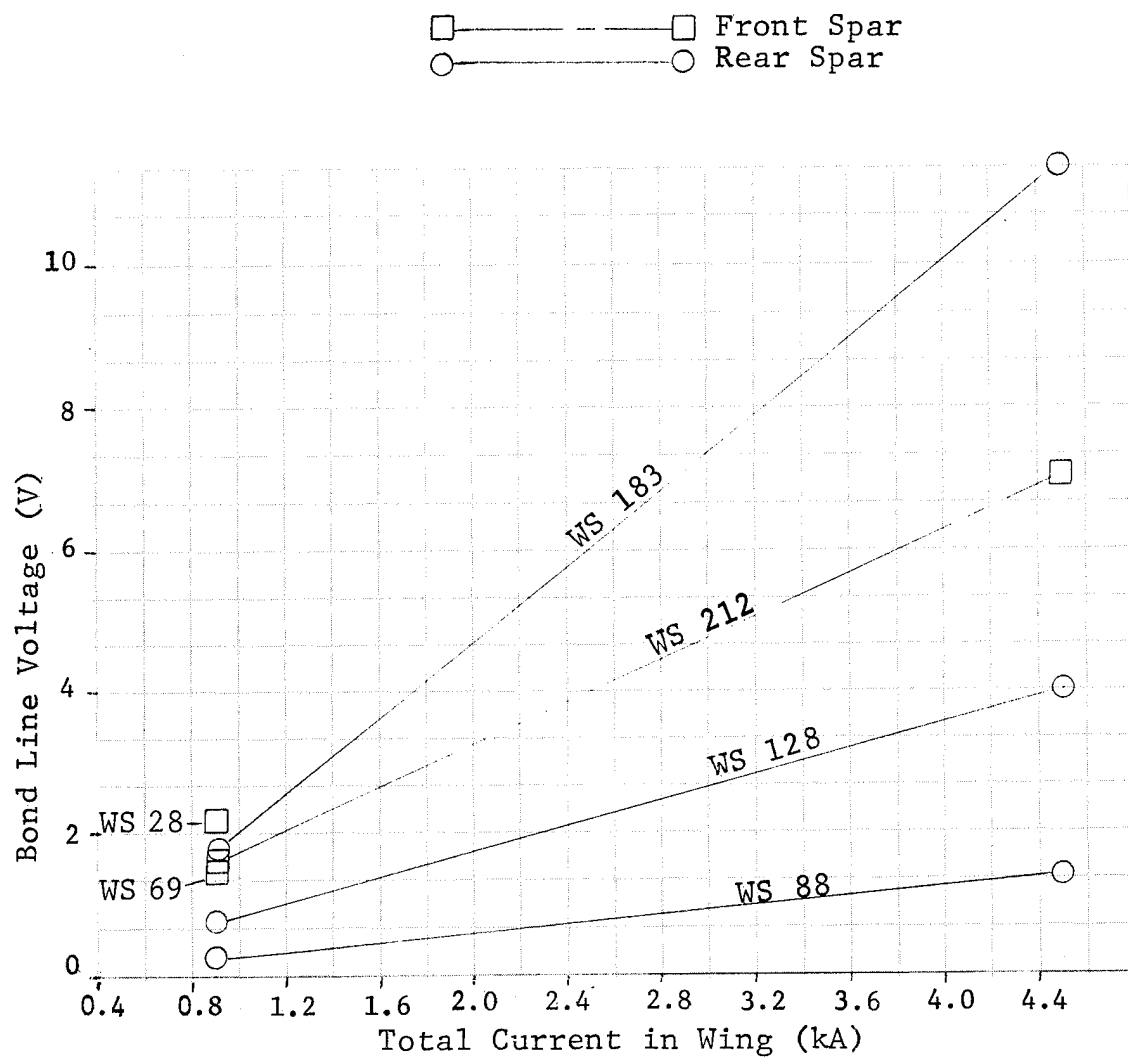


Figure 3.41 - Bond Line Voltages between Front and Rear Spars and Upper gr/E Wing Skin.

voltage potential developed along a wing, as the result of currents flowing through the wing skin, is highest at the point of entry (tip) and decreases as the measurement location approaches the current exit point (wing root reference plane).

Fuel probe to skin voltage measurement levels resulting from 900 A and 190 kA test current levels are plotted in Figure 3.42. Fuel probe and bond line voltages measured at location WS 88 are plotted in Figures 3.43 and 3.44. During these tests, the fuel probes were electrically connected to the reference ground plane at the wing root but were electrically isolated from the wing skin at their points of attachment; thus, the fuel probe voltage readings were actually a measurement of the wing skin potential with respect to the reference ground plane. It should be noted that the fuel probe voltage amplitude levels varied in a manner similar to the bond line voltages discussed above, i.e. the amplitude level was the highest at the point of current entry (tip) and decreased as the measurement location approached the point of current exit (wing root reference plane). Measurements of the peak amplitude voltage between the fuel probes and each wing skin surface indicated that an insignificant difference in voltage potential existed between the two surfaces.

Figures 3.43 and 3.44 are graphs of fuel probe and bond line voltages at wing location WS 88 as a function of test current amplitude. The graphs indicate that the wing skin resistance was non-linear, i.e., the resistance decreased as the peak current amplitude increased.

Table 3-15 shows the fuel probe-to-skin voltages measured during application of 190 kA conducted simulated lightning strikes to the aluminum closeout rib at WS 226. Calculations of the predicted voltage level at each fuel probe location for a 200 kA strike current were made based on wing resistance measurements recorded during previous laboratory tests at low current levels (~ 3 A) and were based on the assumption that WS 28 was at zero potential.

Table 3-15 shows that the actual voltages which existed in the wing were 20-40% lower than predicted (with the exception of WS 29.03). As mentioned above, the resistance of the wing structure material decreased as the conducted current level increased; thus voltage measurements recorded during the 190 kA strike predictably would be lower than voltages calculated based on resistance data obtained at 3 amperes.

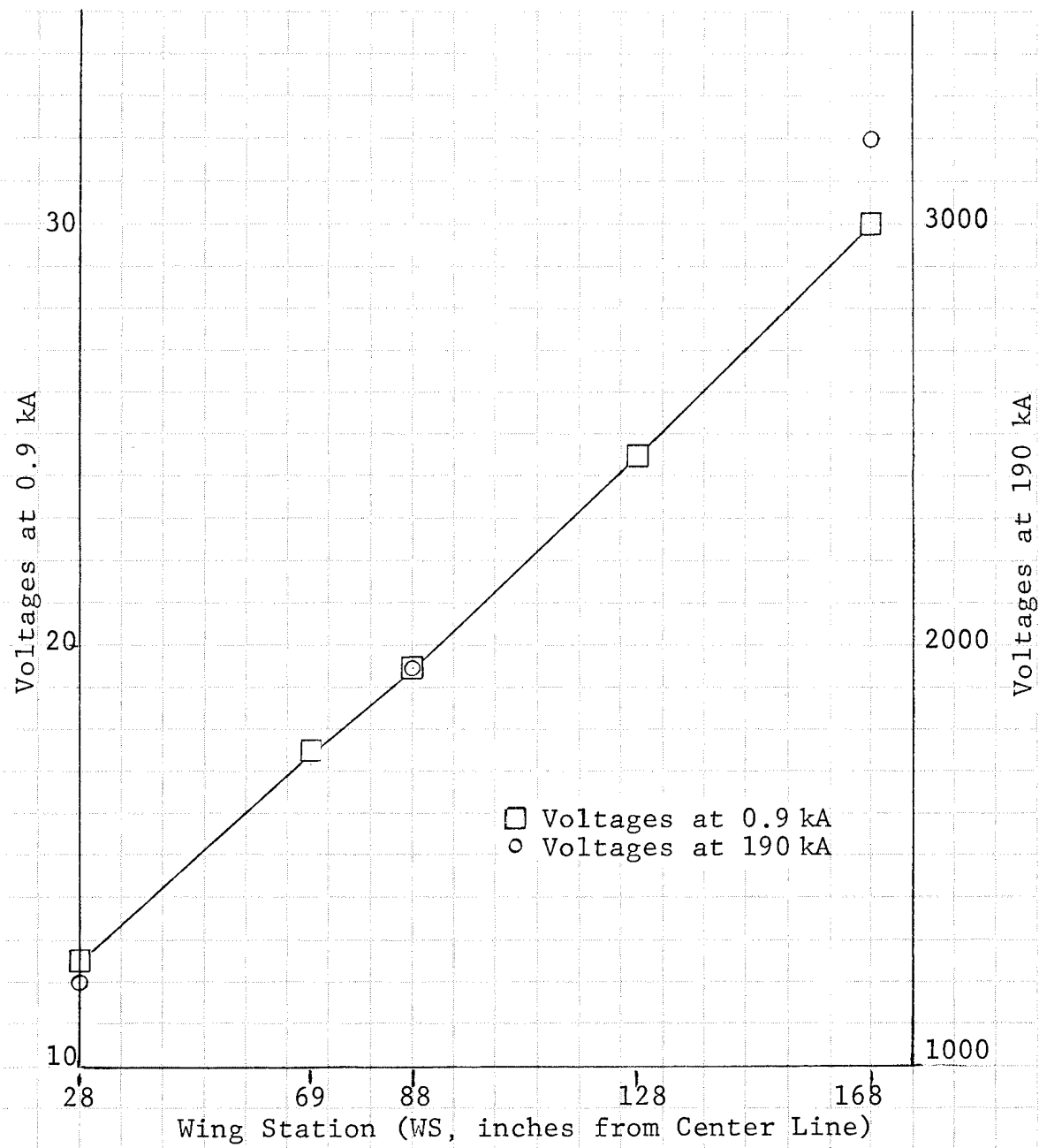


Figure 3.42 - Voltages between Fuel Probes and Top or Bottom Skins at Each Probe for gr/E Wing.

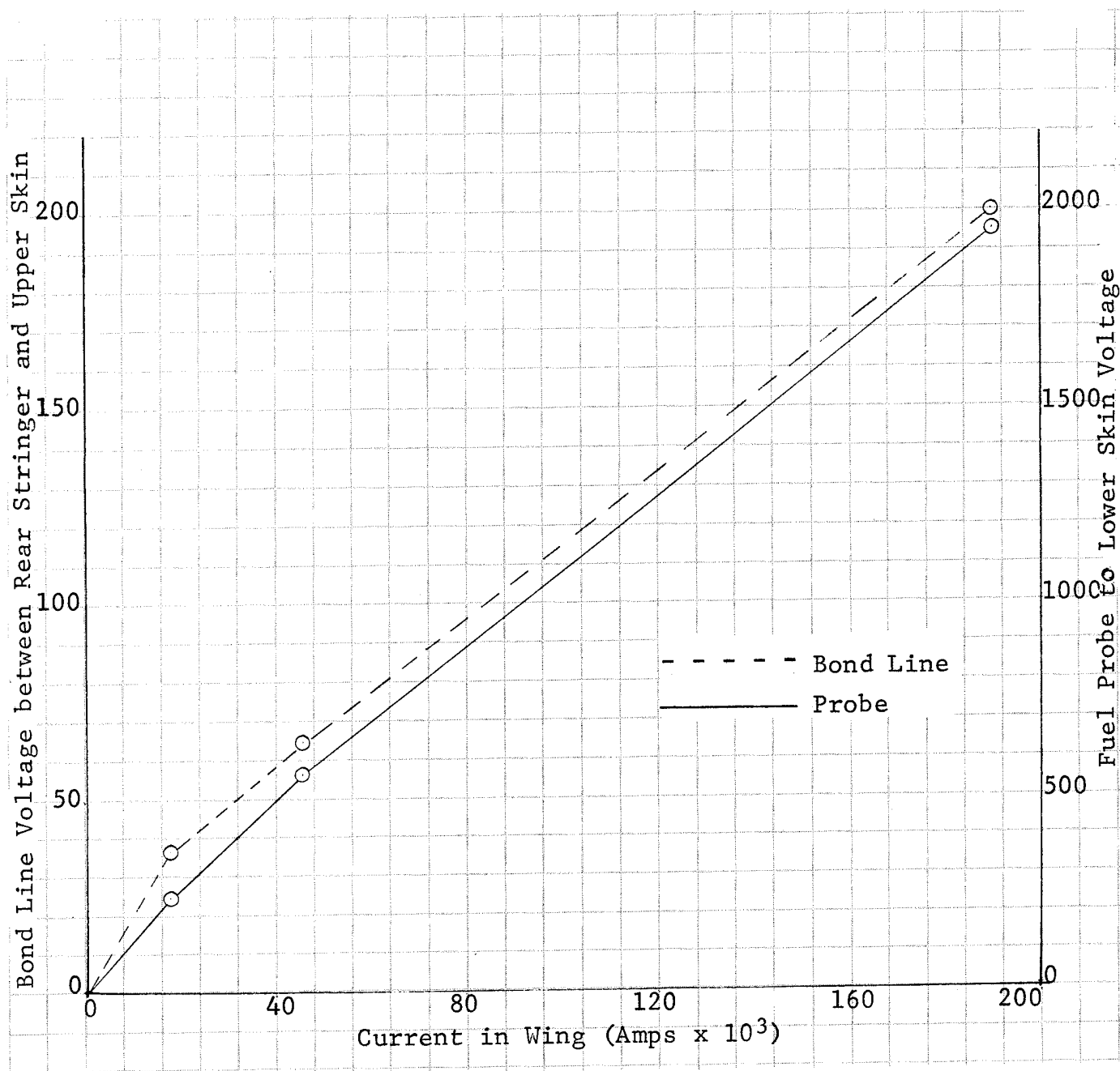


Figure 3.43 - Fuel Probe and Bond Line Voltages at WS 88 of the gr/E Wing.

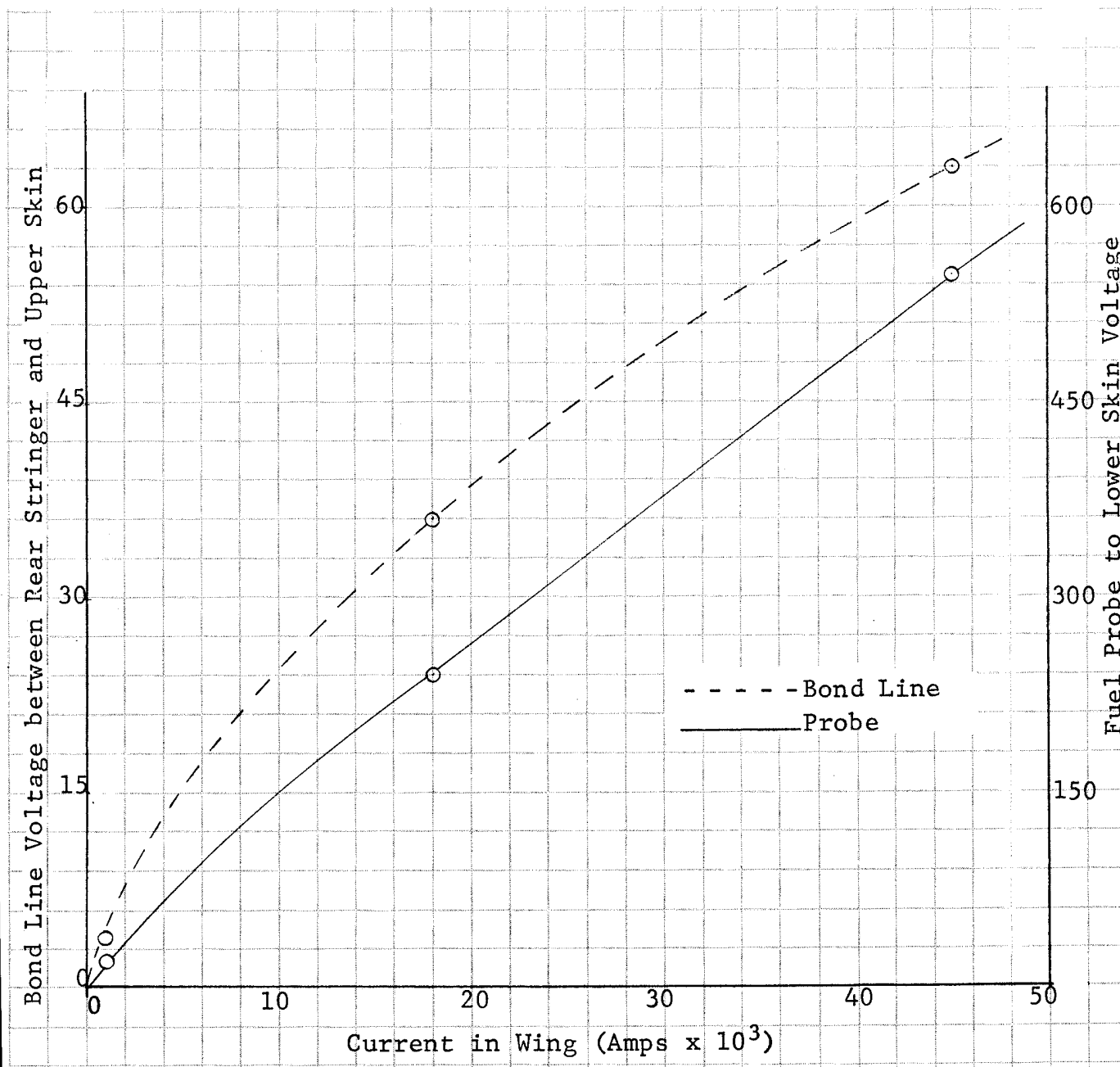


Figure 3.44 - Fuel Probe and Bond Line Voltages at WS 88 of the gr/E Wing.

Table 3-15 - Voltage between Fuel Probe and Adjacent Skin for Simulated Strike to WS 226 Rib in gr/E Wing

<u>Probe No.</u>	<u>Wing Station</u>	<u>Predicted at 200kA(a) (V)</u>	<u>Measured at 190kA (V)</u>
1	WS 29.03	40	1200
2	WS 70.53	1720	--
3	WS 89.03	2470	1950
4	WS129.03	4080	--
5	WS169.03	5700	3200

(a) from structural resistance measurements made at 3A

3.4.4.3 Induced voltages in wing electrical wiring

The results of the induced voltage test measurements are summarized in Table 3-16 and typical test current and measurement voltage oscillograms are shown in Figure 3.45.

The 36 kA conducted entry strikes resulted in measured voltages of 80 to 300 volts. If a linear relationship between the measured voltage and the test current amplitude is assumed, then the range of voltages expected to appear on the conduit wire harness circuits for a full threat 200 kA strike would be 450 V to 1.8 kV. The 170 kA arc entry test to the navigation light resulted in a peak voltage of 1350 volts. Again, assuming a linear relationship, the voltage reading for a full threat level strike current of 200 kA would be 1.6 kV.

3.4.4.4 Magnetic field measurements

Prior to initiation of the magnetic field measurements, the integrated output response of the 20 turn multi-layer coil was compared with that of the test current. The result, which is shown in the oscillogram of Figure 3.46, indicated close correlation between the integrated coil response and the test current waveform.

Table 3-16 - Summary of Voltages Measured in Leading Edge Conduit Wire Bundle Circuits during Simulated Lightning Strikes to Navigation Light in gr/E Wing

<u>Circuit Measured</u>	<u>Current Entry Configuration</u>	<u>Peak Test Current (kA)</u>	<u>Peak Measurement Voltage (V)</u>
Navigation and Position Light (Pin 8)	Conducted Entry to NAV Light Housing	36	330
Pot Control (Pin 1)	"	"	120
Pot Control (Pin 2)	"	"	120
Power to Motor (Pin 6)	"	"	230
Power to Motor (Pin 7)	"	"	230
Power to Power Supply (Pin 11)	"	"	320
Power to Power Supply (Pin 12)	"	"	320
Pot Control (Pin 3)	"	"	260
Chassis Ground (Pin 4)	"	"	80
Noise Check	"	"	4
Navigation and Position Light (Pin 8)	Arc Entry to NAV Light	170	1350

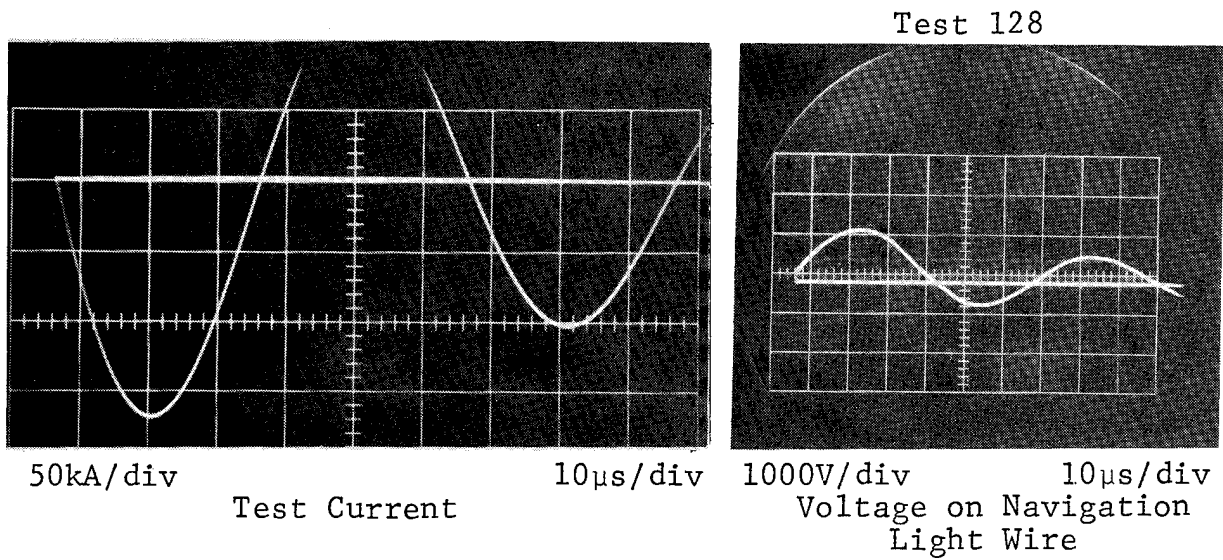


Figure 3.45 - Test Current and Voltage Measurement Oscillograms Obtained during 170 kA Arc Entry Strike to Navigation Light in gr/E Wing.

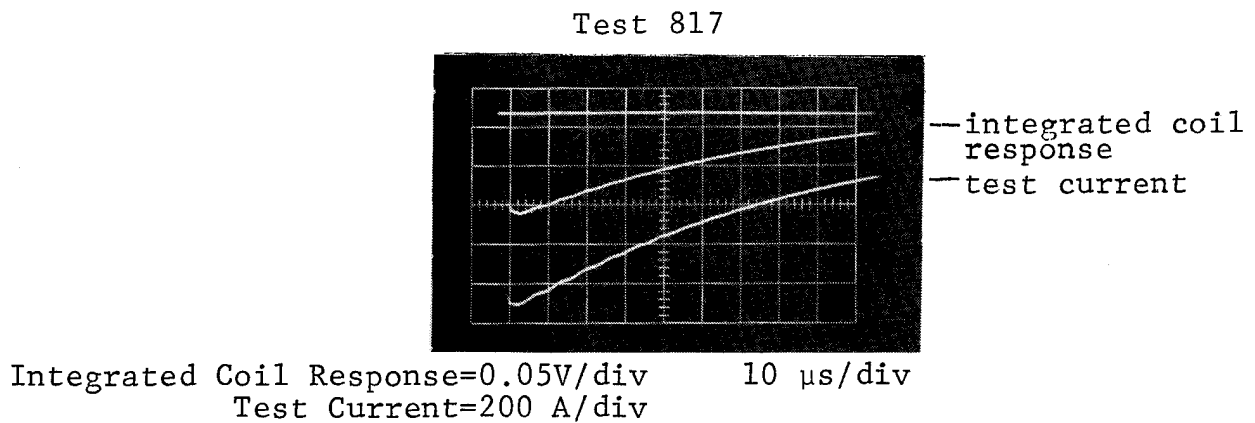


Figure 3.46 - Comparison of Search Coil Integrated Output Response with Test Current.

Figure 3.47 is a schematic representation of the wing showing the measurement location with the magnitude and direction of the magnetic field readings obtained during 900 A simulated strikes conducted into the wing tip static discharger. The oscillograms show the search coil response waveforms for the Z axis (skin-to-skin) magnetic field for each of the measurement locations.

Examination of the data presented in Figure 3.47 reveals that the internal magnetic field intensity was highest in the Z-axis direction (upper to lower) and that the highest Z-axis readings occurred at WS 182 and WS 216 in the vicinity of the wing tip and WS 40 located near the wing root.

Since an inverse proportionality exists between the circumference of a current-carrying conductor (wing skin) and its external magnetic field intensity, it follows that the average external field intensity at the wing tip (which is the smallest circumference) should be greater than the average intensity inboard near the wing root (largest circumference). The internal field intensity, which results from diffusion and aperture penetration of the external field, would follow a similar pattern.

The access door at WS 40 was constructed of kevlar rather than gr/E as in the other door locations. The tests at this location were performed without the use of aluminum flashing shield to simulate the electromagnetic environment that would exist with the kevlar door in place. The test results show a high Z-axis field intensity at this location comparable in magnitude to the measurement recorded at the wing tip locations but higher than the reading obtained at the adjacent access door location which used a gr/E door. The high field readings may also be due to other fields in the vicinity such as the field produced by current flowing in the leading edge conduit. The influence of the conduit field may also be the reason for the pronounced dip in the leading edge of WS 40 to WS 138 waveforms of Figure 3.47.

The second highest readings occurred during tests in which the coil axis was oriented to measure the leading to trailing edge magnetic field (Y-axis). The waveforms from these measurements, as shown on Figure 3.48 for a typical example, rise to peak more rapidly than do the Z-axis waveforms; thus, these fields appear to be more dependent on aperture-type field coupling than the Z-axis field measurements which appear to be more dependent on diffusion of the external fields through the skin material.

The lowest readings occurred for fields in the X-axis direction (wing inboard to outboard). Measurements ranged from 2A/ft (7 A/m) to 6A/ft (21 A/m); this compares to electrical "noise" readings of 1 A/ft (4 A/m) to 3 A/ft (10 A/m).

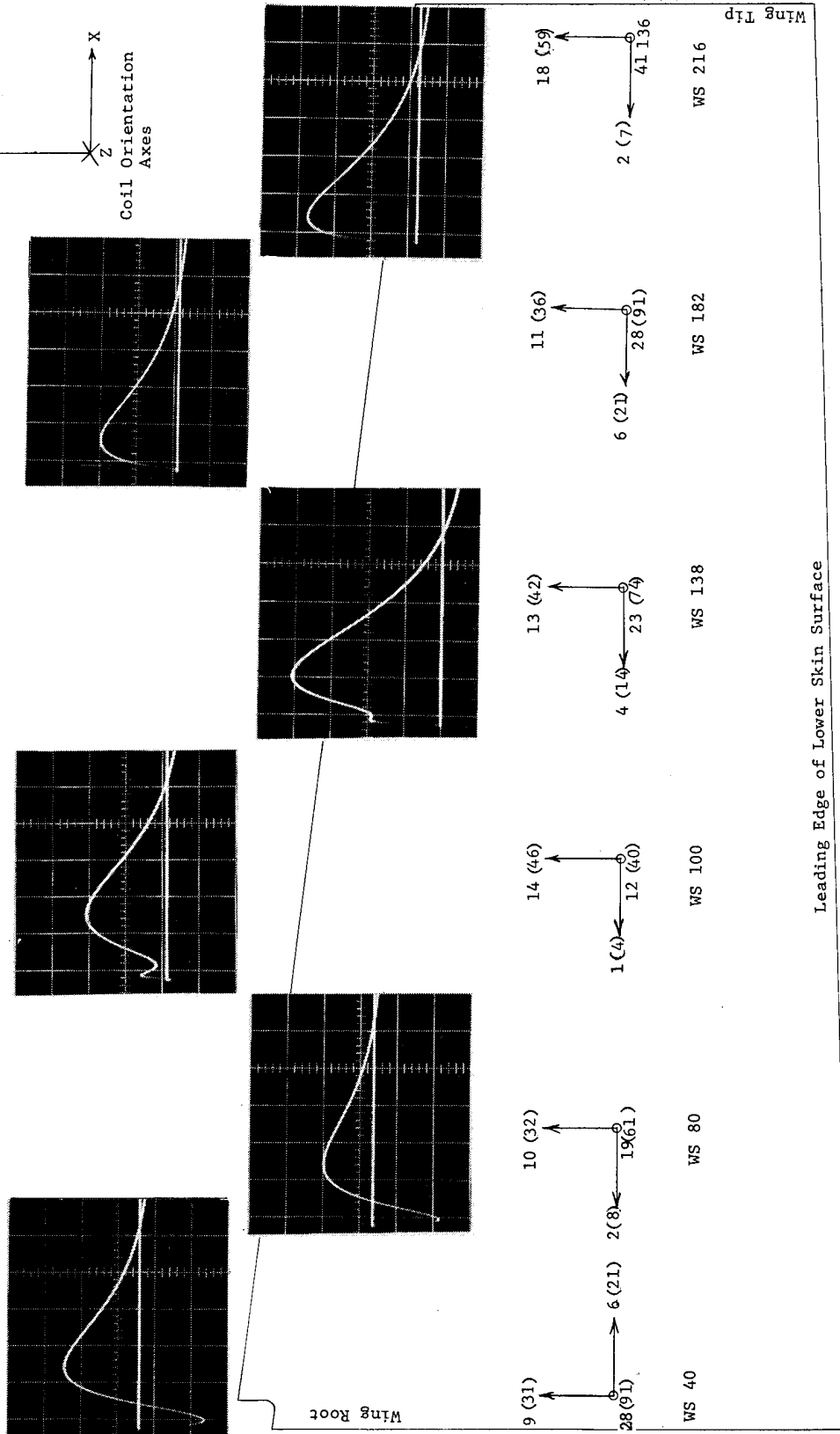
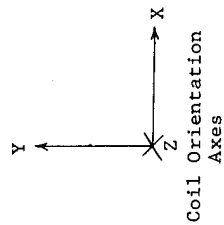


Figure 3.47 - Internal Magnetic Field Intensity Measurements in gr/E Wing for 900 A Test Current. Oscillograms show skin-to-skin waveforms (Sweep speed is 50 μ s/div). Data shows peak readings in A/ft (A/m). Note: Z-axis vector is directed out of the plane of the paper (Upper skin to lower skin).

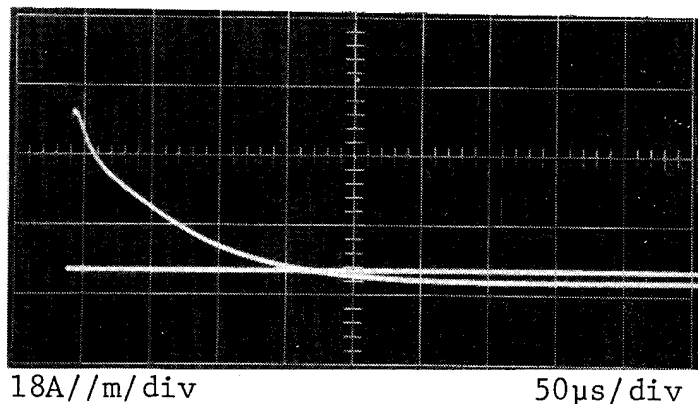


Figure 3.48 - Typical Oscillogram of Integrated Coil Response to Y-Axis Field at WS 138 in gr/E wing.

The results of the external field measurements are shown in Figures 3.49 and 3.50. Figure 3.51 shows typical oscillograms of the test current and the integrated coil response.

As discussed in paragraph 3.3.4.5, the average magnetic field intensity surrounding a current carrying conductor is calculated by dividing the conducted current by the circumference of the conductor. The circumference of the wing at location WS 182 (not including the control surfaces) was approximately 52 in. For a test current of 900 A, the theoretical average field intensity at WS 182 should have been 208 A/ft (692 A/m). At WS 80, with a circumference of approximately 84 in. (not including the control surfaces) the average field intensity should have been 129 A/ft (423 A/m). Comparison of the calculated average magnetic field intensity magnitudes with the recorded values obtained at WS 182 and WS 80 shows that in both cases the measured values are lower than expected.

Variation of the field intensity magnitude with location along the wing perimeter agrees with the theoretical prediction; i.e., the magnetic field intensity amplitude at locations with a smaller than average radius of curvature will be greater than average. The readings obtained at locations 1 and 10 (leading edge), where the radius of curvature was smaller than average, were higher than at any other locations. Readings obtained at locations where the radius of curvature was larger than average, as midway between the leading and trailing edges, were lower than average. The test reading amplitudes again increased at locations 4 and 7 where the radius of curvature again became smaller than average. Measurement points 5 and 6 were located at the trailing edge of the flaps approximately eight inches from the current-carrying wing, thus the field readings were understandably low.

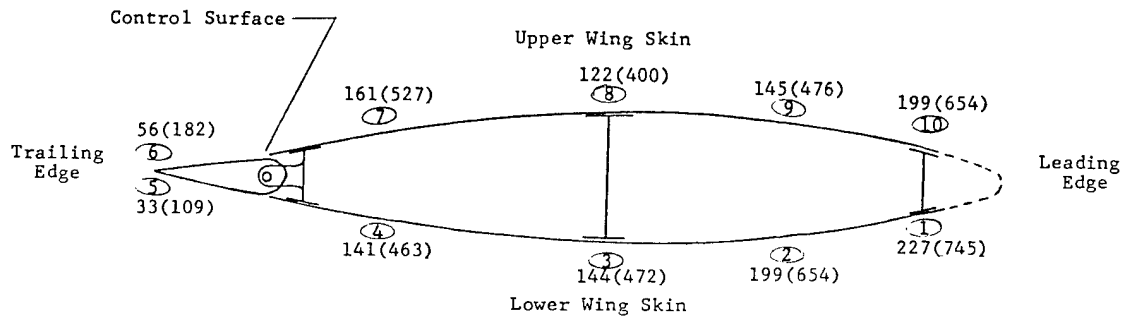


Figure 3.49 - Peak External Magnetic Field Intensity Levels at WS 182 in gr/E Wing. Test current was 900A. Measurements are in A/ft (A/m). Distance between measurement locations (circled numbers) is approximately 8 in.

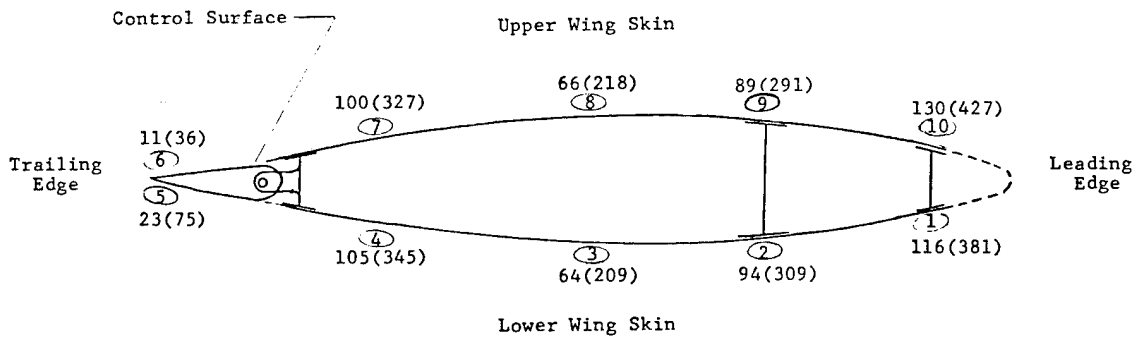


Figure 3.50 - Peak External Magnetic Field Intensity Levels at WS 80 in gr/E Wing. Test current was 900A. Measurements are in A/ft (A/m). Distance between measurement locations (circled numbers) is approximately 14 in.

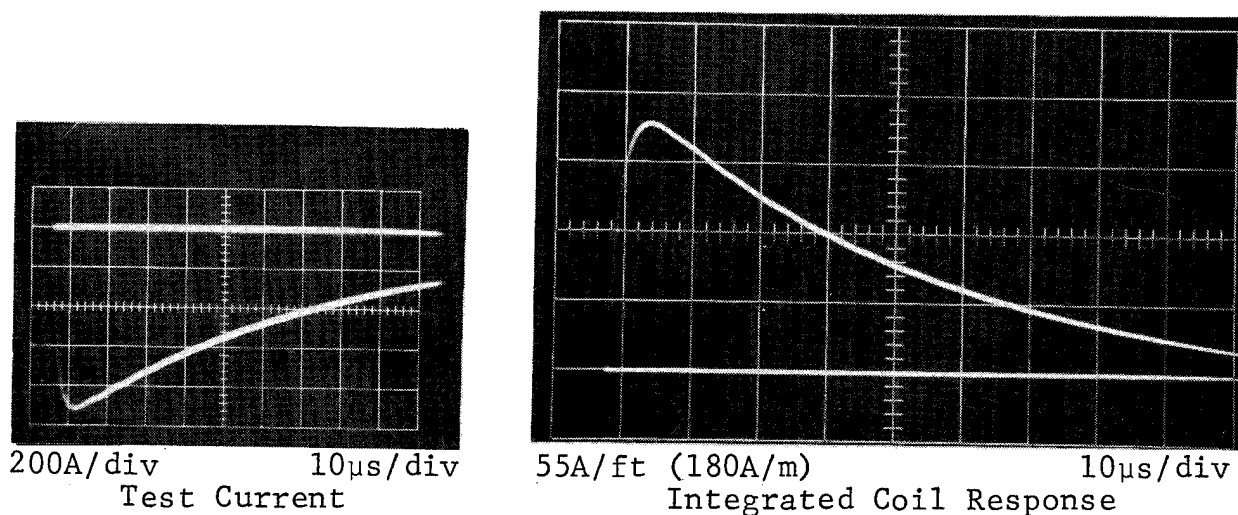


Figure 3.51 - Typical Oscillograms of Test Current and Integrated Coil Response Obtained during External Magnetic Field Measurements at WS 182 on gr/E Wing.

3.5 Discussion of Results

3.5.1 Comparison of the full scale structural environment with the subelement test results

3.5.1.1 Bonded aluminum wing

3.5.1.1.1 Current distribution.- Currents in the wing fuel lines (external to the fuel tank) were recorded during applied current strikes of up to 88 kA peak amplitude to the wing tip. The results are shown in Table 3-2. The maximum fuel line current amplitude recorded was 160A for the 88 kA strike; when extrapolated for a full threat strike of 200 kA, the expected fuel line current amplitude would be 364 A. Table 2-10 lists the spark threshold levels of bonded aluminum fuel line bracket subelement specimens and shows that visible sparks occurred at current levels of 0.10 kA - 10 kA for specimens which exhibited electrical conductivity prior to test. Thus the current levels measured in the full scale structure indicated that the possibility for ignition source sparking would exist if the following conditions were met:

- a) One hundred amperes (or higher) of fuel line current flowed through a fuel line bracket to the aluminum wing skin. Since no evidence of internal fuel tank

sparkling was recorded during the ignition source tests (Figures 3.17 through 3.20), either the current flowing through individual fuel line brackets was less than the spark threshold level, or the bracket adhesive was electrically nonconductive.

- b) A voltage potential of 100 volts or higher existed between a fuel line bracket and the wing skin (see the fuel line bracket subelement test results shown in Table 2-9). Again, the lack of internal fuel tank sparking during the ignition source tests indicated that the fuel line bracket-to-skin voltage potential did not exceed the breakdown voltage level threshold indicated in Table 2-9.

Interpretation of possible fuel tank sparking based on fuel line current measurements must be made with care. Currents flowing between fuel lines and wing skin return may follow several paths and may distribute unequally through several fuel line brackets. Thus, fuel line current levels which exceed the subelement spark threshold levels may not result in fuel ignition sparks at the bracket/wing skin interface since any one bracket may carry only a fraction of the total current.

3.5.1.1.2 Bond line voltages.- Bond line voltages recorded within the fuel tank for test current levels of 7 kA and 11 kA were 0.14 volts or less as shown in Table 3-3. Extrapolation of this reading for a 200 kA, full threat lightning strike results in a projected bond line voltage difference of 2.5 volts. This low voltage level indicates that continuity existed between the stringers, ribs, and aluminum skin. A check with a battery operated ohmmeter confirmed that continuity did exist between the adherends and, therefore, it would not be possible to develop a voltage potential between them. Thus, any sparks occurring in the fuel tank would be the result of current amplitudes which exceeded the current spark threshold level of the bonds. Table 2-6 shows the spark threshold levels of several adhesives tested on the subelement lap joint specimens. In particular, EA 9602.3 adhesive, which was utilized on the full scale structure, had a current spark threshold level of 200 amperes when current was conducted through a bonded surface area of 1 in.².

Photographs taken during the ignition source tests (Figures 3.17 through 3.20) indicated that no internal fuel tank sparking existed during 85 - 100 kA wing tip strikes. Thus, currents flowing between the adherends (wing skin and ribs or stringers) apparently had not exceeded the current density spark threshold level of 200 A/in.².

3.5.1.2 gr/E wing

3.5.1.2.1 Bond line voltage and current thresholds.- The full scale structure bond line voltage test results are tabulated in Table 3-13. For test current of 900 A, the bond line voltages ranged from 0.07 volts to 4.4 volts. If a linear relationship is assumed and the bond line voltages obtained during the 900 A current strikes are extrapolated for a full threat current strike level of 200 kA, the range of anticipated bond line voltages would be 16 to 980 volts. The rear stringer-to-skin bond line at WS 88, which recorded the higher bond line voltage at 900A, was measured during a 45 kA strike to the wing tip and found to be 63 volts. This value extrapolates to 280 volts for a 200 kA strike. A retest of this bond line at the 900 A strike level showed the bond line voltages to be 1.8 volts, down from its original level of 4.4 volts. This result would seem to indicate that either the first measurement circuit contained a high resistance connection causing a higher than normal voltage reading or the conduction of the 45 kA current through the wing resulted in the formation of additional conductive paths in the gr/E skin which reduced the voltage potential rise within the skin.

Table 3-14 shows a comparison between the original 900 A test current bond line readings at WS 88 and those recorded following twenty 190 kA current strikes to the wing. With one exception (rear spar to upper skin), the latter bond line voltage measurements were lower than the initial ones. This result would tend to corroborate the conclusion that currents through the structure form additional conductive paths thus reducing the voltage potential rise in the structure skin.

A graph of bond line voltage at WS 88 (Fig. 3.43) versus test current amplitude indicates that the resistivity of the gr/E skin was not linear but decreased with increasing current amplitude. Thus, if bond line voltage levels obtained with 900 A test currents, are used to predict bond line voltages resulting from 200 kA test currents, the predicted results will be higher than the actual measured voltages. Examination of the test data presented in Table 3-13 shows this to be true. At WS 88, the initial 900 A rear stringer-to-skin bond line voltage was 4.4 volts. If the resistivity of the gr/E skin were linear, the expected bond line voltage for a 200 kA strike would be 980 volts. The table indicates that the actual bond line voltage for a 190 kA strike was 200 volts, approximately 20% of the predicted value.

Table 2-15 tabulates the results of voltage breakdown tests on nonconductive subelement lap joint specimens. With the exception of one test specimen, the voltage breakdown levels ranged

from 1200V to 8000V. (The voltage breakdown level of the one specimen was less than 100 V. Pretest continuity measurements with a battery-operated ohmmeter had indicated that the bond line of this specimen was electrically nonconductive. Due to the difficulty of probing through epoxy resin with test probes, it is possible that good electrical contact with the graphite fiber was not made and that the specimen may have actually been conductive prior to the voltage breakdown tests. A conductive specimen would, of course, require no voltage to initiate conductivity).

The bond line voltages obtained on the full scale gr/E structure for a 200 kA current strike indicated the worst case bond line voltage level expected within a wing is approximately 1/6 of the minimum voltage breakdown level determined by the subelement test results. Thus, sparking at the bond lines would not be expected as a result of voltage breakdown.

If a bond line was electrically conductive, voltage potential could not be developed across it; hence, a fuel ignition spark would not result from bond line voltage breakdown. An ignition spark could result, however, if the current flowing through the conductive bond line were to exceed the current density spark threshold level. Table 2-18 shows the current density spark threshold level resulting from tests on the gr/E subelement lap joint specimens. Six of the specimens exhibited current spark threshold levels of less than 100 A/in.². These specimens had previously shown edge sparking during the voltage breakdown tests and thus would conduct no appreciable current before sparking.

The results of tests on the remaining specimens indicated that the current density spark threshold level ranged between 250 A/in.² and 5000 A/in.². An estimate of the current density level occurring within the full scale gr/E wing can be approximated from its physical dimensions. A worst case current density level would result by assuming that all of the skin current is transferred to the full length spars through the spar caps. If it is assumed that the average width of the spar caps is 2 in. and the length of each spar is 226 in., then the current density is given by:

$$\begin{aligned} \text{average current density} &= \frac{\text{strike current peak amplitude}}{\text{spar cap width} \times \text{spar length} \times \text{no. of}} \\ \text{through spar caps} &\quad \text{spars} \times \text{no. of skin surfaces} \\ &= \frac{200 \text{ kA}}{2 \text{ in.} \times 226 \text{ in.} \times 3 \times 2} \end{aligned}$$

$$\text{Average current density through spar caps} \approx 75 \text{ A/in.}^2.$$

The above analysis indicates that the current density in gr/E wing spar caps is approximately 30% of the level required to produce visible sparks as indicated by the subelement lap joint test results. This result is on the conservative side. Figure 3.36 indicates that at the time of the test current peak amplitude (approximately 4 μ s), the wing skin conducted only 74% of the test current; hence, the current density through the spar caps is approximately 75% of 75 A/in.² or 55 A/in.² which represents about 25% of the current density required to cause sparking.

Peak current amplitudes in the fuel lines measured 2 kA during a 190 kA simulated strike - this level is below the spark threshold level of 10 kA determined from the subelement fuel line feed-through test specimens, as shown in Figure 2.44.

3.5.2 Comparison of the bonded aluminum wing with the gr/E wing

3.5.2.1 Bond line voltage and wing resistance

The bonded aluminum wing exhibited extremely low bond line voltage readings indicating that electrical contact probably existed between the structural members and the wing skin; thus, projected bond line voltages for a severe 200 kA lightning strike were approximately 2.5 volts. This contrasts with the gr/E wing results where a maximum bond line voltage of 200 volts was measured for a 190 kA test current, as shown on Table 3-13.

The resistance of the bonded aluminum wing skin was determined to be 0.3 m Ω and calculated from the test oscillogram of voltage induced in the taxi light wiring, as shown in Figure 3.23 and on Table 3-6. The resistance was calculated by dividing the voltage by the current at the time, t , at which the rate of current change was zero. A schematic representation of this measurement is shown in Figure 3.52.

Calculation of the gr/E wing resistance can be made with a knowledge of the fuel probe-to-skin voltage measurements. As described in Para. 3.4.4.2, the fuel probes were electrically tied to ground through a dummy fuel quantity meter circuit and thus the probe-to-skin voltages actually represented the wing skin voltage potential with respect to the reference ground plane, as shown in Figure 3.53.

Fuel probe voltage readings are plotted in Figures 3.43 and 3.44 as a function of wing current for the probe at wing station WS 88. The structural resistance is the slope of the line which best fits the data points on the graphs and can be determined using the statistical method of linear regression.

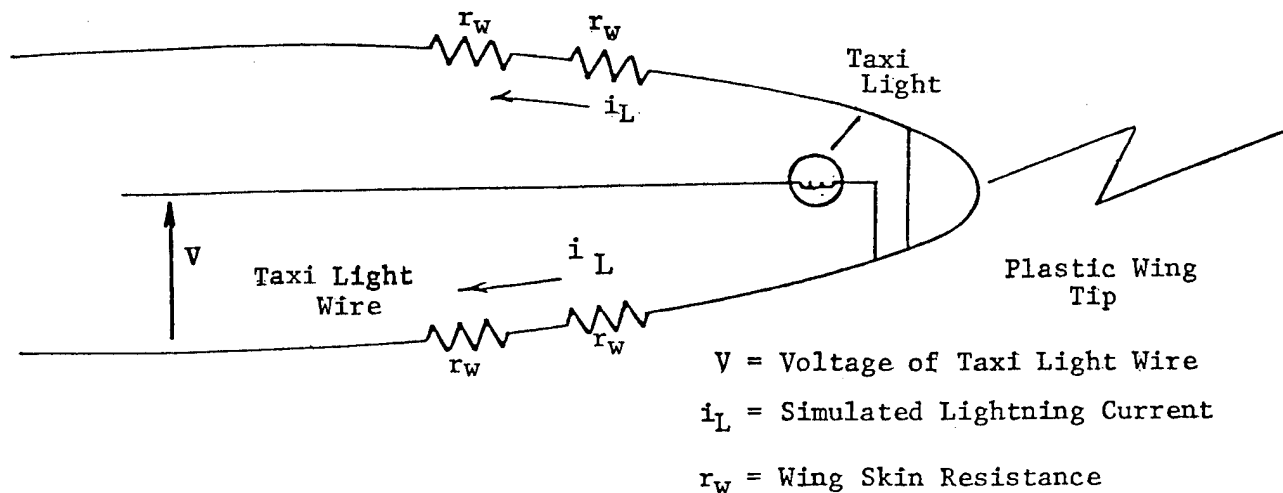


Figure 3.52 - Bonded Aluminum Wing Skin Resistance Measurement ($di/dt = 0$).

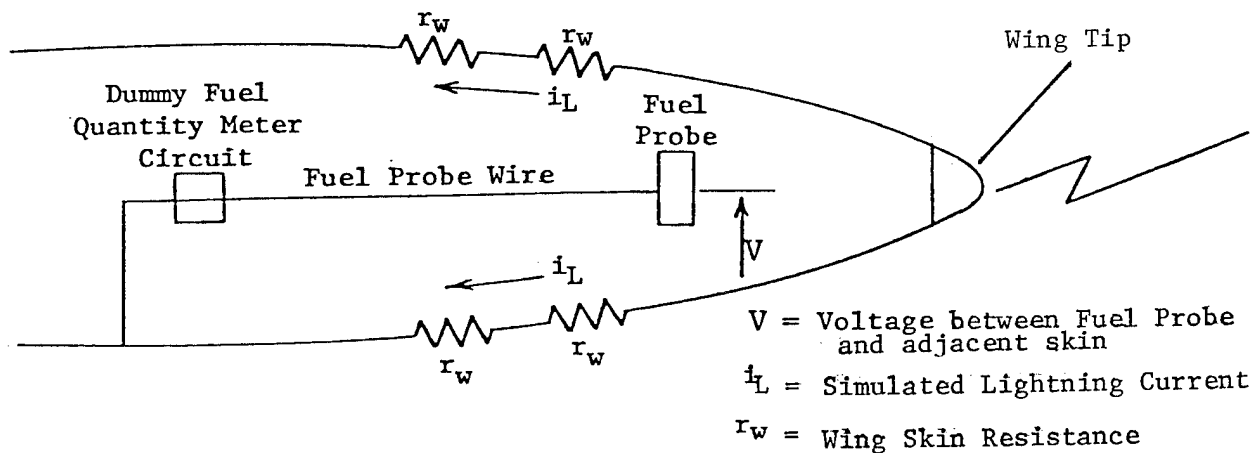


Figure 3.53 - gr/E Wing Skin Resistance Measurement.

This calculation indicated that the resistance between the reference ground plane and location WS 88 was $10.1 \times 10^{-3} \Omega/\text{in.}$ The structural resistance to the closeout rib at WS 226 was then $226 \text{ in.} \times 115 \times 10^{-6} \Omega/\text{in.} = 25.8 \times 10^{-3} \Omega.$

The test results and calculations above show that the resistances of the two wings were $0.3 \text{ m}\Omega$ for the bonded aluminum wing and $25.8 \text{ m}\Omega$ for the gr/E wing. The ratio of wing resistances was then:

$$\frac{\text{gr/E wing resistance}}{\text{bonded aluminum wing resistance}} = \frac{25.8 \text{ m}\Omega}{0.3 \text{ m}\Omega} \approx 100:1$$

3.5.2.2 Magnetic fields

Some interesting comparisons can be derived from the magnetic field data obtained on the bonded aluminum and gr/E wings. The data were previously presented in Table 3-12 and Figure 3.28 for the bonded aluminum wing and Figures 3.47 and 3.49 for the gr/E wing.

The ratio of the external to internal magnetic field intensities for the two wings can be calculated by normalizing the field intensity measurements with respect to test current levels.

For the bonded aluminum wing, this ratio can be determined as follows (measurements are at the fuel filler cap location):

$$\begin{aligned} \text{exterior to interior magnetic} \\ \text{field intensity ratio at WS 160} &= \frac{\text{peak exterior field intensity/test current}}{\text{peak interior field intensity/test current}} \\ (\text{Bonded Aluminum Wing}) &= \frac{2.1(10^3) \text{ A/ft } (6.6(10^3) \text{ A/m})/12 \text{ kA}}{20 \text{ A/ft } (66 \text{ A/m})/2.4 \text{ kA}} \\ &= \frac{175 \text{ A/ft/kA } (570 \text{ A/m/kA})}{8.3 \text{ A/ft/kA } (27 \text{ A/m/kA})} \end{aligned}$$

$$\begin{aligned} \text{exterior to interior magnetic} \\ \text{field intensity ratio at WS 160} &\approx 20:1 \\ (\text{Bonded Aluminum Wing}) \end{aligned}$$

In a similar manner, the external to internal field ratio for the gr/E wing can be calculated.

$$\begin{aligned} \text{exterior to interior} \\ \text{magnetic field intensity} &= \frac{\text{peak exterior field intensity/test current}}{\text{peak interior field intensity/test current}} \\ &\text{at WS 182} \\ &\text{(gr/E wing)} \end{aligned}$$

$$= \frac{145 \text{ A/ft (480 A/m)/0.9kA}}{28 \text{ A/ft (92A/m)/1.9kA}}$$

$$= \frac{145 \text{ A/ft/kA (480 A/m)}}{28 \text{ A/ft/kA (92 A/m)}}$$

$$\begin{aligned} \text{Exterior to interior} \\ \text{magnetic field intensity} &\approx 5:1 \\ &\text{at WS 182} \\ &\text{(gr/E wing)} \end{aligned}$$

A comparison can also be made between the three orthogonal field intensity measurements within the bonded aluminum wing with those in the gr/E wing. Again, data from bonded aluminum wing location WS 160 will be compared to gr/E wing location WS 182, as shown in Table 3-17.

Comparison of exterior to interior magnetic field ratios between the two wings shows that the shielding provided by the aluminum skin was approximately four times more effective than that provided by the gr/E skin. This correlates closely with the internal field ratio comparison of 3.7.1 between the wings for the Z-axis field orientation.

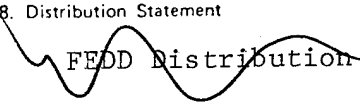
Table 3-17 - Data Tabulation and Results for
Internal Magnetic Field Comparison
between Bonded Aluminum and gr/E
Wings

<u>Coil Orientation (a)</u>	<u>X</u>	<u>Y</u>	<u>Z</u>
Peak Magnetic Intensity (H) A/ft (A/m) Bonded aluminum wing WS 160	5.5(18)	8.5(28)	20(64)
Peak Test Current (kA) Bonded aluminum wing WS 160	2.4	2.4	2.4
Normalized Magnetic Intensity. A/ft/kA (A/m/kA)	2.3(7.5)	3.5(12)	8.3(27)
Peak Magnetic Intensity (H) A/ft (A/m) gr/E wing WS 182	6 (21)	11 (36)	28 (91)
Peak Test Current (kA) gr/E wing	0.9	0.9	0.9
Normalized Magnetic Intensity. A/ft/kA (A/m/kA) gr/E wing WS 182	6.7(23)	12 (40)	31 (100)
<u>gr/E Wing Internal Field</u> Bonded Aluminum Wing In- ternal Field	~3:1	~3.5:1	~3.7:1

(a) See Figure 3.13

References

1. Fisher, F.A. and Plumer, J.A.: "Lightning Protection of Aircraft". NASA RP-1008, 1977, pp. 35-55.
2. "Lightning Test Waveforms and Techniques for Aerospace Vehicles and Hardware". Report of SAE Committee AE4L, June 1978.
3. Plumer, J.A.: "Further Thoughts on Location of Lightning Strike Zones on Aircraft". Lightning Technology, Suppl. NASA CP-2128, FAA-RD-80-30, 1981, pp. 81-98.
4. "Lightning Test Waveforms and Techniques for Aerospace Vehicles and Hardware". Report of SAE Committee AE4L, June 1978, Para. 2.0.
5. "Lightning Test Waveforms and Techniques for Aerospace Vehicles and Hardware". Report of SAE Committee AE4L, June 1978, Table 1.
6. "Lightning Qualification Test Techniques for Aerospace Vehicles and Hardware". MIL-STD-1757, June 1980.
7. Fisher, F.A. and Plumer, J.A.: "Lightning Protection of Aircraft". NASA RP-1008, 1977, p. 190.
8. Gerstein, M. and Allen, Robert D.: "Fire Protection Research Program for Supersonic Transport". Report of Dynamic Science Corporation, SN-4400, 1964, p. 112.
9. Fisher, F.A. and Plumer, J.A.: "Lightning Protection of Aircraft". NASA RP-1008, 1977, pp. 441-446.
10. Gerstein, M. and Allen, Robert D.: "Fire Protection Research Program for Supersonic Transport". Report of Dynamic Science Corporation, SN-4400, 1964, p. 113.
11. U.S. MIL-STD MIL A-25465, Rev. B. "Adhesive, Film Form, Metallic Structural Sandwich Construction", March 1982.
12. U.S. Federal Specification MMM-A-132. "Adhesives, Heat Resistant, Airframe Structure, Metal to Metal", October 1964.

1. Report No. NASA CR-3762		2. Government Accession No.		3. Recipient's Catalog No.	
4. Title and Subtitle LIGHTNING PROTECTION GUIDELINES AND TEST DATA FOR ADHESIVELY BONDED AIRCRAFT STRUCTURES				5. Report Date January 1984	
				6. Performing Organization Code	
7. Author(s) J.E. Pryzby and J.A. Plumer				8. Performing Organization Report No. LT-83-155	
				10. Work Unit No.	
9. Performing Organization Name and Address Lightning Technologies, Inc. 10 Downing Parkway Pittsfield, MA 01201				11. Contract or Grant No. NAS1-15884	
				13. Type of Report and Period Covered Contractor Report	
12. Sponsoring Agency Name and Address National Aeronautics and Space Administration Washington, DC 20546				14. Sponsoring Agency Code 505-45-03-01	
15. Supplementary Notes Langley Technical Monitors - Bruce D. Fisher and William E. Howell					
16. Abstract <p>The highly competitive marketplace and increasing cost of energy has motivated manufacturers of general aviation aircraft to utilize composite materials and metal-to-metal bonding in place of conventional fasteners and rivets to reduce weight, obtain smoother outside surfaces and reduce drag. The purpose of this program was protection of these new structures from hazardous lightning effects.</p> <p>The program began with a survey of advance-technology materials and fabrication methods under consideration for future designs. Sub-element specimens were subjected to simulated lightning voltages and currents. Measurements of bond line voltages, electrical sparking, and mechanical strength degradation were made to comprise a data base of electrical properties for new technology materials and basic structural configurations. The second phase of the program involved tests upon full scale wing structures which contained integral fuel tanks and which were representative of examples of new technology structures and fuel systems. The purpose of these tests was to provide a comparison between full scale structural measurements and those obtained from the "sub-element" specimens.</p>					
17. Key Words (Suggested by Author(s)) Lightning protection Fuel systems Lightning effects General aviation Composites Adhesive bonding Structures				18. Distribution Statement  Subject Category 05	
19. Security Classif. (of this report) Unclassified		20. Security Classif. (of this page) Unclassified		21. No. of Pages 173	
22. Price					